Geothermal Field Development Strategies Based on Economic and Fault Stability Analysis

A Case Study for the Delft Sandstone Area

Caroline Zaal

MSc Thesis Petroleum Engineering and Geosciences
Delft University of Technology

May 2020

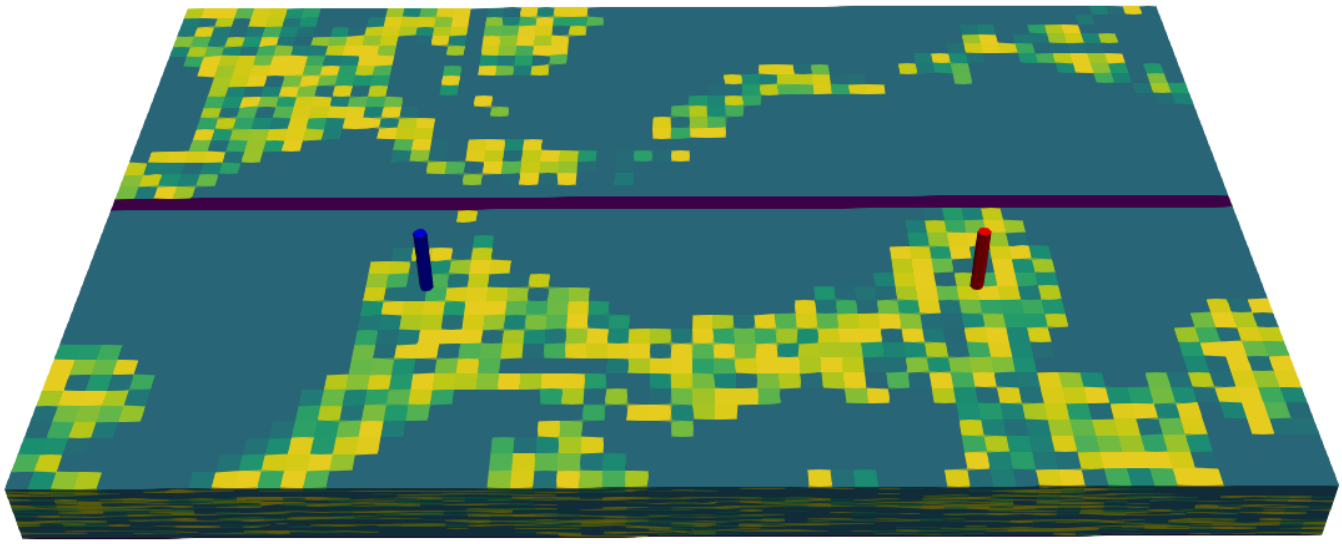

TU Delft

Geothermal Field Development Strategies Based on Economic and Fault Stability Analysis

A Case Study for the Delft Sandstone Area

by

Caroline Zaal

To obtain the degree of Master of Science in:
Petroleum Engineering and Geosciences
Faculty of Civil Engineering and Geosciences,
Delft University of Technology

To be defended publicly on Thursday May 7, 2020 at 10:00 AM.

Student number:	4307836	
Project duration:	May, 2019 – May, 2020	
Thesis committee:	Dr. Ir. F.C. Vossepoel,	TU Delft, Supervisor and Committee Chair
	Dr. A. Daniilidis,	TU Delft, Supervisor
	Prof. Dr. D. Bruhn,	TU Delft
	Dr. A. Correlje,	TU Delft

This thesis is confidential and cannot be made public until May 7, 2020.

TU Delft

Abstract

The main objective of this thesis is to assess the combined influences of specified reservoir conditions and operational parameters on the profitability of a geothermal project and on the potential for fault reactivation. The aim is to propose potential development strategies to maximize the profitability and minimize the potential for slip and reactivation of pre-existing critically stressed faults. The reservoir conditions of interest in this study include the fault permeability, the fault throw and the friction coefficient of the sandstone. The operational parameters of interest are the flowrate, the injection temperature of the re-injected water and the distance between the wells and the fault. As a case study a simplified homogeneous 3D box-shaped reservoir model is simulated based on the Delft Sandstone Member in the West Netherlands Basin, using the Delft Advanced Research Terra Simulator (DARTS). Reservoir production data and local pore pressure data are generated with DARTS and serve as the input data for the fault stability model and the economic model, which are both built in Python.

The fault stability model is built based on the method of Mohr circles, regional stress values in the Delft area and the failure criterion of sandstone and allows to assess the fault slip tendency of a pre-existing fault. The economic model is based on the Dutch fiscal system and policies and includes the costs of the phases of a geothermal project and required energy calculations. The outputs of the model allow to assess the profitability of a geothermal project based on the Net Present Value (NPV).

Outcomes of this study have shown that the profitability and the fault stability depend highly on the joint influences of specific reservoir conditions and operational options. Sealing faults generally have a negative influence on both the NPV outcomes and the fault stability as the presence leads to decreasing heat production, higher pumping costs and higher pressure build up near the fault. This influence is strengthened when the wells are placed close to the fault, while it is reduced by placing the wells far from the fault. The flowrate and the used injection temperature are found to be the most important operational options, regardless of the reservoir conditions. Combining the highest possible flowrates and the lowest possible injection temperature maximizes the NPV outcomes. As it is found that NPV outcomes increase by a factor 6 when increasing the flowrate 2.5 times and decreasing the injection temperature by 5 K may increase the NPV values up to 19% to 43% depending on the flowrate.

With respect to the reservoir conditions the study has shown that the fault permeability and the sandstone friction coefficient are the most important influencing reservoir conditions, compared to the fault throw. The risk for fault instability increases with decreasing value of the friction coefficient and of the fault permeability. With respect to the operational options the potential for fault slip is minimized when the lowest possible flowrate is combined with the highest possible injection temperature. However, the use of a 5 K higher injection temperature allows the use of a 600 m^3/day higher flowrate. Placing the wells minimally 200 m from a fault in the homogeneous reservoir and using a minimum flowrate of 7200 m^3/day maximizes the NPV outcomes and fault reactivation is reduced as much as possible. The assessment of the fault stability and the profitability is however very sensitive to the reservoir conditions, which is explicitly found from the results comparing a homogeneous and a heterogeneous reservoir. This makes the potential development strategies extremely prone to heterogeneity effects and subsurface conditions which makes them highly dependent on locations specific properties. Though, the general influences of the reservoir conditions and operational options on a heterogeneous reservoir are similar to those found for the homogeneous reservoir.

Acknowledgement

With this thesis I am ending my studies at the Delft University of Technology and this final project would have not came to a success without the help of several people. With this I would like to thank all of them. First and foremost I want to thank my supervisors Alex Daniilidis and Femke Vossepoel who both have been so engaged during the entire process. Alex was my daily supervisor and has given me great guidance throughout the project by always challenging and forcing me to think further, answering my questions with counter questions and he always took time to help me out with a lot of patience. A big thank you to Femke who also supported me greatly despite her busy schedule and gave valuable suggestions and comments on my work. I am very grateful to have had you both as my supervisors. Also I would like to thank David Bruhn and Aad Correlje for taking place in my graduation committee and providing me with useful and valuable feedback on my report and presentations. Special thanks go to Yang Wang who has helped multiple times resolving technical issues and difficulties on DARTS and Python.

This project has been a challenging journey with ups and downs, which I would not have been able to complete without the continuous support from my family and friends. First of all, I want to especially thank my parents. My father, always willing to think with me about the goals and content of my project, providing feedback where possible and getting me in touch with contacts who could help me out with additional relevant information. And my mother for being the best mental advisor and always being there to help put my worries and demotivations into perspective. Both my parents have helped greatly in keeping me motivated throughout the entire process. Also I want to thank my MV and Petro/Civil study mates for all the coffee breaks and lunches at the faculty. The many laughs and joint complaining sessions have helped keeping me motivated and keep the entire process enjoyable most of the time. Finally, thanks to my roommates and Fleur for the fun digital conversations and support which have kept the final stage of my thesis bearable during the Corona crisis.

Caroline Zaal
Delft, May 2020

Contents

Abbreviations

AbEx	Abandonment Expenditures
BHP	Bottom Hole Pressure
CapEx	Capital Expenditures
CBS	Centraal Bureau van Statistiek
CPB	Centraal Planbureau
DAGO	Dutch Association for Geothermal Operators
DARTS	Delft Advanced Research Terra Simulator
DCF	Discounted Cashflow
DSSM	Delft Sandstone Member
EBN B.V.	Energie Beheer Nederland B.V.
ECN	Energieonderzoek Centrum Nederland
ESP	Electricle Submersible Pump
EZK	Ministerie van Economische Zaken & Klimaat (Dutch Ministry of Economic Affairs and Climate)
HHV	High Heating Value
KEV	Klimaat- en Energieverkenning
kW	kilo Watt
LCOH	Levelized Cost of Heat
LHV	Low Heating Value
MC	Mohr-Coulomb
NPV	Net Present Value
OBL	Operator-Based Linearization
OpEx	Operational Expenditures
PBL	Planbureau voor de Leefomgeving
PI	Profitability Index
PJ	Peta Joule
PV	Present Value
RNES	Regeling National EZ-Subsidies
SDE	Stimulering Duurzame Energie
SodM	Staatstoezicht op de Mijnen
Tcbb	Technical Committee Ground Movement

THP	Tubing Head Pressure
TNO	Toegepast Natuurwetenschappelijk Onderzoek - Advisory Group for Economic Affairs
WACC	Weighted Average Cost of Capital
WN	Stichting Warmtenetwerk
WNB	West Netherlands Basin

List of Figures

List of Tables

1

Introduction

Geothermal energy is on the rise and is a promising, renewable energy source which can deliver baseload energy for industrial and domestic usage. The annual energy consumption in the Netherlands is approximately 3156 PJ of which 5.7% (181 PJ) is covered by renewable energy (EBN, 2017). Geothermal energy delivers 1.7% (3 PJ) from this renewable energy, produced by 18 geothermal doublets. Figure 1.0.1 shows these doublets and their status in June 2019.

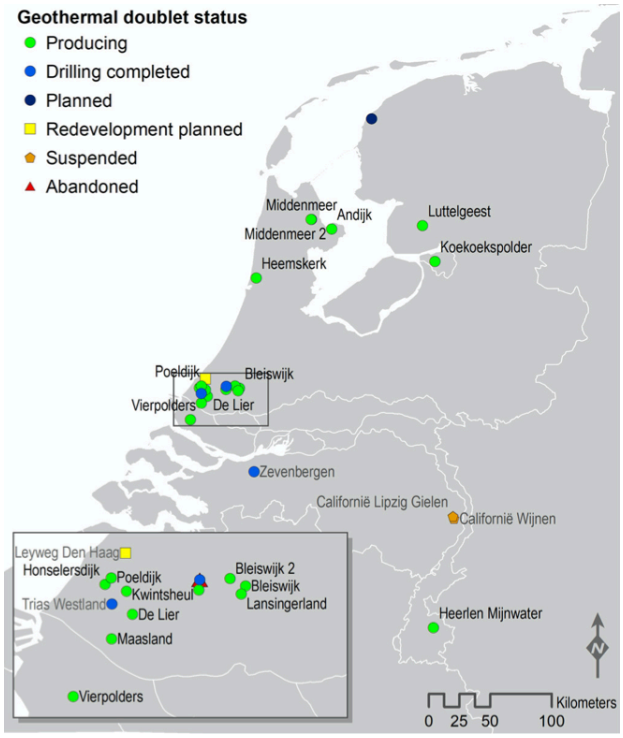

Figure 1.0.1: Geothermal doublets in the Netherlands and their status in June 2019 (Buijze et al., 2019a)

In order to meet the conditions of the Paris Climate agreement of 2015, the Netherlands needs to reduce their CO_2 emmissions by 49% by 2030 and by 95% in 2050 compared to 1990 (Schoof et al., 2018). Current geothermal sources in the Netherlands emit in average 13 kg CO_2/GJ, which is an 80% reduction in comparison to 66 kg/GJ CO_2 emissions due to hydrocarbon sources (Stichting Platform Geothermie, 2019). This makes geothermal energy a source with high potential for the Dutch government in their aim to accelerate the sustainable transition by six times and to reduce CO_2 emissions (Schoof et al., 2018). To stimulate the acceleration of sustainable energy production in the Netherlands, a masterplan was set up in 2018 by a collaboration of geothermal organizations Platform Geothermie, DAGO, WN and EBN to

accelerate the development of geothermal energy applications. The goal of this masterplan is to increase the annual geothermal production from 3 PJ in 2018 to 50 PJ in 2030 and to more than 200 PJ in 2050. One PJ per year can provide heat to approximately 20,000 households in the Netherlands (Schoof et al., 2018). In order to meet this aim the amount of geothermal developments in the Netherlands need to be accelerated and this should be accompanied by specific assessments on the profitability and safety risks associated with prospective projects. Namely, for any geothermal operation to be successful it must not only be profitable, it should also not pose any environmental or societal risks. An important risk to consider, is the risk of induced seismicity.

1.1. Problem Statement

The acceleration of geothermal heat production requires development of a large variety of target formations, even the targets that are more challenging to develop (Buijze et al., 2019b). This acceleration would result in a higher density of geothermal systems and this means there will be more mutual interference between the systems and more interaction with structural subsurface elements such as faults (Daniilidis et al., 2020a; Willems et al., 2017). The social acceptance of the accelerated development of this 'new' energy source depends on the management and assessments of safety and potential risks associated (Buijze et al., 2019b). Any concerns that are related to the potential for disturbances or induced seismicity could delay or even hold back the development of a geothermal energy production (Buijze et al., 2019b; Gaucher et al., 2015). Therefore it is essential to properly assess, evaluate and mitigate safety risks for the local community and the environment, due to potential induced seismic events. In addition, a geothermal project needs to stay economically attractive for a developer and for potential investors in order to execute a geothermal development. This thesis is about these two important considerations in geothermal operations and can help operators to assess the viability of their (future) projects, based on the combined assessment of the impact of specific reservoir conditions and operational options on the profitability and induced seismicity.

Profitability

In order to produce 50 PJ of geothermal energy by 2030, 160 doublets need to be realized between now and 2030 (Schoof et al., 2018). This requires an investment of approximately two billion euros. Between 2030 and 2050, 450 additional doublets should be realized to meet the energy goals. This still requires another four billion euros, even if the realization costs can be reduced by 40% due to growing experience and coordinated exploration and production. To be able to finance this fast growing development a few requirements should bet met. Firstly, according to the Dutch mining act it is required that the financial carrying capacity of a geothermal operator is sufficient throughout the entire geothermal project (Wiebes, 2018). This is obligatory in order to be able to compensate any financial setbacks because of potential technical problems during the development or production. Therefore, operators need sufficient initial capital and their project needs to be profitable. For a project to be profitable it requires secure and stable revenues and reductions in development and operations costs. Secondly, investors are required to finance these projects. In order to attract investors for geothermal projects, it is required to ensure a stable yield of geothermal projects and make sure that financial risks are reduced as much as possible (Schoof et al., 2018). Reducing financial risks is done by reducing the probability and the start of low-yield projects and mitigating the impacts of these projects (Schoof et al., 2018), which requires sufficient capital, insurance systems and increase in knowledge and experience in geothermal energy and the Dutch subsurface. Therefore it is important to research the profitability of a potential reservoir in the Netherlands and research its expected yield. In this way it should be possible to research its ability in providing high yield and revenues and with this optimise investment decisions for potential investors and stakeholders.

Operators can increase their expected NPV by opting for increased flowrates, as higher flowrates (like 400 m^3/hr) generate higher NPV compared to lower flowrates of for example 100 m^3/hr (Daniilidis et al., 2020a). However, still there is a potential risk of fault reactivation (possibly leading to induced seismicity) due to the injection of water. The potential for seismicity could already be present in the area of interest before it is even identified as a risk, especially when a prospected project is planned near a pre-existing fault. Any risk of fault reactivation could withhold investors and citizens in surrounding area of accepting the geothermal project. Fault reactivation is even a potential reason of a project being less profitable than expected as it might be needed to cut off a running project earlier than expected if reactivation occurs.

Therefore the assessment of any possible reactivation of faults nearby the geothermal reservoir is crucial as well.

Induced seismicity

Induced seismicity is found to be a key issue for the development and application of geothermal projects and has already caused delays or cancellations of some developments (Gaucher et al., 2015). In the public view seismic risks are a concern in terms of its direct impact on local damages, but also in terms of their perception on subsurface energy production in general. Compared to cases worldwide, Buijze et al. (2019b) have shown that the seismic potential is generally low for the current sandstone targets in the Netherlands. However, recent seismic events have occurred in the South-Eastern part of the Netherlands near the Californie geothermal sites in Limburg and in Groningen (Buijze et al., 2019b). This is also visible in Figure 1.1.1, which shows the active faults in the Netherlands and the areas in which both natural and induced seismic events have occurred. According to Figure 1.1.1 the seismic events in Limburg are natural, however there may be a link to the ongoing geothermal projects in the area (SodM, 2018). Especially since some operators in the South-Eastern part of the Netherlands have chosen to make use of the present faults as they promote the flow of water and allow the production of water with higher temperatures (SodM, 2017). However, studies have shown that placing a geothermal doublet close to faults, hence injecting water close to faults almost always goes paired with seismic events (SodM, 2017). Therefore it is crucial to research if there is potential for seismic events resulting from geothermal operations in other parts of the Netherlands as well.

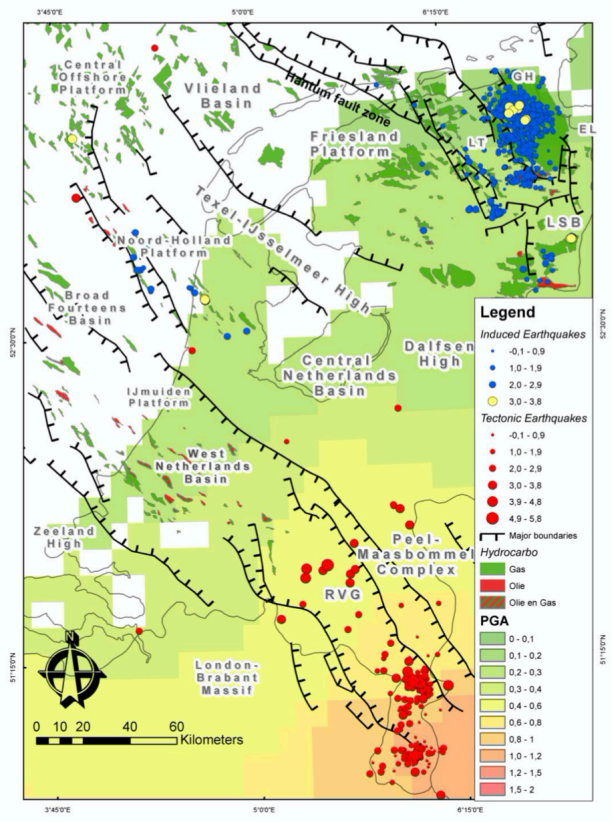

Figure 1.1.1: Map of the Netherlands showing present active faults and encountered earthquakes (induced and natural) in Dutch area (Buijze et al., 2019b)

The earthquakes in Groningen are a result of hydrocarbon operations, which has different mechanisms behind fault reactivation compared to those of geothermal operations (Buijze et al., 2019b). Hydrocarbon operations lead to stress reductions potentially resulting in fault reactivation, while geothermal operations lead to stress increases. The strength of a specific point at a faults surface is determined by the the effective stress. Fault reactivation due to fluid injection (geothermal operations) is caused because increased pore pressure and total stresses push shear stresses to the point of failure of a fault (Fitts,

2013). As a result the local effective stress at that point decreases. The extraction of subsurface fluids and gas (hydrocarbon operations), on the other hand, reduces the local pore pressure and this increases the effective stress, which could potentially lead to compaction of the rock mass at that location (Grasso, 1992). This compaction leads to strain accumulation and if this exceeds the strength of the fault surface it could cause reactivation (Pennington et al., 1986).

Fault slip can be seismic or aseismic (Figure 1.1.2), which are identified as two different modes of fault growth as a result of differing slip velocities (Preuss et al., 2019).

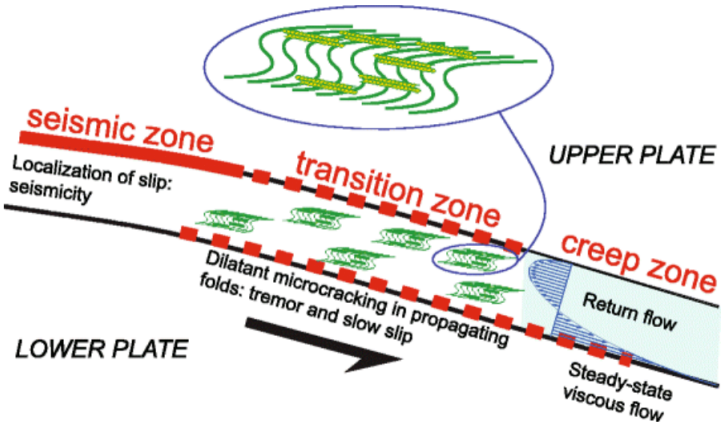

Figure 1.1.2: The relationship between seismic and aseismic fault slip. Seismic slip occurs in the seismic zone (generally at relatively shallow depth down to 20 km) and occurs fast and causes earthquakes. Aseismic slip (creep zone) occurs in a slow and steady pace and does not induce noticeable earthquakes as this generally happens deep in the subsurface. The two zones are separated by the transition zone in which fault slip may cause vibrations or happens slowly (Platt et al., 2018)

If the resistance to fault slip is decreased faster compared to how fast the fault adapts to this stress decrease, sudden slip may occur and this may radiate seismic waves causing earthquakes (Schwarts and Rokosky, 2007). This is called seismic slip and occurs in the seismic zone at depths down to approximately 20 km (Platt et al., 2018). If the resistance to fault slip decreases in a slow and relatively steady pace, stable sliding occurs and this does not radiate seismic waves as large amounts of energy dissipate during deformation. This is called aseismic slip, or creep and is often caused by postseismic relaxation. Induced seismicity is the result of rapid, seismic slip on a plane of weakness in the subsurface, which is related to fault reactivation by Amonton's law (Buijze et al., 2019a; National Research Council, 2013). The occurrence of fault reactivation is determined by a combination of geological and operational factors (Candela et al., 2018). Examples of natural conditions are the presence of pre-existing faults and the local stress levels near a potential geothermal reservoir. This in combination with operational parameters like the production and injection rate may reactivate faults. Re-injection of water into the subsurface, adds stress to the total stress field in nearby rocks and local pore pressure is increased as water flows into permeable rocks (Fitts, 2013). This increased pore pressure front diffuses along with the flowing water and once this pressure reaches a fault near its point of failure, even a very small increase in pore pressure or total stress could trigger fault reactivation (Candela et al., 2018). The occurence of seismicity depends on multiple factors. These are the inititation of fault slip, the propagation of fault slip and seismicity generation (Platteeuw, 2018). It should however be noted that seismicity is not always generated as result of slip initiation and propagation. Therefore, to assess and mitigate any safety risks this thesis focuses only on the initiation of fault slip, which may initiate fault reactivation. The analysis is therefore considered as a worst-case scenario.

In order to research the potential for fault slip it is needed to address the subsurface properties at potential geothermal locations, the structures of any present faults and how these properties affect this reactivation. In this also operational parameters like the distance from the wells to the fault, the production/injection rate and the injection temperature are important. These reservoir conditions and operational parameters however also influence the profitability of a project. As mentioned, Daniilidis et al. (2020a) have shown that profitability increases by using higher flowrates during geothermal production, however it is essential to investigate how this use of increased flowrates influences the fault reactivation.

A prospective project may result in high profits, but at the same may induce fault reactivation which makes the project possibly unsafe for local citizens. Hence, the project could be cut off earlier than expected or not start at all, which might result in severe economic losses when the project had already started. Therefore, the presence of certain reservoir conditions and use of operational parameters may have a positive impact on the profitability, but on the contrary can have a negative impact on the fault stability and vice versa. In order to attract investors and local citizens to accept and finance a geothermal project the profitability needs to be maximized, while the safety risks due to potential reactivation must be minimized. Therefore, specific reservoir conditions and operational parameters must be investigated on their combined effects on profitability and fault stability. As a result of this research it should be possible to make an effort in lowering seismic risks and maximize profits by designing potential development strategies such that the risk of slip and reactivation of critically-stressed faults is lowered as much as possible, while remaining profitable.

1.2. Research Questions

The link between the above mentioned problems will be addressed using the following research questions.

- How does the presence of a sealing or a non-sealing fault in a reservoir influence the economics of a geothermal project?
- What combination of reservoir conditions and operational options are of key importance in making a geothermal project profitable?
- What reservoir conditions are of key importance for the possible occurrence of fault reactivation?
- How sensitive is the possibility of fault reactivation in the Delft Sandstone Member to different development options?
- What regulations and guidelines need to be considered for the potential development strategies in the Netherlands?

1.3. Research Approach

In order to assess the profitability and risk of fault reactivation a case study is done on a real-life reservoir of which petro-physical and geological data is available to make the results as realistic as possible. Currently a lot of research is done into the Delft area in which two geothermal systems are already operational (by greenhouse companies Ammerlaan and Duijvestijn) and a third well is upcoming on the campus of the TU Delft, which will be realized by the Delft Aardwarmte Project (Donselaar et al., 2015). The model simulated in this thesis is therefore based on reservoir characteristics of the Delft Sandstone Member in the Delft area, which is part of the Lower Cretaceous Nieuwerkerk Formation in the West Netherlands Basin.

A simplified homogeneous 3D box-shaped reservoir model is simulated using Delft Advanced Research Terra Simulator (DARTS). With respect to the assessment of fault slip initiation a pre-existing fault is assumed, which does not vary in vertical orientations. Production and pressure data generated with DARTS are the inputs for the fault stability model and economic model, which are both built in Python. The economic model is based on the costs for each phase of a geothermal project and on the Dutch economic system and policies, which is all found from literature research and earlier studies (Daniilidis et al., 2017; van Dongen, 2019a). This economic model allows us to assess the project profitability based on outputs such as the net present value, levelized cost of heat and profitability index. The fault stability model is built such that it allows to assess the slip tendency using the method of Mohr circles which are based on regional stress values in the subsurface of the Delft area, the local pore pressure changes near the fault extracted from the reservoir model and the Mohr failure criterion based on the characteristics of the Delft Sandstone. The fault stability and the profitability are researched for different test cases in the Delft area. These test cases differ in reservoir conditions and operating options. Reservoir conditions are varied in the values for fault throw, fault permeability (sealing or non-sealing) and the friction coefficient of sandstone. Operating options are varied in flow rate in the injector and producer, the distance between the wells and the fault and the injection temperature of the water. The found profitability and fault stability are compared with simulations of a heterogeneous 3D box-shaped reservoir model based on the realistic

porosity and permeability found in the Delft Sandstone. Comparing the results of the homogeneous and the heterogeneous reservoir puts the results into perspective and helps to contextualize the outcomes of the homogeneous reservoir. In addition the economic and technical robustness and sensitivity of the two models are investigated. A schematic of the used workflow in this thesis is shown by Figure 1.3.1.

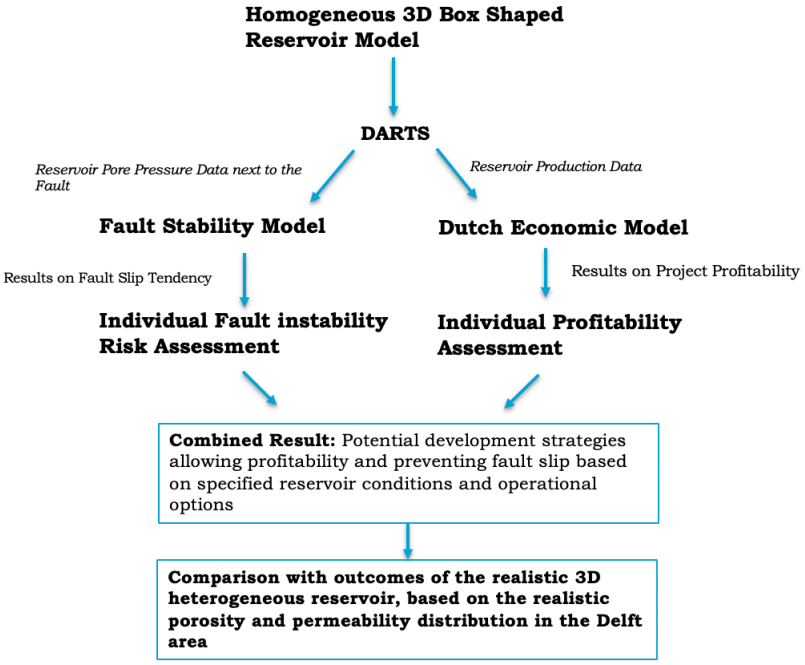

Figure 1.3.1: Schematic of the used workflow in this thesis

1.4. Thesis Outline

This thesis starts with a literature review on the geological history and geological setting of the Delft Sandstone area in Chapter 2. This is followed by the description of the reservoir simulation model in DARTS and the used input parameters in Chapter 3. The methodology, background information of governing equations and the used input parameters of the fault stability model and the economic model are described in Chapter 4 and Chapter 5 respectively. This is followed by Chapter 6 which presents and describes the individual results of the different reservoir conditions and development parameters on the fault stability and profitability of the homogeneous Delft Sandstone reservoir. The combined impact of these parameters on the fault stability and profitability are shown in Chapter 7 and discusses potential reservoir development strategies based on the presence of a sealing, a medium sealing or a permeable fault. Chapter 8 presents the sensitivity study in which the results of simulations of the realistic 3D heterogeneous reservoir are shown and compared to those of the homogeneous reservoir. Additionally, the outcomes of specific economic and technical sensitivity checks are presented and discussed to put the results into perspective. Chapter 9 firstly discusses the results of the homogeneous and heterogeneous reservoir by taking into account regulations and guidelines in the Netherlands and this is followed by the overall conclusions of this study. The thesis is finalized with recommendations for future studies in Chapter 10.

2

Geological Setting

Most prospective areas for geothermal energy in the Netherlands correspond largely to areas of Dutch hydrocarbon explorations and production (Pluymaekers et al., 2012). Therefore the determination of aquifer properties benefits greatly from retrieved well log interpretations, core plug measurements and core descriptions during these explorations. The Dutch area has five major stratigraphic formations in which aquifers are present (Pluymaekers et al., 2012):

- The Slochteren formation (Permian Rotliegendes sandstone)
- Main Buntsandstein formation (Triassic)
- Nieuwerkerk formation (Jurassic Schieland group)
- Vlieland formation (Early Cretaceous)
- Dinantian formation (Carboniferous)

A map showing the distribution of deep aquifers with geothermal potential in the Netherlands is shown in Figure 2.0.1.

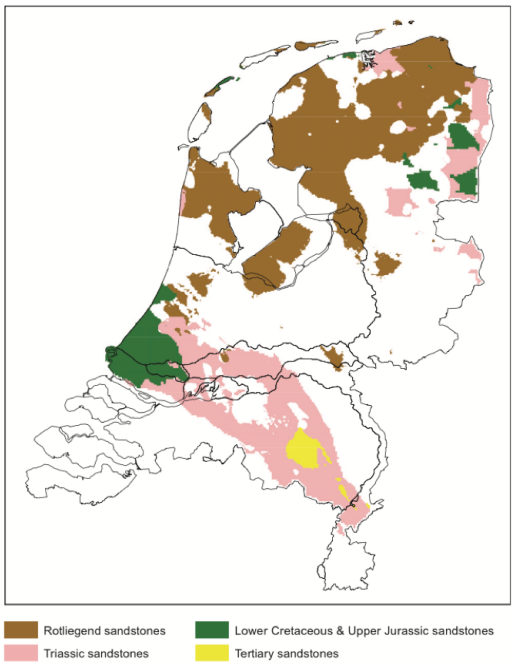

Figure 2.0.1: Distribution of deep aquifers with geothermal potential in the Netherlands (Pluymaekers et al., 2012)

The target reservoir of this thesis is the Delft Sandstone Member (DSSM), which is part of the Nieuwerkerk formation in the West Netherlands Basin (WNB). The WNB is a 60 km wide trans-tensional basin, located in the southwestern parts of the Netherlands and contains stratigraphic formations of the Late Jurassic/ Early Cretaceous (Bonte et al., 2012; Pluymaekers et al., 2012). It is structurally bounded in the North by the Zandvoort Ridge and IJmuiden High from the Central Netherlands Basin, in the South it is bounded by the London Brabant Massif and towards the South-East it merges with the Roer Valley Graben (Van Adrichem Boogaert and Kouwe, 1993). A simplified structural map of the Dutch area is shown in Figure 2.0.2.

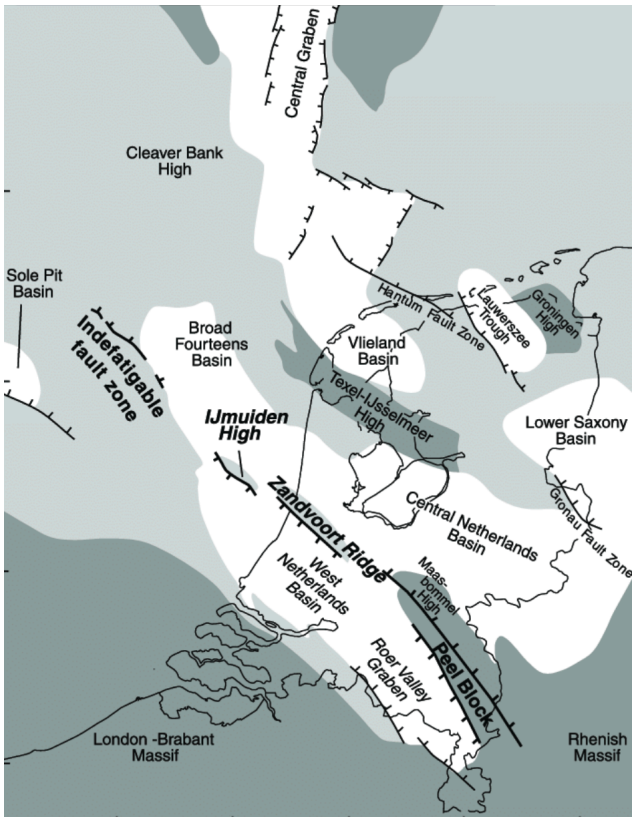

Figure 2.0.2: Simplified structural map of the Netherlands (Michon et al., 2003)

The evolution of the basin is complex and consists of four major phases (van Balen et al., 2000).

Late Carboniferous - Early Permian Stage
The evolution of the basin started with the Variscan orogeny, in which especially the northern part of the Zandvoort Ridge was uplifted and eroded (van Balen et al., 2000). The southern part of the basin was much less uplifted and eroded. As time passed the basin was filled with fine-grained sediments and by the end of the Late Carboniferous the basin was filled with shales and coal-bearing sediments (Van Adrichem Boogaert and Kouwe, 1993).

Late Permian - Middle Jurassic
This stage of the WNB evolution is called the 'Prerift stage'. During the Late Permian sedimentation of fluvial and aeolian sandstones was ongoing, this consisted of the sandstones we now know as the Rotliegend sandstone group (van Balen et al., 2000). These were followed by the deposition of claystones, siltstones and carbonates of the Zechstein group. During the Late Permian there was a short uplift, which was followed by regional thermal subsidence during the Early Triassic (Nelskamp and Verweij, 2016). Triassic sediments were fine-grained lacustrine and sandy fluvial and aeolian deposits, which are known as the Main Buntsandstein Group (Van Adrichem Boogaert and Kouwe, 1993). From the Middle to Late Triassic tectonic movement of the Early Kimmerian phase took place, during which the WNB formed a large half-graben. After that faulting caused subsidence and as a result subunits formed in the basin.

Late Jurassic - Early Cretaceous
During the Late Jurassic to the Early Cretaceous the strongest rifting of the basin occured; therefore this phase is called the 'synrift' phase (Nelskamp and Verweij, 2016; van Balen et al., 2000). This rifting happened in short duration pulses, which caused the basin to brake up in multiple subunits. In addition, Late Jurassic sedimentation caused large thickness variations.

Late Cretaceous - Quartenary
The 'postrifting' phase of the WNB took place during Late Cretaceous, in which the WNB inverted due to compressive forces (van Wijhe, 1987). Reverse movements took place in major fault zones of the basin, which resulted in the formation of many oil-bearing structures (van Balen et al., 2000). In the latest age of the Late Cretaceous the inversion movements ceased and the basin was again covered with Early Paleocene sediments. A cross-section of the WNB is shown in Figure 2.0.3 and a more detailed overview of the stratigraphy in the Delft area is given by Figure 2.0.4. The Delft Sandstone Member is part of the Schieland Group.

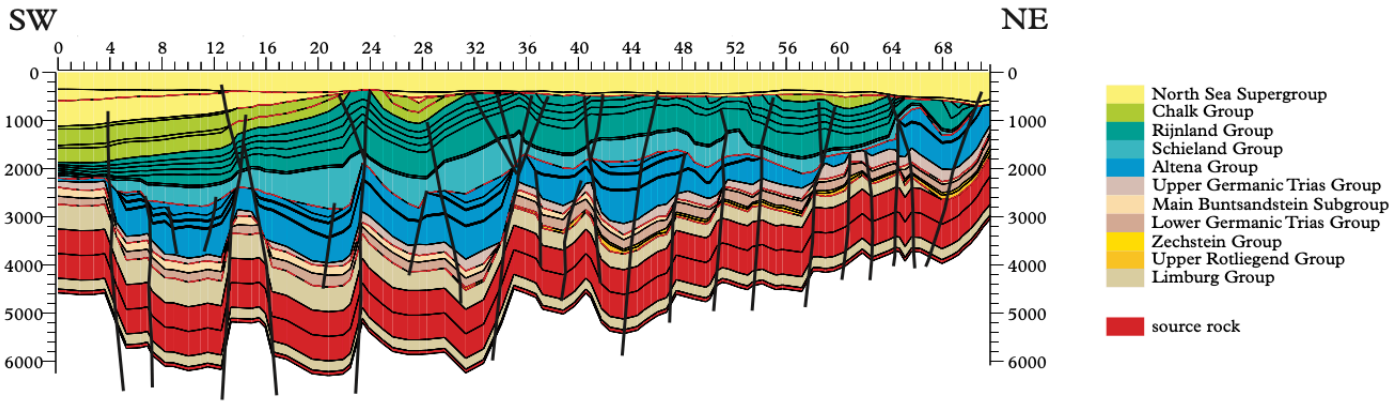

Figure 2.0.3: Stratigraphic cross-section of the West Netherlands Basin. The Delft Sandstone Member is part of the Schieland Group. Source rock in this figure indicates source rocks for hydrocarbons (van Balen et al., 2000).

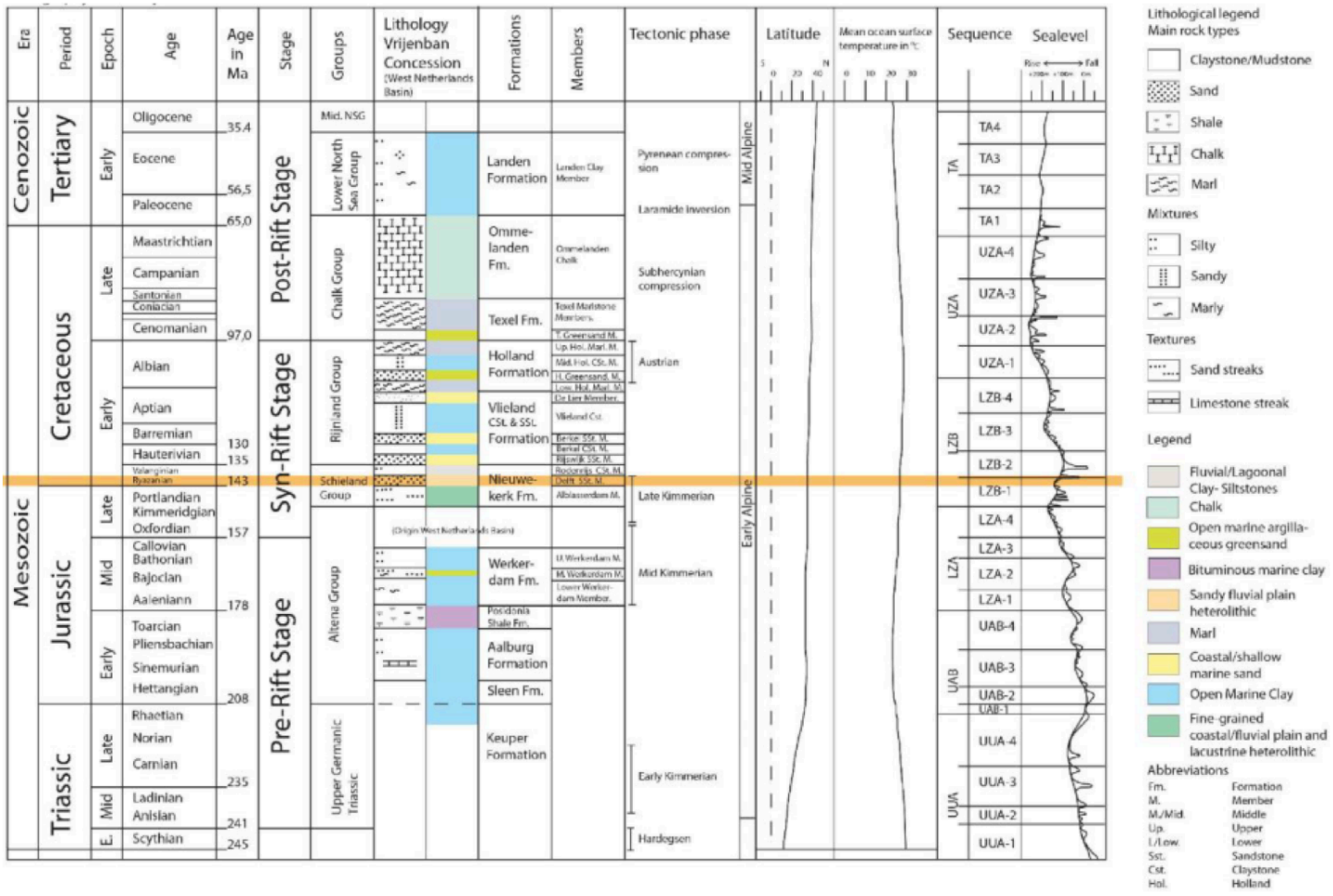

Figure 2.0.4: Regional stratigraphy of the Delft area. Lithology based on wells DEL-3, DEL-8, PNA-13, PNA-15 and RWK-1. The brown line indicates the stratigraphic position of DSSM (Donselaar et al., 2015)

2.1. Regional Stratigraphy of the Delft Area

During the syn-rift stage of the WNB a lithological group called the Schieland Group was deposited and the Nieuwerkerk formation is part of this group. As also visible from the stratigraphy in Figure 2.0.4, the Nieuwerkerk formation consists from base to top of the Alblasserdam Member, the DSSM and the Rodenrijs Claystone Member (Van Adrichem Boogaert and Kouwe, 1993).

2.1.1. Alblasserdam Member

The Alblasserdam Member is present throughout the entire WNB and overlies Middle Jurassic shallow-marine limestone and shelf mudstone of the Brabant and Werkendam formations (Vondrak et al., 2018). The member contains high sandstone/shale ratios which are deposited in braided fluviatile environments (Den Hartog Jager, 1996; DeVault and Jeremiah, 2002). The sandstones are typically fine to medium grained or coarse-grained and the geometries consists of sheets and isolated or stacked channels because of their fluvial origin (Donselaar et al., 2015; Van Adrichem Boogaert and Kouwe, 1993). The shale layers typically contain clay and siltstones. In the WNB thicknesses of the Alblasserdam member range from less than 100 to over 1300 m. From wells DEL-03 and PNA-13 it is found that the thicknesses are respectively 300 m and 500 m in the Delft area, however this goes paired with high uncertainty as neither of the wells directly penetrate the base of the member (Donselaar et al., 2015).

2.1.2. Delft Sandstone Member

On top of the Alblasserdam Member lies the Delft Sandstone Member, which is mainly present in the western and central parts of the WNB (Donselaar et al., 2015). The DSSM is layered and consists of fine to coarse gravelly sandstone sequences deposited by a north-west flowing meandering river and bands of silt- and claystones deposited as floodplains in a lower coastal plain setting (Donselaar et al., 2015; Gilding, 2010; Van Adrichem Boogaert and Kouwe, 1993). Detailed core- and cuttings and well logs analyses have been done from wells penetrating DSSM in the Delft area and these have shown that DSSM can be subdivided into three different depositional units. This subdivision is based on characteristics such as the sand/clay ratio, N/G ratio, varying thickness and the amount of present floodplain fines in a unit (Gilding, 2010). Table 2.1.1 summarizes the properties of each unit.

Table 2.1.1: Geological properties of the three units of the Delft Sandstone Member

Property	Unit 1	Unit 2	Unit 3
Thickness (m)	10 - 60	3 - 18	about 30
Porosity (%)	19	extremely low	30
Permeability (mD)	90 - 295	extremely low	725 - 1130

Unit 1, called the Lower Delft Sandstone Member unit, consists of loosely-stacked single-storey meandering river sandstone bodies interbedded with fine-grained floodplain clay- and siltstones (Donselaar et al., 2015; Gilding, 2010). The thickness varies between 10 and 60 m, the average porosity is approximately 19% and the permeability ranges from 90 mD at the base to 295 mD at the top (Donselaar et al., 2015). Unit 2, called the Middle Delft Sandstone Member unit, overall has a low sand content and contains interbedded clay- and siltstones with coal layers. Due to these fine grained sediments this unit has extremely low permeability and porosity (Donselaar et al., 2015). It has a thickness ranging from 3 to 18 meters, with an average of 8 m (Gilding, 2010). Unit 3, the Upper Delft Sandstone Member unit, has a thickness of about 30 m and consists of stacked, multi-storey and laterally-amalgamated meandering river sandstones which are coarse to large or even gravelly (Dinoloket, 2020; Donselaar et al., 2015; Gilding, 2010). These sandstones are interbedded with minor mudstone intervals. The unit has high lateral and vertical sandstone-to-sandstone connectivity, the average porosity is 30% and permeability varies between 725 and 1130 mD. These characteristics make unit 3 the most promising target for the production of geothermal energy and therefore the properties of unit 3 are used as input in the reservoir model. The large differences in thickness between the units are the result of differential subsidence caused by local fault movements. This differential subsidence also caused the spatial difference in amounts of deposited sand bodies in each unit. Figure 2.1.1 shows the different units and variations in thickness and sand bodies.

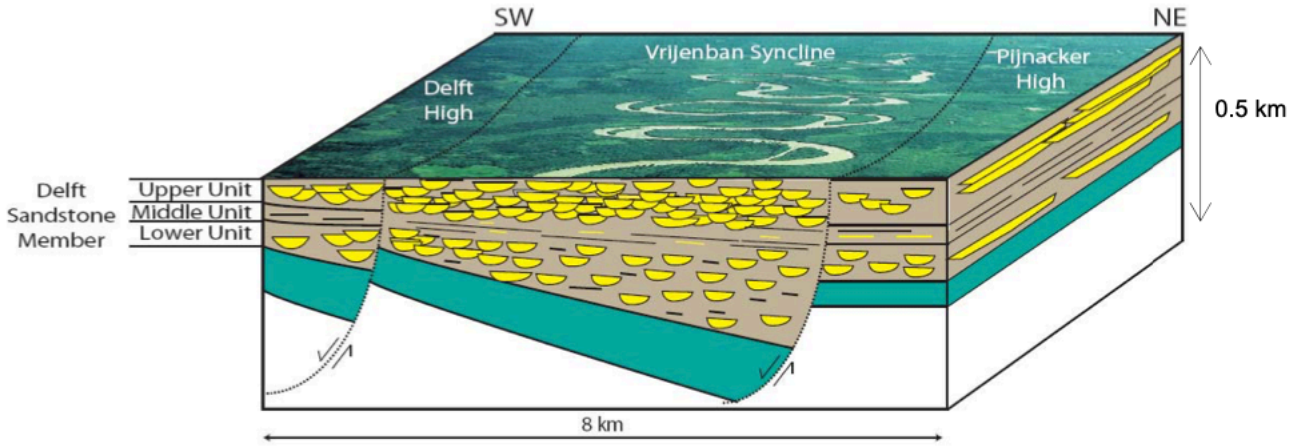

Figure 2.1.1: Depositional setting of the Delft Sandstone Member showing the three different units, divided based on the sand/clay ratio, N/G ratio, varying thickness and the amount of present floodplain fines in a unit (Gilding, 2010)

2.1.3. Rodenrijs Claystone Member

The DSSM is conformably overlain by the organic-rich claystone of the Rodenrijs Claystone Member, which is the youngest deposit of the Schieland Group (Van Adrichem Boogaert and Kouwe, 1993). This member consists of laminated grey lignitic clay-, silt- and sandstones with lignite and coal beds containing well-preserved plant fossils. It is found in all wells in the Delft area that are drilled beyond Cretaceous aged deposits and analyses of these well logs show thicknesses ranging from 30 to 100 meters (Gilding, 2010). The fine grained silt- and claystones are deposited in a low energetic area and the presence of horizontal organic bands indicate plant growth in the area at the time of deposition. This clay composition and the fact that no fluvial sand deposits or fossil contents were found indicate a floodplain to near coastal environment. The age of this member is found to be Late Valengian to Early Hauterivian, based on absence of sporomorphs which were present in the earlier deposits (Van Adrichem Boogaert and Kouwe, 1993). These times are known as periods with relative warm climates, which resulted in eustatic sea-level rises creating higher marine influences. Especially in the transition from fluvial to coastal environments this resulted in lagoonal environments. The Rijswijk Member, which is part of the Rijnland Group, overlies the Rodenrijs Claystone Member and is found to be a transgressive marine sandstone (Van Adrichem Boogaert and Kouwe, 1993). The interpretation of this Rijswijk member and the origins of the fluvial DSSM and near coastal Rodenrijs Claystone Member, indicate that Rodenrijs Claystone Member is a transitional lower coastal plain to lagoonal deposit between the fluvial and marine influences.

2.2. Structural Setting of the Delft Area

A part of the focus of this thesis is on the fault stability in the Delft area and therefore it is important to highlight the structural setting in this area based on the main present folds and faults. The deposits in the WNB have large thickness variations, which are the result of extensional and compressional faulting. Because of the present faults three main anticlinal and synclinal structures can be classified: the Delft High, the Pijnacker High and the Vrijenban Syncline which lies in between the two 'Highs' (Gilding, 2010). A simplified cross-section of this setting in the Delft area is shown in Figure 2.2.1. From this figure it is visible that Delft High and Pijnacker High both have a pop-up structure. Pop-up structures, also called flower-structures, are formed due to the inversion of the WNB during the compressional post-rifting phase and form trapping mechanisms for hydrocarbons (Den Hartog Jager, 1996). The highest part of the Vrijenban Syncline near the Delft High is found at 1900 m true vertical depth and the top of the DSSM is at 2200 m true vertical depth. The syncline is bounded by two main faults. The Delft main boundary fault (DA) in the southwest and the Pijnacker main boundary fault (PA) in the northwest.

2.2.1. The Pijnacker High

The Pijnacker High is located in the northeast of the Vrijenban syncline, has a length of 10 km and is at least 0.5 km wide at the top of DSSM (Gilding, 2010). The Pijnacker High consists of a pop-up structure and a horst structure, called the Pijnacker Horst. This pop-up structure is formed by the intersection of an inverted normal fault and a reverse fault. The Pijnacker pop-up contains hydrocarbons in the Rijswijk member. The Pijnacker main boundary fault (PA in Figure 2.2.1) is a 70° southwest dipping synsedimentary fault that divides the Vrijenban syncline and the Pijnacker Horst (Gilding, 2010). The downthrow of the syncline block resulted in a fault throw that varies laterally between 50 and 200 meters at the top of the DSSM. A throw of 80 m was found near the Pijnacker 13 well. Movement of the PA fault created thickness differences between the Schieland Group depositions in the Vrijenban syncline and the Pijnacker Horst. After deposition of the Schieland Group the movement of the syncline block along the PA fault continued, which reactivated and inversed the fault. Reversed normal fault PB1 was created during this inversion and on its own partly faults and throws the Schieland Group members on the southwestern side of the Pijnacker pop-up. Fault PB1 formed throws in the DSSM of up to 50 meters and research and earlier productions in the Pijnacker oilfield have demonstrated possible sealing capacity. Both the throw and the sealing capacity of the faults are very important parameters in the fault stability analysis as they affect the flow and pressure build up in the reservoir.

2.2.2. The Delft High

The Delft High is located in the southwest of the Vrijenban syncline. From seismics it is found that its length is approxamtely 10 km and has a width of 1 to 2 km at the top of the DSSM (Gilding, 2010). The Delft High pop-up structure is bounded by an inversed normal fault (DA1) and a reverse fault (DB2), which both fault the Schieland Group members. Fault DA1 is also a synsedimentary growth fault, similar to the PA fault, and resulted in throws varying laterally from 75 m in the southwest to 150 m in the northwest at the top of the Schieland Group (Gilding, 2010). Fault DB2 and several other faults were formed by the same processes as the formation of fault PB1 in the Pijnacker High and also in the Delft High seismic data show variations in thickness of the Schieland Group members which indicate synsedimentary growth. The Delft High contains the Delft oil field in the Rijswijk member. The Delft Sandstone Member is the most promising target for the production of geothermal energy, which is highlighted yellow in Figure 2.2.1. The reservoir model is based on a reservoir thickness of 105 m and therefore a throw is taken into account that varies between 0 and 75 m.

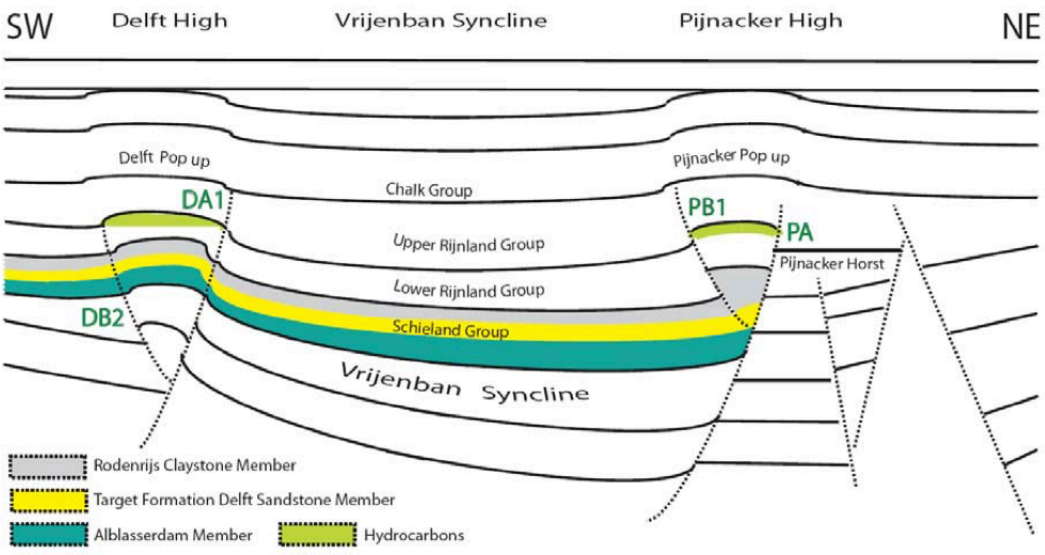

Figure 2.2.1: Symplified cross-section of the structural setting in the Delft area. The target DSSM indicated with yellow. (Gilding, 2010)

3

Reservoir Simulation

This chapter describes the governing equations of the used reservoir simulator in Section 3.1, followed by the input data and description of the varying parameters in Section 3.2.1.

3.1. Delft Advanced Research Terra Simulator (DARTS)

The Delft Advanced Research Terra Simulator (DARTS) is a Python and C++ based geothermal dynamic reservoir simulator, developed at the faculty of Civil Engineering of the Delft University of Technology. This simulator provides fast and accurate flow response of a geothermal field and with this predicts temperature and pressure distributions during geothermal productions (Wang et al., 2019, 2020). It is based on the framework of Operator-Based Linearization (OBL), which makes it fit for complex multiphase flow and transport applications (Khait and Voskov, 2018b).

For the simulation of geothermal reservoirs three fundamental conservation equations are used, which are the Conservation of Mass, Conservation of Energy and Darcy's law for fluid flow in porous media (O'Sullivan et al., 2000). The conservation of mass states that the mass of a system must remain constant over time for any closed system. Which means that a change in mass in an open system must be balanced. The conservation of mass equation with n_c components and n_p phases is given by equation 3.1 (Voskov, 2017). In which the three terms denote respectively the change in mass with time, the mass flux due to flow and a source term if any mass changes occur apart from the boundary.

$$\frac{\partial}{\partial t}\left(\phi \sum_{j=1}^{n_p} x_{cj}\rho_j s_j\right) - \nabla \cdot \sum_{j=1}^{n_p} x_{cj}\rho_j v_j \; + \sum_{j=1}^{n_p} x_{cj}\rho_j \tilde{q}_j = 0, \qquad c = 1, \ldots, n_c \tag{3.1}$$

With:

- ϕ = Porosity
- x_{cj} = The mole fraction of component c in phase j
- s_j = Phase saturations
- ρ_j = Phase molar density
- n_p = Number of phases
- n_c = Number of components
- $\tilde{q}_j$ = Phase rate per unit volume
- v_j = Phase velocity

The conservation of energy equation is very similar to the conservation of mass, given by equation 3.2 (Khait and Voskov, 2018b). Energy migrates through the subsurface via thermal conduction and convection. Thermal conduction is the transfer of kinetic and potential energy via collision and movement of particles within a rock body. The speed of this energy transfer depends on the thermal gradient and the thermal conductivity of the rock material. The principle of thermal conduction is shown by 3.2.

$$\frac{\partial}{\partial t}\left(\phi \sum_{j=1}^{n_p} \rho_j s_j U_j + (1-\phi)U_r\right) - \nabla \cdot \sum_{j=1}^{n_p} h_j \rho_j v_j \; + \nabla \cdot (\kappa \nabla T) + \sum_{j=1}^{n_p} x_{cj} h_j \rho_j \tilde{q}_j = 0 \tag{3.2}$$

With:

- U_j = Phase internal energy
- U_r = Rock internal energy
- h_j = Phase enthalpy
- κ = Thermal conductivity
- ∇T = Temperature gradient

Thermal convection is the transfer of heat by the movement of fluids and is controlled by Darcy's Law. This law describes the flow of fluid through porous media and is generally used to determine the velocity of a fluid, based on the rock permeability and the fluids pressure drop and viscosity. Darcy's law is given by equation 3.3 (Voskov, 2017).

$$v_j = -\left(K \frac{k_{rj}}{\mu_j}(\nabla p_j - g_j \nabla d)\right), \quad j = 1, \ldots, n_p \tag{3.3}$$

With:

- K = Permeability tensor
- k_{rj} = Relative permeability
- μ_j = Phase viscosity
- p_j = Vector of pressures in phase j
- g_j = Gravity term
- ∇d = Vector of depths

The three conservation equations are transformed into equations 3.4 and 3.5, which are the discretized formulations of flow and transport for general multi-component fluids and this makes them suitable for geothermal reservoir simulations (Khait and Voskov, 2018b; Voskov, 2017). These transformations are done by applying finite-volume discretization and backward Euler approximation in time.

$$V\left[\left(\phi \sum_{j=1}^{n_p} x_c j \rho_j s_j\right)^{n+1} - \left(\phi \sum_{j=1}^{n_p} x_c j \rho_j s_j\right)^{n}\right] - \Delta t \sum_{l}\left(\sum_{j=1}^{n_p} x_{cj}^{l} \rho_j^{l} \Gamma_j^{l} \Delta \psi^{l}\right) + \Delta t \sum_{j=1}^{n_p} \rho_p x_{cj} q_j = 0, \quad c = 1, \ldots, n_c \tag{3.4}$$

$$V\left[\left(\phi \sum_{j=1}^{n_p} \rho_j s_j U_j + (1-\phi)U_r\right)^{n+1} - \left(\phi \sum_{j=1}^{n_p} \rho_j s_j U_j + (1-\phi)U_r\right)^{n}\right] - \Delta t \sum_{l}\left(\sum_{j=1}^{n_p} h_j^{l} \rho_j^{l} \Gamma_j^{l} \Delta \psi^{l} + \Gamma_c^{l} \Delta T^{l}\right) + \Delta t \sum_{j=1}^{n_p} h_j \rho_j q_j = 0 \tag{3.5}$$

With:

- V = Control volume
- $q_j = \tilde{q}_j V$ = a source of phase j
- $\Delta\psi^l$ = Difference in pressures between blocks connected via interface l
- ΔT^l = Difference in temperature between blocks connected via interface l
- $\Gamma_j^l = \frac{\Gamma^l k_{rj}^l}{\mu_j^l}$ = Phase transmissibility
- Γ^l = Constant geometrical part of transmissibility
- $\Gamma_c^l = \Gamma^l \kappa = \phi\left(\sum_{j=1}^{n_p} s_j^l \gamma_j^l - \kappa_r\right) + \kappa_r$ = Thermal transmissibility

Both equations 3.4 and 3.5 are approximated in time using a Fully Implicit Method, which introduces non-linearity to the system (Voskov, 2017). Solving this non-linear system is normally done using a conventional linearization approach called the Newton-Raphson method (Khait and Voskov, 2018b). However, this system is based on complex combinations of non-linear properties and relations and therefore linearizing this with Newton-Rhapson may lead to various errors (Voskov, 2017). Linearization in DARTS is done using the Operator-Based Linearization approach (OBL) which is developed by Voskov (2017). OBL simplifies the complicated non-linear physics by parameterizising the different operators in physical space with a limited number of supporting points, making it able to represent the operators piece-wise (Khait and Voskov, 2018a,b; Wang et al., 2019). During simulations the operators are evaluated based on multi-linear interpolations, which reduces and improves the non-linear behaviour of the system. The successful application of OBL in thermal multi-component and multiphase flow simulations has been proven by multiple researches and publications such as Voskov (2017), Khait and Voskov (2018a,b) and Wang et al. (2019, 2020). Further discussion of the complex mathematics behind DARTS is outside the scope of this thesis.

3.2. Input Data

For the simulation of the reservoir a simplified 3D box-shaped model is developed based on the characteristics of the Delft Sandstone Member. A base case of the box-model is made based on homogeneous porosity and permeability (Figure 3.2.1). All simulations are run for 30 years with time steps of 365 days to have equal comparisons of the different test cases. The input data for the base case reservoir model include the parameters shown in Table 3.2.1, of which five of the parameters will be varied in value for the test scenario's. At the top and the bottom the reservoir is bounded by layers which act as infinitely large domains with a fixed temperature and which provide conductive thermal recharge to the reservoir (Daniilidis et al., 2020b).

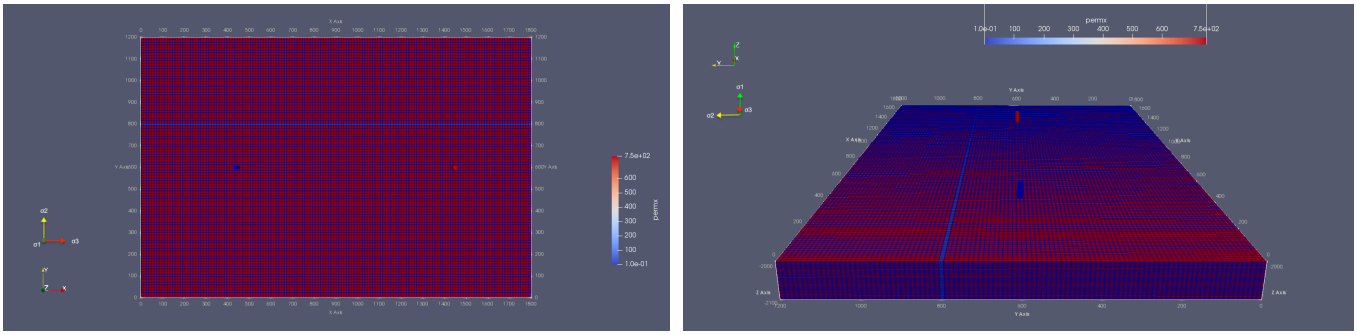

Figure 3.2.1: 3D box models of the reservoir simulator, with the injection well indicated blue and production well indicated red. Figure a shows the reservoir from the Z-angle. Figure b shows the reservoir from the X-angle.

The DSSM is overlain by the Rodenrijs Claystone member and therefore, the overburden permeability is based on values for argillaceous units. These units contain a substantial amount of fine-grained

components, predominantly shales and clays. Permeability research of these units has shown that values range between 10^{-7} to 10^{-1} mD (Neuzil, 1994). The presence of gas or water in the formations impacts these permeability values. In the presence of gas the permeability increases to values between 10^{-2} to 1 mD and in presence of water the values range between 10^{-5} to 10^{-3} mD (Mezger, 2014). The Delft study area contains hydrocarbon fields and geothermal production can be accompanied by gas co-production. To take into account both possible present fluids, therefore an overburden permeability of 10^{-3} mD is used in the modelling of the reservoir.

Table 3.2.1: Input data for the base case of the reservoir model

Parameter	Value	Unit
nx*ny*nz	150*100*42	-
dx*dy*dz	12*12*2.5	m
Location producer	444,600	m (X,Y)
Location injector	1440,600	m (X,Y)
Location fault	1800,636,105	m (X,Y,Z)
Fault permeability	750 perm	mD
Fault throw	0	m
Uniform reservoir and fault porosity	24	%
Uniform reservoir permeability	$7.4x10^{-9}$ (750)	m^2 (mD)
Overburden permeability	$9.9x10^{-15}$ (0.001)	m^2 (mD)
Top reservoir depth	2000	m
Model reservoir thickness	105	m
Fault-wells distance	192	m
Uniform initial pressure	20.1	MPa
Uniform initial temperature	345.75	K
Flowrate prod/inj	4200	m^3/day
Injection temperature	308.15	K
Simulation time	30*365	days
Thermal conductivity rock	100	kJ/m/day/K
Heat capacity rock	2200	kJ/m^3/K

3.2.1. Varying Parameters

To be able to find potential development strategies with respect to fault stability and profitability in a geothermal project, different test scenario's are simulated. These scenario's are formed by varying two types of parameters: reservoir conditions and operating options. Table 3.2.2 displays the values of the considered parameters.

Table 3.2.2: Varying parameters of the reservoir model

Parameter	Value	Unit
Flowrate	3600, 4200, 4800, 5400, 6000, 6600, 7200, 7800, 8400, 9000	m^3/day
Fault throw	0, 25, 75	m
Fault permeability	750, 75, 0.1	mD
Injection temperature	303.15, 308.15, 313.15	K
Fault-wells distance	12, 24, 36, 60, 96, 192, 300, 396	m

Reservoir Conditions

In terms of reservoir conditions the test cases are varied in values for:

- Fault permeability
- Fault throw
- Friction coefficient of the sandstone

The fault permeability determines if the fault is sealing or non-sealing. It is found that a sealing fault does not allow flow across the fault and therefore pressure build-up will occur next to the fault, which has effects on its stability (Daniilidis et al., 2016, 2020a). A non-sealing fault on the other hand is much more permeable and should allow flow, which should result in a larger reservoir volume accessible by the well and less pressure build up next to the fault.

An additional important parameter with respect to faults is the fault throw (Daniilidis et al., 2020a). Throw is the vertical component of separation between a hanging and a footwall of a fault. Especially in the case of non-sealing faults this throw is of importance as it may seal part of the fault from flow. The values for fault throws found in the Delft Sandstone are described in Chapter 2 and the test cases are based on these values.

The friction coefficient of sandstone and varying values are described in Chapter 4.

Operational Options
The varying operational options considered in this thesis are:

- Flowrate of the injector and producer (The flowrate of the two wells is always equal)
- Injection temperature of the water
- Distance between the wells and fault

The flowrate and injection temperature are both proven to have a positive influence on the thermal power output of the doublet (Daniilidis et al., 2016, 2020a; Saeid et al., 2015). The thermal output increases with increasing flowrates and with decreasing injection temperature and therefore also positively influences the NPV. Considering the doublet placing with respect to the fault, Daniilidis et al. (2020a) has shown that the sensitivity of the doublet positioning increases with increasing fault permeability. However, limited research has been done on how these three operational options influence the fault stability and how this impacts a development strategy.

3.2.2. Mesh Grid

The mesh grid size used in the simulations for this thesis are 150x100x42, which results to 630,000 grid cells. The choice for this mesh size is based on mesh grid sensitivity performed for the production temperature and pressure near the present fault, given in Figure 3.2.2. Increasing the 60x40x42 mesh to the 150x120x42 mesh, increases the temperature accuracy 33% and the pressure accuracy by 25%. However, this increase in mesh size also increases the simulation time from approximately 80 seconds to almost 1007 seconds. For larger mesh sizes it is visible that the accuracy of the results does not increase significantly, but the simulation time does. To exemplify, using the grid of 150x100x42 (yellow) instead of the 150x120x42 grid (green) saves about 319 sec in simulation time, which is an approximate decrease of 32% in time.

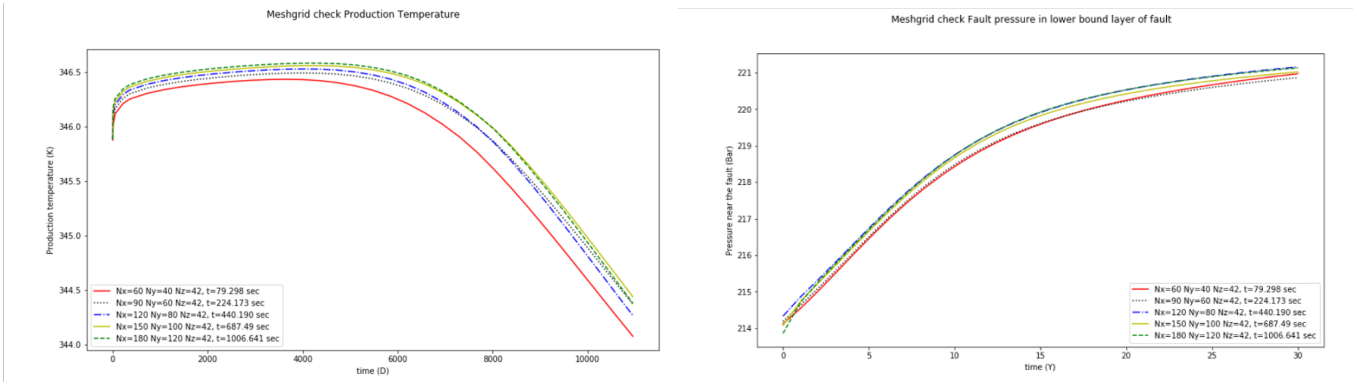

(a) Mesh grid check based on production temperature

(b) Mesh grid check based on pressure build up next to the fault

Figure 3.2.2: Mesh grid sensitivity checks based on the production temperature (a) and the pressure near the fault (b)

4

Development of the Fault Stability Model

This chapter describes the development of the fault stability model. An overview of the described input parameters is given in Section 4.3. Section 4.1 describes the mechanics of deformation with the focus on stress and pore pressure. This is followed by the description of Mohr circles used in the model in section 4.2.

4.1. Mechanisms of deformation

Mechanics deal with the effects of forces on bodies which as a result tend to change in shape, direction or placement (Burg, 2018). In the subsurface the most important forces are due to gravity and to relative motions of large rock masses in the earth's crust and mantle (Burg, 2018). Subsurface deformations are generally permanent and produce failure structures like folds and faults in rock layers. The deformation of rocks is influenced by different physical and chemical parameters, such as stress and pore pressure. Stress and pore pressure are the main parameters taken into account in the fault stability model.

4.1.1. Stress

Stress is a force what tends to deform a body and controls the deformation of a rock. A stress is divided into three components, of which one is directed perpendicular to the surface on which the stress is applied (the normal force) and two components are applied parallel to the surface (the shear forces) (Burg, 2018). All components act on a certain plane and in a certain direction and these specific orientations are given by means of the Cartesian coordinates system. The state of stress of a certain point in the subsurface is three-dimensional and is therefore defined by nine stress components which can be visualized by means of a cube, given in Figure 4.1.1.

The stress components are mathematically defined in the stress tensor matrix, which is given by 4.1 (Heidbach et al., 2016):

$$\sigma_{ij} = \begin{vmatrix} \sigma_{xx} & \sigma_{xy} & \sigma_{xz} \\ \sigma_{yx} & \sigma_{yy} & \sigma_{yz} \\ \sigma_{zx} & \sigma_{zy} & \sigma_{zz} \end{vmatrix} \tag{4.1}$$

With:

- i = The plane on which the component is acting
- j = The direction of the component
- $\sigma_{i=j}$ = Normal stress
- $\sigma_{i\neq j}$ = Shear stress

The shear stress components are interchangeable and equal when they act on mutually perpendicular planes and if the body does not rotate. In that case the shear stresses are given by $\sigma_{ij} = \sigma_{ji}$, by which three shear components can be neglected and the state of stress at a certain point is specified by six

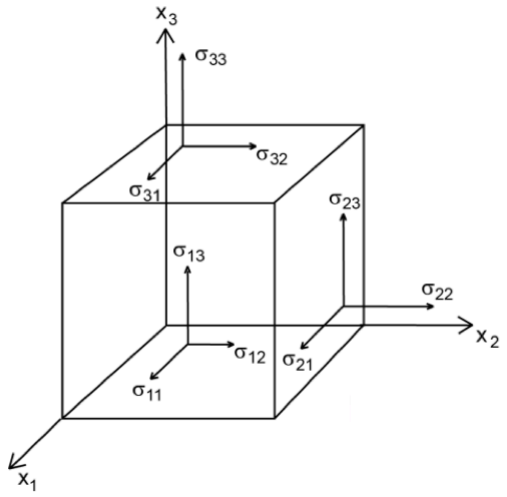

Figure 4.1.1: Components of stress at a cubic points given in Cartesian coordinates (Heidbach et al., 2016)

independent stress components.

At any point in the subsurface with a homogeneous stress field it is possible to find a rotated rock with its planes oriented parallel to the normal stress planes. As a result the shear stresses vanish and normal stress components form the principal axis coordinate system (Heidbach et al., 2016). In that case the normal stresses describe the stress state and they are called the principal stresses, denoted by σ_1, σ_2 and σ_3, which respectively are the maximum, intermediate and minimum principal stress. The orientations of the principal stresses in the rotated stress cube are given in Figure 4.1.2.

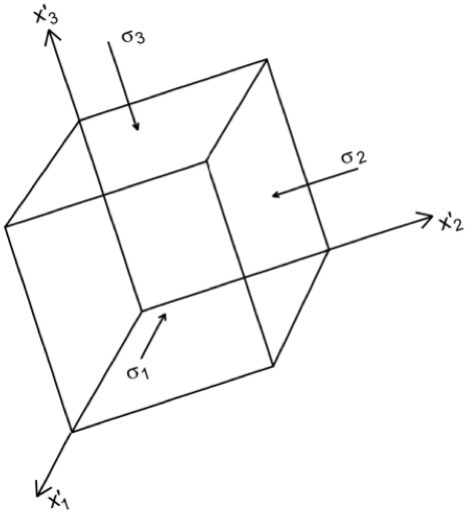

Figure 4.1.2: Principal stress orientations in rotated cubic point (Heidbach et al., 2016)

The principal stress magnitudes are key elements in determining the regional stress field at any depth (Kidambi and Kumar, 2016) and therefore it is helpful to consider them in terms of vertical stress (σ_v), minimum horizontal stress (σ_h) and maximum horizontal stress (σ_H) (Anderson, 1951). The vertical component of the stress field is due to the overburden weight and is determined by an integration of rock density with depth, given by equation 4.2 (Zoback et al., 2003).

$$\sigma_V = \int_0^z \rho(z) g dz \approx \bar{\rho} g z \tag{4.2}$$

With:

- $\rho(z)$ = Density as function of depth (kg/m^3)
- g = Gravitational acceleration (m/s^2)
- z = Depth (m)
- $\bar{\rho}$ = Mean overburden density (kg/m^3)

The vertical stress value is translated into horizontal stress values with the help of the Poisson's ratio (ν) and a gravity based model. This model is based on the assumption that overburden pressure is the only source of horizontal stress and that this horizontal stress increases in all directions due to the effect of Poisson's ratio (Mechelse, 2017). Poisson's ratio differs for each rock body and therefore the extent to which the horizontal stress increases depends on this value. The equation for this model is given by equation 4.3.

$$\sigma_h = \frac{\nu}{1-\nu}(\sigma_v - Pp) + Pp \tag{4.3}$$

With:

- ν = Poisson's ratio (-)
- Pp = Pore pressure (MPa)

The coupling of the principal stresses to σ_V, σ_H and σ_h is defined by Anderson, who used the vertical stress as a reference (Anderson, 1951). As a result, principal stresses occur in different configurations which coincide with three different tectonic stress regimes in the subsurface: the tensional regime, the strike-slip regime and the compressive regime. These regimes define how the rock will deform.

In a tensional stress regime deformation is driven by gravity and fault slip occurs when the minimum horizontal stress reaches a sufficiently low value depending on depth and pore pressure (Zoback et al., 2003). In this case vertical stress is the dominating stress and minimum horizontal stress is the minimum stress, resulting in deformation by means of normal faulting. With normal faulting the hanging wall moves downdip with respect to the foot wall, which is visible in Figure 4.1.3.

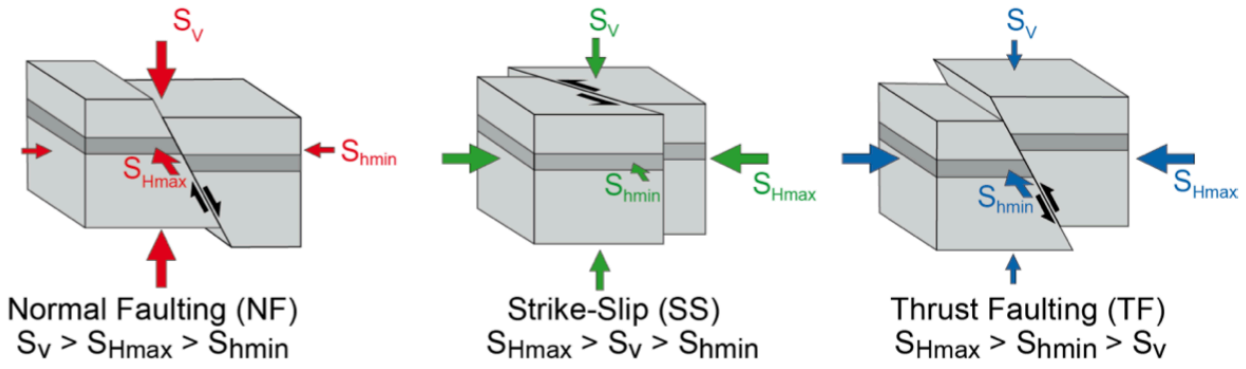

Figure 4.1.3: Overview of three different types of deformation (Heidbach et al., 2016)

The second stress regime is an intermediate stress state, in which strike-slip faulting occurs when the difference between the minimum and maximum horizontal stress is sufficiently large. In strike-slip faulting the hanging wall and footwall move along each other, as shown in Figure 4.1.3. Folding and thrust faulting occurs in a compressive regime, in which the hanging wall moves updip with respect to

the foot wall (thrust faulting) or folds. This results when both horizontal stresses exceed the vertical stress and the maximum horizontal stress is sufficiently large compared to the vertical stress. An overview of the three stress configurations and their coinciding regime and type of deformation are given in table 4.1.1.

Table 4.1.1: Overview of the three principal stress configurations and their coincided stress regime and type of deformation (Zoback et al., 2003)

σ_1	σ_2	σ_3	**Stress regime**	**Deformation type**
σ_V	σ_H	σ_h	Tensional	Normal faulting
σ_H	σ_V	σ_h	Strike-slip	Strike-slip faulting
σ_H	σ_h	σ_V	Compressive	Folding and thrust faulting

4.1.2. Pore Pressure

Another important factor in deformation is the influence of the pore pressure in the subsurface. The pore pressure is the pressure exerted by fluids present in cracks and pores of subsurface materials. When water is injected or an external load is applied, the pore pressure in the subsurface changes. Any increased pore water pressure significantly reduces the rock strength (Waltham, 2009), which causes deformation.

The total stress on a rock in the subsurface is built up of two forces: the pore water pressure and the force in the solid matrix (Fitts, 2013). The force of the solid matrix acts through the grains network of the rock and the pore pressure acts along the entire surface of the rock. Terzaghi found in 1925 that the force acting through the matrix is the effective stress, which can be determined as a function of the total stress and the pore pressure as given by equation 4.4.

$$\sigma_e = \sigma_t - P \tag{4.4}$$

With:

- σ_e = Effective stress (MPa)
- σ_t = Total stress (MPa)
- P = Pore water pressure (MPa)

It is found that failure occurs between the particles of the rock and with this it occurs in the rock matrix (Platteeuw, 2018). This means that resistance to failure is controlled by the effective stress and not by the total normal stress (Hillis, 2000). Local effective stresses result in a shear stress and an effective normal stress, which together drive slip along faults (Buijze et al., 2019b). As visible from equation 4.4, the pore pressure acts in opposition of the effective normal stress and this means that failure can be induced by the effect of pore pressure.

The stress state at faults is determined using the differential stress, the difference between the maximum and minimum principal stress (Buijze et al., 2019b). When the three principal stresses are equal the stress state is called isotropic. In these conditions fault slip is not likely to occur. When differential stress starts increasing, the stress state becomes anisotropic and the principal stress values are no longer equal to each other. In this anisotropic stress state, faults become critically stressed and seismic slip along faults becomes favorable (Buijze et al., 2019b). In most subsurface conditions the stress state is anisotropic.

The dominating stress state in the Netherlands is the tensional state, which generally promotes normal faulting.

4.2. Mohr Circles

Fault slip may occur when the failure strength of the fault is reached or exceeded. The slip tendency depends on the regional stress field (stress tensor), the orientation of the fault surface, its rock frictional characteristics (e.g. cohesive strength and friction coefficient) and the ratio between shear and normal stresses acting on the fault (Morris et al., 1996). The friction coefficient is often considered as the fault

strength in the analysis of induced seismicity mechanisms and is the value that may cause slip in case of a cohesionless surface (Morris et al., 1996). A practical way of visualizing the stress at certain locations is by the use of Mohr circles, which relates stress points to material planes (Burg, 2018). Mohr circles in combination with the Mohr-Coulomb failure criterion visualize clearly if slip and/or failure will occur at a certain point.

4.2.1. Basic Principles

A Mohr circle visualizes the magnitudes and orientations of shear stress as a function of the effective normal stress (Burg, 2018). With this a specific point on the Mohr circle represents the shear and effective normal stresses on a plane in a specific state of stress and orientation. In this thesis two-dimensional Mohr-circles are used to visualize the stress states near the fault as a result of production and reinjection of water.

A two dimensional Mohr circle is plotted with the help of the standard circle equation (eq. 4.5) in a coordinate axis with effective normal forces on the horizontal x-axis and shear forces on the vertical y-axis.

$$(x-h)^2 + (y-k)^2 = r^2 \tag{4.5}$$

With:

- (x, y) = Coordinate plane
- (h, k) = Circle centre
- r = Circle radius

The radius of the stress circle is defined by equation 4.6. This radius also denotes the maximum shear stress (τ_{max}), which is the maximum value the rock can handle before failure occurs (Platteeuw, 2018).

$$r = \frac{\sigma_1 - \sigma_3}{2} \tag{4.6}$$

A circle with its center given by equation 4.7 and a diameter of σ_1-σ_3 is constructed through points σ_1 and σ_3. In this circle the maximum principal stress σ_1 is at the right extremety of the circles and minimum principal stress σ_3 is at the left. The principal stresses hereby form the boundaries of the circle, showing the planes at which the shear stresses are zero. In between those boundaries the shear and normal forces have different orientations and magnitudes.

$$Center = \frac{\sigma_1 + \sigma_3}{2} \tag{4.7}$$

The fault stability model developed in this thesis is based on the 2D- circle equation, given by equation 4.5. Principal stress values σ_1 and σ_3 are based on regional stress values in the Netherlands and the pore pressure is found from the production data generated with DARTS. The input data used in the model are given in Section 4.3.

4.2.2. Mohr-Coulomb Failure Criterion

The slip tendency is based on the governing equation of fault reactivation, which is described by Amonton's law given by equation 4.8 (Moeck et al., 2009).

$$\tau_f = C + \mu(\sigma_{ft} - P) \tag{4.8}$$

With:

- τ_f = Shear strength of the rock (MPa)
- C = Cohesion of the rock (MPa)
- μ = Coefficient of internal friction (-)
- σ_{ft} = Total stress normal to the failure plane (MPa)
- P = Pore pressure (MPa)

- $\sigma_{ft} - P$ denotes the effective stress σ'_{ft}

This law states that stability or failure of a fault is determined by the ratio of shear to normal stresses acting on a surface and this also defines the slip tendency (Morris et al., 1996). Slip likely occurs when the resolved shear stress (τ) equals or exceeds the frictional sliding resistance, also called the failure shear stress (τ_f) (Jaeger and Cook, 1979). Hence the tendency for fault slip is given by equation 4.9.

$$\tau \geq \tau_f = C + \mu(\sigma'_{ft}) \tag{4.9}$$

In this the failure stress is proportional to the normal stress acting on the surface.

A commonly used way of modelling the shear strength of a rock is by the use of the Mohr-Coulomb failure criterion in combination with the Mohr circles. Equation 4.8 shows the slip tendency of a fault in a specific stress field and is therefore used as the failure criterion. This criterion shows the shear strength of the rock and in combination with the Mohr circle it shows the rock stability. Empirically, it holds that failure occurs if the Mohr circle touches or intersects the failure criterion. This is the point at which the shear stress exceeds or equals the failure shear stress of the fault.

As visible from equation 4.8, the slip tendency also depends on the pore pressure near the fault. This dependence is visualized in Figure 4.2.1. When pore pressure increases, due to for example injection of water, the rocks shear strength decreases. As a result the Mohr circle moves to the left, increasing the chance of failure (Circle 1 in Figure 4.2.1) (Hillis, 2000). However, when pore pressure decreases, because of water production, the shear strength increases and the Mohr circle moves to the right decreasing the chance of failure (Circle 2). Circle 3 shows a situation in which the the failure envelope is reached and failure occurs.

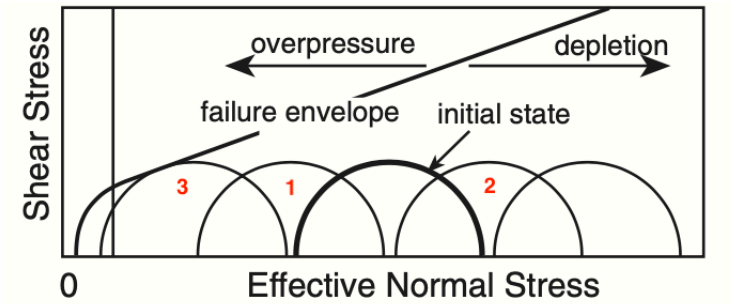

Figure 4.2.1: Mohr circle diagrams illustrating the effects of pore pressure. Increase of pore pressure shifts the circle left, decreasing shear strength and increasing chance of failure (Circle 1). Decrease in pore pressure, decreases the chance of failure and shifts the circle left (Circle 2). Failure occurs when the failure envelope is reached (Circle 3). (Hillis, 2000)

4.3. Model Input

Table 4.3.1: Input data for the fault model

Parameter	Value	Unit	Source
σ_1	45	MPa	-
σ_2	34	MPa	(Bakker, 2019)
σ_3	30	MPa	(Bakker, 2019)
Poisson's ratio	0.25	-	(Bakker, 2019)
Friction coefficient	Range	-	(Samuelson and Spiers, 2012; Takahashi et al., 2007)
Cohesion coefficient	0	MPa	(Taghipour et al., 2019)
Inital pore pressure	20.1	MPa	Assigned in DARTS

4.3.1. Local Stress Values

The local stress values in the fault stability model are based on the pore pressure values found within two y-layers within the production block (the side on which the wells are positioned) and two y-layers outside the production block. The stress values are found from the production data generated with DARTS. Four specific layers in the y-direction are of interest for the local pressure values, which each have a width of 12 m in the reservoir model. The layers of interest are the first and the second layers on either sides directly next to the fault, which together comprise an interval of 24 m on either sides of the fault. An illustration of how the local pressure values are extracted is given in Figure 4.3.1. The black line in the figure indicates the position of a fault and the red outline indicates one of the layers of interest within the production block. Each of the layers of interest consist of 6300 cells and these cells are analyzed individually on their pressure values for every year of production (Figure 4.3.2). For every year the maximum pressure value encountered in these 6300 cells is registered, which in the end gives an overview of the maximum pressures encountered in each layer of interest. This is done for all four layers next to the fault. The result is an overview of the maximum pressure values for the full production cycle and for each test case. The maximum of these maximum values is the input for the Mohr circles described in Section 4.2. During the simulations the location of all maximum pressure values are encountered within the black box in Figure 4.3.1, which comprises about 10% of the fault surface.

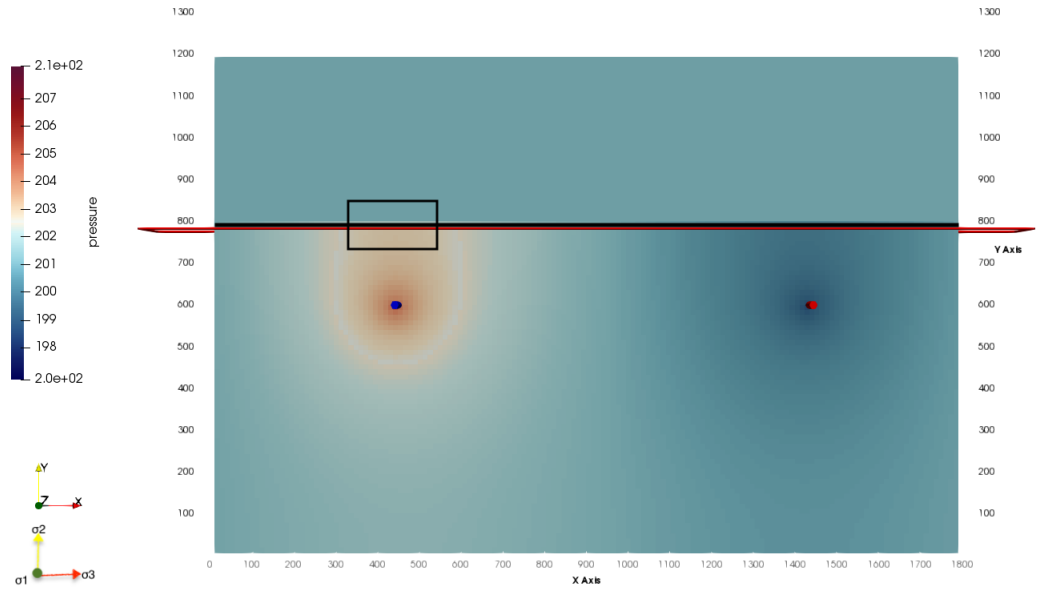

Figure 4.3.1: Figure showing the layers from which pore pressure values are extracted for local pressure values. The black line indicates a fault, the red line shows one of the four layers from which pore pressure values are extracted. The black box indicates the location of the pressure build up in all simulations.

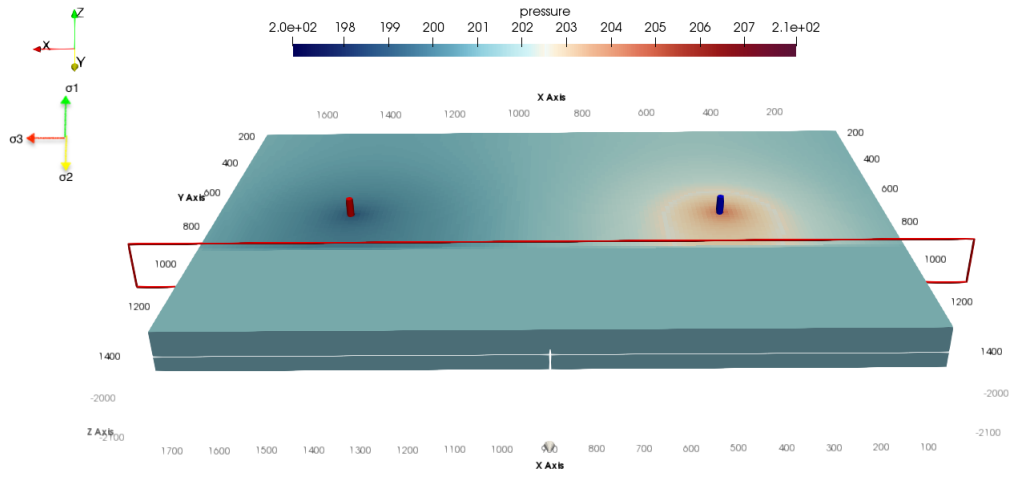

Figure 4.3.2: Figure showing the Y-angle of the layers from which pore pressure values are extracted for local pressure values. The red slice shows one of the four layers from which pore pressure values are extracted. This slice consists of 6300 cells which are all evaluated on their pore pressure.

4.3.2. Regional Stress Values

The vertical stress is the result of cumulative effect of body forces acting on the DSSM. Therefore the vertical stress value is calculated by integrating the bulk density over the depth of each lithological unit (equation 4.2). The thicknesses of the lithological units are based on data found in well GT2 in the Delft area and bulk densities are based on earlier research (Bakker, 2019; Mechelse, 2017; TNO, 2020). Horizontal stress values are derived from equation 4.3 and a Poisson's ratio of 0.25 (Bakker, 2019).

4.3.3. Friction and Cohesion Coefficient

Mineralogy compositions of sandstone differ widely and as a result the friction coefficients of different sandstones vary as well. Fluids such as water in the subsurface influence this friction coefficient, especially when clay minerals are present which lower the coefficient value (Samuelson and Spiers, 2012). Earlier research has shown that in the presence of brine the friction coefficient is 0.7 and 0.45 for a sandstone with a clay content of respectively 0% and 50% (Samuelson and Spiers, 2012; Takahashi et al., 2007). It is found that parts of the Delft sandstone contain about 50% of clay minerals (Bakker, 2019). Therefore, the fault stability model incorporates a range of values for friction coefficient to take into account this variability in possible values for the Delft sandstone. The values range between 0.4, to take into account the maximum clay content, to 0.7 in increasing steps of 0.1.

With respect to the cohesion coefficient, pre-existing faults are assumed in this thesis. The cohesion of a rock with pre-existing faults is therefore set to zero (Taghipour et al., 2019).

5

Development of an Economic Model under Dutch Fiscal Conditions

The costs of a geothermal project depends on multiple factors such as the costs of different phases of the project, geological uncertainties, government policies and heat demand in the surrounding area (Schoof et al., 2018). This chapter describes the development of the economic model and its inputs based on literature and earlier studies (Daniilidis et al., 2017; van Dongen, 2019a). An overview of the input parameters is given in Section 5.1. This is followed by the description of all the phases of a geothermal project and the associated costs in Section 5.2. The governing equations of the energy calculations are described in Section 5.3. Section 5.4 describes all expenditures associated with a geothermal project and 5.6 shows and describes the governing equations for the financial parameters used to assess profitability.

5.1. Model Input

The economic model is designed to evaluate the feasibility of geothermal projects in the Netherlands. The inputs of the model are all based on Dutch financial regulations and therefore only hold for Dutch geothermal projects. The inputs used in the model are given in Table 5.1.1.

Table 5.1.1: Inputs for the economic model

Parameter	Value	Unit	Sample frequency	Source
Production time	30	years	-	-
No. of doublets	1	-	-	-
No. of wells	2	-	-	-
Exploration costs	460,000	€	Once	van den Bosch et al. (2013)
ESP costs	800,000	Euro	Every 5 years	van 't Spijker and Ungemach (2016)
Power facility	1,500,000	€	Once	van den Bosch et al. (2013)
Drill location	300,000	€	Once	van den Bosch et al. (2013)
Unforeseen costs	5	% of construction costs	Once	van Dongen (2019a)
ESP downtime	15	days	Every 5 years	Daniilidis et al. (2017); van Dongen (2019a)
ESP efficiency	55	%	-	van 't Spijker and Ungemach (2016)
Electricity price	0.071	€/kWh	-	CBS (2019)
Gas price	0.016	€/kWh	-	-
Fixed OpEx	5	% of CapEx	Annually	de Boer et al. (2016); van Dongen (2019b)
Drill insurance	7	% of maximum compensation available	Once	Rijksdienst voor Ondernemend Nederland (2019a)
$/€conversion	0.90	-	-	-
AbEx single well	1,275,500	€	Once	Osundare et al. (2018)
Market value of equity	0.3	-	-	Rijksdienst voor Ondernemend Nederland (2019b)
Market value of debt	0.7	-	-	Rijksdienst voor Ondernemend Nederland (2019b)
Cost of equity	14.5	%	-	Rijksdienst voor Ondernemend Nederland (2019b)
Cost of debt	2	%	-	Rijksdienst voor Ondernemend Nederland (2019b)
Corporate tax	25	%	-	Rijksoverheid (2019)

5.2. Phases of a Geothermal Project and their Costs

A geothermal project is developed in multiple stages which all contribute to the total costs of the project. These stages are the research phase, exploratory phase, development and production phase and the abandonment phase. These phases all contribute to the total costs of a geothermal project, depending on multiple factors such as the costs of different phases of the project, geological uncertainties, government policies and heat demand in the surrounding area (Schoof et al., 2018). This section describes each phase of the project and its associated costs. The described costs are used as input data in the economic model, which is further discussed in Chapter 5.

5.2.1. Research Phase

An exploration permit and an environmental permit are required prior to starting the realization of a geothermal project (van den Bosch et al., 2013). The exploration permit is needed to receive exclusivity to research an area for geothermal potential. To receive this permit, multiple factors need to be analyzed which is done during the research phase (van den Bosch et al., 2013).

The research phase starts with a quick scan in which geological research is done into the regional and local geology and the subsurface of the area. With this geological data the potential of producing geother-

mal heat is determined, by means of the presence of aquifers, the potential for water flow, the depth, any neighboring fields and faults. This quick scan is based on interpolations and models generated with the available data of the area. With the results of the quick scan the operator makes a probability estimation of the exploitable potential of geothermal heat. If it turns out there is a probable potential to produce geothermal energy, the operator sets up an exploration plan. This plan describes in general what the geological situation is in the area, how the operator is planning to do the exploration and exploitation and where he is planning to locate the drill site. In addition this exploration plan must include an analysis of potential seismic risks resulting from the geothermal operations (SodM, 2016). The third key element needed for the permit request is the safety policy during the project, to ensure the health and safety of the surrounding area and employees. The last request element is evidence showing the operator is able to fulfill the project financially and technically.

With this package of information, the operator requests an exploration permit at the Dutch Ministry of Economic Affairs and Climate (EZK) and with advice from the Staatstoezicht op de Mijnen (SodM) they will grant permission for exploration (van den Bosch et al., 2013).

5.2.2. Exploratory Phase

When the exploration permit is granted, more detailed research of the geology is conducted, to generate a detailed subsurface model and minimize risks related to resource temperature, depth and productivity prior to drilling (Hanson, 2019). This research is based on data from existing wells, previous drillings and seismic surveys to model the subsurface. It is meant to give more detailed information about the layering, structure and thickness of the subsurface and make a preliminary estimation of the amount of heat that could be exploited (Daniilidis et al., 2017). In addition, the data should give insights in what possible risks could be encountered during drilling (van den Bosch et al., 2013). The research also includes surface studies to assess possible locations for a drilling site and to investigate the heat demand at the locations of the potential reservoirs, to generate a match between the heat demand and the potential heat supply (Schoof et al., 2018). All data from the geological study are used for the feasibility study, in which the economic potential of the project is evaluated.

Using the results of the geological study the operator sets up a drill design. This drill design takes into account possible drill locations, considers the most efficient way to arrange the equipment at the location and how the production facilities will be connected to the regional heat network. The well design is submitted to the Dutch regulator SodM that checks the design for compliance with the requirements and safety qualifications (Schoof et al., 2018). After completing the drill design an environmental permit is requested from the Ministry of Economic Affairs and Climate, which allows the drilling and installation of the drill site.

The research and the exploratory phase are the riskiest parts of the entire project as they are based on high geological uncertainties and risks. As a result, these higher levels of risks contribute to possible higher initial project costs. The costs associated to every part of these phases are given in Table 5.2.1.

Table 5.2.1: Costs of research and exploratory phase (van den Bosch et al., 2013)

	Minimum Costs (€)	**Maximum Costs (€)**
Quick Scan	10.000	20.000
Geological Research	25.000	250.000
Permit requests and required research	30.000	70.000
Drill design documentation and research	70.000	120.000

The total costs of the research and exploratory phase are between €135.000 to €460.000 euro. The economic model incorporates the most conservative costs to take into account the risks encountered during exploration.

5.2.3. Development, Realization and Exploitation

When the environmental permit is issued the realization phase of the geothermal project is started. This phase includes installation of the drilling site and required equipment and drilling of the doublet. These

different elements all contribute to the total investments costs of the project and are further discussed in the following sections.

Drilling Location
The drilling location is the place at the surface where the production facilities and buildings are placed. The costs of this drilling location depend highly on the goal of the geothermal project, the used drilling rig and on how the wells are drilled (deviated or not).

Earlier geothermal projects in the Netherlands have shown that total drilling location costs are between €150.000 and €300.000 euros (van den Bosch et al., 2013). This includes costs for the preparation, installation and drilling on the specific location. As mentioned, the exact amount depends on many different factors and therefore the most conservative amount of costs is taken into account in the economic model.

Doublet Drilling
A geothermal doublet consists of two wells, a production and an injection well. The costs of drilling these wells depend on the depth as is given in equation 5.1 (TNO, 2019) .

$$Wellcosts = 375000 + 1150 * depth + 0.3 * depth^2 \quad (5.1)$$

The costs are given in euro's and the output of the equation are the well and installation costs of a single well.

When drilling the first well in a new geothermal project, the prior knowledge and experience may be limited. Therefore, the first well is riskier compared to drilling additional wells due to unexpected difficulties during drilling and this could result in additional costs. A contingency factor of 110% is added to the model to take into account these additional costs (van Dongen, 2019a).

After the first well is drilled,it is tested to check if it is able to produce at desired rates. The well is also tested with an injection test to check if the water is reinjected easily into the subsurface. When the test gives a positive result a second well is drilled. In case of a negative result an alternative design is made to ensure better results and in addition available subsidies provided by the government can help to compensate in any costs to still be able to continue the project. In the worst case the project is abandoned.

The operator gains experience and knowledge from drilling and testing the first well, which results in a learning curve. This learning curve could result in more efficient production or drilling strategies and with this it has a positive influence on the well costs (Lukawski et al., 2014). Research has shown that with average industry learning rate, the 5th geothermal well drilled in a given field is likely to cost no more than 80% of the first well (Lukawski et al., 2014). According to this research the average learning curve for the second well is 0.925. This learning curve is included in the model for every new drilled well.

Equipment
Dutch geothermal projects consist of some standard necessary equipment. These include equipment for the circulation of water, filters and screens, an injection pump and an Electrical Submersible Pump (ESP) and a heat exchanger. The ESP is installed in the production well and lifts the water to the surface. The entire production process is regulated by a process computer, which conducts continuous measurements on the produced water.

Most geothermal production wells in the Netherlands are equipped with a Baker Hughes ESP (van 't Spijker and Ungemach, 2016). An ESP is built up of several different components and if properly designed, it should be able to achieve an efficiency of 55% in most configurations operating with rates between 100 and 300 m3/h (van 't Spijker and Ungemach, 2016). The lifetime of the ESP's in Dutch geothermal projects is researched by Baker Hughes and they estimate a lifetime of 5 years (van 't Spijker and Ungemach, 2016), after which it needs to be replaced. The investment costs of an ESP are based on purchases in the Paris Basin of France and are estimated to be between €180.000 and €300.000 euro for a pump with capacity between 250 and 500 kW (van 't Spijker and Ungemach, 2016). The costs increase with increasing required capacity. Due to limited availability of the ESP costs data, an estimation

is made for the costs for higher capacity pumps (van Dongen, 2019a). The estimated costs are given in Table 5.2.2.

Table 5.2.2: Estimated costs ESP (van Dongen, 2019a)

ESP capacity (kW)	Estimated costs (k€)
250-500	300
500-800	600
800-1000	800
1000-1200	1000
>1200	1200

The model incorporates €800,000 for the ESP costs (Daniilidis et al., 2017; van Dongen, 2019a).

The water circulation pump, injection pump, the screens and filters and the heat exchanger are located at the surface and are called the surface facilities. The costs for this surface facility range from €500.000 to €1.500.000 euro (van den Bosch et al., 2013). The most conservative amount is used in the model.

After installation of all equipment the operator needs an exploitation permit and an approved exploitation plan, after which he can start the production of geothermal energy. This project is estimated to go on for 30 years.

5.2.4. Abandonment

After the production lifetime the wells are abandoned. The abandonment consists of plugging and closing the wells and returning the production site to its original state. Abandonment happens mostly at the end of the production cycle but can also be done earlier if the wells do not deliver the required amount of heat to keep the project economically feasible (van Adrichem, et. al., 2014).

Abandonment costs of geothermal wells in the Netherlands are scarce, so the costs implemented in the model are based on values found in earlier European geothermal projects. This investigation focused on the guiding regulations in Germany, the Netherlands, Norway and the United Kingdom in designing the abandonment plan (Osundare et al., 2018). The authors mention a minimum abandonment and plugging cost of 1.275.500 dollar per well (Osundare et al., 2018). This is implemented into the model with a USD/EUR conversion factor of 0.90.

5.3. Energy Calculations

During the exploitation phase hot water is pumped from the subsurface and energy is extracted by a heat exchanger. However, running the pumps to produce this energy also requires energy. The governing equations used in the model to determine the amount of produced and required energy are discussed in the following subsections.

5.3.1. Produced Energy

The amount of produced energy is found in two steps. First the amount of power produced from the production well is determined. This is done using the flowrate, the temperature difference between the produced and injected water and the volumetric heat capacity. The equation is given by equation 5.2 (Doddema, 2012).

$$P_{doublet} = q * \Delta T * C_{fluid} \tag{5.2}$$

With:

- $P_{doublet}$ = Thermal power produced by the well (W)
- q = Flow rate (m^3/s)
- ΔT = Temperature difference between the produced and injected water (K)

- C_{brine} = Volumetric heat capacity of the fluid (J/m^{3}K)

The volumetric heat capacity is determined from the specific heat capacity and the density of the fluid, which in this case is water (Doddema, 2012). The properties are computed using the IAPWS97 thermodynamics module in Python (Romera, 2020) and the temperature and pressure data generated with DARTS.

$$C_{fluid} = C_{fluid} * \rho_b \tag{5.3}$$

With:

- C_P = Specific heat capacity at constant pressure (J/kgK)
- ρ_b = Density fluid (kg/m^3)

The second step is the conversion of produced thermal power into produced amount of energy. The produced energy at timestep i is the thermal power produced at timestep i, multiplied by the time difference between the current and the previous timestep. The energy calculation is given by equation 5.4.

$$E = P_{well} * \Delta t \tag{5.4}$$

With:

- E = Produced Energy (Wh)
- P_{well} = Thermal power of the well (W)
- Δt = Time difference between t_i and t_{i-1} (hr)

5.3.2. Required Energy

Multiple facilities are used for the production of geothermal energy, which include the injector pump and an ESP. Both these facilities require power to run and this required power is determined as the product of the flowrate and the pressure difference between the ESP and injector pump. The equation is given by equation 5.5 (van 't Spijker and Ungemach, 2016).

$$P_{pump} = \frac{q * \Delta P}{\eta} \tag{5.5}$$

With:

- P_{pump} = Power required by the pump (W)
- q = Flow rate (m^3/s)
- ΔP = Pressure difference between ESP and injector (Pa)
- η = Pump efficiency (55%, (van 't Spijker and Ungemach, 2016))

The energy required for production is determined from the power by integrating it over time.

5.4. Project Expenditures

An important part of the exploration phase is the determination of the project economics. An operator and also the permit guarantees need insights in the profitability and total costs of the project. The following subsections give a description of the expenditures accompanied with a production project.

5.4.1. Capital Expenditures

The capital expenditures, abbreviated by CapEx are the total investment costs of the project. The CapEx consists of the exploration, construction and unforeseen construction costs.

Construction costs consist of all costs associated to preparation, drilling and installation of the equipment and drill site. This includes the doublet drilling, the pumps, the heat exchanger and the screens and filters. The costs of the components are discussed in Section 5.2.3. The total exploration costs are

discussed in Section 5.2.2.

During drilling and installation any unexpected difficulties or problems may occur, and this contributes to extra costs. This is due to for example geological uncercainties, poor initial project design, corrosion, filter clogging or required skin removal. These additional costs are taken into account as unforeseen costs and are calculated as 5% of the construction costs (van Dongen, 2019a).

5.4.2. Operational Expenditures

Operational Expenditures, Abbreviated by OpEx , are all costs made during production. The total OpEx consists of the variable and the fixed OpEx. The variable OpEx are the costs that fluctuate over time, depending on the power required for production and the electricity prices. Fixed OpEx are the costs that remain unchanged during the entire production process.

Variable OpEx

The variable OpEx depend on the amount of energy required by the ESP and injection pump and the market price of electricity. The current electricity price for industry users is 0.071 euro/kWh (CBS, 2019). The future electricity price, however, is very volatile as it is influenced by many factors, such as the gas prices, fluctuations in energy demand and by national and international energy policies and events (Schoots and Hammingh, 2019). Therefore predictions of the future electricity prices are made by Planbureau voor de Leefomgeving (PBL) in cooperation with other Dutch research institutes and these are set up in a document called The Klimaat- en Energieverkenning (KEV) 2019 (Schoots and Hammingh, 2019). The document gives an overview of the current status of the Dutch energy management and forecasts of the energy system, their prices and CO_2 emissions. The document acts until 2030 as the base scenario for future analyses for emissions and the energy system (Schoots and Hammingh, 2019). Electricity prices are very volatile and therefore the predictions made in the KEV are highly uncertain. To take into account this uncertainty they implemented an uncertainty bandwidth, which shows the range in which the prices can vary over time. The forecasted electricity prices and their bandwidth are given in Figure 5.4.1.

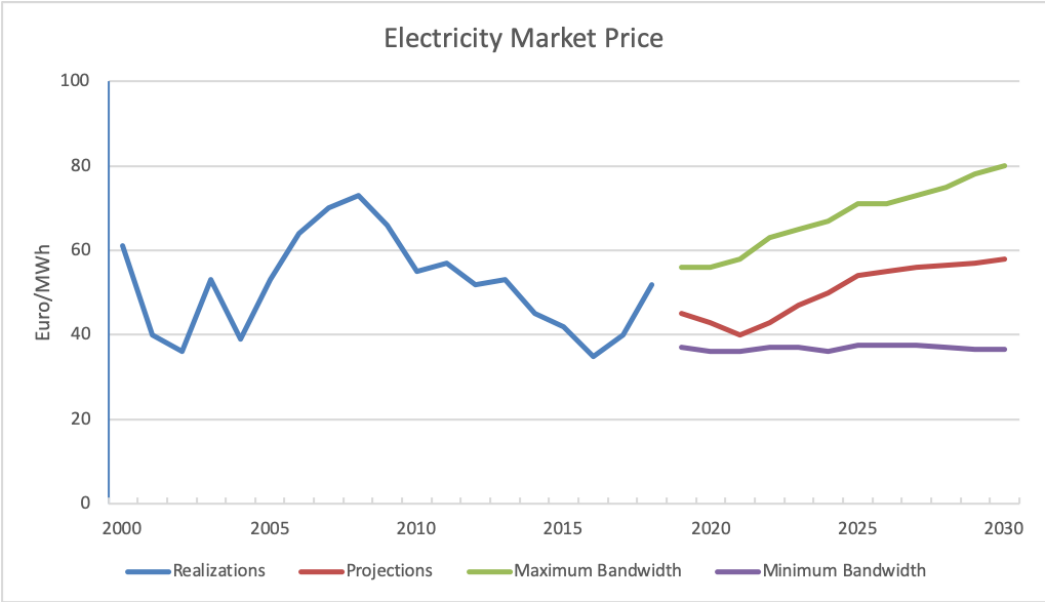

Figure 5.4.1: Forecasted Dutch electricity prices (Schoots and Hammingh, 2019)

The prices given in Figure 5.4.1 are the base electricity prices, without the addition of taxes. The tax for the use of electricity in industry is 0.01421 euro/kWh (Belastingdienst, 2019). In the model this is added to the base electricity price.

Fixed OpEx

As mentioned, fixed OpEx are the annual costs that do not change over time. In general, fixed OpEx include the maintenance and workover costs, rent of facilities, staff payment and insurance costs.

Workovers and Maintenance

Workovers and maintenance are done regularly throughout the production process. During workovers and maintenance operations the facilities are inspected and cleaned annually. The total annual costs for workovers and maintenance are estimated at 5% of the project's CapEx, which are build up by two elements. Annual costs for inspection, maintenance, workovers and costs for staffing are determined as 4% of the project's CapEx. This percentage is found by Energieonderzoek Centrum Nederland (ECN) and is based on data from Dutch geothermal projects (de Boer et al., 2016). Heat network maintenance is not included in this 4%. In practice it turns out that the pipelines for the heat network hardly require any maintenance once they are installed. From existing projects in the Netherlands, it is found that maintenance costs for the heat network are 1% of the project's capex (van Dongen, 2019b). Which makes a total of about 5% for the calculation of the fixed OpEx. The income not generated during maintenance and workovers are added to the fixed OpEx to take into account the effects of the downtime (Daniilidis et al., 2017).

Insurance

The production of geothermal energy is associated with a lot of risks and one of them is the geological uncertainty. After drilling the production well the operator can encounter a lower than expected temperature or production volume of the water. In that case the aquifer does not have the capacity as initially expected and this results in a lower than expected heat production.

For many investors this so called 'miss drilling' risk formed a barrier for making investments into geothermal energy (Rijksdienst voor Ondernemend Nederland, 2019a). As a solution the Ministry of Economic Affairs and Climate set up the 'Risico's dekken voor aardwarmte' program, abbreviated by RNES Aardwarmte (Rijksdienst voor Ondernemend Nederland, 2019a). This is an insurance that compensates part of the drilling expenses in case the expected P90 production of heat is not met. The P90 production is the amount of heat that is expected to be produced with 90% probability. The insurance is bound to strict regulations and only compensates for the geological risks associated to the aquifer parameters, such as the temperature or the volume of water that could be produced from it. The risks of possible induced seismicity or any coproduction of oil or gas are not part of the insurance (Rijksdienst voor Ondernemend Nederland, 2019a).

The maximum amount of compensation depends on the drilled depths. The different amounts are given in Table 5.4.1.

Table 5.4.1: Overview of maximum amount of insurance per geothermal project (Rijksdienst voor Ondernemend Nederland, 2019a)

Project	Depth (m)	Maximum compensation (€)
Regular	2000-3500	11.050.000
Deep	> 3500	18.700.000

These compensations are financed by the Ministry of Economic Affairs, the program Kas als Energiebron and by the issuers themselves, who pay a premium to the government to get this insurance. This premium accounts for 7% of the maximum compensation available (Table 5.4.1) for the project (Rijksdienst voor Ondernemend Nederland, 2019a). Since the Delft Sandstone is located at a depth of about 2000 m, the premium is included once in the model based on 7% of the maximum compensation for a regular geothermal project.

5.4.3. Abandonment Expenditures

The Abandonment Expenditures (AbEx) consist of the costs for abandonment and plugging of wells, mentioned in Section 5.2.4.

5.5. Project Revenues

The project's revenues include the income generated by the delivered heat and from the Sustainable Duurzame Energyproductie (SDE+) subsidy.

5.5.1. Production Revenues

In the Netherlands the heat price is determined as 90% of the Dutch market price of gas (TTF) (Ministerie van Economische Zaken en Klimaat, 2019). This TTF price is based on the High Heating Value (HHV) of gas. The ratio between the HHV and Low Heating Value (LHV) of gas is 90%, which makes the heat price essentially the same as the costs for LHV gas. The current market price of gas is 0.016 euro/kWh.

The KEV 2019 made forecasts for the future gas prices until 2030. And similar to the electricity prices the gas prices are highly volatile as well. Due to the volatility the forecasted gas prices are also incorporated with a bandwidth, showing the range in which the price can vary. This bandwidth is based on scenario's made by CPB and PBL (Schoots and Hammingh, 2019). The forecasted gas prices are given in Figure 5.5.1.

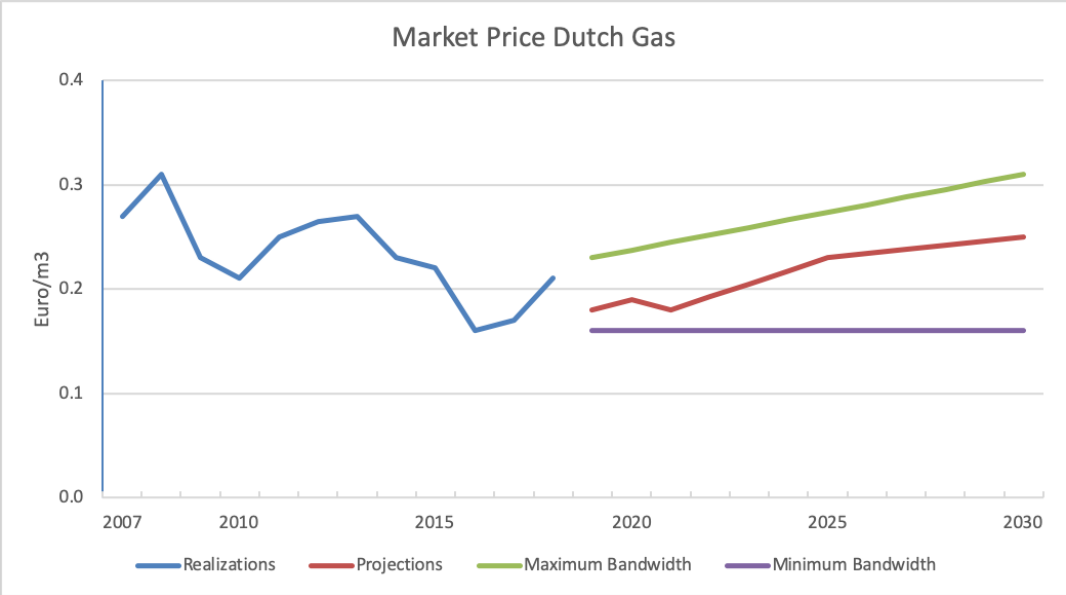

Figure 5.5.1: Forecasted market prices of Dutch gas (Schoots and Hammingh, 2019)

.

5.5.2. SDE+ Subsidy

The production of sustainable energy is not always profitable, because the production costs are generally higher compared to producing energy from fossil fuels. As a solution, producers of geothermal energy are allowed to request an SDE+ subsidy. This subsidy provides financial compensation for the costs for the production of sustainable energy (Rijksdienst voor Ondernemend Nederland, 2019b). The maximum subsidy period is 15 years and the amount of compensation depends on the project itself.

The subsidy is buildup of the base amount of the energy and the correction amount (Rijksdienst voor Ondernemend Nederland, 2019b). The base amount is the production cost of the thermal energy and is fixed over the entire duration of the subsidy. The correction amount is the market price of the thermal energy and is revised every year, based on the market price development (Rijksdienst voor Ondernemend Nederland, 2019b). This correction amount is determined the same way as the market price, which is 90% of the TTF price (Ministerie van Economische Zaken en Klimaat, 2019). The maximum amount of subsidy is determined as given in equation 5.6.

$$SDE+ = Baseamount - Correctionamount \tag{5.6}$$

This makes the amount of SDE+ contribution dependent on the heat price. When the heat price is higher than expected in the SDE+ regulations, the operator receives less SDE+ subsidy but on the contrary earns more from the produced heat. When the heat price is lower than expected, the operator earns less from selling the heat, but receives more SDE+ subsidy. The SDE+ regulations take into account a minimum market price, which is called the base energy rate. This base energy rate is the minimum amount of the correction sum and results in a maximum amount of subsidy if the market price is equal to the base energy price (Rijksdienst voor Ondernemend Nederland, 2019b).

The subsidy is available for four different categories (Rijksdienst voor Ondernemend Nederland, 2019b):

- Geothermal energy from a depth of minimum 500 meters
- Geothermal energy from a depth of minimum 4000 meters
- Geothermal energy from a depth of minimum 500 meters, in which one or two abandoned oil or gas wells are used in the doublet
- Geothermal energy from a depth of minimum 500 meters, in which the production installation is expanded with at least one extra well

Table 5.5.1 gives the prices on which the subsidy is based for every kind of project in 2019.

Table 5.5.1: SDE+ 2019 prices (Rijksdienst voor Ondernemend Nederland, 2019b)

Geothermal Project 2019	**>500 m**	**>500 m, use of oil/gas well**	**>500 m, extra well**	**>4000 m**
Base Amount (€/kWh)	0.052	0.052	0.032	0.067
Base Energy Rate (€/kWh)	0.013	0.013	0.013	0.013
Correction Amount (€/kWh)	0.019	0.019	0.019	0.019
Full capacity hours per year	6000	6000	6000	7000
Maximum subsidy duration (years)	15	15	15	15

At the start of each production year an estimation is made for the total heat production and the gas market price. Based on these two estimated parameters the amount of subsidy is determined and is paid to the producer at the beginning of the year. In this it should be noted that not the entire amount of production is subsidized. Depending on the type of geothermal production a maximum of 6000 to 7000 full capacity production hours are subsidized over a maximum period of 15 years (Rijksdienst voor Ondernemend Nederland, 2019b). At the end of each production year the production and energy prices are evaluated and any potential differences are compensated or paid back by the operator.

The model takes into account the 'regular' geothermal projects at depths between 500 and 4000 meters. The subsidy payouts in the model are based on equation 5.6, the prices given in Table 5.5.1 and the amount of full capacity hours per year and are implemented on a yearly base for 15 years.

5.6. Financial Parameters

Combining the projects revenues and costs give the cashflows generated during the project. However, these cashflows give minimum details on the financial performance of the project. Therefore, different financial evaluation methods are used to evaluate this performance.

5.6.1. Weighted Average Cost of Capital

Before starting any project, most initiative takers try to get investors for their project, which can invest in a project by means of equity or debt. The Weighted Average Cost of Capital (WACC) is a weighted average of the costs of a company's capital and debt. Lenders and equity holders expect to receive a certain return on the capital or funds they provided and this expected return is given by the WACC. With this, the company can determine how much interest they owe for every euro financed. It gives the average cost of finance of the business. The WACC is also seen as the minimum required return of a company, which gives the minimum amount of profit in order to achieve a return on the investment. This is especially helpful in the comparison of other projects in the same risk category.

In the Netherlands, projects that may be subsidized with the SDE+ regulation are financed in a 70/30 debt over equity ratio. For geothermal projects the cost of debt is set at 2% and the cost of equity is 14.5% (van der Welle and Lensing, 2018). These percentages depend on the risk profile of the project category and whether it is applicable for the 'groenfinanciering'. For geothermal projects the cost of equity is set at the highest percentage as they are generally accompanied with high risk (van der Welle and Lensing, 2018). The WACC is calculated using equation 5.7.

$$WACC = \frac{E}{V} * Re + \frac{D}{V} * Rd * (1 - Tc) \tag{5.7}$$

With:

- Re = Cost of equity
- Rd = Cost of debt
- E = Market value of equity (0.3)
- D = Market value of debt (0.7)
- V = Total market value of the project's financing (E+D)
- Tc = Corporate tax rate

The corporate tax is a direct tax imposed on the income or capital of companies. In the Netherlands, this tax is 25% for companies or projects exceeding an annual profit of 200.000 euros (Rijksoverheid, 2019). With the use of equation 5.7, the value of the WACC for geothermal projects is 5.4%.

5.6.2. Discounted Cashflow and Net Present Value

To make a valuable analysis of cashflows generated in the future, it is required to discount them to their present value (PV) . The PV is today's value of the amount of money paid or received in the future. The value of money changes constantly and therefore it is most relevant to know present values of cashflows to get a clear perspective with respect to for example other projects. This present value is determined by discounting the future cashflows with a discount rate and the elapsed time since the start of production. This is also called the discounted cashflow (DCF) and is given by equation 5.8.

$$DCF = \frac{C_t}{(1 + r)^t} \tag{5.8}$$

With:

- C_t = Cashflow generated at time t (Euro)
- r = Monthly discount rate [-]
- t = Elapsed time since project start (30 days assumed in this thesis)

From the DCF the net present value (NPV) can be determined, which is the sum of the discounted cashflows minus the investment costs. The NPV calculation is given in equation 5.9.

$$NPV = \Sigma \frac{C_t}{(1 + r)^t} - C_0 \tag{5.9}$$

In general, it holds that an investment is profitable if the NPV is positive. If the NPV is zero, no profit or losses are made and negative NPV will result in loss of money. With this the general rule of the NPV holds that only investments with a positive NPV should be considered as a worthwhile investment.

Any rate can be used for the discount rate, but it is very useful to set the WACC as the discount rate. As mentioned earlier, the WACC gives the average cost of finance of the business and therefore the costs of finance are automatically incorporated into the NPV when discounting with the WACC. As a result, if the NPV is positive it means that the stake- and shareholders are being repaid and the project generates profit. If the NPV is zero, it means that the stake-and shareholders are being repaid, but no profit is generated. A company can also decide to use a discount rate higher than the WACC. In that case the goal of the project is set higher and more heat needs to be produced. But as a result, it means that in

the case of zero NPV, the stakeholders are being repaid and the project earns profit. In this it should be noted that the WACC is initially on yearly basis and the DCF and NPV calculations are done on monthly basis. Therefore the WACC is converted to its monthly rate in order to use it as the discount rate in the model.

5.6.3. Levelized Cost of Heat

Another useful index to research the economic performance of a geothermal project is the use of levelized cost of heat (LCOH). This is a measure of the present value of the costs made to produce one kWh of energy at a specific time. The LCOH helps to make a qualitative comparison between different energy sources, like oil, gas or other renewable energy sources. The LCOH is determined using equation 5.10.

$$LCOH = \frac{\Sigma \frac{Capex_t + Opex_t}{(1+r)^t}}{\Sigma \frac{Heat_t}{(1+r)^t}} \tag{5.10}$$

With:

- $Capex_t$ = Capital expenditures at time t (Euro)
- $Opex_t$ = Operational expenditures at time t (Euro)
- $Heat_t$ = Produced heat at time t (kWh)

5.6.4. Profitability Index

The profitability index is the ratio between the discounted cashflows and the initial investment and is determined using equation 5.11.

$$PI = \frac{\frac{C_t}{(1+t)^t}}{C_0} \tag{5.11}$$

In general it holds that a profitability index greater than one indicates a profitable project. Any value lower than one indicates that the present value of future cashflows is less compared to the initial investment. With this, the financial attractiveness of an investment increases with increasing profitability index. It should be noted that the profitability index does not take into account the size of the project. As a result, the PI is only a reliable comparison method when comparing the same kind of investments. So, investments with the similar size and similar amount of initial investment costs.

6

Individual Parameter Influences on Profitability and Fault Stability

This chapter shows and describes the individual influences of the considered reservoir conditions and operational options on the profitability and fault stability of the homogeneous Delft Sandstone reservoir. The parameters are simulated over 30 years of production with the base case values for the reservoir which are listed in Table 3.2.1 in Chapter 3. All parameter values are kept constant at base case values unless indicated different or in case a specific parameter is being highlighted. With respect to the varying parameters the base case values are as follows:

- Flowrate: 4200 m^3/day
- Injection temperature: 308.15 K
- Distance between the wells and the fault: 192 m
- Fault permeability: 750 mD
- Fault throw: 0 m
- Friction coefficient of the sandstone: 0.5

The chapter is divided in sections describing the results for fault stability and profitability separately. Each section is subdivided into the two parameter categories and discusses the results for each varying input.

6.1. Individual Results for the Fault Stability

This section shows how fault slip and reactivation are influenced by the considered reservoir conditions and operational options.

6.1.1. Reservoir Conditions

Fault Permeability

Figure 6.1.1 shows the influence of the fault permeability on the fault stability. Narrowing the results down to the build up next to the fault in the layers within the production block (solid line) and outside of the production block (dashed line) we see multiple different influences. With respect to the pressure build up within the production block it is clear that pressure builds up more rapidly in presence of a sealing fault. The maximum pressure encountered in case of a sealing fault is 20.24 MPa after 30 years, while this is 20.19 MPa and 20.18 MPa for permeabilities of 75 mD and 750 mD respectively. In presence of a sealing fault (figure a) the pressure in the layers outside the production block remains stable at reservoir pressure, meaning that injection of water does not influence layers on the block across a sealing fault. This results from the fact that a sealing fault forms a barrier to flow and therefore injected water is not able to move across the fault. Pressure accumulation happens near the fault on the side within the production block and therefore fault slip is not likely to occur due to pressure build up in the layers

outside the production block. However, from Figures 6.1.1b and 6.1.1c we see that in the presence of more permeable faults the pressure values inside and outside the production block tend to converge. This means that pressure build up in the layers outside the production block becomes similar to that of the layers within the production block as fault permeability increases. This makes the investigation into the layers outside the production block less meaningful and therefore the fault stability research will only focus on the influence of the layers within the production block.

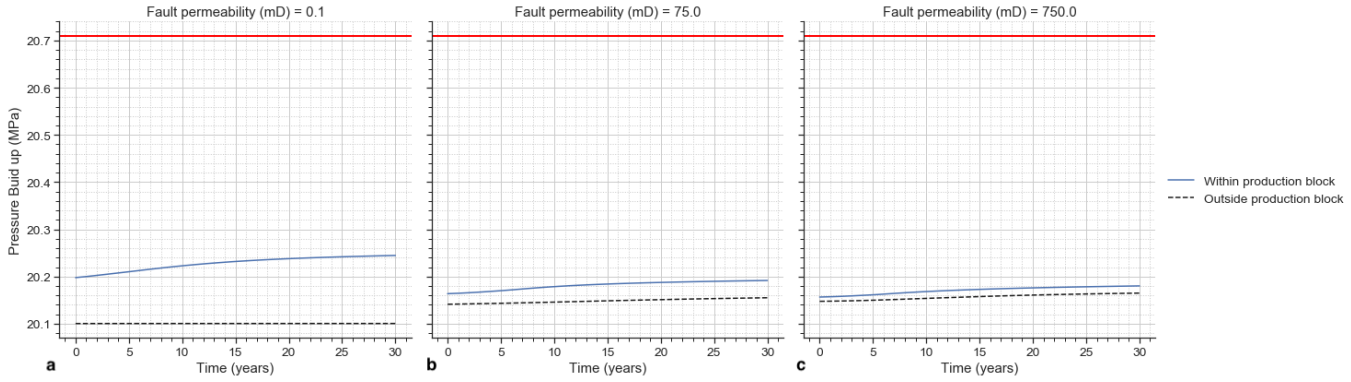

Figure 6.1.1: Influence of the fault permeability on the pressure build up near the fault as result of a flowrate of 4200 m^3/day, 192 m distance between the fault and the wells and injection temperature of 308.15 K. Figure a shows permeability of 0.1 mD, figure b shows 75 mD and figure c shows 750 mD. The failure pressure is 20.71 MPa, indicated by the red horizontal line. This failure pressure is determined using the Mohr circles and the stress values as discussed in Chapter 4.

Fault Throw

The pressure build up as result of the fault throw is very similar to the fault permeability. Figure 6.1.2 shows that the pressure generally builds up more rapidly in case of a throw of 75 m (black, dotted line). The maximum encountered pressure next to the fault is 20.18 MPa in case of zero throw (green, solid line) and this increases with about 0.01 MPa for every 25 m of additional throw length. The overburden has a low permeability because of the relative high clay and shale content and therefore acts as a barrier to flow, similar to a sealing fault. This is especially visible in the case shown in Figure 6.1.2 since a fault permeability of 750 mD is considered. Therefore, less flow is possible through the fault when the throw increases and this results in more pressure build up next to the fault.

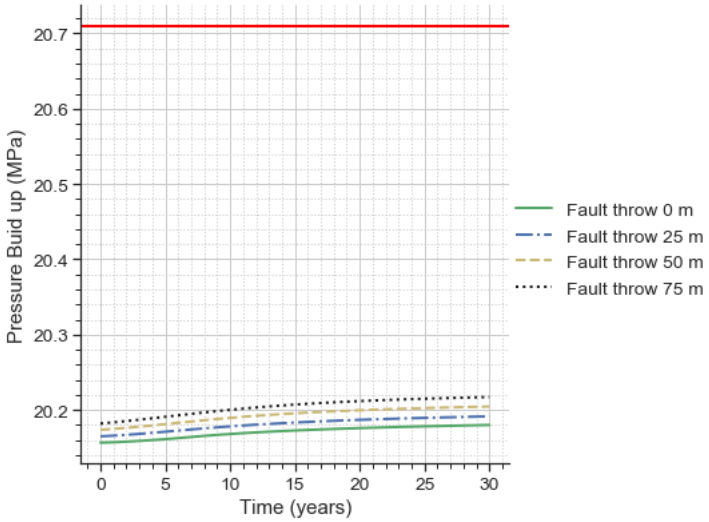

Figure 6.1.2: Influence of the fault throw on the pressure build up near the fault in the base case reservoir. With a flowrate of 4200 m^3/day, 192 m distance between the fault and the wells and an injection temperature of 308.15 K. The fault permeability is 750 mD. The values of the throws are: 0 m (green, solid), 25 m (blue, dash-dotted), 50 m (yellow, dashed) and 75 m (black, dotted). Failure pressure is 20.71 MPa, indicated by the red horizontal line. This failure pressure is determined using the Mohr circles and the stress values as discussed in Chapter 4.

Friction Coefficient

As mentioned earlier the slip tendency of a fault does not only depend on the stress fields and their orientations, but also on rock frictional characteristics such as the friction coefficient. Figure 6.1.3 shows the stress state of the base case reservoir with four different friction coefficient values for the Delft sandstone. The figure shows that slip and thus reactivation is theoretically very likely to occur if the sandstone has a friction coefficient of 0.4 as the red Mohr circle intersects the failure criterion. Still, it is not certain that slip and reactivation will occur as this Mohr circle is based on the highest value of the encountered pore pressure in the base case reservoir after 30 years of production. In addition these pore pressures are all encountered on one specific location at the fault, which exhibits about 10% of the fault surface as mentioned in Section 4.3.1 of Chapter 4. Slip and failure does not occur for the case of a friction coefficient of 0.5. The maximum encountered pore pressure in the case of Figure 6.1.3 is 20.18 MPa and an additional pressure of 0.55 MPa (5.5 bar) is required for failure. The fault is theoretically stable if Delft sandstone has a friction coefficient of 0.6 or 0.7, which require an additional pressure of respectively 1.41 MPa (14.1 bar) and 2.43 (24.3 bar) for slip to occur.

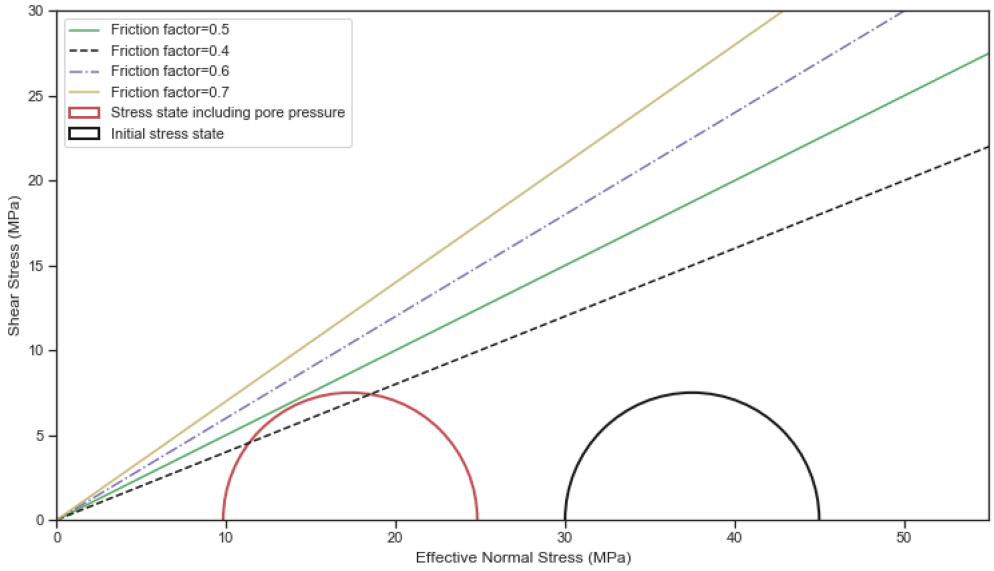

Figure 6.1.3: Mohr circles showing the stress state as result of different values for friction coefficient in the base case reservoir. The maximum encountered pore pressure in the base case reservoir is 20.18 MPa. The initial stress state is visualized with the black circle and the red circle visualizes stress state including maximum encountered pore pressure of 20.18 MPa.

6.1.2. Operational Options

Flow Rate

Figure 6.1.4 shows the maximum encountered pore pressures after 30 years of production as a result of increasing flow rates of the doublet. from this figure we see that pore pressure increases with flowrate and it increases about 0.01 MPa with every 600 m^3/day.

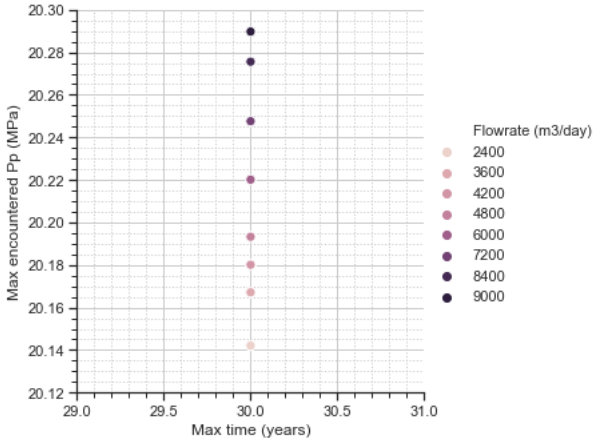

Figure 6.1.4: The influence of flowrates between 2400 and 9000 m^3/day on the maximum pore pressure next to the fault with permeability 750 mD. The wells are placed a distance of 192 m from the fault and an injection temperature of 308.15 K is used.

Injection Temperature

The influence of the injection temperature on the fault stability is very minimal. This is visible from Figure 6.1.5, which shows the maximum pore pressure encountered after 30 years of production. From the figure we see that a 10 degrees difference in temperature makes a difference of 0.007 MPa in the pore pressure, therefore the conclusion is drawn that injection temperature has minimal influence on the fault stability. This is due to the fact that mechanics of rock properties like thermo-elasticity effects are not directly taken into account in this thesis when considering the fault stability. Still, the difference in pore pressure is not zero and we see that pressure builds up with decreasing temperature. This is caused by the change in density and viscosity of the water with temperature. The density and viscosity are positively correlated and increase with decreasing water temperature (Figure C.0.1 in Appendix C). The colder the injection water, the higher the water density and viscosity and this makes the fluids more resistant to flow. As flowrate is kept constant this resistance to flow builds up pressure in the reservoir.

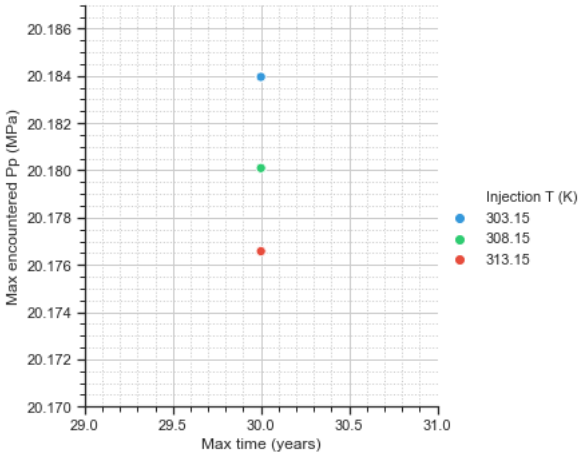

Figure 6.1.5: The influence of the injection temperature of 303.15, 308.15 and 313.15 K on the maximum encountered pore pressure next to the fault with permeability 750 mD. The wells are placed 192 m from the fault, the flowrate is 4200 m^3/day.

Distance between the Wells and Fault

Figure 6.1.6 shows the pore pressure build up next to a permeable fault (750 mD) as result of varying distance between the wells and the fault. As visible from the figure, maximum encountered pore pressure values are significantly higher when the wells are placed close to the fault. Values of 20.48 MPa are encountered after 30 years of production when the wells are placed 12 or 24 m from the fault and at a distance of 96 m the maximum pore pressure builds up to 20.24 MPa. While maximum pressures of

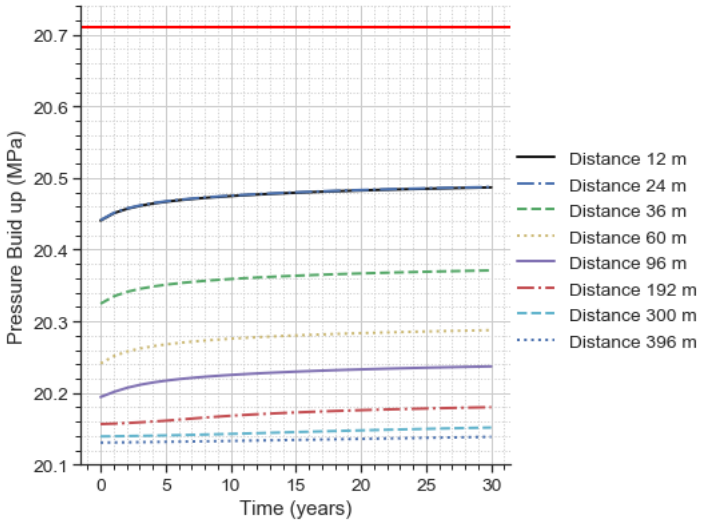

Figure 6.1.6: The influence of distance 12, 24, 36, 60, 96, 192, 300 and 396 m between the wells and fault on the pressure build up near a non-sealing fault (0.1 mD). The used flowrate is 4200 m^3/day and the injection temperature is 308.15 K. The red horizontal line indicates the failure pressure of 20.71 MPa when the sandstone has a friction coefficient of 0.5. This failure pressure is determined using the Mohr circles and the stress values as discussed in Chapter 4.

20.18, 20.15 MPa and 20.14 MPa are encountered at distances of 192, 300 and 396 m respectively after the same amount of production time. The closer the wells are positioned to the fault, the extent of the pressure build up near the fault increases. This means that the distance has a direct influence on the pore pressure next to the fault, hence on the potential for fault slip. On the contrary the amount of pressure build up and the encountered maximum pore pressure after 30 years are comparable at distances of 300 and 396 m. It should be noted that the 12 m distance plot overlies the 24 m distance plot, meaning that the same maximum pressures are encountered. This results from the fact that the two layers directly next to the fault are analyzed on their pressure values. These two layers together comprise 24 m next to the fault, which means that the wells are placed within this vicinity when they are placed 12 m or 24 m from the fault. The figure shows the maximum encountered pressures within these two layers and this happens near the injector well when the well is placed 12 m or 24 m from the fault. Since the well injects water with a constant rate, the pressure build up therefore shows similar trends.

6.2. Individual Results for the Profitability

This section shows how the projects profitability is influenced by the considered reservoir conditions and operational options.

6.2.1. Reservoir Conditions

The influence of the fault permeability and fault throw are described below. The friction coefficient is also considered as a reservoir property, but has no influence on the project's profitability as it defines the rock strength. Therefore the friction coefficient is not further highlighted in terms of profitability.

Fault Permeability

The influences of the fault permeability on the project economics are visualized in Figure 6.2.1, which show the net present values as a function of the profitability index and levelized cost of heat after 30 years of production. It is visible that the NPV values between the three fault types do not differ significantly when the reservoir conditions and operational options are kept constant, considering the fact that the total NPV outcomes are in the scale of millions. Still, a bigger contrast in NPV outcomes is visible between the sealing fault and the more permeable fault. These differences are caused by the pumping costs to produce the energy, shown by Figure H.4.1. Higher pumping costs are required when operating in the presence of a sealing fault, compared to when more permeable faults are present. Over time the bottom hole pressure (BHP), which is the formation pressure at the bottom of the hole, increases. This BHP increase is larger when a sealing fault is present because it acts as a barrier to flow and pressure

builds up. The required energy of the pumps is based on equation 5.5 and in this research case only the pressure difference between the ESP and the injector varies. The BHP increases and as a consequence the injector pressure increases to maintain constant flowrate. This results in a larger pressure difference between the injector and the producer, hence resulting in higher required energy in the presence of a sealing fault and in higher pumping costs.

Looking at the cumulative amount of produced energy after 30 years we see that the total amount of produced energy between the three fault types differ minimally (Figure H.3.1 in Appendix H). These differences are between 200 and 700 kWh on a total produced amount of 162 GWh. Yet, the presence of a sealing fault does impact the heat production which is visible from Figure H.1.1 in Appendix H showing the produced amount of energy in kWh in the presence of the three different faults. The heat production drops significantly after approximately 20 years in presence of a sealing fault, while the heat production remains almost constant for 30 years in presence of more permeable faults. This drop in heat production is related to a drop in production temperature after 20 years (Figure H.2.1). From this it turns out that steady heat productions can be guaranteed more reliably when reservoirs have faults with increasing permeabilities. The higher the fault permeability, the more lateral flow is possible and this allows larger available water volumes for production. This is also visible from the temperature maps shown in Appendix A.1.1, which show that the amount of flow increases with increasing fault permeability.

It should be noted that the NPV differences are also caused by the relative contrast between the fault permeabilities and the reservoir permeability. The difference between the two permeable faults is only a factor 10, while the difference between the 0.1 mD and 75 mD fault is a factor 750. Scaling this to the NPV we see that the difference in NPV is much larger for higher fault permeabilities, compared to the sealing fault permeabilities. With respect to the LCOH, the outcomes of the NPV values consequently turn out in lower values for increasing fault permeability. Regarding the profitability index, shown in figure b, the values are quite similar but do increase slightly with increasing fault permeability.

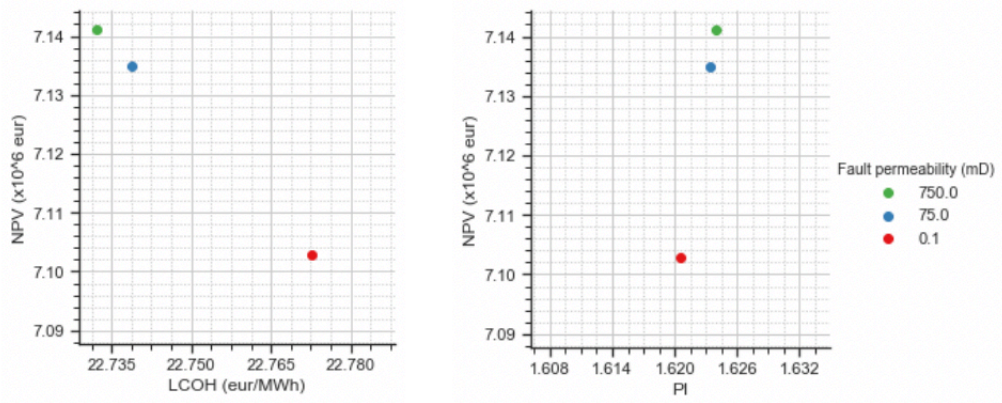

(a) Net Present Value vs Levelized Cost of Heat (b) Net Present Value vs Profitability Index

Figure 6.2.1: The influence of fault permeability 0.1, 75 and 750 mD on the NPV, LCOH and profitability index. The used flowrate is 4200 m^3/day, the distance between the fault and the wells is 192 m, the injection temperature is 308.15 K and the fault permeability is 750 mD.

Fault Throw

Figure 6.2.2 shows how the fault throw influences profitability of a geothermal project. As visible from figure a the NPV values decrease with increasing fault throw. However, the differences in NPV due to the fault throw are minor relative to the total NPV of €7 million. The delta NPV values with increasing throw are displayed in Table 6.2.1.

The overburden has a low permeability because of the relative high clay and shale content and therefore acts as a barrier to flow, similar to a sealing fault. This is especially visible in this case since a fault permeability of 750 mD is considered. With increasing throw, there is a larger flow barrier and therefore less amount of heat is extracted. This is also visible from the temperature plot over time in Figure I.1.1 in Appendix I, which shows that the production temperature starts dropping earlier during the project

Table 6.2.1: NPV differences as a result of increasing fault throw

Fault throw (m)	Delta NPV (x10^6€)
0-25	-0.005
25-50	-0.007
50-75	-0.008
0-75	-0.02

as the throw increases. As a result the energy production drops as well which is visible from Figure I.2.1 in the same Appendix. Still, in the case of 25 m throw there is 80 m in depth of reservoir left from which heat can be laterally extracted across the fault. With increasing throw this area becomes smaller and this affects the heat production and thus the NPV (visible in Figure 3.2.1 and temperature maps in Figure A.2.1 of Appendix A). A decreasing amount of heat production as a consequence also influences the LCOH, which decreases with decreasing amount of throw. The influence of the throw value on the PI is similar to the influence of the fault permeability.

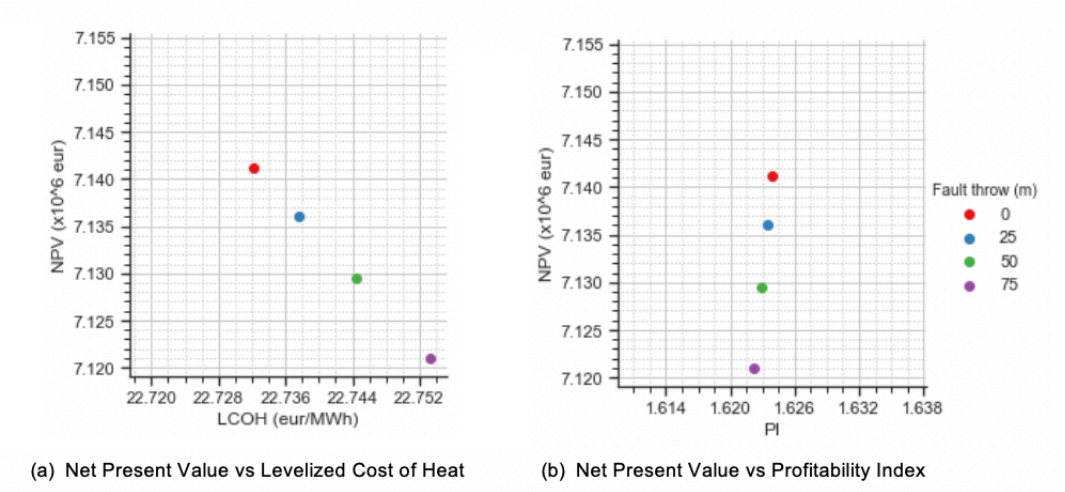

(a) Net Present Value vs Levelized Cost of Heat (b) Net Present Value vs Profitability Index

Figure 6.2.2: The influence of fault throw 0, 25, 50 and 75 m on the NPV, lCOH and profitability index. The used flowrate is 4200 m^3/day, the distance between the fault and the wells is 192 m, the injection temperature is 308.15 K and the fault permeability is 750 mD.

6.2.2. Operational Options

Flow rate

The NPV values as result of increasing flow rates of the doublet are visualized in figure 6.2.3 and the corresponding trends of the cumulative discounted cashflows are visualized in figure B.0.1 in Appendix B. Both figures show that the profitability of a geothermal project increases with flowrate. It should be noted that friction of water inside the wells is not taken into account. Friction of water inside the wells grows with increasing flowrate and therefore this will lower the NPV. In the case of the wells placed at a constant distance of 192 m from the fault and a non-sealing fault the NPV increases with approximately 3.7 million euros with every 600 m^3/day increase in flowrate. Larger water volumes are extracted with higher rates and this results in higher NPV and consequently in lower LCOH values. However, it is visible that decrease in values of LCOH flattens as rates get higher. Especially from rates of 7200 m^3/day and higher, which means that the costs of producing one MWh of energy are of more importance when considering rates between 3600 and 7200 m^3/day. The profitability index increases approximately 0.33 with every 25 m^3/hr increase in flowrate. Last important result is the one at 2400 m^3/day, which gives a negative NPV and a PI lower than one. Both values are indicators that a project in the base case of the homogeneous reservoir with a rate of 2400 m^3/day would not be profitable at all and therefore the project will not be started.

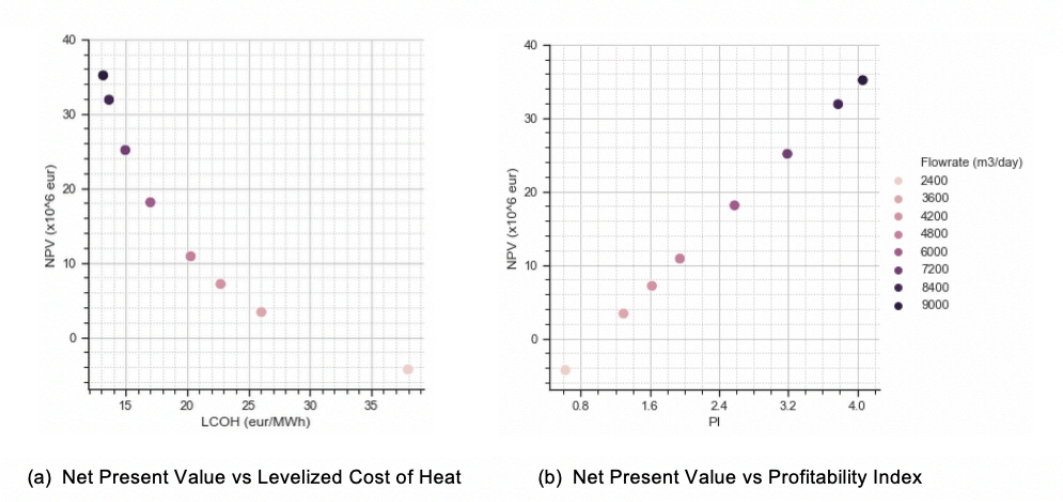

Figure 6.2.3: The influence of flow rate between 2400 and 9000 m^3/day on the NPV, LCOH and profitability index. The distance between the fault and the wells is 192 m, the injection temperature is 308.15 K and the fault permeability is 750 mD.

Injection Temperature

Re-injecting water at lower temperature means that more heat is extracted. Logically this results in higher profits as showcased in Figure 6.2.4. Injecting water at a temperature of 303.15 K results in almost €11 million NPV, while injecting water at 308.15 and 313.15 K results in approximately €7 and €3.3 million euros respectively. An increase in temperature of 5 K thus decreases the NPV with about €3 million. As a result, the injection temperature also has significant influences on the LCOH. 10 degrees lower water temperature reduces the costs to produce one MWh of geothermal energy by almost 6 euros. The same decrease in temperature increases the profitability index by 0.65. These results show that the injection temperature can make a significant difference in the profitability of a geothermal project.

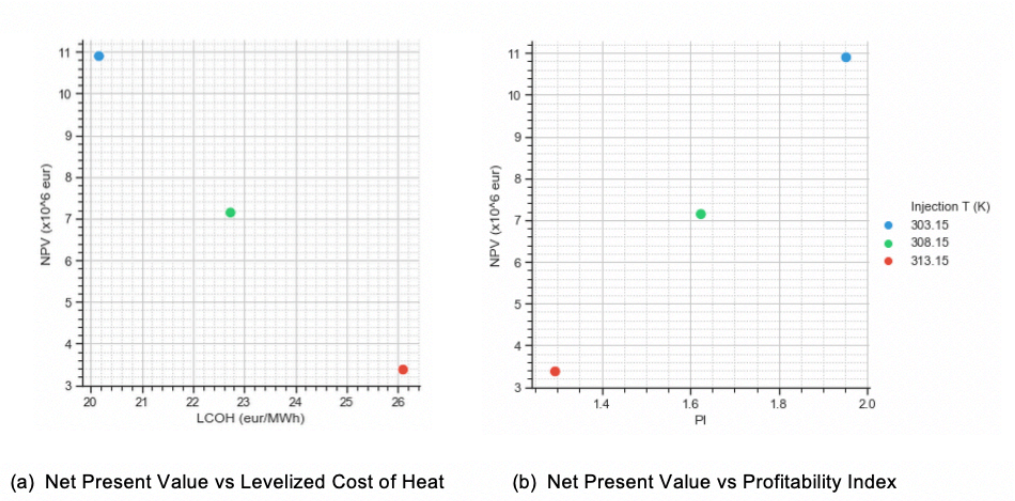

Figure 6.2.4: The influence of injection temperature 303.15, 308.15 and 313.15 K on the NPV, LCOH and profitability index. The used flowrate is 4200 m^3/day, the distance between the fault and the wells is 192 m and the fault permeability is 750 mD.

Distance between the Wells and Fault

With respect to the distance between the fault and the wells it is found that the NPV outcomes increase with increasing distance from a sealing fault and that the increase in NPV outcomes diminishes when the wells are placed a distance of 192 m and further from a sealing fault. This is visualized in Figure 6.2.5, which shows the influences of the distance between the wells and a sealing fault (0.1 mD). Relative larger increases in NPV values, between €30,000 and 50,000, are visible when wells are placed between 12 and

192 m from the fault. Between 192 m and 300 m between the wells and the fault the NPV increase is about €25,000 and the NPV increase between distance 300 and 396 m from the fault is only €10,000. The higher profits with increasing distance in the presence of a sealing fault results again from the earlier mentioned barrier to flow. A sealing fault forms a flow barrier and therefore the lateral volume from which water is produced is smaller when the wells are placed for example 36 m from the fault, compared to a distance of 300 m. This is visualized in figure A.3.1 in Appendix A. It should be noted that these differences are relative minor taking into account that these projects have NPV's in the range of million's.

The influence of the distance between the wells and the fault on the profitability is directly related to the fault permeability. In the presence of a non-sealing fault with permeability of 750 mD the NPV values are very similar at each distance from the fault (Figure D.0.1 in Appendix D), meaning that profitability is not influenced by the distance when a fully permeable fault is present.

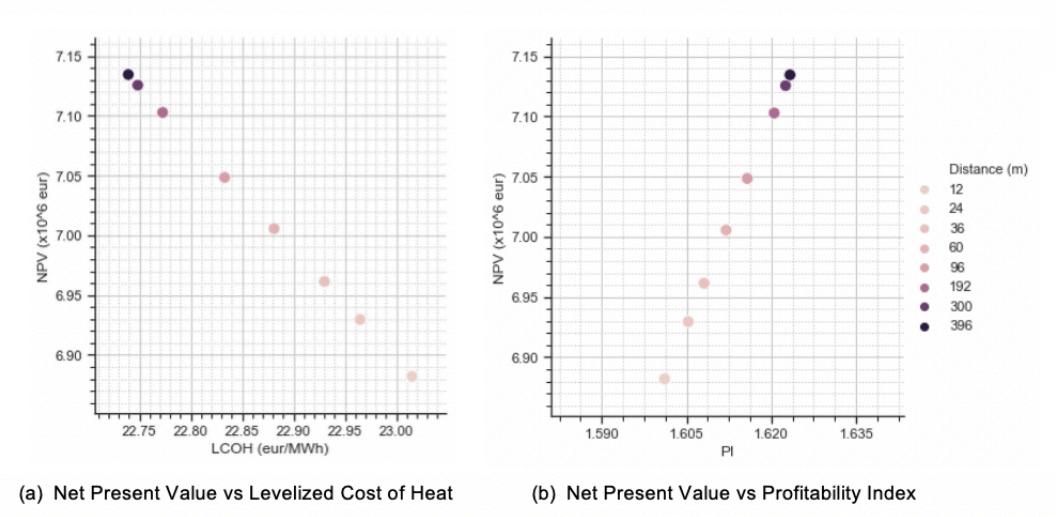

(a) Net Present Value vs Levelized Cost of Heat (b) Net Present Value vs Profitability Index

Figure 6.2.5: The influence of 12, 24, 36, 60, 96, 192, 300 and 396 m distance between the wells and a sealing fault on the NPV, LCOH and profitability index. The used flowrate is 4200 m^3/day, the injection temperature is 308.15 K and the fault permeability is 0.1 mD.

7

Reservoir Development Strategies

This chapter shows and describes the combined influences of the considered reservoir conditions and operational options on the Delft sandstone reservoir with homogeneous permeability and porosity. The results are divided based on the the fault permeability as this is a relative fixed condition in real life. The effects of the fault throw and the operational options are tested with respect to each fault type and based on that optimal development strategies will be discussed.

In both the minimum and maximum case of fault permeability it is found that producing geothermal heat in the Delft area at rates of 2400 m^3/day and 3000 m^3/day would not be profitable using an injection temperature of 308.15 K (Figure E.1.1 in Appendix E). These projects would lead to a negative NPV, hence the project would not commence. The same holds when combining a rate of 2400 m^3/day with an injection temperature of 303.15 K. The best possible option to generate positive NPV outcomes with a rate of 3000 m^3/day is when this is combined with an injection temperature of 303.15 K, generating an NPV of about €2 million. Fault slip is not likely to occur with either flowrate. No further research is done for rates of 2400 m^3/day and 3000 m^3/day.

7.1. Development in the Presence of a Sealing Fault (0.1 mD)

The results of the homogeneous reservoir in the presence of a sealing fault with 0.1 mD permeability are discussed in this section. The results are presented and discussed based on the combined effects on the NPV and on the fault stability, after which potential development strategies are discussed.

Combining the effects of the fault throw with a sealing fault it is found that the throw has no influences on the pressure build up or the NPV, regardless of the used flowrate. These results are visualized in Appendix E.2. The outcomes for the maximum encountered pressures next to the fault are very similar for every value of the throw, independent of the used flowrate. To exemplify, the maximum encountered pressure next to the fault as result of a 6000 m^3/day flowrate is 20.46 MPa at each considered throw of 0 m, 25 m and 75 m. In terms of the profitability we see that NPV values also do not change as result of increasing throw (Figure E.3.1). This means that the increasing NPV and pressure next to the fault is fully caused by the higher flowrates of the injection well. As mentioned in Section 6.1 the overburden has low permeability due to the high clay and shale content and therefore acts as a barrier to flow. So both the fault and the throw have sealing properties, through which the throw does not additionally influence the flow properties of the fault. Therefore the fault throw is not further taken into account in the development strategies when a sealing fault is present.

7.1.1. Net Present Value

With respect to the profitability in the presence of a sealing fault it is found that the flowrate and the injection temperature are the most important influencing factors. The higher the flowrate and the lower the injection temperature, the more profits are generated during the project. Additionally, it holds for all combinations of flowrates and injection temperatures that placing the wells at a minimum distance of 192 m from the fault provides the highest NPV values. Combining this wells placement with a minimum

flowrate of 7200 m^3/day allows an operator to increase the NPV by €2 to €3 million euros, regardless of the used injection temperature. This is all visualized by Figure 7.1.1, which shows the combined influence of the injection temperature, the distance between the wells and the fault and the flowrate on the NPV outcomes in the presence of a sealing fault.

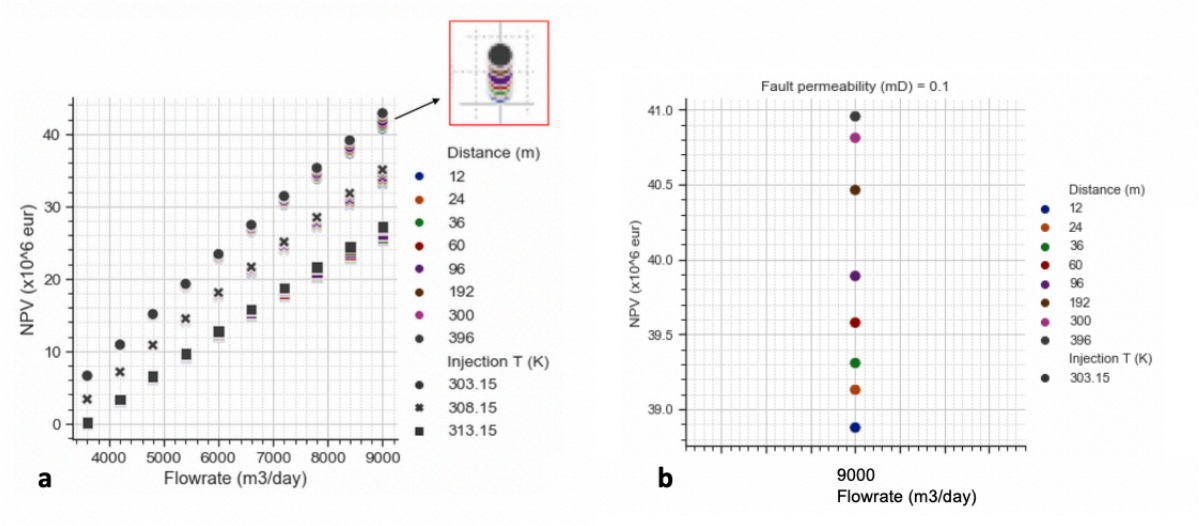

Figure 7.1.1: The combined influence of injection temperature, distance between the fault and the wells and flowrates between 3600 and 9000 m^3/day on the NPV in presence of a sealing fault, shown in Figure a. The red outlined box shows a zoomed-in view of the NPV values generated with a flowrate of 9000 m^3/day, 303.15 K injection temperature and wells placed between 12 m and 396 m from the fault. One vertical distance in a grid cell of the plot indicates €2 million NPV. Figure b shows this zoom-in in more detail.

As already found and discussed in Section 6.2 the NPV increases with increasing flowrate and with decreasing injection temperature. Logically, the combination of these two parameters strengthens this effect and this is visible from the figure. To give an example, with an injection temperature of 313.15 K the NPV outcome increases by €3.2 million when the flowrate is increased from 3600 m^3/day to 4200 m^3/day. With an injection temperature of 308.15 K this NPV increase between the two rates is €3.8 million and at a temperature of 303.15 K this is €4.1 million. This same amount of increase in NPV at each injection temperature is seen for every 600 m^3/day increase in flowrate.

In Section 6.2 it is also found that higher NPV outcomes are generated with increasing distance between the wells and the fault. The results in Figure 7.1.1 confirm this and show that this outcome strengthens with increasing flowrate. The figure shows that the interdependency between the wells placement and the used flowrate makes a more significant difference in NPV when a minimum flowrate of 7200 m^3/day is used. Namely, using a flowrate of 7200 m^3/day and higher could increase the NPV outcomes up to €2 million euros if the wells are placed 396 m from the fault instead of 12 m. This is better visualized by the red box in Figure 7.1.1.a, which shows a zoom-in of the NPV values resulting from a flowrate of 9000 m^3/day, an injection temperature of 303.15 K and wells placed distances 12 m to 396 m from the fault. One vertical distance in a grid cell of the plot indicates €2 million. Figure 7.1.1.b shows the zoom-in in more detail. This zoom-in also shows that the NPV increases less significantly with values up to €300,000 when the wells are placed a minimum distance of 192 m from the fault (Figure E.3.2 in Appendix E.3). The relative difference in growth of NPV between distances up to 192 m and further than 192 m is thus much larger as flowrates are higher. This means that the distance at which the doublet is placed plays a less significant role in terms of the NPV when it is placed at a minimum distance of 192 m from the fault, which was also found by Daniilidis et al. (2020a). The same results are found at the considered injection temperatures and that means injection temperature and distance are not influencing each other. If an operator uses flowrates between 3600 and 6600 m^3/day, we see from Figure 7.1.1 that the distance between the wells and the fault does not make a distinct difference in NPV, regardless of the used injection temperature.

Lastly, Figure 7.1.1 shows that flowrate 3600 m^3/day is the minimum profitable flowrate to use for a homogeneous reservoir using data from the Delft area. At the highest considered injection temperature of

313.15 K this rate results in a negative NPV of -€33,000 when the doublet is placed 12 m from the fault, hence this project would not commence. At a distance of 24 m the NPV is -€980, which is still a loss but it comes very close to breakeven. This means that breakeven of a geothermal project in the homogeneous Delft area in presence of a sealing fault is achieved with an injection temperature of 313.15 K and an approximate distance between 24 m and 36 m from the fault. The exact distance could however not be researched because of the used grid size in this thesis, which allows steps of 12 m. At 36 m distance and 313.15 K temperature this rate results in €20,000 NPV. This makes the flowrate of 3600 m^3/day the minimum profitable flowrate in the homogeneous Delft area, provided that the doublet is placed at a distance larger than 24 m from the fault.

7.1.2. Fault Stability

The use of each operational option and the presence of specific reservoir conditions should be checked on their effects on the fault stability in order to find the best possible development strategy. In this development strategy it is important to take into account the friction coefficient of the sandstone. As discussed in Chapter 4 this value varies between 0.4 and 0.7. However, fault stability results of the homogeneous reservoir with respect to the friction coefficient show that a range of values between 0.48 and 0.53 are of interest in presence of a sealing fault. Appendix E.4 shows the maximum pressures encountered within the first 24 m distance from the fault inside the production block as a result of sandstones with friction coefficients of 0.4, 0.47, 0.53, 0.54 and 0.6. A friction coefficient lower than 0.48 would always result in failure based on the Mohr-Coulomb (MC) failure criterion for all rates, injection temperature and distance combinations considered in this study as the failure criteria are exceeded. Conversely, a friction coefficient higher than 0.54 would remain stable based on the MC failure criterion at every considered flowrate, distance and injection temperature. With a friction coefficient of 0.53 only a rate of 9000 m^3/day, an injection temperature of 303.15 K and wells placed 12 m from the fault exceeds the failure pressure, hence might cause slip.

The combined influence of flowrate, injection temperature and distance between the fault and the wells on the highest maximum encountered pressure next to the fault is visualized in Figure 7.1.2. This figure also shows the failure pressures due to the different friction coefficients.

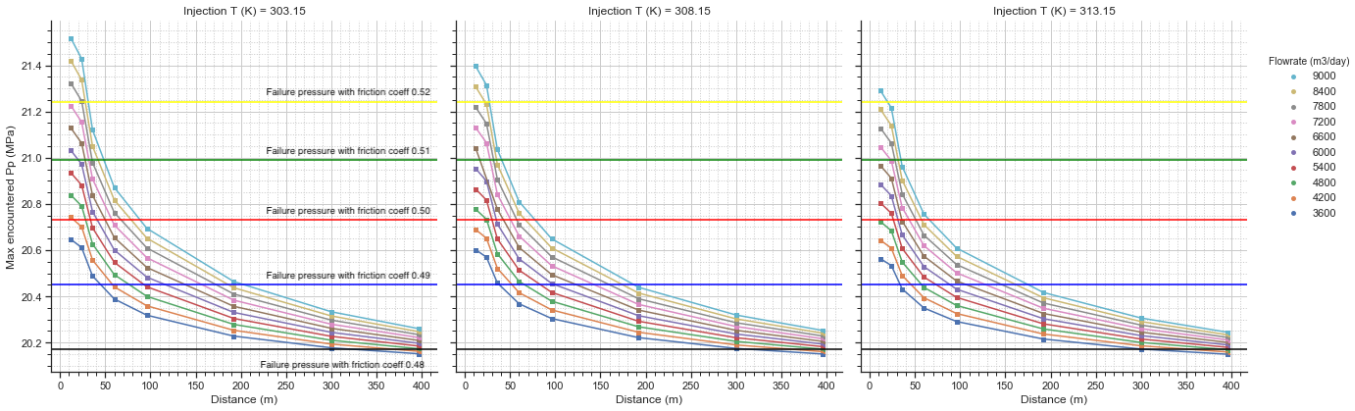

Figure 7.1.2: Maximum encountered pressures next to a sealing fault after 30 years as result of distance of 12 m, 24 m, 36 m, 60 m, 96 m, 192 m, 300 m and 396 m between the fault and the wells, flowrates between 3600 and 9000 m^3/day and injection temperatures of 303.15 K, 308.15 K and 313.15 K. The horizontal lines indicate the failure pressures as result of coefficients 0.48 (Black), 0.49 (Blue), 0.5 (Red), 0.51 (Green) and 0.52 (Yellow)

In general Figure 7.1.2 shows that an increasing friction coefficient allows the use of higher flowrates at shorter distances between the wells and the fault without crossing the MC failure criterion. As the fault stability increases with increasing friction coefficient of the sandstone. Additionally, including the injection temperature we see from the figure that this is a critical factor for minimizing the risk of failure. Using a 5 K higher temperature for the injection water results in lower pressure values encountered next to the fault, dependent on the flowrate. This results from the viscosity and density changes of the water, discussed in Chapter 6. The effects of the injection temperature imply that increasing the temperature could be an important factor in minimizing fault slip when wells are placed close to the fault or when

the sandstone has a lower than expected friction coefficient. Using a 5 K higher injection temperature also allows an operator to use a 600 m^3/day higher flowrate, without crossing the MC failure criterion. However, it still depends on the sandstone friction coefficient what minimum distance between the wells and the fault and what maximum possible flowrate would remain safe from fault slip.

With respect to the influence of the flowrate and the distance between the wells and the fault on the pressure build up, Figure 6.1 shows that higher values for the maximum pressure are encountered next to the fault with increasing flowrates and with decreasing distance. This means that the influences of the flowrate and the distance strengthen each other. This strengthening effect is also visible from the cross sections and pressure build up plots in Appendix E.5, showing the pressure build up next to the fault. From these figures it is clearly visible that the closer the wells are placed to the fault and the higher the used flowrate, the higher the pressure builds up. To exemplify, if the wells are placed 24 m from the fault the pressure next to the fault after 30 years is 20.57 MPa with a rate of 3600 m^3/day. While the pressure after 30 years is about 20.69 MPa due to a rate of 5400 m^3/day for wells at the same distance. If the wells are placed 192 m from the fault the difference in pressure after 30 years is about 0.4 MPa lower at both flowrates. This shows that the increase in maximum pore pressures are less significant for each flowrate when the wells are placed a minimum of 192 m from the fault.

7.1.3. Potential Development Strategy

The aim of this study is to find potential development strategies which maximize the profitability and minimize the risk of potential fault slip. The combined outcomes of the NPV and fault stability in Figure 7.1.3 show that the fault stability is the decisive factor in terms of the development strategy. What flowrate and wells placement remains safe from fault slip depends on the used injection temperature and the friction coefficient of the sandstone. The risk of exceeding the MC failure criterion, hence the potential risk for fault slip, increases with decreasing friction coefficient. This makes it essential to characterize the real value of the friction coefficient to make meaningful predictions on the fault slip tendency. In the presence of a sealing fault a friction coefficient lower than 0.48 will certainly result in exceedance of the failure criteria, while sandstones with values above 0.54 are always safe regardless of the used flowrates, injection temperatures and wells placement from the fault.

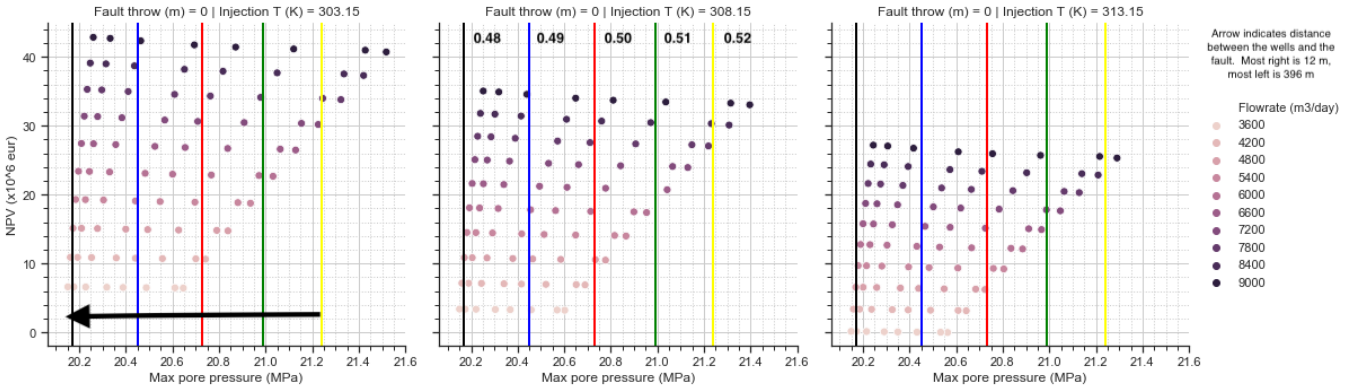

Figure 7.1.3: NPV and Maximum encountered pore pressures after 30 years as result of rates between 3600 and 9000 m^3/day in presence of a sealing fault. The vertical lines indicate the failure pressures for friction coefficients: 0.48 (Black), 0.49 (Blue), 0.50 (Red), 0.51 (Green) and 0.52 (Yellow). The arrow indicates increasing distance between the wells and the fault from right to left. Most right indicates 12 m between the wells and the fault and most left is 396 m.

We have seen that higher flowrates can be used during the production when the sandstone has a higher friction coefficient. As a result, also more profit can be made due to higher friction coefficients. The NPV outcomes are maximized when the wells are placed a minimum distance of 192 m from the fault and if a minimum rate of 7200 m^3/day is used. For these NPV maximizing conditions, Figure 7.1.3 shows that sandstones with a minimum friction coefficient of 0.50 remain stable from fault slip and allow the operator independence of the injection temperature. The amount of profit, on the other hand, does depend on the injection temperature and can be maximized by using a low as possible temperature. Namely, using a temperature of 303.15 K results in NPV between €31 and €42 million, using 308.15 K results between €22 and €35 million and using 313.15 K results between €18 and €28 million. In case

an operator plans to use the NPV maximizing conditions to make the highest NPV, but the sandstone has a lower than expected friction coefficient fault slip can be minimized by using a higher injection temperature.

Regarding the allowable distance between the wells and the fault, Figure 7.1.3 shows that this increases significantly with decreasing friction coefficient. The wells should be placed far from the fault in order to not exceed the MC failure criterion if the sandstone has a lower than expected friction coefficient. According to the figure a minimum distance of 192 m should suffice in order to not exceed a relative low failure pressure, though it does depend on the used flowrate and injection temperature. In restricted cases, like a lower than expected friction coefficient or a lower than expected allowable flowrate, the combination of flowrate and injection temperature is essential in terms of the NPV outcomes. Closer inspection of the figures show that higher profits are provided when a 600 m^3/day lower flowrate is combined with a 5 K lower injection temperature, compared to using a 600 m^3/day higher flowrate combined with a 5 K higher injection temperature.

7.2. Development in the Presence of a Medium Sealing Fault (75 mD)

This section presents and discusses the results of a reservoir in presence of a medium sealing fault with permeability of 75 mD. Again the results are presented and discussed based on the combined effects on the NPV and on the fault stability, after which the optimal development strategy is discussed.

7.2.1. Net Present Value

The combined influences of the fault throw, flowrate, wells placement with respect to the fault and injection temperature in the presence of a medium sealing fault are shown in Figure 7.2.1. Generally the combined influences of the used flowrate, injection temperature and distance between the wells and the fault are similar to those found for the situation with a sealing fault. The effects of the fault throw with a medium sealing fault are very minimal, comparable to the individual results found in Section 6.2. With each considered injection temperature and for a constant rate the NPV decreases between €20,000 and €50,000 with every 25 m increase of fault throw, which is very small compared the total extent of the NPV values in the range of millions. Adding the wells placement with respect to the fault, we see no differences in NPV in the presence of throws of 0 m and 25 m. These findings suggest that the combined influence of the fault throw and the distance between the fault and the wells influences the NPV outcomes minimally. In the presence of a 75 m throw, however, minor changes are visible with respect to wells placement. With this extent of the throw we see that a 384 m increase in distance between the wells and the fault increases the NPV values by €1 million for flowrates of minimally 7200 m^3/day (zoom-in in Figure 7.2.1). While this increase in NPV is about 10% of that amount using lower rates. In addition, the NPV remains relatively constant when wells are placed a minimum of 192 m from a medium sealing fault (Figure F.1.1 in Appendix F). The NPV results for the presence of a 75 m throw are comparable to the effects of a sealing fault as the overburden has a low permeability due to its relative high clay and shale content. From this we derive that a fault throw influences the NPV in the presence of a medium sealing fault if it has a minimal extent of 75 m. It is highly likely that a throw as large as reservoir thickness shows approximately the same results as the presence of a sealing fault.

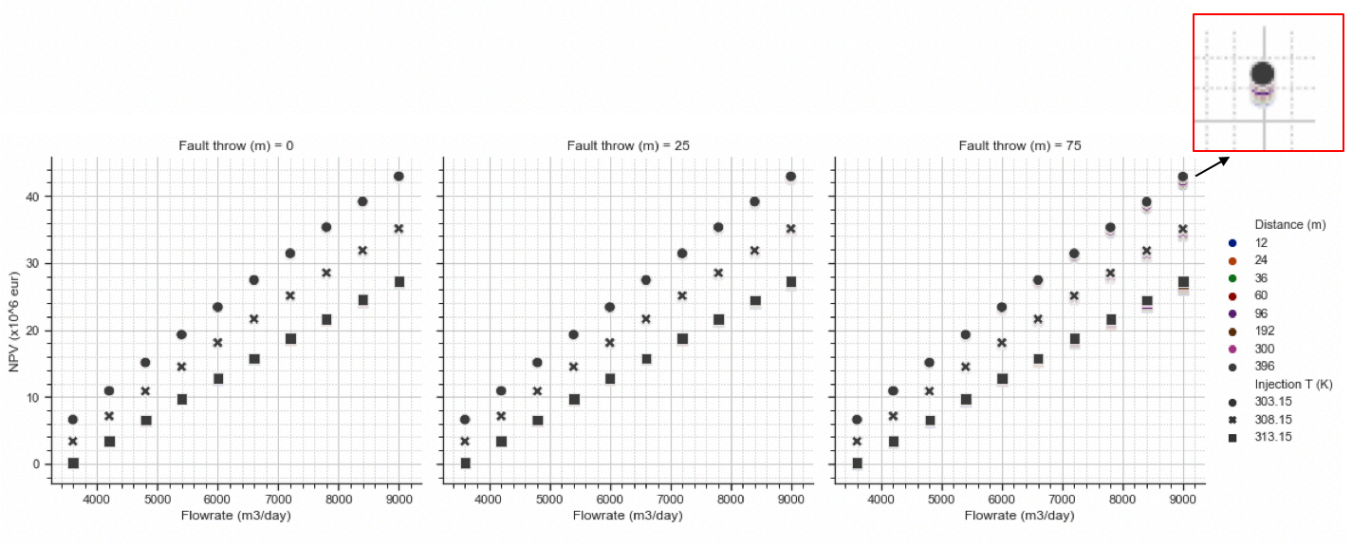

Figure 7.2.1: The combined influence of injection temperature, distance between the fault and the wells and flowrates between 3600 and 9000 m^3/day on the NPV in presence of a medium sealing fault. The red outlined box shows a zoomed-in view of the NPV values generated with a flowrate of 9000 m^3/day, 303.15 K injection temperature and wells placed between 12 m and 396 m from the fault. One vertical distance of a minor grid cell of the plot indicates €2 million.

7.2.2. Fault Stability

In the presence of a medium sealing fault the general effects of the flowrate, the distance between the fault and the wells and the injection temperature are found to be similar to those found for a sealing fault. Though, the encountered pressures next to a medium sealing fault are generally lower compared to a sealing fault as the injected water is able to flow across the fault more easily and thus accumulates less next to the fault. Hence leading to lower pressure build up. The presence of a large fault throw increases the maximum encountered pressures, especially when this is combined with high flowrates and short distances between the wells and the fault. This is visualized in Figure 7.2.2, which shows the maximum encountered pore pressures next to the fault after 30 years of production as a result of a constant injection temperature of 303.15 K and fault throws of 0 m, 25 m and 75 m. This figure is narrowed down to only the fault throw, to make the influences more clear. The complete figure showing the encountered pressures next to the fault as a result of all considered reservoir conditions and operational options is visualized in F.2 in Appendix F. The varying parameters in these figures are the flowrate and the distance between the fault and the wells.

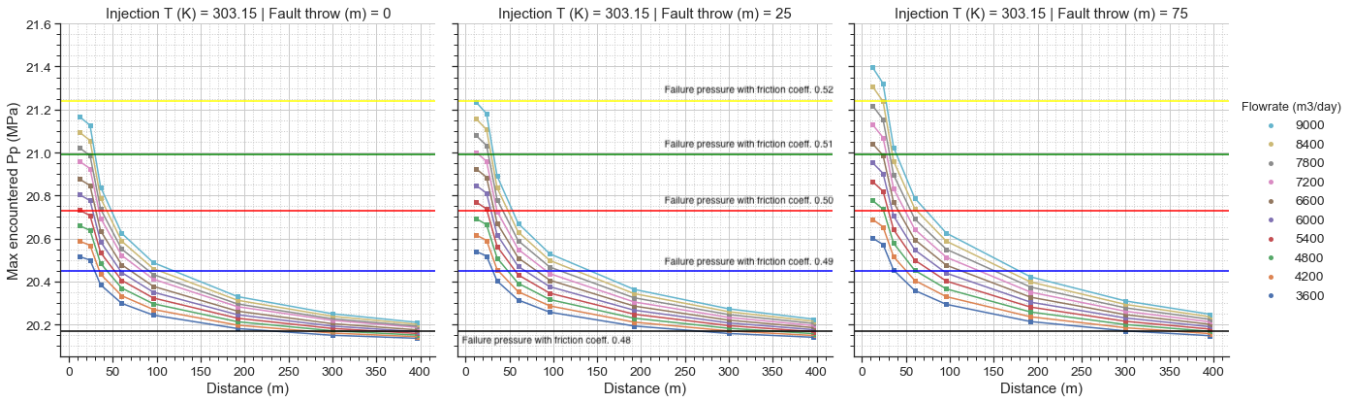

Figure 7.2.2: Maximum encountered pressures next to a medium sealing fault after 30 years as result of distance of 12 m, 24 m, 36 m, 60 m, 96 m, 192 m, 300 m and 396 m between the fault and the wells, flowrates between 3600 and 9000 m^3/day, fault throw of 0 m, 25 m and 75 m and a constant injection temperature of 303.15 K. The horizontal lines indicate the failure pressures as result of coefficients 0.48 (Black), 0.49 (Blue), 0.5 (Red), 0.51 (Green) and 0.52 (Yellow).

From Figure 7.2.2 it is visible that at distances shorter than 192 m between the fault and the wells,

a 25 m increase in fault throw makes a 600 m^3/day lower flowrate exceed the MC failure criteria. This holds for each of the three considered injection temperatures. These findings imply that the fault throw is a more important factor in terms of the fault stability when the wells are placed closer than 192 m from the fault and that the influences of the fault throw might be minimized by placing the wells at this distance or further from the fault. In addition the maximum pore pressures increase less significantly for each flowrate when the wells are placed at this distance. Also with respect to the sandstone friction coefficient it is visible that the wells should be placed minimally 192 m from the fault in order to minimize the risk of exceeding the MC failure criterion, especially when the friction coefficient is relatively low. Similar to the results for the sealing fault it is found that a friction coefficient of 0.47 is the maximum value with which fault slip is very likely to occur and with a value of 0.54 the sandstone is always stable from slip, regardless of the used flowrate and injection temperature. Though, as mentioned the encountered pressures are found to be lower compared to those found next to a sealing fault, regardless of the presence of a fault throw. To exemplify, in the presence of a medium sealing fault and zero fault throw and using an injection temperature of 303.15 K a flowrate of 9000 m^3/day at a distance of 60 m from the fault results in a maximum pressure of 20.62 MPa, while this is 20.87 MPa under the same conditions but in the presence of a sealing fault. In the presence of a 75 m fault throw next to a medium sealing fault this maximum pressure is 20.79 MPa under these conditions. This shows that the presence of a large fault throw has similar influences to those of a sealing fault, but still have smaller effects on the pressure build up.

With respect to the influence of the used injection temperature we see consistent effects with the case in which a sealing fault is present. Namely, that every 5 K increase in injection temperature results in a 600 m^3/day higher flowrate remaining safe from potentially inducing fault slip. This holds for each extent of the fault throw in case a medium sealing fault is present. The combined effects of the injection temperature and the fault throw (Combination A) and the wells distance to the fault and the fault throw (Combination B) have exact counteracting influences on what flowrate remains safe from inducing fault slip. Increasing the throw 25 m, while the wells are placed 60 m from the fault allows a maximum flowrate of 5400 m^3/day with an injection temperature of 303.15 K. While this maximum allowable flowrate is 6000 m^3/day if the throw is 0 m. Consequently, a 600 m^3/day higher flowrate is allowable if the injection temperature of the two cases is increased to 308.15 K. Combining A and B results in a balance between the two influences on the flowrate. An example of this implication is shown by Figure 7.2.3. Combining a throw of 25 m and an injection temperature of 308.15 K results in the same maximum flowrates remaining safe from inducing fault slip as using an injection temperature of 303.15 K when no throw is present. These findings suggest that the effects of the fault throw on the fault stability can be minimized by increasing the injection temperature.

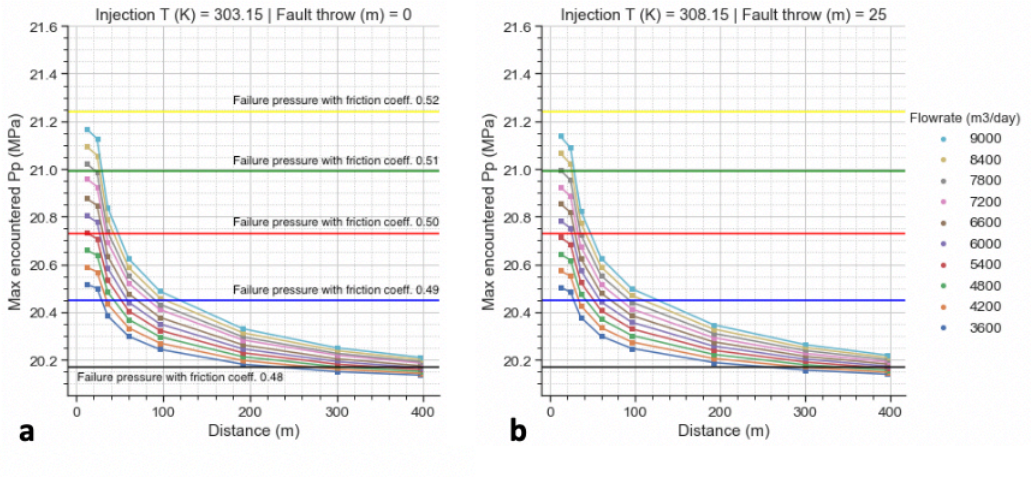

Figure 7.2.3: Comparison of the maximum encountered pressures after 30 years as result of injection temperatures of 303.15 K and 308.15 K and with a fault throw of respectively 0 m and 25 m. Both with increasing flowrate between 3600 and 9000 m^3/day and distance between the wells and the fault between 12 m and 396 m. Figure a shows the maximum encountered pressures next to a medium sealing fault when no throw is present and when an injection temperature of 303.15 K is used. Figure b shows the maximum encountered pressures next to a medium sealing fault when 25 m throw is present and when an injection temperature of 308.15 K is used.

7.2.3. Potential Development Strategy

In the presence of a medium sealing fault NPV outcomes up to €42.5 million can be reached, dependent on the used flowrate and injection temperature. Compared to the presence of a sealing fault higher profits between €130,000 and €540,000 are realizable if a medium sealing fault is present in the homogeneous Delft Sandstone reservoir. This is however minimal compared to the total range of the NPV outcomes in the extent of millions. The Highest NPV values are reached when wells are placed a minimum distance of 192 m from the fault and if a minimum rate of 7200 m^3/day is used. This strategy allows an operator independence of the used injection temperature and the fault throw to not exceed the MC failure criterion, even if the sandstone has relatively low values for the friction coefficient. Though, the injection temperature has a maximizing effect on the amount of NPV an operator can generate. This is all visible from Figure 7.2.4, which shows the profitability and the maximum encountered pore pressures for a reservoir with a medium sealing fault when no throw is present. Again, this is a narrowed down figure to discuss the outcomes with more simplicity. The combined results for all varying parameters in reservoir conditions and operational options on profitability and fault stability are given in Figure F.2.2 in Appendix F.

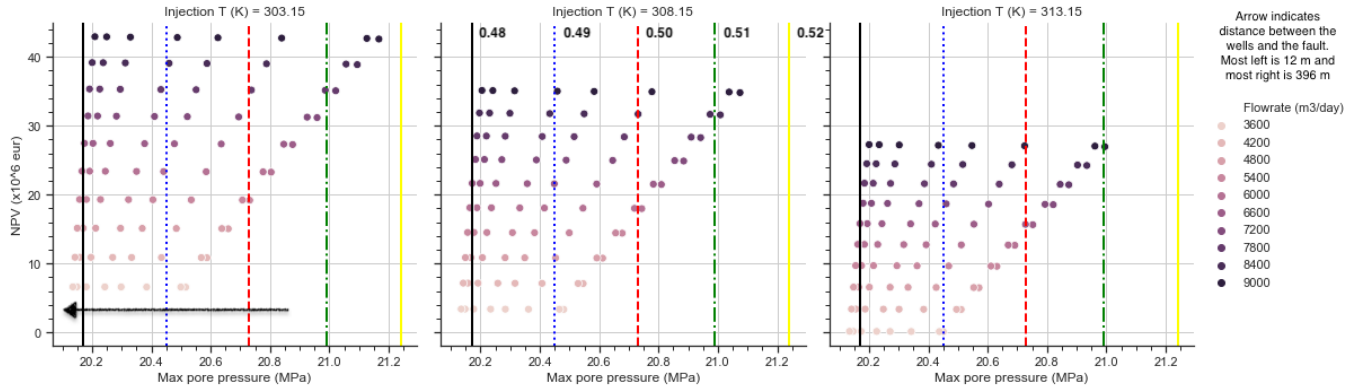

Figure 7.2.4: NPV and Maximum encountered pore pressures after 30 years as result of injection temperatures 303.15 K, 308.15 K and 313.15 K, increasing flowrate between 3600 and 9000 m^3/day and distance between the wells and the fault for a reservoir with a medium sealing fault when no throw is present. The vertical lines indicate the failure pressures for friction coefficients: 0.48 (Black), 0.49 (Blue), 0.50 (Red), 0.51 (Green) and 0.52 (Yellow). The arrow indicates increasing distance between the wells and the fault from right to left. Most right indicates 12 m between the wells and the fault and most left is 396 m.

As found earlier, the influences of the fault throw on the NPV outcomes are negligibly small considering the fact that the total profits of the project is in the extent of tens of millions. The fault throw does however influence the pressure build up next to the fault, but this can be minimized by placing the wells minimally 192 m from the fault. As discussed in the previous subsection, when wells are placed closer than 192 m from the fault every 25 m increase in fault throw makes a 600 m^3/day lower flowrate induce fault slip independent of the used injection temperature. Hence forcing an operator to use lower flowrates, resulting in about 13% lower NPV with every 600 m^3/day lower used flowrate. This is visible from Figure 7.2.5, which shows the profitability and fault stability as a result of increasing fault throw from 0 m, 25 m and 75 m and a constant injection temperature of 303.15 K. The figure also shows that using a higher injection temperature can make up for the loss in NPV due to the fault throw as it allows to use a 600 m^3/day flowrate. Therefore, it is essential for an operator to know the exact values of the fault permeability and friction coefficient of the sandstone in order to make the best possible combinations of operational options.

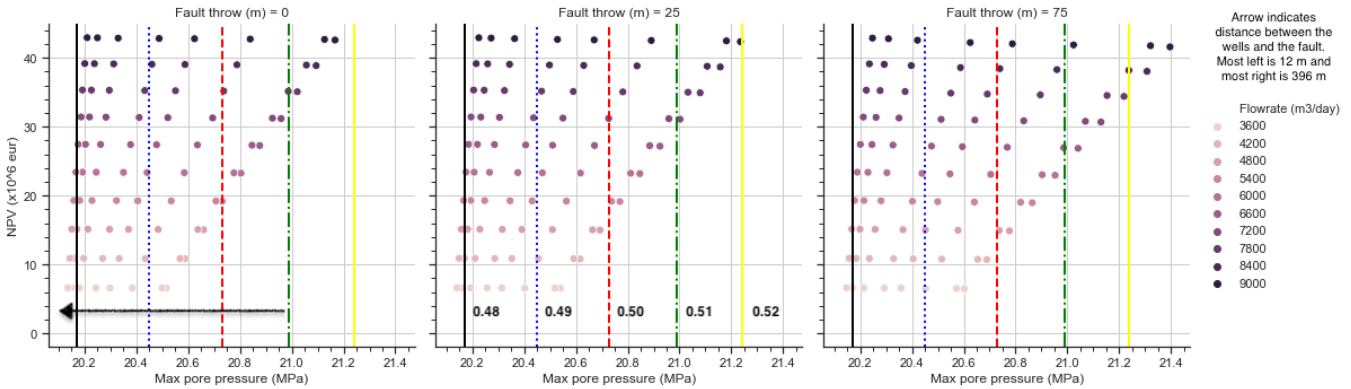

Figure 7.2.5: NPV and Maximum encountered pore pressures after 30 years as result of fault throws of 0 m, 25 m and 75 m, increasing flowrate between 3600 and 9000 m^3/day and distance between the wells and the fault for a reservoir with a medium sealing fault using a constant injection temperature of 303.15 K. The vertical lines indicate the failure pressures for friction coefficients: 0.48 (Black), 0.49 (Blue), 0.50 (Red), 0.51 (Green) and 0.52 (Yellow). The arrow indicates increasing distance between the wells and the fault from right to left. Most right indicates 12 m between the wells and the fault and most left is 396 m.

7.3. Development in the Presence of a Transparent Fault (750 mD)

This section presents and discusses the results of a reservoir in presence of a fully permeable fault with permeability of 750 mD. The results are presented and discussed based on the combined effects on the NPV and on the fault stability, after which the optimal development strategy is discussed.

7.3.1. Net Present Value

In the scenario of a homogeneous reservoir with a transparent fault it is again found that the influences of the injection temperature and the flowrate are consistent with those found for the presence of a sealing and a medium sealing fault. Additionally, it is found that the fault throw and the distance between the wells and the fault have extremely minimal influences on the NPV outcomes when a transparent fault is present. Minor influences are only noticeable when the throw has a large extent of minimally 75 m and when high flowrates are used, resulting from increasing distance between the wells and the fault. These differences range between €50,000 and €925,000 for increasing distance and when high flowrates of minimally 7200 m^3/day are used. This is visible from Figure 7.3.1. For throws of 0 m and 25 m the figure shows overlapping NPV outcomes, which means that the NPV values do not differ with increasing distance between the wells and the fault.

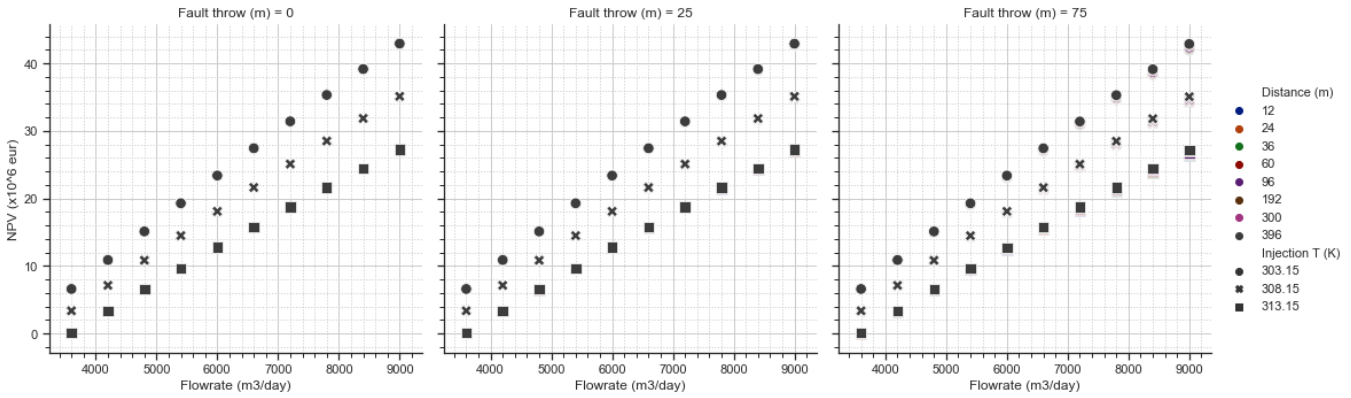

Figure 7.3.1: The combined influence of injection temperature, distance between the fault and the wells and flowrates between 3600 and 9000 m^3/day on the NPV in presence of a fully transparent fault.

7.3.2. Fault Stability

In general the maximum encountered pore pressure next to a transparent fault increases with increasing flowrate, decreasing distance between the wells and the fault and increasing fault throw, consistent with

the previous fault types. Additionally, it is found that in the presence of a transparent fault the sandstone can have lower friction coefficients without the MC failure criterion being exceeded. As a result higher flowrates could be used and the wells could be placed closer to the fault. It should however be noted that the presence of the fault throw might change this influence of a transparent fault on the pressure values when the wells are placed close to the fault. This is visible from Figure 7.3.2 showing the maximum encountered pore pressures next to the fully transparent fault for increasing fault throws of 0 m, 25 m and 75m. This figure shows results for flowrates between 3600 m^3/day and 9000 m^3/day, a fixed injection temperature of 303.15 K and increasing distance between the wells and the fault from 12 m to 396 m. A 25 m increase in fault throw makes a 600 m^3/day lower flowrate induce fault slip. This holds for each of the three considered injection temperatures, similar to the findings of the medium sealing fault.

With respect to the maximum encountered pressures next to a transparent fault it is found that the pressure values build up to significantly lower values compared to those found next to the medium sealing and a sealing fault. This results from the fact that injected water is able to flow across the fault, without any obstructions. Hence, the water does not accumulate directly next to the fault and this results in less pressure build up. This implies that the risk of fault slip is generally much smaller in the presence of a transparent fault, compared to the presence of a medium sealing or a sealing fault.

The complete figure of the resulting maximum pore pressures next to the fault as a result of the different reservoir conditions and operational options is given by Figure G.3 in Appendix G.

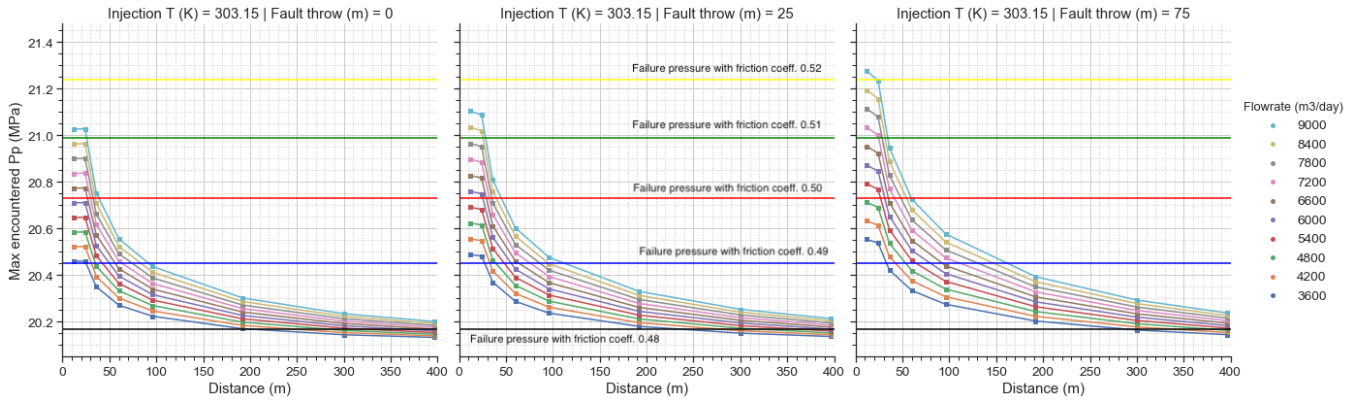

Figure 7.3.2: Maximum encountered pressures next to a transparent fault after 30 years as result of distance of 12 m, 24 m, 36 m, 60 m, 96 m, 192 m, 300 m and 396 m between the fault and the wells, flowrates between 3600 and 9000 m^3/day, fault throw of 0 m, 25 m and 75 m and a constant injection temperature of 303.15 K. The horizontal lines indicate the failure pressures as result of coefficients 0.48 (Black), 0.49 (Blue), 0.5 (Red), 0.51 (Green) and 0.52 (Yellow).

A note of caution in Figure 7.3.2 are the maximum encountered pressure values when the wells are placed 12 m from the fault, at which the curves are flattening. All encountered pressure values follow a reciprocal trend with decreasing distance between the wells and the fault, except for the pressure values at the closest distance of 12 m. These pressure values show a smaller increase compared to the others and this observation is strengthened by the extent of the fault throw. Namely, the maximum encountered pressure values in the presence of zero fault throw are equal when the wells are placed 12 m or 24 m from the fault. While the pressure values increase 0.1 MPa between the two distances when 25 m throw is present and about 0.5 MPa when 75 m throw is present. This observation can be explained by the influence of the fault throw and the positioning of the wells with respect to the fault. These influences are visualized by cross-sections of the reservoir showing the pressure distributions between the injection well and a transparent fault as result of 0 m throw, 25 m throw and 75 m throw are given by Figures G.2.2, G.2.3 and G.2.4 in Appendix G. When a 75 m throw is present next to the fault, only 30 m of transparent fault is left. This means that the injected water and built up pressure can only diverge to the other side of the fault via this 30 m of transparent fault. This is shown by the red plume on the left side of the fault in Figure G.2.4. The remaining 75 m of the fault, which is sealed due to the throw does not allow flow to adjacent blocks and therefore the pressure builds up. Placing the wells 24 m from the fault increases the lateral surrounding volume around the well, allowing the water and pressure to diverge into a larger volume. Because of this the pressure builds up to lower values. The same happens when a 25 m throw

is present next to the fault. Only 25 m of impermeable throw forms a barrier to flow, leaving 80 m of transparent fault left for the injected water and pressure to diverge. This causes a slight pressure build up compared to when the wells are placed 24 m from the fault. When zero throw is present the injected water and built up pressure can diverge easily to the other side of the fault, which spreads the pressure build up. As described in Chapter 4 the pressure build up is measured for the two layers directly next to the fault. When the wells are placed 12 m from the fault this means that the wells are in the vicinity of these two layers from which the pressure build up is analyzed. The maximum encountered pressure when the wells are placed 12 m from the fault shows the pressure in the first layer next to the fault. Which is the layer separating the fault and the injection well in Figure a of G.2.2. When the wells are placed 24 m from the fault the maximum encountered pressure is found in the second layer next to the fault, as this is closest to the injection well. As the water is injected with the same constant rate and at both distances the water can diverge away in the exact the same way, this results in the same values of the maximum encountered pressures for the two distances.

7.3.3. Potential Developement Strategy

Combining the results of the NPV and maximum encountered pore pressures next to the fault we see that placing the wells minimally 192 m from the fault and using a minimum flowrate of 7200 m^3/day maximizes the NPV outcomes and remains safe from inducing fault slip, provided that the friction coefficient is higher than 0.49. This applies to each used injection temperature and each considered value of the fault throw. This is visualized in Figure G.3.1 in Appendix G. As found from the previous results and consistent with the outcomes of a sealing and a medium sealing fault, the highest NPV outcomes of approximately €43 million result when using the lowest possible injection temperature. Figure 7.3.3 shows the NPV and maximum encountered pore pressures next to the fault when zero throw is present and for the three different injection temperatures. Compared to using an injection temperature of 303.15 K, increasing the temperature with 5 K decreases the maximum NPV outcomes by 17%. And increasing the temperature 10 K decreases the NPV outcomes by 35%. With respect to the fault stability, using a higher injection temperature allow as operator to use higher flowrates. A note of caution in the figure is in the presence of zero throw, for which the pressure at distances of 12 m and 24 m between the wells and the fault are equal. The reason for this is explained in the previous subsection.

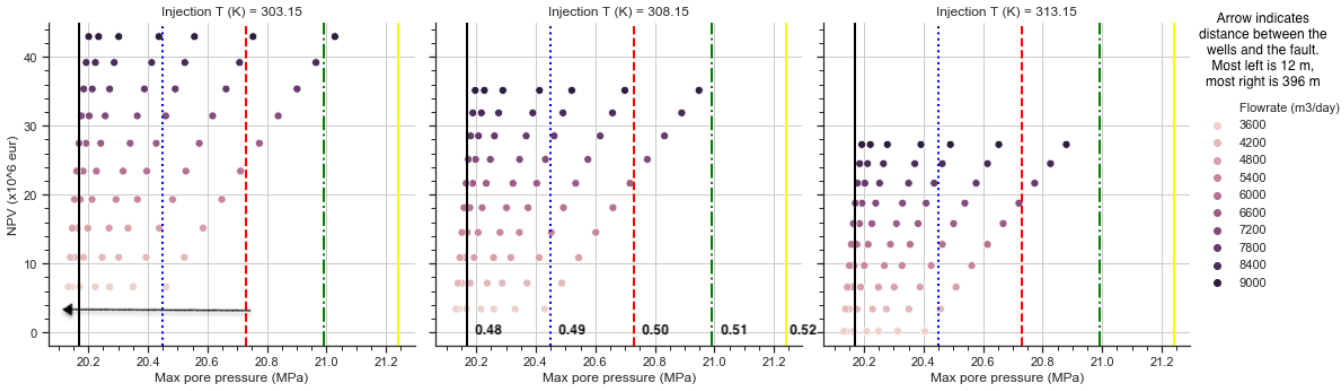

Figure 7.3.3: NPV and Maximum encountered pore pressures after 30 years as result of injection temperatures 303.15 K, 308.15 K and 313.15 K, increasing flowrate between 3600 and 9000 m^3/day and distance between the wells and the fault for a reservoir with a transparent fault when no throw is present. The vertical lines indicate the failure pressures for friction coefficients: 0.48 (Black), 0.49 (Blue), 0.50 (Red), 0.51 (Green) and 0.52 (Yellow). The arrow indicates increasing distance between the wells and the fault from right to left. Most right indicates 12 m between the wells and the fault and most left is 396 m.

Figure 7.3.4 shows the NPV and maximum encountered pressures next to the fault as result of increasing throw and a constant injection temperature of 303.15 K. With respect to the NPV maximizing strategy the fault throw has no significant influences. The fault throw does influence the fault stability when wells are placed closer than 192 m to the fault or when the sandstone has a lower than expected friction coefficient. However, similar to the previous two fault types the allowable injection temperature and flowrate to not exceed the MC failure criterion depend on the friction coefficient of the sandstone.

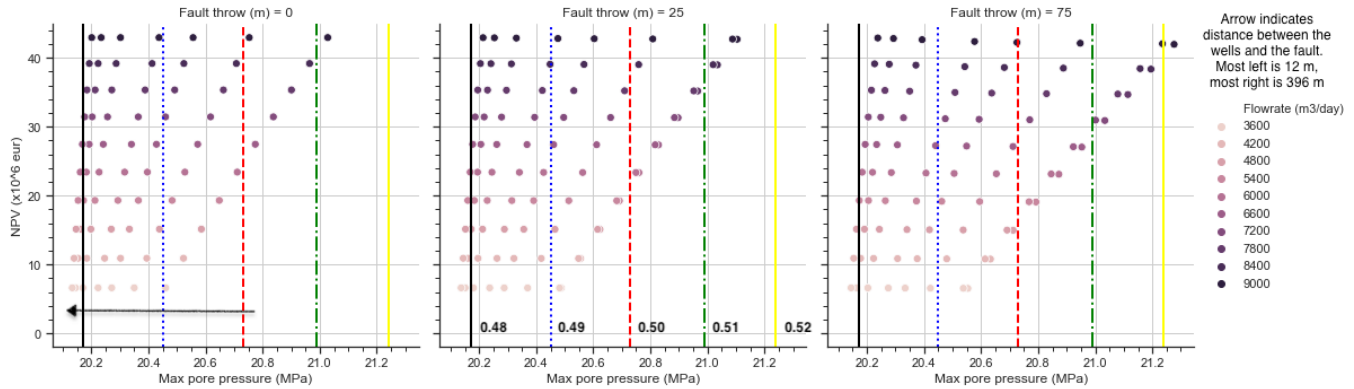

Figure 7.3.4: NPV and Maximum encountered pore pressures after 30 years as result of fault throws of 0 m, 25 m and 75 m, increasing flowrate between 3600 and 9000 m^3/day and distance between the wells and the fault for a reservoir with a transparent fault using a constant injection temperature of 303.15 K. The vertical lines indicate the failure pressures for friction coefficients: 0.48 (Black), 0.49 (Blue), 0.50 (Red), 0.51 (Green) and 0.52 (Yellow). The arrow indicates increasing distance between the wells and the fault from right to left. Most right indicates 12 m between the wells and the fault and most left is 396 m.

7.4. Comparison of the Development in Presence of a Sealing, Medium Sealing and a Transparent Fault

In this section the profitability and fault stability outcomes are compared of reservoirs in which a sealing fault, a medium sealing fault and a transparent fault are present. For consistency, the results are again discussed based on NPV outcomes, fault stability and finalized with the development strategies. The results in this section are simplified to four values for the flowrate and distance between the wells and the fault to keep the differences clear. For flowrate the used values are 3600, 5400, 7200 and 9000 m^3/day and for the distance between the wells and the fault the used values are 12 m, 60 m, 192 m and 396 m.

7.4.1. Net Present Value

Figure 7.4.1 shows a comparison of the NPV results for the three different faults when no throw is present.

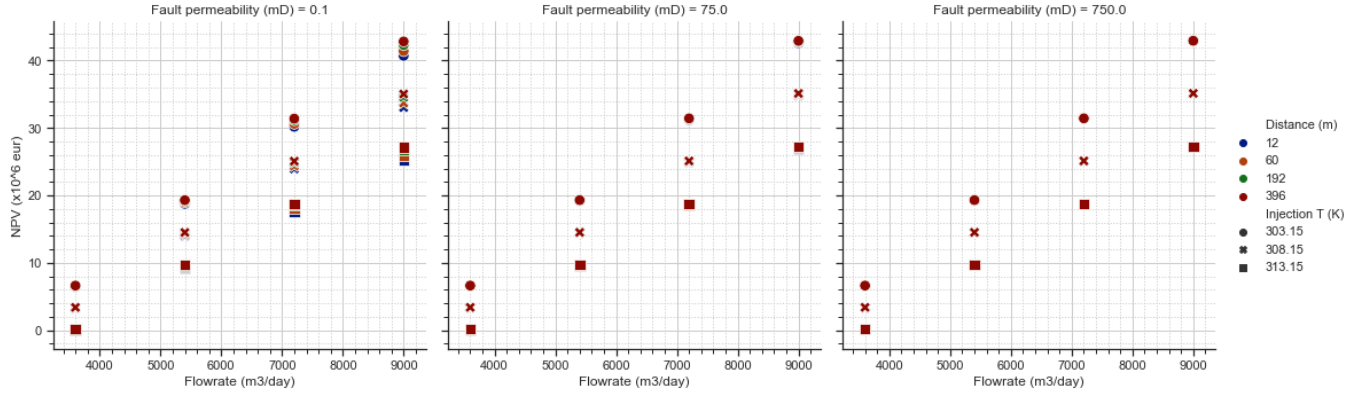

Figure 7.4.1: Comparison of the combined influence of injection temperature, distance between the fault and the wells and flowrates between 3600 and 9000 m^3/day on the NPV in presence of a sealing, a medium sealing and a transparent fault when zero throw is present

Comparing the NPV outcomes for situations in which the three different faults are present, we can say that injection temperature and flowrate are the main influencing operational parameters. NPV outcomes increase with increasing flowrate and decreasing injection temperature. With respect to the distance between the wells and the faults we see this is only influencing NPV outcomes significantly when the fault is sealing, since the NPV results are diverging with increasing distance. While the NPV results are roughly overlapping for the different distances when the faults are more permeable. In addition, the NPV outcomes at high flowrates converge towards a similar maximum value with increasing fault permeabilities and increasing distance between the wells and the fault. This is better visualized by Figure

J.1.1 in Appendix J, which shows the NPV outcomes with increasing distance for a rate of 9000 m^3/day and an injection temperature of 303.15 K. Increasing the wells distance from a sealing fault to 396 m compared to 12 m and using high flowrates of minimum 7200 m^3/day, increases the NPV approximately €2 million to €3 million. While this NPV increase is approximately €350,000 for the same distances in presence of a medium sealing and a transparent fault. In each of the three cases of the fault permeability the maximum NPV value is about €43 million when a flowrate of 9000 m^3/day is used and when the wells are placed 396 m from the fault. These maximum NPV outcomes for the three fault types differ in a range between €100,000 and €140,000 which is negligible. These results imply that NPV outcomes of a geothermal project have a plateau outcome and that NPV outcomes are positively affected by increasing fault permeability, as the wells placement with respect to the fault becomes less influencing. The latter is explained by two main reasons, which are the heat production and the pumping costs.

Heat Production

For more permeable faults the produced amount of energy is found to be relatively constant and similar at each flowrate and each distance between the wells and the fault (Figure J.2.1 in Appendix J). This amount of produced energy differs however significantly by the influences of the flowrate and the distance between the wells and the fault when a sealing fault present, especially when high flowrates are used and wells are placed close to the fault. This is visible from Figure 7.4.2, which shows the produced energy in kWh over time in the presence of a sealing fault. This figure and the mentioned figure in Appendix J assumes an injection temperature of 303.15 K and zero throw.

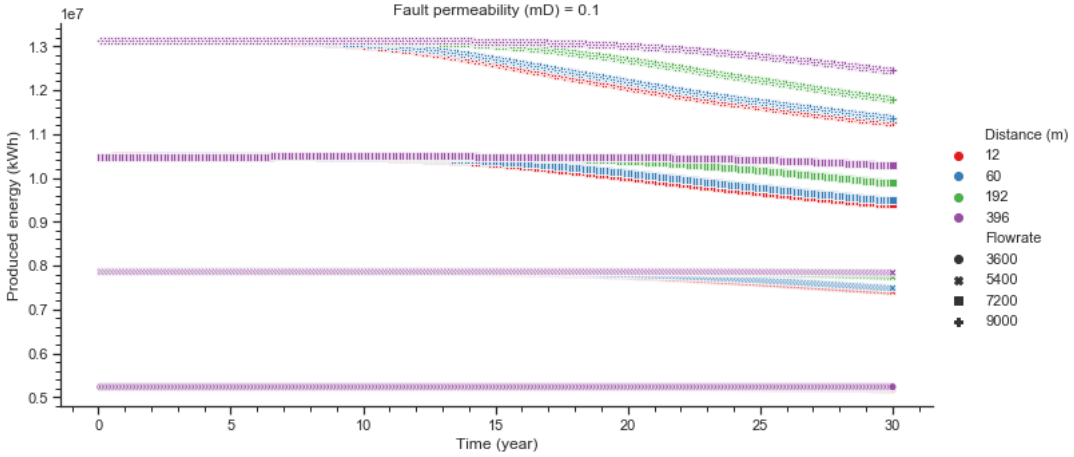

Figure 7.4.2: The combined influence of an injection temperature of 303.15 K, distance between the wells and the fault between 12 m and 396 m and flowrates between 3600 and 9000 m^3/day on the produced energy in the presence of a sealing fault

The energy production is coupled to the temperature of the production water. The production temperature starts dropping after approximately 10 years when a flowrate of 9000 m^3/day is used and the wells are placed 12 m from the fault, this is visualized by Figure J.3.1 in Appendix J showing the temperature of the produced water over time for the three different fault types and the same flowrates and distances between the wells and the fault. As a consequence of this temperature drop, the energy production starts dropping after 10 years as well which is visible from Figure 7.4.2. This decrease in production temperature and produced energy starts after approximately 20 years and in a much smaller extent when the wells are placed 396 m from the fault or when low flowrates are used. The earlier decline in production due to the close wells placement is explained by the barrier to flow formed by the sealing fault, which was also discussed in Chapter 6.2. The barrier to flow inhibits any connection between the blocks on each side of the fault, through which no flow is possible between the two sides. This results in a decrease of the lateral volume from which the wells produce heat. When the wells are placed close to the fault this lateral volume is decreased further, as the sealing fault forms an obstacle for flow. The influence of the sealing fault is avoided when the wells are placed far from the fault, resulting in a larger reservoir volume from which the wells produce heat. Hence, this results in a slower decrease of the temperature of the produced water, thus in higher amounts of produced heat and a higher NPV. The avoidance of the fault influence also explains the fact that maximum NPV values are similar for the three different faults.

For the more permeable faults flow between adjacent sides of the fault is possible, which increases the lateral volume from which heat can be produced. Closer placement of the wells to more permeable faults, therefore has less effects on the heat production. So when wells are placed further away from a sealing fault, the NPV outcomes become similar to those when more permeable faults are present.

Pumping Costs

The pumping costs have similar influences on the NPV outcomes. Similar to the trends of the produced heat, the pumping costs do not or minimally differ at each flowrate and distance between the wells and the fault when the faults are more permeable (Figure J.4.1 in Appendix J). For a sealing fault, however, the pumping costs increase more significantly when wells are placed close to the fault. Especially when high flowrates are used, as visible from Figure 7.4.3. This figure also uses data where the fault has zero throw.

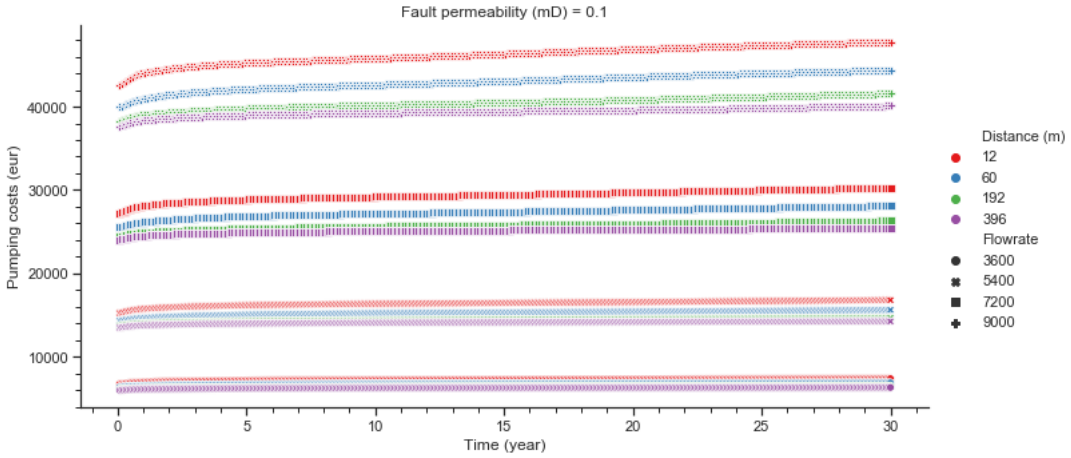

Figure 7.4.3: The combined influence of an injection temperature of 303.15 K, distance between the wells and the fault between 12 m and 396 m and flowrates between 3600 and 9000 m^3/day on the pumping costs in the presence of a sealing fault

This again results from the barrier to flow, blocking any interaction between the two fault blocks at each side of the fault. As explained earlier, placing the wells closer to a sealing fault further decreases the lateral area around a well. When wells are placed close to the fault and the injector well injects water, pore pressure builds up. Because of the smaller lateral volume the injected water and pressure diverge away less easily and cause a larger BHP build up (visualized in Figure J.6.1 in Appendix J). This study assumes constant flowrates during the entire production. To maintain constant flowrates and overcome the pressure build up, higher pumping pressures need to be applied. This increases the amount of energy required for production and injection, which increases the pumping costs. Hence lowering the NPV. On the contrary, when faults are more permeable the injected water and built up pressure can diverge across the fault causing less BHP pressure and decreasing the required energy and pumping costs (Figure J.6.1 in Appendix J).

With respect to the fault throw we have seen from previous results that this influences the NPV outcomes in combination with a more permeable fault and when it has a large extent of 75 m, though the influence is minimal (Figure J.1.2 in Appendix J). It is however found that NPV results show similar trends to the results in presence of a sealing fault, when a large fault throw is present next to a more permeable fault. This makes the distance between the wells and the faults more influencing in terms of the NPV outcomes with increasing fault throw. For a medium sealing fault NPV outcome increase with up to approximately €1.5 million when increasing distances between the wells and the faults from 12 to 396 m and using high flowrates. While this increase is up to approximately €0.9 million for the same parameters when a 75 m throw is present next to a fully transparent fault. The differences in NPV are caused by the earlier explained changes in heat production and pumping costs. Corresponding plots of the heat production and pumping costs are shown in Figures J.2.2 and J.4.2 in Appendix J. Throw does not influence a sealing fault, since it is already a barrier to flow. This is visible as NPV outcomes do not change with increasing fault throw. For all three cases of the fault permeability and independent of the

present fault throw it is found that NPV outcomes are maximized when wells are placed minimal 192 m from the fault and when a minimum flowrate of 7200 m^3/day is used.

7.4.2. Fault Stability

Figure 7.4.4 shows the maximum encountered pressures next to a sealing fault, a medium sealing fault and a transparent fault when zero throw is present and when an injection temperature of 303.15 K is used. As found in the previous results, with respect to the pressure build up next to the faults higher maximum pressures are encountered with increasing flowrates and with decreasing distance between the fault and the wells. When wells are placed close to the fault it is clear that lower pressure values are encountered next to faults with increasing permeability, as injected water and pressure diffuse away more easily when faults are more permeable. It depends on the friction coefficient of the sandstone what flowrate and wells placement stay below the MC failure criterion. Independent of the used operational options it is found for all three cases of the fault permeability, a friction coefficient of 0.47 and lower will definitely induce fault slip. While it is not likely that slip will be induced if the sandstone has friction coefficients of minimal 0.54. If the Delft Sandstone has a friction coefficient ranging between 0.47 and 0.54 it is highly essential to identify the exact value in order to adapt the used operational options such that the MC failure criterion is not reached. For a medium sealing and a transparent fault, Figure 7.4.4 shows that the sandstone can have a minimum friction coefficient of 0.49 to use all flowrates ranging between 3600 and 9000 m^3/day and when the wells are placed minimal 192 m from the faults. While for a sealing fault this minimum friction coefficient is 0.5 for the same operational parameters, as a rate of 9000 m^3/day induces fault slip if the sandstone has a friction coefficient of 0.49. If the wells need to be placed closer to the fault the combined influence of the friction coefficient, flowrate and fault permeability become essential to minimize fault slip.

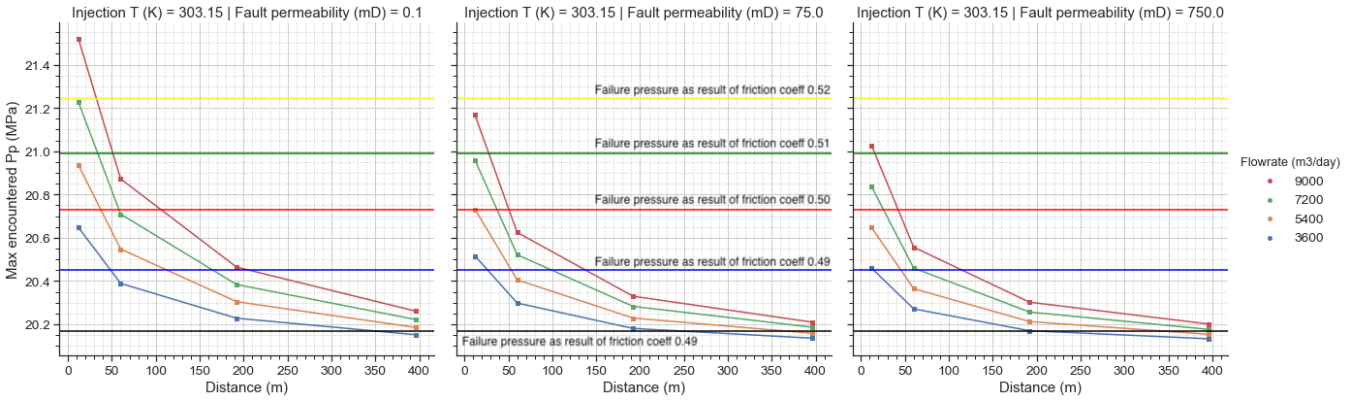

Figure 7.4.4: Comparison of the maximum encountered pressures next to a sealing, a medium sealing and a transparent fault after 30 years of production in presence of zero throw. As result of 303.15 K injection temperature, increasing flowrate between 3600 and 9000 m^3/day and distance between the wells and the fault of 12 m, 60 m, 192 m and 396 m. The figures show the results from left to right: sealing, medium sealing and transparent.

In general it is found for each of the three fault types that increasing the injection temperature 5 K, allows the use of a 600 m^3/day higher flowrate without exceeding the MC failure criterion. Additionally, the use of a higher injection temperature makes it possible to safely operate in a sandstone with a lower than expected friction coefficient without exceeding this failure criterion. Especially when a sealing fault is present in the reservoir. Using a higher injection temperature decreases the maximum encountered pore pressures next to the three different faults, as density and viscosity of the water decrease with increasing temperature. This improves the ability of flow of the water and results in lower pressure build up. Figure 7.4.5 shows the maximum encountered pressures next to the faults as result of using an injection temperature of 313.15 K. For the more permeable faults it still holds that a minimum friction coefficient of 0.49 allows to use all flowrates when the wells are placed minimal 192 m from the fault, without exceeding the MC failure criterion. However, for the sealing fault we see that increasing the injection temperature by 10 K allows a minimum friction coefficient of 0.49 as well to use all flowrates without exceeding the MC failure criterion. This is in contrary to using a 303.15 K injection temperature with which a rate of 9000 m^3/day exceeds the failure criterion if the sandstone has this friction coefficient.

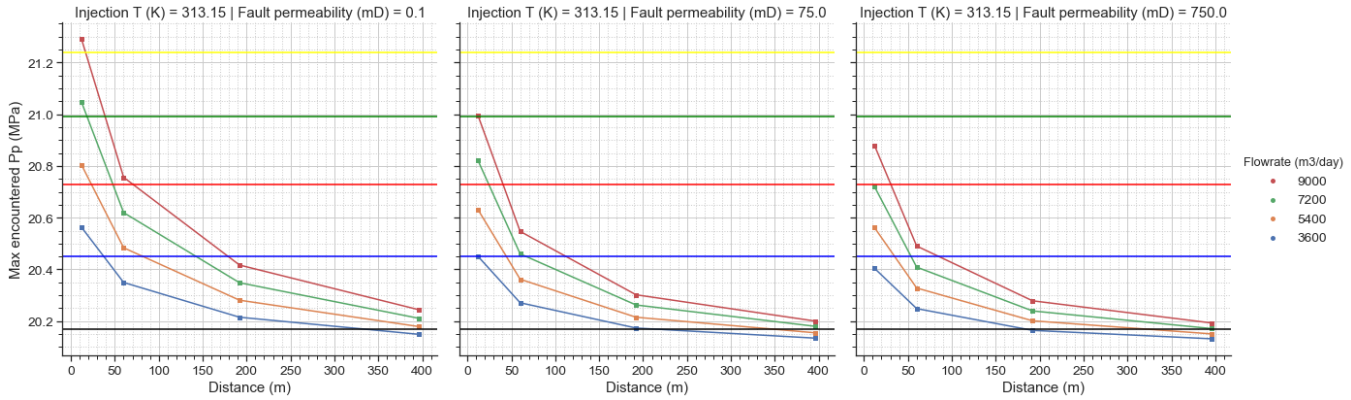

Figure 7.4.5: Comparison of the maximum encountered pressures next to a sealing, a medium sealing and a transparent fault after 30 years of production in presence of zero throw. As result of 313.15 K injection temperature, increasing flowrate between 3600 and 9000 m^3/day and distance between the wells and the fault of 12 m, 60 m, 192 m and 396 m. The figures show the results from left to right: sealing, medium sealing and transparent.

With respect to the fault throw influences we have seen that a large throw of 75 m could lead to increased pore pressures next to more permeable faults, compared to when zero or small throws of 25 are present. When no throw is present we see from Figure 7.4.4 that the maximum encountered pressures near more permeable faults are significantly lower compared to the pressures next to a sealing fault. However, when a medium sealing and a transparent fault are combined with 75 m throw we see from Figure7.4.6 that the encountered pressures are more similar to the results of a sealing fault, especially when low rates are used. We see no significant differences compared to when zero throw is present when the wells are placed minimally 192 m from the fault, which means that the fault throw influences are minimized by placing the wells far from the fault. If the wells need to be placed closer to the fault it is again important to look closely into what maximum flowrate and minimum injection temperature can be used in order to not exceed the MC failure criterion and risk fault slip.

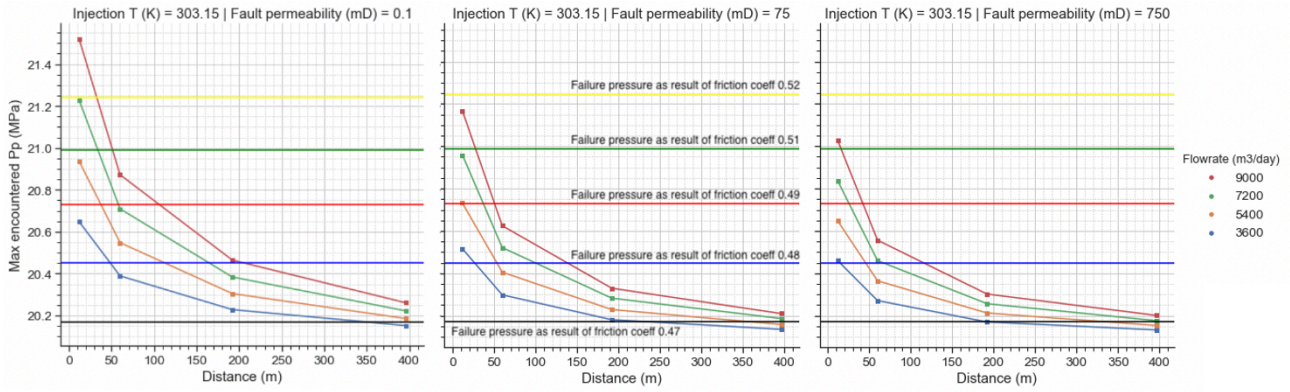

Figure 7.4.6: Comparison of the maximum encountered pressures next to a sealing, a medium sealing and a transparent fault after 30 years of production in presence of 75 m throw. As result of 303.15 K injection temperature, increasing flowrate between 3600 and 9000 m^3/day and distance between the wells and the fault of 12 m, 60 m, 192 m and 396 m. The figures show the results from left to right: sealing, medium sealing and transparent.

7.4.3. Potential Development Strategy

Figure 7.4.7 shows the NPV and maximum encountered pore pressures next to the three fault types when zero fault throw is present. The highest NPV outcomes are reached when the wells are placed minimally 192 m from the fault and when a minimum flowrate of 7200 m^3/day is used. Provided that the sandstone has a minimum friction coefficient of 0.5 if the fault is sealing and 0.49 if the fault is more permeable in order to prevent exceedance of the MC failure criterion with this strategy. With respect to the fault stability it is found that increasing the injection temperature by 5 K, allows an operator to safely increase the flowrate by 600 m^3/day and that the risk of exceeding the MC failure criterion decreases when lower

flowrates are used. These findings do however depend strongly on the permeability of the present fault and on the sandstone friction coefficient. If the friction coefficient is lower than expected or the wells are placed closer than 192 m to the fault an operator should carefully look into what combinations of flowrate and injection temperature he can safely use without inducing fault slip and at the same time generate high NPV outcomes. This means the operator should make a trade-off between the two parameters, which was also found by Daniilidis et al. (2016). Possible trade-offs are explained using a few examples given in Figure 7.4.7. According to Figure 7.4.7 lower maximum encountered pressure values and a 10% higher NPV could result from using an 1800 m^3/day lower flowrate combined with 10 K lower injection temperature, compared to the reversed combination. This is visualized by the dark box in the figure, which shows two data points of flowrates which are not likely to induce fault slip if the sandstone has a friction coefficient of 0.50. It should however be noted that this observation highly depends on the range of the considered flowrates and injection temperatures for the operation. For relatively low flowrates it is found that the use of an 1800 m^3/day higher flowrate with a 10 K higher injection temperature would still result in about 22% more profits compared to a low flowrate of for example 3600 m^3/day combined with an injection temperature of 303.15 K. A consequence is however that the pressure values increase as well. This is all visualized by the circle in Figure 7.4.7. Additionally, previous findings have shown that increasing NPV values result when relatively high flowrates are combined with a low as possible injection temperature. However, again the figure shows this goes paired with pressure increases. Based on these findings there are three possible strategies which could be used for the trade-off between the flowrate and the injection temperature. It is however important to note that it strongly depends on the friction coefficient and the fault permeability what actual values could be safely used for the operational parameters without exceeding the MC failure criteria. Additionally, it is important to investigate the freedom an operator has in making his choices with respect to the used operational options. Lastly, thermo-elastic properties of the sandstone are not taken into account in this study but may be influenced by the injection water with relatively low temperatures.

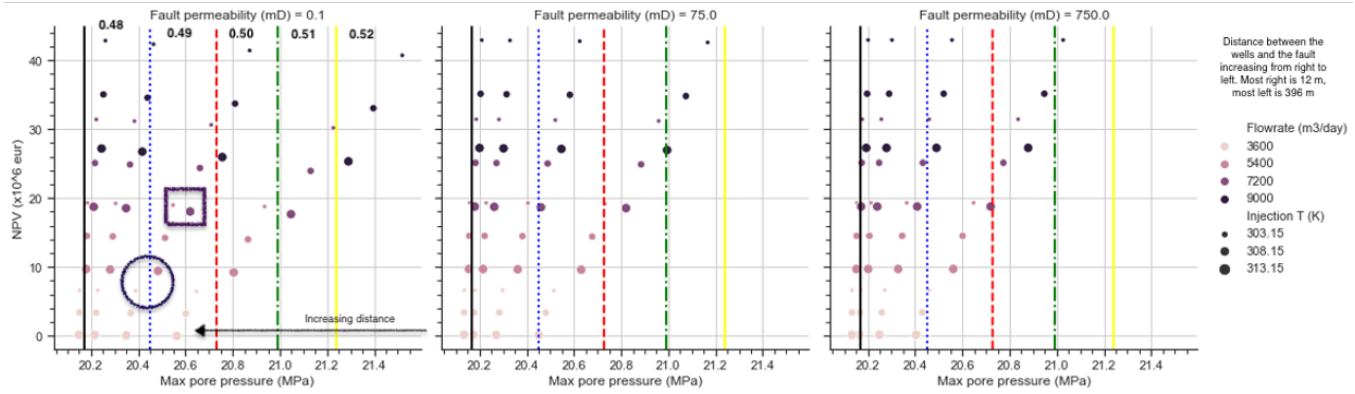

Figure 7.4.7: NPV and maximum encountered pore pressures next to the fault in presence of a sealing, a medium sealing fault and a fully transparent fault and when zero throw is present. Comparison of the combined influence of injection temperature, distance between the fault and the wells of 12 m, 60 m, 192 m and 396 m and flowrates between 3600 and 9000 m^3/day. The dark box highlights the NPV resulting from 7200 m^3/day flowrate combined with 308.15 K injection temperature and flowrate 5400 m^3/day combined with 303.15 K injection temperature. The circle highlights NPV resulting from 5400 m^3/day flowrate combined with 313.15 K injection temperature and flowrate 3600 m^3/day combined with 303.15 K injection temperature

The fault throw has no significant influences on the NPV, but does have influences on the maximum encountered pressures next to the fault. Which makes the fault permeability and the sandstone friction coefficient more important parameters to characterize compared to the fault throw. Figure J.5.1 in Appendix J shows all the results for the different fault throws and injection temperatures for the same four flowrates and distances between the wells and the fault.

8

Sensitivity Study

This chapter presents profitability and fault stability results of heterogeneous reservoir simulations based on the realistic Delft Sandstone reservoir used in this thesis to make a comparison with the outcomes of the homogeneous Delft reservoir and place this analysis in perspective. This is followed by the results of a sensitivity study to investigate the economic and technical robustness of the geothermal projects in the Delft reservoir.

8.1. Simulations with a Heterogeneous Delft Sandstone Reservoir

To better contextualize the results for the homogeneous reservoir, the profitability and fault stability are also researched for a 3D heterogeneous reservoir in the Delft area. This reservoir is based on the channelized DSSM and is modelled using the realistic porosity and permeability data of the real reservoir, visualized by figure 8.1.1. The properties of the simulated fault are assumed with the same values as used for the homogeneous reservoir.

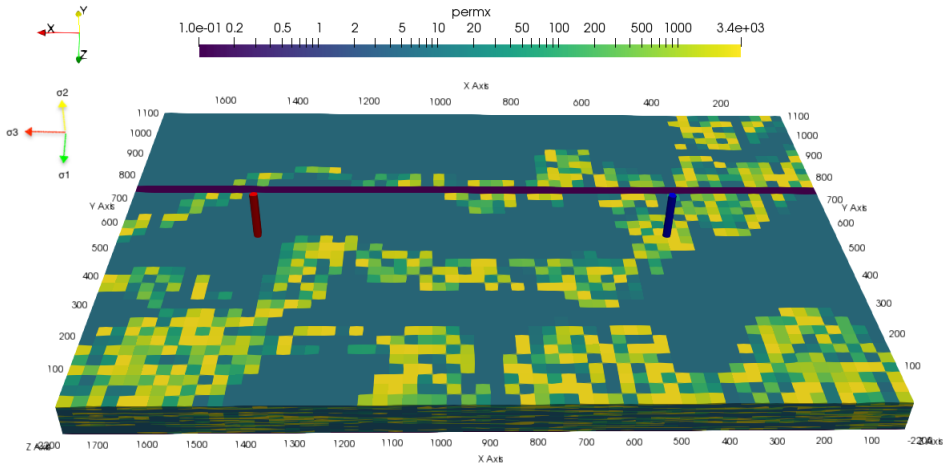

Figure 8.1.1: Angled overview of the 3D box model of the heterogeneous Delft Sandstone reservoir, with the injection well indicated blue and production well indicated red. Each cell is 30 m by 30 m by 2.5 m (x,y,z)

The simulations done for this reservoir have a mesh grid of 60 by 40 by 42 (x,y,z), which comprises 100,800 cells and the cells have dimensions 30 m by 30 m by 2.5 m. This mesh size is used as the poro-perm data is provided in this mesh grid. This makes the results for the heterogeneous reservoir slightly different compared to the results of the homogeneous reservoir which is simulated with a finer model resolution. An assumed fault is simulated with permeabilities of 0.1 mD and 750 mD and because of the used grid size this fault has a thickness of 30 m, while the fault in the homogeneous reservoir is 12 m.

The wells in this reservoir are positioned with a well spacing of 990 m, the injector well is positioned 450 m by 600 m (x,y) and the producer well is positioned 1440 m by 600 m (x,y). The depth of this reservoir is 2200 m. The remaining parameters remain the same as assumed for the homogeneous reservoir and this also holds for the varying parameters.

Figure 8.1.2 shows the profitability and the maximum encountered pore pressure next to the fault for the heterogeneous reservoir in the presence of a sealing and a transparent fault. These results are showing the influences of injection temperatures of 303.15 K and 313.15 K, flowrates between 3600 m^3/day and 9000 m^3/day and the distance between the wells and the fault of 60 m, 90 m, 180 m and 390 m. These distances are a proxy to the distances used in the simulations of the homogeneous reservoir, adjusted to the mesh size. A note of caution is the fact that the distance between the wells and the fault is adjusted by moving the fault. Hence, the fault location changes for each considered distance while the wells positioning remains fixed for all the simulations.

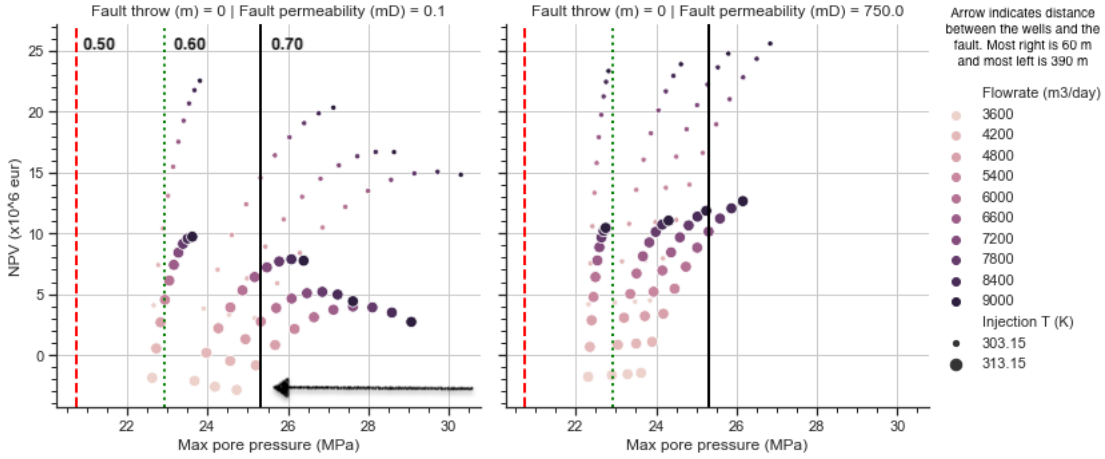

Figure 8.1.2: NPV and maximum encountered pore pressures next to a sealing and a transparent fault in the heterogeneous Delft Sandstone reservoir after 30 years of production. As result of 303.15 and 313.15 K injection temperature, increasing flowrate between 3600 and 9000 m^3/day and distance between the wells and the fault of 60 m, 90 m, 180 m and 390 m. Zero fault throw is assumed. The strong bend in the outcomes for the sealing fault result from the heterogeneity effects of the permeability on the NPV, caused by increased pumping costs and decreased heat production.

With respect to the NPV outcomes the figure shows that the maximum possible values depend highly on the fault permeability combined with the distance between the fault and the wells. In the presence of a sealing fault the NPV outcomes decrease significantly by approximately €2 million with decreasing the distance between the wells and the fault. Contrary to expectations based on the findings in the homogeneous reservoir, the NPV outcomes increase by €1 million with decreasing distance in the presence of a transparent fault. This discrepancy could be attributed to the heterogeneity effects on the energy required for the pumping, hence on the pumping costs. Plots of the required pumping energy are visualized in Figure K.2.1 of Appendix K. These figures show the required amount of energy as a result of the presence of the two different fault types and the earlier mentioned values for the operational options. The influences of the operational options on the required amount of energy during production are similar with the results found for the homogeneous reservoir when a sealing fault is present. The required amount of energy increases with increasing flowrate and with decreasing distance between the fault and the wells. In the presence of a transparent fault it is visible that higher amounts of energy are required with increasing distance between the fault and the wells and with increasing flowrate. The heterogeneous reservoir is a channelized reservoir, through which the permeability and porosity vary in space. In addition, the fault permeability is very high compared to the average reservoir permeability which means that the transparent fault enhances the reservoir permeability over a vicinity of 30 m. When the wells are placed 60 m from the fault the injected water, thus the pressure build up, must diffuse through 'only' 60 m of heterogeneous sediment after which the permeability is enhanced and the water can flow easier over a vicinity of 30 m. Hence, the pressure build up in the reservoir especially near the injection well (BHP) becomes relatively lower compared to when this enhancement is not taking place as is the case when a sealing fault is present (Figures K.3.1 and K.3.3 in Appendix K). When the wells are placed 390

m from the transparent fault this means the diffusion of the injected water is impeded over a larger area until the water reaches the fault. This results in a larger pressure build up in the reservoir, especially near the injection well which increases the BHP and therefore higher injection pressures are required to maintain steady flowrates (Figure K.3.2). The influences of the operational parameters and the reservoir conditions on the BHP are visualized in Figures K.4.1 and K.4.2 in Appendix K. The required amount of energy increases when higher pressures need to be applied which also means higher pumping costs. With respect to the amount of produced heat the results show consistent results compared to the homogeneous reservoir, namely the heat production increases with increasing distance between the fault and the wells and with increasing flowrate (Figure K.1.1).

Another clear result with respect of the NPV are the decreasing outcomes when the wells are placed closer to a sealing fault. This was also visible in the homogeneous reservoir, but the effects of the decreasing distance are intensified in the case of a heterogeneous reservoir. The reason for this is the barrier to flow caused by the sealing fault and the influence of the heterogeneous porosity and permeability on the flow. Varying permeability and porosity in a heterogeneous reservoir decreases the ability for flow, compared to the ability for flow in a homogeneous reservoir as the latter has constant flow properties throughout the entire reservoir. These heterogeneity properties are strengthened when combined with a sealing fault. As discussed in Chapters 6 and 7 placing the wells close to the fault increases the influence of the sealing fault as this decreases the volume available for heat production and water injection further, hence decreases the amount of produced heat and increases the pumping costs. The presence of a sealing fault results in $1x10^6$ kWh less energy production compared to a transparent fault as shown in Figure K.1.1 in Appendix K.

With respect to the maximum encountered pore pressure next to the fault it is visible from Figure 8.1.2 that higher friction coefficients of the sandstone are required in order to not exceed the MC failure criterion in the heterogeneous reservoir, compared to the homogeneous reservoir. In addition, the choice of the operational options depends highly on the fault permeability. When the wells are placed 390 m from the fault and the sandstone has a friction coefficient of 0.6 the maximum flowrate that does not reach the MC failure criterion is 4200 m^3/day with a sealing fault and 9000 m^3/day with a transparent fault. This is a significant difference and this affects the NPV drastically as it results in €1 million to €4 million NPV for the first case and in up to €23 million NPV for the second case. More operational options are available when the sandstone has a friction coefficient of 0.7.

Combining the profitability and fault stability results of the heterogeneous reservoir, we can say that the general influences of the considered reservoir and operational parameters of interest are similar for the homogeneous and the heterogeneous reservoir. However, the development strategies found for the homogeneous reservoir need to be adapted based on the fault permeability and the friction coefficient of the sandstone to make them suitable for the heterogeneous reservoir. Namely, placing the wells minimally 180 m from the fault (180 m in the heterogeneous reservoir is the proxy for the 192 m distance in the homogeneous reservoir) and using a minimum flowrate of 7200 m^3/day result in significantly different NPV outcomes in the presence of a sealing or a transparent fault. In addition we see that a high injection temperature combined with the distance between the wells and the fault influences the NPV outcomes largely when a sealing fault is present as this strengthens the effects of the heterogeneity and the barrier to flow on the heat production.

Comparing the outcomes of the homogeneous and the heterogeneous reservoir it is clear that the results in general show similarities with respect to the influences of the reservoir conditions and the operational options on the profitability and fault stability. The homogeneous reservoir simulations serve as a valid indication of the general influences of specific parameters on the geothermal production and the fault stability and based on these results good first indications and boundaries can be made in terms of possible development strategies. However, heterogeneous reservoir simulations are crucial in order to find the exact influences of specific parameters and to set up a development strategy. Nonetheless, the results for the heterogeneous reservoir are a clear indication that geothermal development strategies of geothermal reservoirs depend highly on the subsurface conditions. Therefore, the potential development strategies and the composition of the planned operational options are strongly related to geological uncertainties. This makes the identification of the rock frictional characteristic values and regional stress

values important in order to make valuable recommendations on the development strategy in order to maximize the profitability and minimize the fault stability risk. Similar to the homogeneous reservoir the profitability and fault stability of the heterogeneous reservoir depend highly on the positioning of the doublet, especially when a sealing fault is present. For the heterogeneous reservoir this is even strengthened due to the additional heterogeneity effects. Changing the doublet position can have big impacts as the permeable sandstone bodies differ in space. Researching the optimization of the wells placement is outside the scope of this thesis, but work on this topic has been done by Shetty (2017) and further investigation in this is highly recommended for future studies. Finally, the grid resolution of the porosity/permeability dataset should be refined in order to make more precise simulations of the DSSM reservoir and to make a more specific assessment of the profitability and fault stability risk of a geothermal reservoir.

8.2. Economic Robustness

As mentioned in Chapter 1 it is stated by the Dutch mining law that geothermal operators are required to have sufficient financial carrying capacity to compensate any financial setbacks due to technical problems encountered during development and production. This carrying capacity is required to be plentiful over the entire life cycle of the project and is checked when permits are requested, when the drilling and production operations commence and at several times during the production process (Wiebes, 2018). For operators it is therefore important to research the economic sensitivity and robustness of their prospected geothermal systems. In this thesis the economic robustness of the homogeneous Delft reservoir is researched in case of an economic downside and if subsidies would not be available. The economic downside is based on a low gas price caused by for example an oil crisis or an economic crisis.

8.2.1. Low Gas Price

Geothermal revenues are currently based on 90% of the TTF gas price and this research assumes a fixed gas market price of 0.016 eur/kWh. However, it is commonly known that the gas market price is highly volatile and depends on many political, social and natural circumstances. Especially a crisis such as the economic crisis from 2007 to 2009 influenced the gas prices drastically. Therefore it is essential to research the effects of such economical downtimes on the profitability of geothermal projects. Historical trading data over the last 10 years have shown that in times of low natural gas prices the prices were approximately 20% to 23% lower compared to the overall mean price during this time span (Trading Economics , 2020). Although this remains an approximation, a 23% lower gas price is therefore used to investigate the profitability sensitivity of a homogeneous geothermal reservoir. This gives a low gas price of 0.0123 eur/kWh. All other economic parameters remain unchanged and the results include SDE+ subsidies.

Figure 8.2.1.a shows the general trend of the NPV outcomes for the three different types of faults in case of a low natural gas price. These NPV outcomes result from flowrates between 3600 and 9000 m^3/day, distance between the fault and the wells between 12 m and 396 m and injection temperatures of 303.15 K, 308.15 K and 313.15 K. According to Figure a, the homogeneous reservoir can still result in a maximum NPV of €35 million in times of low gas prices. This is a 16.7% decrease compared to the economic output with the initially assumed gas price. The relative influence of the low gas price is bigger when low flowrates are used as is visible from Figure b, which shows the difference between the NPV outcomes for an injection temperature of 303.15 K and the considered flowrates and distances between the fault and the wells. Compared to the decrease in NPV outcomes with a rate of 9000 m^3/day, this decrease between times of normal gas prices and low gas prices is 20% for a rate of 6000 m^3/day and almost 30% for a rate of 4200 m^3/day. This results from the combined effects of the lower revenue price and the fact that relatively less heat is produced over time with lower flowrates.

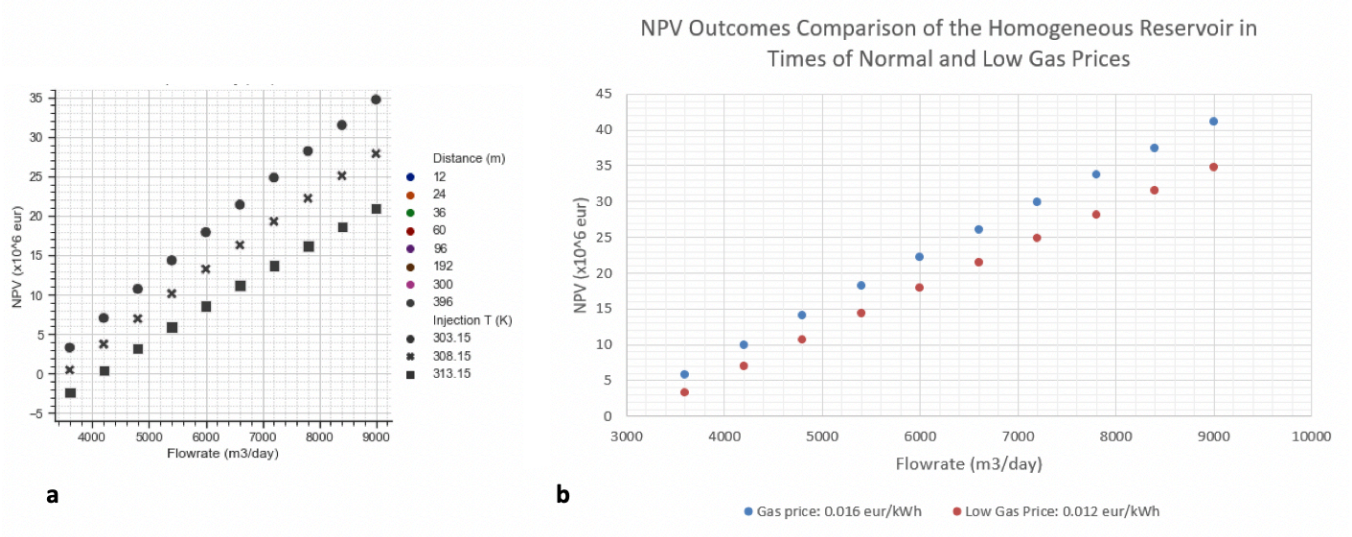

Figure 8.2.1: Comparison of the NPV outcomes in case of a low and a normal gas price in a homogeneous reservoir in the presence of a sealing, medium sealing and transparent fault. Figure a shows the general trend of the NPV outcomes as a result of a gas price of 0.0123 eur/kWh. Figure b shows the comparison between the NPV outcomes with injection temperature of 303.15 K and the considered flowrates in times of a normal gas price (0.016 eur/kWh) and in times of low gas prices. The assumed flowrates are between 3600 and 9000 m^3/day, the injection temperatures are 303.15 K, 308.15 K and 313.15 K and the distance between the fault and the wells is between 12 m and 396 m.

In times of low gas prices the real heterogeneous DSSM reservoir remains profitable with maximum NPV outcomes up to €15 million in the presence of a sealing fault and up to €19 million in the presence of a transparent fault, both provided that an injection temperature of 303.15 K is used. This is shown by Figure 8.2.2. For the heterogeneous reservoir this means a 35% and 27% decrease respectively compared to the NPV outcomes in times of normal gas prices. The NPV outcomes in times of normal gas prices are visualized in Figure K.5.1 in Appendix K.

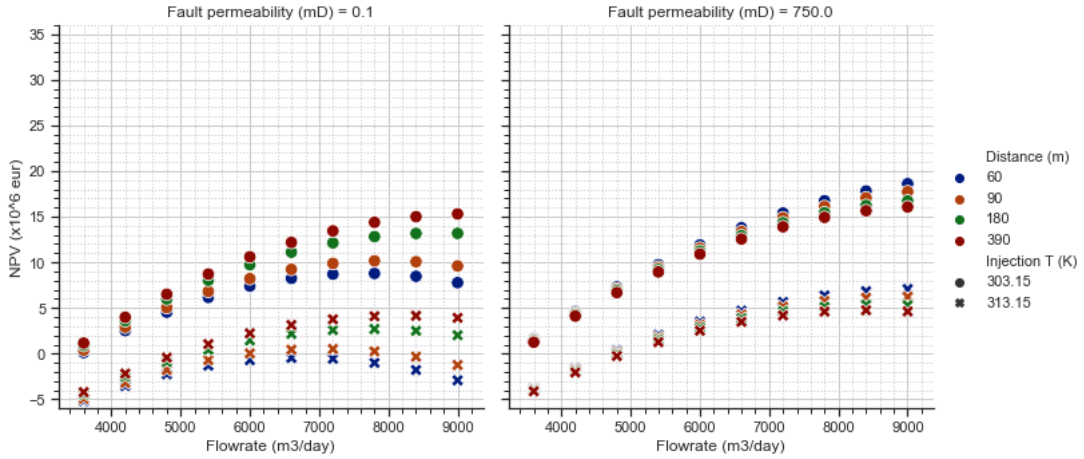

Figure 8.2.2: NPV outcomes of the heterogeneous reservoir in times of a low gas price of 0.012 eur/kWh in the presence of a sealing fault and a transparent fault. The results show the combined influence of 303.15 K and 313.15 K injection temperatures, flowrates between 3600 and 9000 m^3/day and distance between the fault and the wells of 60 m, 90 m, 180 m and 390 m.

An important note is the fact that the use of high flowrates combined with short distances between the wells and a sealing fault can result in negative NPV outcomes in times of low gas prices. This happens when an injection temperature of 313.15 K is used and is caused by the earlier discussed combined influence of the heterogeneous porosity and permeability of the reservoir and of the sealing fault, which inhibits flow. Both parameters influence the ability of flow and additionally the sealing fault decreases the lateral volume from which heat can be extracted and in which water is re-injected. As a result less

heat is extracted and the reservoir pressure builds up to larger values, which increases the pumping costs. Placing the wells close to the fault and increasing the flowrate increases this effect. The negative outcomes using high flowrates can be prevented by placing the wells minimally 180 m from a sealing fault.

8.2.2. Exclusion of the SDE+ Subsidy

The SDE+ subsidy provides financial compensation for the costs of the production of geothermal energy. Operators may request the subsidy if the expected amount of produced heat is estimated with 50% probability (Mijnlieff et al., 2017). The granting of the subsidy may be declined if this P50 probability is not met or if any geological or operational data is not provided in good order. Therefore it is interesting to investigate the sensitivity of the homogeneous Delft reservoir on its profitability if the SDE+ subsidy would be excluded from the total revenues. Figure 8.2.3.a shows the general trends of the NPV outcomes for the three fault types in a homogeneous reservoir when no subsidies are granted. Generally it is visible that homogeneous geothermal reservoirs could remain profitable without subsidies and result in a maximum NPV of €6 million. However, the profitability depends highly on the gas price volatility and therefore the gas prices are required to remain 'normal' (0.016 eur/kWh) in order to maintain this profitability. The figure shows that relatively high flowrates starting from 6600 m^3/day are required to remain profitable. In addition, if any regulations regarding the minimum injection temperature will be made the flowrate should even increase further for the project to remain profitable and this can influence the fault stability. In addition it is found that the wells positioning to the fault play an important role in the profitability, especially when a sealing fault is present. The wells need to be placed minimally 200 m from the fault to remain profitable. For shorter distances between the wells and the fault the NPV outcomes are negative. In all three cases of the fault permeability the project would breakeven if a flowrate of 6000 m^3/day is used combined with an injection temperature of 303.15 K, provided that the wells are placed minimally 192 m from a sealing fault.

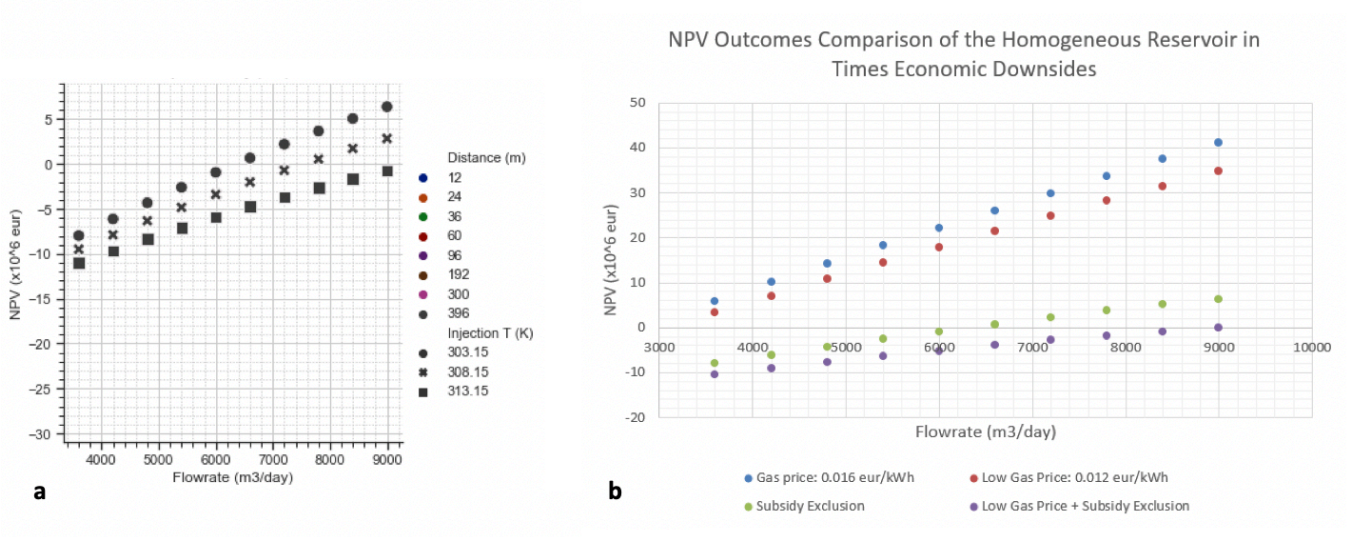

Figure 8.2.3: Comparison of the NPV outcomes in case of the exclusion of SDE+ subsidies in a homogeneous reservoir in the presence of a sealing, medium sealing and transparent fault. Figure a shows the general trend of the NPV outcomes for the three fault types when SDE+ subsudies are excluded. Figure b shows the overall results of the considered economic downsides for an injection temperature of 303.15 K, being times of low gas prices (0.0123 eur/kWh), exclusion of the subsidies and the combination of the two. The results show the combined influence of injection temperatures, distance between the fault and the wells between 12 m and 396 m and flowrates between 3600 and 9000 m^3/day.

In contrast to the results of the homogeneous reservoir, the NPV outcomes of the heterogeneous reservoir show that the project would result in negative outcomes for every considered combination of the operational options as shown in Figure 8.2.4. This means that a geothermal operation would not be able to commence in the real DSSM reservoir when subsidies are not available.

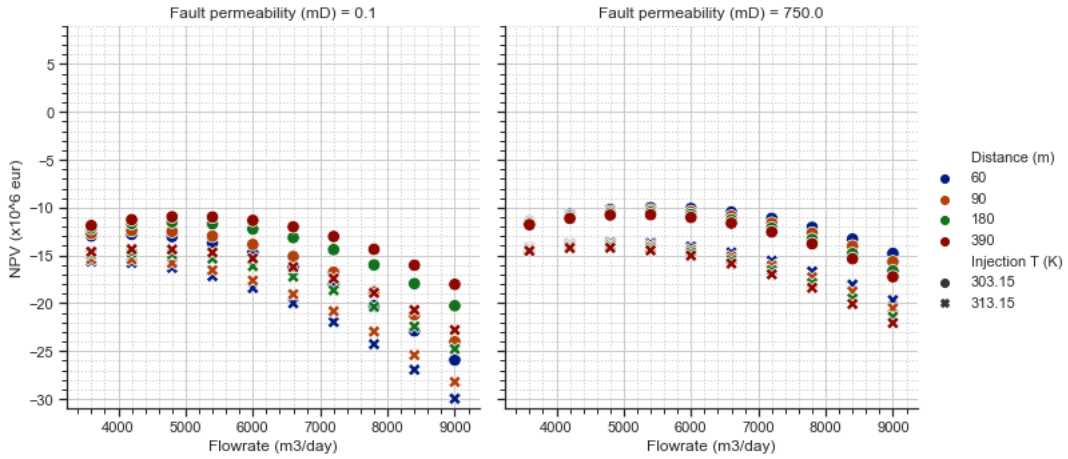

Figure 8.2.4: NPV outcomes of the heterogeneous reservoir when no SDE+ subsidy is granted in the presence of a sealing fault and a transparent fault. The results show the combined influence of 303.15 K and 313.15 K injection temperatures, flowrates between 3600 and 9000 m^3/day and distance between the fault and the wells of 60 m, 90 m, 180 m and 390 m.

A worst-case scenario for geothermal operators is the case in which the SDE+ subsidy is not granted paired with times of low gas prices. These outcomes for a homogeneous reservoir are visualized in Figure 8.2.3.b which shows a comparison of the NPV outcomes for each of the considered economic downsides and for the normal gas price. The outcomes show that it is impossible to commence geothermal operations in times of low gas prices if SDE+ subsidies are not available as all options result in negative NPV's. A project in the homogeneous Delft Sandstone would only breakeven if the operator uses a flowrate of 9000 m3/day, places his wells far from the fault and if an injection temperature of 303.15 K is used. However, a breakeven of the project is presumably not the aim of an operator and therefore this option would probably not commence. Regarding the heterogeneous reservoir this worst-case scenario results in only negative NPV outcomes (Figure K.5.2), since the outcomes are already negative when subsidies are excluded in times of normal gas prices.

The results of the economic sensitivity show that Dutch geothermal operators currently depend highly on the SDE+ subsidies in order to make high NPV profits and to make profits in general if they are producing with low flowrates between 3600 and 6000 m^3/day. This also means that the subsidies are very important for operators in order to maintain their financial carrying capacity. This outcome implies that geothermal operations are not possible in the Netherlands if the subsidies for geothermal operations would not be available or for some reason would no longer be granted. Especially if geothermal revenues remain coupled to the gas prices as these are highly volatile. It might therefore be worthwile to investigate the effects on the profitability if geothermal energy would be based on a heat price that does not depend of the gas price.

8.3. Technical Robustness: Different Regional Stress Values

The fault stability depends on the regional stresses in the surrounding area and on the rock frictional properties which determine the strength of the fault, like the friction and the cohesion coefficient. As a result, the stresses acting on a fault are partly defined by the orientation of the fault with respect to the regional stresses (Baisch et al., 2016). Depending on the regional stress field pre-existing faults can be oriented favourably for fault slip and others can be locked and therefore may not slip at all due to pressure increases. In this study one regional stress field is assumed with specific values and orientations of the principal stresses, which together assumes a certain fault orientation in the reservoir. It is therefore interesting to investigate the sensitivity of the fault stability in the reservoir if the fault orientation is assumed differently, by interchanging the values of the principal stress values. Especially since the regional pressure values remain uncertain, as they are based on assumptions. For the sensitivity research of the fault stability the values of the horizontal stresses, σ_2 and σ_3, are interchanged giving values of respectively 30 MPa and 34 MPa. The vertical stress, σ_1, remains unchanged as this stress originates from the overburden pressure.

Figure 8.3.1 shows the maximum encountered pore pressures next to a sealing, a medium sealing and a transparent fault in the homogeneous reservoir. The results are shown for an injection temperature of 303.15 K. All values of the maximum encountered pore pressures next to the three fault types remain below the failure pressure of a sandstone with a friction coefficient of 0.4. The minimum friction coefficient of a sandstone is 0.4, which means that the MC failure criterion is not reached in the homogeneous reservoir when the horizontal stress values are inversed compared to the original considered stress field.

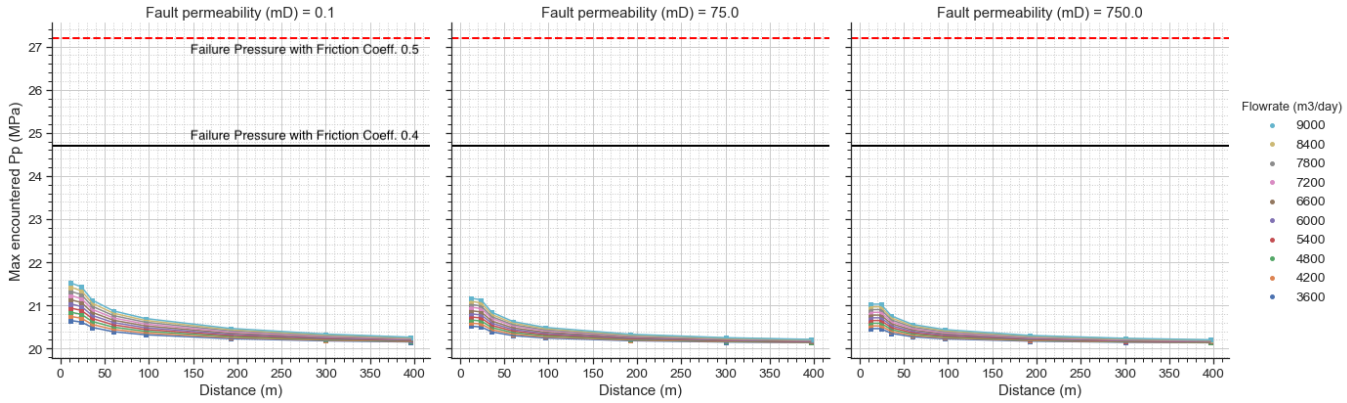

Figure 8.3.1: Comparison of the maximum encountered pore pressures in case of inversed horizontal stress values in a homogeneous reservoir in the presence of a sealing, medium sealing and transparent fault. The results show the combined influence of 303.15 K injection temperature, distance between the fault and the wells between 12 m and 396 m and flowrates between 3600 and 9000 m^3/day.

This large difference in fault stability compared to the original stress field is explained by the Mohr's circles in Figure 8.3.2. In the scenario of the original stress values the Mohr's circle has a three times larger circle radius compared to the circle in the scenario of the inversed stress values. Additionally, the circle center of the original stress field is located at a 2 MPa larger stress as the value for σ_3 is assumed to be 30 MPa in the original stress field and 34 MPa in the inversed stress field. The Mohr's circles show that a fault in the original stress field is likely to withstand less large pressure increases compared to a fault in the stress field with inversed horizontal stresses. More specifically, slip of a fault in the latter regional stress field is highly unlikely as a pressure increase of almost 20 MPa is required to exceed the MC failure criterion. With respect to the fault orientations in the homogeneous reservoir this implies that a fault in the reversed stress field is locked and a fault in the original stress field is oriented favourably for slip. Regarding the heterogeneous DSSM reservoir the reversed stress field allows the sandstone to have a lower minimum friction coefficient of the sandstone to not exceed the MC failure criterion, compared to when the original considered stress field is present. Although, it still depends on the fault permeability what operational options are safe to use to not exceed the failure criterion.

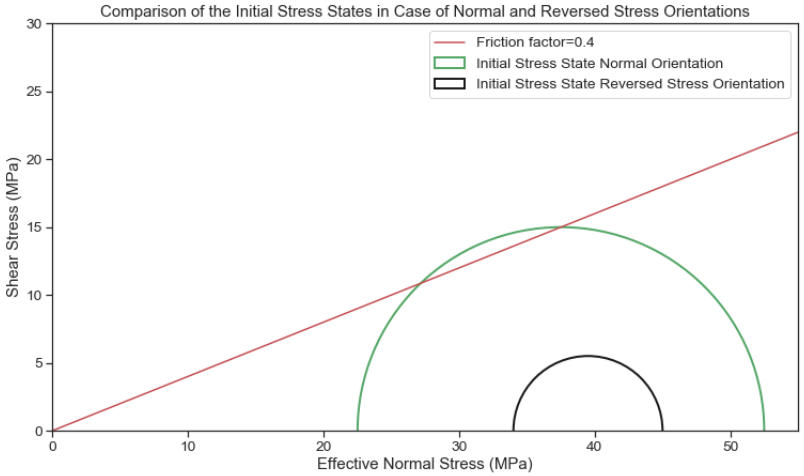

Figure 8.3.2: Comparison of the Mohr's circles in the scenario of the original considered regional stress values and the inversed regional stress values. Original stress values are: σ_1 = 45 MPa, σ_2 = 34 MPa and σ_3 = 30 MPa and the inversed stress values are: σ_1 = 45 MPa, σ_2 = 30 MPa and σ_3 = 34 MPa.

These findings show clearly what significant impacts different regional stress values and fault orientation can have on the fault stability. In the original considered stress field slip may be induced due to a very small increase in pore pressure, while the fault remains stable regardless of the amount of pressure increase when the principal stresses are slightly different. More specifically, even a very small alteration in the regional stress field may change the slip favorability of the fault. Based on the fault stability results of the research and the sensitivity it is clear that specific knowledge of the stress distribution in the subsurface is required to make a quantitative assessment of the fault stability. Especially the assessment of horizontal stress values in the subsurface is highly recommended as limited data on these values is available for the Netherlands.

9

Discussion and Conclusions

This chapter discusses the outcomes of the research based on defined guidelines by the the Ministry of Economic Affairs and Climate, SodM, the Dutch Mining Council and other involved stakeholders. The chapter is finalized with the conclusions of this thesis.

9.1. Discussion

Regulations for subsurface operations in the Netherlands are documented in the Dutch Mining act, which states that operators are required to submit an exploration plan to the Ministry of Economic Affairs and Climate (EZK) (Dutch Government, 2020). The Ministry grants permission for operations with the advise from SodM. Since 2003 it is required by this act that an exploration plan includes a risk assessment on the seismic risks possibly resulting from the planned subsurface operations (SodM, 2016). Initially it was set up for planned hydrocarbon operations, but nowadays it also holds for geothermal operations. To date there are no strict regulations for the placement of doublets with respect to pre-existing faults. Current practice is based on the risk assessment using the 'Qcon workflow', a three level approach to assess the seismic risk for geothermal fields (Baisch et al., 2016), and project specific requirements of the EZK policy. These practices are based on the technical advise of the SodM, TNO-AGE, the Technical Committee Ground Movement (Tcbb) and the advise of local governments (water boards and municipalities) and finally on recommendations made by the Dutch Mining Council. The Mining Council advises EZK and SodM on the exploration and production of hydrocarbons and geothermal heat, based on the advises of the earlier named stakeholders. A new guideline for geothermal operations is being developed by a number of involved parties, such as EBN, DAGO and TNO (Schoof et al., 2018). The aim is to define measures to prevent unwanted damages and safety risks, such as induced seismic events or groundwater pollution, caused by geothermal operations (Herber, 2020; Straver, 2019). The minimum distance between a geothermal doublet and a fault is to date not quantitatively documented. Because of this absence the Dutch Mining Council in their advise to EZK recommend to place the injection well not closer than 100 m from a fault and to place both the injector and the producer wells on the same side of a fault in order to prevent fault reactivation (Herber, 2020). It is important to note that these practical guidelines are used in the advice of the Dutch Mining Council until new guidelines for the assessment of the risk of seismicity in geothermal operations have been formulated.

The research results have shown that the NPV outcomes are maximized when using the highest possible flowrate. The results have also shown that the BHP in the reservoir increases when the reservoir permeability is low or when a fault with decreasing permeability is present, as the water can not diverge away easily. This pressure build up could lead to the exceedance of the MC failure criterion and hence possibly to fault slip. The used flowrate is correlated to the injection pressure, as higher pressures need be applied when larger flowrates are used and vice versa. With respect to the used flowrate and injection pressure there are no boundaries explicitly stated in the mining act. However, the SodM has set up a protocol with guidelines for the maximum allowable injection pressure (SodM and TNO-AGE, 2013). The protocol is intended to restrict the applied injection pressure in order to limit any negative influences on other nearby geothermal projects, underground gas and CO_2 storages and on subsurface bodies such as

drinking water containing layers and of course on cricitally stressed faults present in the area. According to SodM and TNO-AGE (2013) the applied injection pressure is especially important since water with low temperatures are injected, which additionally increases the pressure build up as the viscosity and the density of the water are lowered due to lower temperatures. Besides this, the injection of cold water may cause fracking as well. Therefore, the protocol states some general guidelines concerning the maximum allowable injection pressure and the used injection temperature according to the 'containment' and 'confinement' principle (SodM and TNO-AGE, 2013). The 'containment' part states that fractures, caused by pressure or temperature influences are acceptable, provided that the fractures appear limited and they only appear within the permitted area of the operator. However, these fractures are not allowed to affect any confining layers and the injected water must remain within the borders of the permitted area. In addition the used pressure and temperature are not allowed to induce any seismic events. Further specific guidelines or regulations concerning the used injection temperature are however not yet available.

The SodM protocol defines an equation for the determination of the maximum allowable Tubing Head Pressure (THP), which is given by equation 9.1 (SodM and TNO-AGE, 2013). For clarification, the THP is measured at the wellhead which is located at the surface.

$$THP_{Max} = Dt * (0.135 - HG_w) \tag{9.1}$$

With:

- THP_{Max} = Maximum allowable Tubing Head Pressure of the injection well (bar)
- Dt = Depth of the injection well from the surface to the top of the reservoir (m, TVD)
- HG_w = Hydraulic gradient of the local injection water as a function of the water salinity. Usually in the range of 0.103 to 0.108 (bar/m)

The maximum allowable THP for an average geothermal reservoir in the Netherlands at a depth of 2000 m and with a hydraulic gradient of 0.105 is 60 bar. The equation can also be defined for the BHP of the injection well and this is given by equation 9.2.

$$BHP_{Max} = Dt * 0.135 \tag{9.2}$$

The depth of the homogeneous Delft reservoir in this thesis is 2000 m, which results in a maximum allowable BHP of 270 bar. As was found from the results in Chapter 7 the BHP increases to higher values when the wells are placed close to the fault, when the fault permeability is low and when low injection temperatures are used (Figure J.6.1 in Appendix J). With respect to the SodM protocol all considered flowrates are safe to use in a homogeneous reservoir as all encountered BHP values are below the maximum allowable pressure. Therefore, in terms of the pressure guidelines it is theoretically unlikely that operations in the homogeneous Delft reservoir will cause any negative influences on nearby projects or subsurface bodies. Therefore the proposed development strategies for the homogeneous reservoir remain unchanged.

For the heterogeneous reservoir the maximum allowable BHP is 297 bar according to the SodM protocol, as the depth of the heterogeneous reservoir is 2200 m. As found in Section 8.1 in Chapter 8 the highest BHP values in the presence of a transparent fault are encountered at a wells positioning of 396 m from the fault, while this is 60 m for a sealing fault (Figure K.4.2 in Appendix K). Additionally the BHP in the heterogeneous reservoir builds up to significantly higher values compared to the homogeneous reservoir, due to the heterogeneity effects. With respect to the SodM protocol the maximum allowable BHP limit is clearly exceeded by the considered flowrates and this has big impacts on the potential development strategies in the real DSSM reservoir, which is also shown by Daniilidis et al. (2020b). Taking into account the protocol guidelines a maximum flowrate of 5400 m^3/day is allowed in the presence of a sealing fault, provided that the doublet is placed minimally 90 m from the fault. This flowrate may be maximized to 6600 m^3/day when an injection temperature of 313.15 K is used. In the scenario of a transparent fault the maximum allowable flowrate is 6000 m^3/day and this can be maximized to 7200 m^3/day with a higher injection temperature. Reflecting these flowrates back to the fault stability and profitability (Figure 8.1.2 in Chapter 8) a sealing fault remains stable if the wells are placed minimally 180 m from the fault and the friction coefficient should be minimally 0.7. The profitability would result

in a maximum NPV of €13 million. A permeable fault combined with a friction coefficient of 0.7 on the other hand remains stable with the maximum allowable flowrate if the wells are placed minimally 60 m from the fault and this results in a maximum NPV of about €25 million.

For the described specific values of the operational options to not exceed the SodM guideline and in both scenario's of the fault type in a heterogeneous reservoir the sandstone must have a minimum friction coefficient of 0.7 in order to not exceed the MC failure criterion. This means that the MC failure criterion could be exceeded with these specific values for the operational options when the sandstone has a lower friction coefficient, while the SodM criterium is not exceeded. Exceeding the MC failure criterion means there is a potential for fault slip to occur, which may reactivate a fault and might result in induced seismic events. The aim of the SodM protocol is to prevent any (damaging) seismic events and to keep the surrounding area of the injection well safe (SodM and TNO-AGE, 2013). The aim of preventing seismic events is therefore not met when taking into account rock frictional properties of the subsurface. Aditionally, there are no indications in the protocol of any inclusion of parameters that take into account the presence of pre-existing faults, which may be already critically stressed prior to the geothermal operations. As found from this study, the choice of the used values for specific operational options are essential in terms of the fault stability. Especially in combination with the present geological parameter values of the reservoir. Without doing any additional research into present faults the outcome of the maximum allowable pressure implies that the operator may use the highest flowrate possible. However, this is not the case when taking into account the friction coefficient of the sandstone, the fault permeability and the placement of the wells with respect to the fault. This implies that the protocol of the SodM is a good initial reference point for the maximum allowable injection pressure and flowrate, but additional in-depth research is required in terms of pre-existing faults and friction coefficient (MC failure criterion) to certainly prevent possible induction of seismic events.

The development strategies and allowable operational options change when taking into account the practical advise of the Mining Council to EZK. As mentioned earlier they generally have two recommendations of which placing the doublet on the same side of the fault is already satisfied in this study. Secondly, they advise to place the wells minimally 100 m from a pre-existing fault. In each of the three cases of the fault type (sealing, medium sealing or transparent) in the homogeneous reservoir the sandstone must have a minimum friction coefficient of 0.5 in order to use a maximum flowrate of 9000 m^3/day and each injection temperature at this well placement from the fault. The operational options are more critical when the sandstone has a friction coefficient of 0.49. Placing the wells minimally 100 m from the fault allows the maximum flowrate to 4800 m^3/day for a sealing fault, for a medium sealing fault to 7800 m^3/day and for a transparent fault to 9000 m^3/day in order to not exceed the MC failure criterion and potentially induce slip. This still results in significant NPV outcomes in the range between €15 and €43 million. Using a higher injection temperature allows the use of higher flowrates but the presence of a large fault throw can again lower the allowed maximum flowrates. The development strategies found in this thesis recommends a minimum distance between the wells and the fault of 192 m, but it should be noted that this also takes into account the maximizing of the NPV outcomes. Based on these outcomes this practical advise is therefore a valid guideline and is in line with the development strategies found in this study. Still, based on the considered MC failure criteria the wells could be placed even closer then 100 m from the fault without exceeding the failure criterion, it depends however strongly on the value of this criterion and the fault permeability. To give an example, for more permeable faults in a homogeneous reservoir it is possible to place the wells 36 m or 60 m from the fault without exceeding the MC failure criterion of a 0.5 friction coefficient with relatively high flowrates. Though, the used flowrates should be adapted accordingly to not exceed the criterion. In the heterogeneous reservoir it is possible to place the wells 60 m from a transparent fault and use a flowrate up to 6600 m^3/day without exceeding the MC failure criterion of 0.7 friction coefficient. It is however not possible to place the wells closer than 100 m to a sealing fault, provided the sandstone has a friction coefficient of 0.7, as this results in negative NPV outcomes and would not commence. The recommendations of the Mining Council to EZK are therefore a safe guideline with respect to exceeding the MC failure criteria and with that minimize the potential risk of fault slip, however if needed because of for example surface spatial planning it is possible to place the wells closer to a more permeable fault without exceeding MC failure criteria.

Regarding the injection temperatures the outcomes of the fault stability show clear indications of trig-

gering exceedance of the MC failure criterion when low temperatures are used and this is line with what is found in literature. The lower the used injection temperature, the higher the pressure build up next to the fault and this influence is strengthened combined with other operational options and by specific reservoir conditions. Especially when the fault has a low permeability and if the rock frictional properties of the sandstone are not favorable the used injection temperature is a critical parameter. Setting up specific regulations regarding the minimum allowable injection temperature based on the reservoir properties, wells positioning with respect to the fault and the maximum allowable flowrate is therefore highly recommended. It should be noted that this study did not take into account the specific thermo-elasticity properties of the subsurface and these properties could have additional effects on the pressure build up as well.

The risks of fault instability due to geothermal operations and possible mitigation options are continuously researched. Possible hazard mitigations by means of potential development strategies are proposed based on the results of this thesis and on the recommendations and regulations defined by EZK, which takes into account the advises of the SodM, the Mining Council and involving stakeholders. It is however important to note that these outcomes go paired with uncertainties as the identification of reservoir conditions such as pre-existing (critically) stressed faults and the sandstone friction coefficient in the area of interest are prone to practical limitations and uncertainties (Baisch et al., 2016). The initial fault strength depends on the regional stress values and the orientation of the fault and therefore it is very important to find the exact values of these parameters in order to do an accurate assessment of the fault stability. In addition, even the most detailed 3D seismic surveys and processing for fault interpretationare subject to resolution limitations and uncertainty regarding the exact fault position (Baisch et al., 2016). This makes the identification of present faults and their properties inherently uncertain. The location of faults in the subsurface could be misinterpreted with tens to hundreds of meters, as result of for example limited seismic data or poor time to depth conversions. Hence, taking into account this uncertainty of the fault location it is on closer inspection a fair point of debate to not place the geothermal doublet closer than 36 m from the fault as the actual fault location could be within this vicinity. Especially taking into account the assumed grid size of this study, which comprises 12 m per cell and is thus also prone to uncertainty.

9.2. Conclusions

The objective of this research was to assess the combined influences of specified reservoir conditions and operational parameters on the profitability and the fault stability of a geothermal project in the Delft Sandstone reservoir. Based on these influences potential development strategies are designed in order to maximize the profitability and to minimize the risk of fault instability, by not exceeding defined Mohr Coulomb failure criteria. The reservoir conditions assessed in this research include the fault permeability, the fault throw and the friction coefficient of the sandstone. The operational parameters include the flowrate of the injector and the producer, the injection temperature and the distance between the wells and the fault. To assess the profitability an economic model is developed, based on the Dutch economic system and this is an expanded and revised version of the models described by Daniilidis et al. (2017); van Dongen (2019a). The fault stability model is based on the theory of Mohr Circles and using regional and local stress values in the reservoir. Both models use production and pressure data simulated with DARTS. The conclusions of this thesis are presented by answering the research questions.

- **How does the presence of a sealing or a non-sealing fault in a reservoir influence the economics of a geothermal project?**

  A sealing or a non-sealing fault influences the project profitability, but the extent to which the NPV changes depend highly on the used operational options. The results of the research show that the NPV outcomes for a homogeneous geothermal reservoir increase with increasing fault permeability. The extent to which the outcomes increase with increasing fault permeability depends highly on the used operational options. An operator makes less profit when a sealing fault is present in the reservoir and this results from higher pumping costs and an earlier decline in the heat production. A sealing fault acts as a barrier to flow and inhibits any flow between the blocks adjacent from the fault. Hence, a sealing fault decreases the lateral volume available for heat extraction. As a result the production temperature starts decreasing earlier during the geothermal project, resulting in a reduced amount of produced energy and NPV as a consequence. These results are in contrast

to a fault with higher permeability, which show almost constant energy production over the entire project lifetime. Additionally, the barrier to flow causes an increasing bottom hole pressure as injected water can flow away less easily. Hence larger pressures need to be applied for pumping to maintain constant flowrates and this results in larger amounts of required pumping energy and thus in higher pumping costs.

- **What combination of reservoir conditions and operational options is of key importance in making a geothermal project profitable?**

The study has shown that the NPV outcomes depend mostly on the used flowrate and injection temperature independent of the present reservoir conditions. Increasing the used flowrate from 3600 m^3/day to 9000 m^3/day increases the resulting NPV almost 6 times. And using a 5 K lower injection temperature increases the NPV outcomes 19% to 43%, depending on the used flowrate. The influence of using a 5 K lower injection temperature is relatively higher on low flowrates (43% for a flowrate of 3600 m^3/day) compared to high flowrates (19% for a flowrate of 9000 m^3/day) as relatively less heat is produced with low flowrates. Still, the NPV outcomes are maximized when high flowrates are combined with the lowest possible injection temperatures. Up to 10% higher NPV values result when combining a 5 K higher injection temperature with a 600 m^3/day lower flowrate. The distance between the wells and the fault is found to have a particularly significant influence in combination with a sealing fault. Due to the barrier to flow caused by the sealing fault, a close placement of the wells to the fault has a negative influence on the heat production as the lateral volume decreases. More specifically, this combined effect of the wells placement and the sealing fault is strengthened when high flowrates are used. It can therefore be concluded that the negative effects of a sealing fault on the profitability can be minimized by placing the wells far from the fault. With respect to the reservoir conditions the simulations with the homogeneous reservoir in Chapter 7 suggest that the fault permeability is the factor that has the largest influence on the profitability of the geothermal project. However, the heterogeneous reservoir simulations suggest that the porosity and permeability distribution of the real reservoir is a highly influencing factor as well. In reality the reservoir conditions cannot be changed (although uncertain) and operational options need to be adjusted to these properties in order for a geothermal project to be profitable. In general it is found for both sealing and more permeable faults in a homogeneous reservoir that the NPV outcomes of a geothermal project can be maximized by placing the wells a minimum distance of 192 m from the fault and using a minimum flowrate of 7200 m^3/day, without exceeding the MC failure criterion and potentially induce fault slip. This strategy is based on the fact that the NPV outcomes of the study tend towards a plateau outcome for each of the three fault types.

- **What reservoir conditions are of key importance for the possible occurrence of fault reactivation?**

From this study it is found that exceeding the Mohr Coulomb failure criterion, hence the fault slip tendency, depends highly on the fault permeability and on rock frictional characteristics of the sandstone, such as the friction coefficient. With respect to the fault permeability the pressure builds up to higher values next to a low permeable (sealing) fault, compared to more permeable faults as it counteracts flow across the fault surface. Hence, slip of a sealing fault is induced faster and from this it can be concluded that the MC failure criteria are more likely to be exceeded in the presence of low permeable faults, compared to more permeable faults. The stability of more permeable faults can however be decreased by the presence of a large throw as a throw acts as an additional barrier to flow. For a homogeneous Delft Sandstone the maximum friction coefficient that will certainly lead to exceeding the MC failure criterion is 0.47, whereas a friction coefficient above 0.54 is always safe, regardless of the used operational options and the fault permeability. For friction coefficients ranging in between these two 'extreme' values it is essential to take into account the fault permeability and the planned operational options when researching the fault slip tendency based on the MC failure criteria. It is therefore highly recommended to characterize the exact value of the friction coefficient to make meaningful predictions on the fault slip. A note of caution is the fact that the framework of this study assumes one specific regional stress field, which defines one specific fault orientation. Additionally, information about regional horizontal stress values in the Netherlands is very limited and therefore the values used in this study are based on assumptions

which makes the outcomes of the study regarding the fault stability conditioned to the availability of better stress field characterization. Interchanging the horizontal stress values has shown that the fault slip tendency depends highly on the fault orientation and the regional stress values, which makes the investigation of the regional stress values a fruitful area for further work.

- **How sensitive is the possibility of fault reactivation in the Delft Sandstone Member to different development options?**

  Critically stressed faults may be stable prior to the production process, but the outcomes of this study have identified the essential influences of the used operational options on the fault stability. The sensitivity of the fault slip tendency depends highly on the used flowrate, injection temperature and the distance between the fault and the wells. However, the combination of the fault permeability and the friction coefficient of the sandstone is the decisive factor in what development options can potentially be used without exceeding MC failure criteria, hence potentially inducing fault slip. In general it is found that the lowest possible flowrates and the highest possible injection temperatures should be used in order to prevent fault slip. As smaller volumes of water are injected per unit of time with low flowrates and higher injection temperatures increase the viscosity and the density of the injection water which allows it to flow more easily, hence resulting in less pressure build up. On the contrary, higher values of the friction coefficient allow the use of larger flowrates and lower injection temperatures to remain safe from exceeding the MC failure criterion. With respect to the operational options the results have shown that using a 5 K lower injection temperature allows the use of a 600 m^3/day higher flowrate. Development strategies depend strongly on the reservoir conditions and the placement of the wells with respect to the fault, which makes it difficult to set up one specific recommendation regarding the development. Altering the value of one specific parameter like the friction coefficient of the sandstone requires alterations of the operational options. Therefore it can be concluded that the chance of reactivation of faults depend on the development options. Based on the study of the homogeneous reservoir a potential strategy is set up in which it is recommended to place the wells minimally 200 m from the fault and use a minimum flowrate of 7200 m^3/day, regardless of the fault type. However, alterations of the used flowrate, injection temperature or the distance between the wells and the fault are needed when taking into account the friction coefficient. It is therefore possible to set up a general development strategy for a geothermal project, but it depends highly on location specific reservoir conditions.

- **What regulations and guidelines need to be considered for the potential development strategies in the Netherlands?**

  Based on the outcomes of this study it is possible to set up a general development strategy in order to prevent exceeding the MC failure criterion and with this the potential for fault slip and to maximize the profitability. The use of these NPV maximizing strategies are however limited by regulations set up by the Dutch government to prevent induced seismicity as much as possible. Official guidelines are still under construction as researches into the induced seismicity effects of geothermal operations are ongoing, but the State Supervision of the Mines (SodM) has set up practical guidelines regarding the maximum allowable injection pressure which regulates the allowable flowrate in order to minimize the risk of induced seismicity. Also with respect to the distance between the fault and the wells there are no officially documented guidelines yet, but the Dutch Mining Council recommend with practical guidelines to EZK to place the wells minimally 100 m from the fault. Regarding potential development strategies in this study it is found that the SodM protocol is a good initial reference point for the maximum allowable injection pressure and flowrate, but the MC failure criteria of the sandstone could still be exceeded, hence fault slip could potentially occur which in the end could induce seismic events, even when adjusting the operational options to meet the SodM protocol. Additional in-depth investigation into the rock frictional characteristics of the subsurface and the presence of (critically) pre-existing faults is required for the protocol to certainly prevent possible induction of seismic events. The recommendation of the Mining Council to EZK are found be generally in line with the findings of this study, though it is possible to place the wells even closer than 100 m from the fault when needed. In general the guidelines limit the choice in operational options as the maximum allowable injection pressure can set the allowable flowrate lower than expected. Combined with the fault stability assessment of this study, which also limits potential operational

options based on the reservoir conditions, the official regulations could have a big impact on the development strategy. It might therefore be reasonable to set up guidelines which adjust according to the location specific properties. Additionally, in terms of profitability it can be concluded that geothermal projects depend eminently on the SDE+ subsidies granted by the Dutch government. In case of subsidy exclusion, high flowrates of minimally 6600 m^3/day are required to breakeven the homogeneous geothermal project which has their influences on the fault stability. In case of a heterogeneous reservoir the project would not be profitable at all and will therefore not commence. These outcomes are detached from times of low gas prices, in which the profitability of geothermal projects without the granting of subsidies remains negative under all considered scenarios. From this it can be concluded that geothermal operations would not be able to commence at all if the SDE+ subsidies are no longer granted.

10

Recommendations

This chapter discusses recommendations for future research based on the outcomes and uncertainties of the research done in this thesis.

- This study has shown that fault slip tendency highly depends on the sandstone friction coefficient. As mentioned it is therefore important to identify the exact values of the sandstone in the reservoir of interest, as this helps to make more accurate interpretations and assessments of the risk for fault, hence more accurate potential development strategies can be set up.
- The Mohr circles used to assess the fault slip tendency in this study are based on constant regional stress values. Besides this, the horizontal stress values used in this study are highly uncertain as very limited data on these values is present for the West Netherlands Basin. Therefore it is recommended to determine the horizontal stress values to make the assessment of the slip tendency more exact.
- In terms of induced seismicity, this study focused on the assessment of the potential for fault slip. However, two more processes are required for induced seismicity to occur: the propagation of fault slip and the generation of seismicity. To make an accurate assessment of the potential for induced seismicity it is therefore needed to look into the further propagation of the slip found in this thesis and if and how seismicity will be generated. In addition the maximum pressures found in this research, which may lead to fault slip, are encountered within a vicinity of about 10% of the fault. There may be other critical places near the fault which can lead to slip as well.
- Currently the heat prices are coupled to hydrocarbon energy prices, which makes the geothermal revenues dependent on the volatile gas price. A profitability assessment on a decoupled heat price might show a more independent performance of geothermal energy. Additionally, it might be reasonable to assess the heat price compared to the price of hydrocarbons if CO_2 pricings are taken into account. Are hydrocarbons still cheaper than using sustainable sources? Lastly, the results have shown that geothermal projects in the Netherlands are not able to commence when SDE+ subsidies are granted, let alone when this is combined with low gas prices. It is therefore a very interesting topic to investigate in what way geothermal projects could still be profitable when this happens.
- In this thesis a constant production rate is assumed throughout the entire year during the full 30 years of the project. However, it is known that heat demand is much lower during summer months compared to winter months. How does a change in flowrate due to heat demand influence the profitability? And how does this influence the fault stability as for example lower rates are used during summer months.
- This study did not take into account the effects of (early) thermal breakthrough. However, this might be an important factor in terms of profitability when this happens early in the production process. For future studies it would be interesting to take this into account and research how this would affect the projects profitability.
- The thermo-elastic properties of the sandstone are not directly taken into account in this thesis, but do influence the subsurface characteristics (DiPippo, 2016) and therefore the fault stability

(Platteeuw, 2018). Investigating the effects of these thermo-elastic properties due to the injection of cold water can make the fault stability assessment much more valuable.

A.1. Fault Permeability Influences

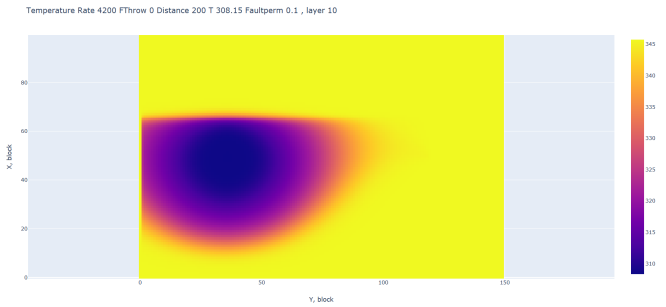

(a) Fault permeability 0.1 mD

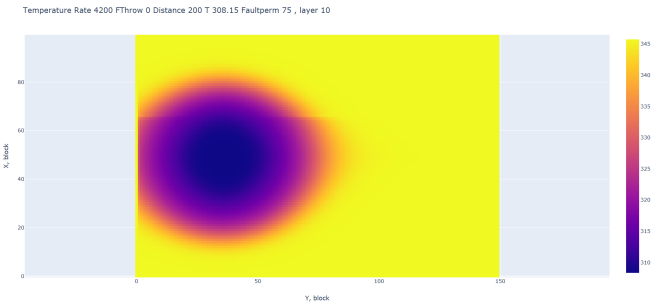

(b) Fault permeability 75 mD

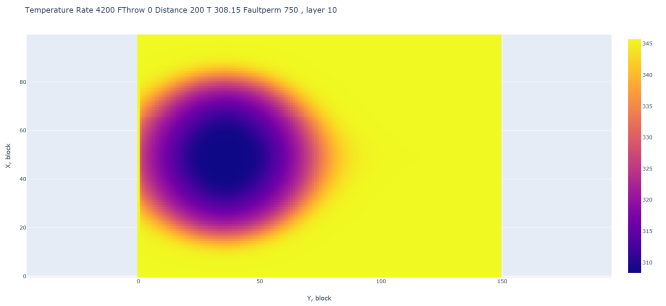

(c) Fault permeability 750 mD

Figure A.1.1: Temperature maps of reservoir layer 10 showing the results of fault permeabilities 0.1, 75 and 750 mD

A.2. Fault Throw Influences

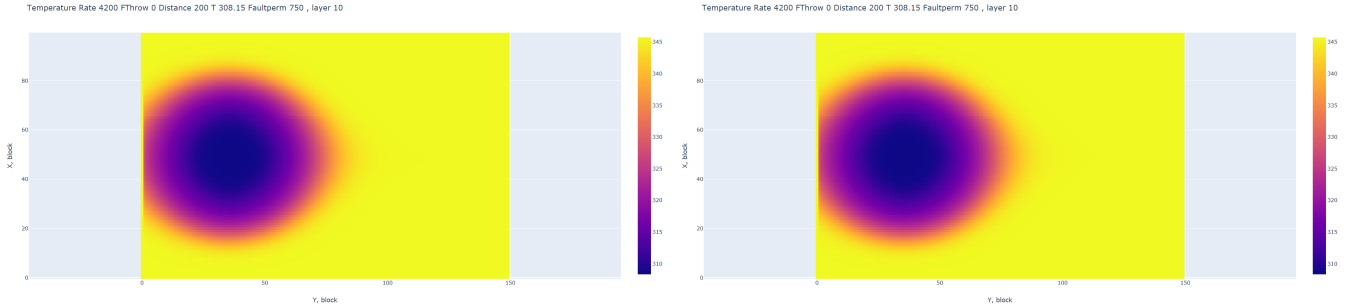

(a) Fault throw 0 m, layer 10

(b) Fault throw 0 m, layer 30

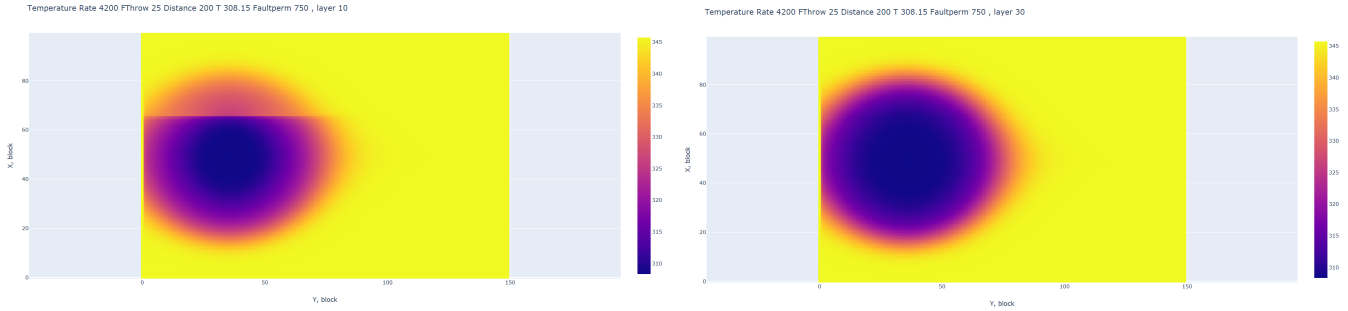

(c) Fault throw 25 m, layer 10

(d) Fault throw 25 m, layer 30

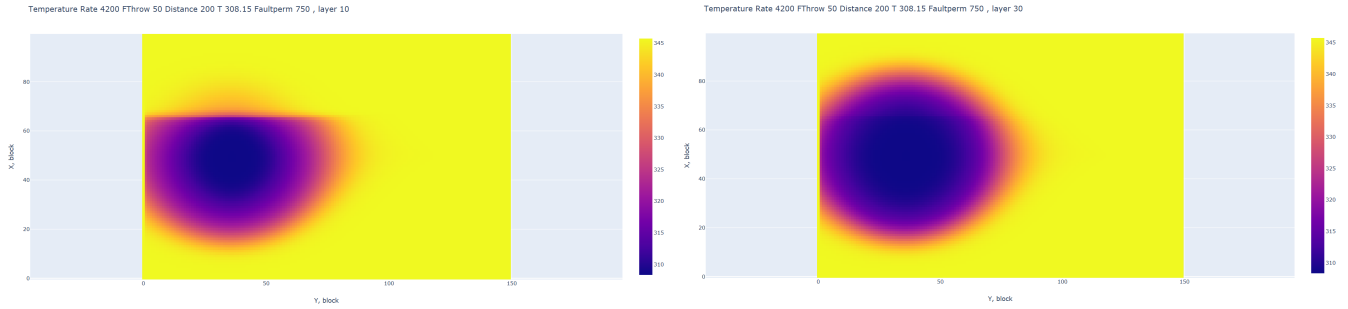

(e) Fault throw 50 m, layer 10

(f) Fault throw 50 m, layer 30

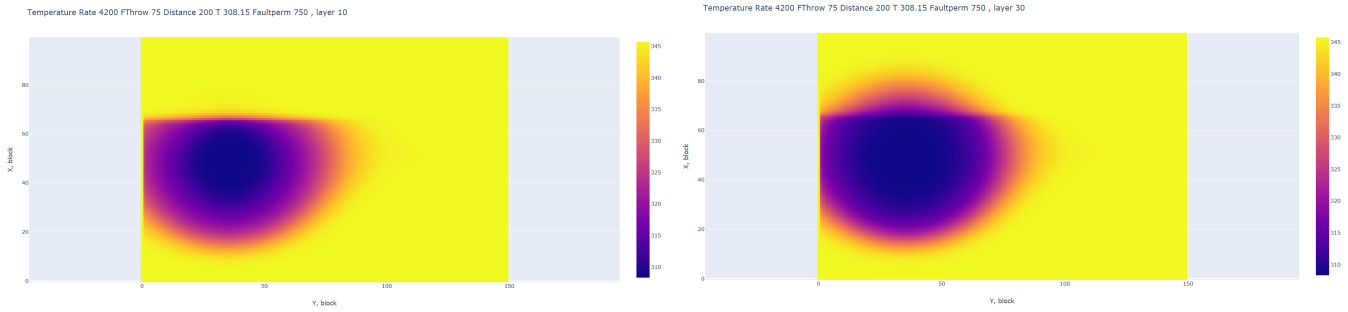

(g) Fault throw 75 m, layer 10

(h) Fault throw 75 m, layer 30

Figure A.2.1: Temperature maps of reservoir layers 10 and 30 showing the results of fault throw 0, 25, 50 and 75 m

A.3. Influences of Wells Distance to the Fault

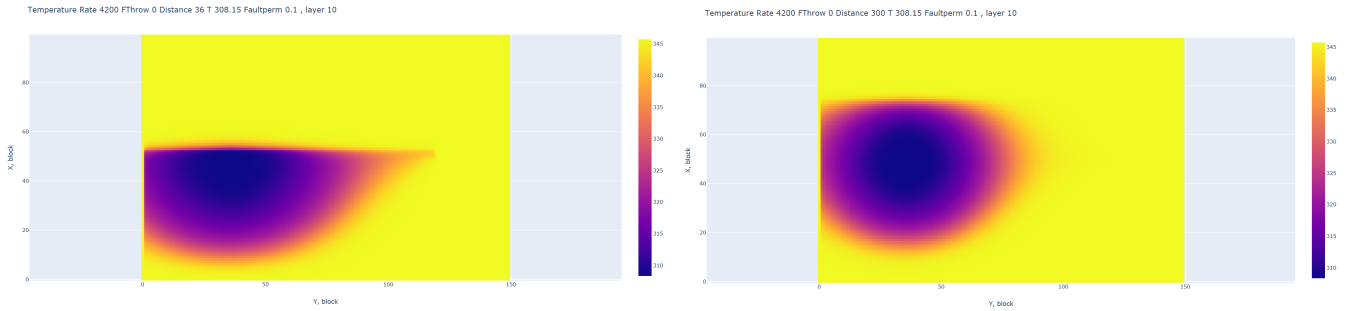

(a) Wells placed 36 m from the fault

(b) Wells placed 300 m from the fault

Figure A.3.1: Temperature maps of reservoir layers 10 showing the results of the wells placed a distance 36 m and 300 m from the fault

B

Flow Rate Influences on Cumulative Discounted Cashflows

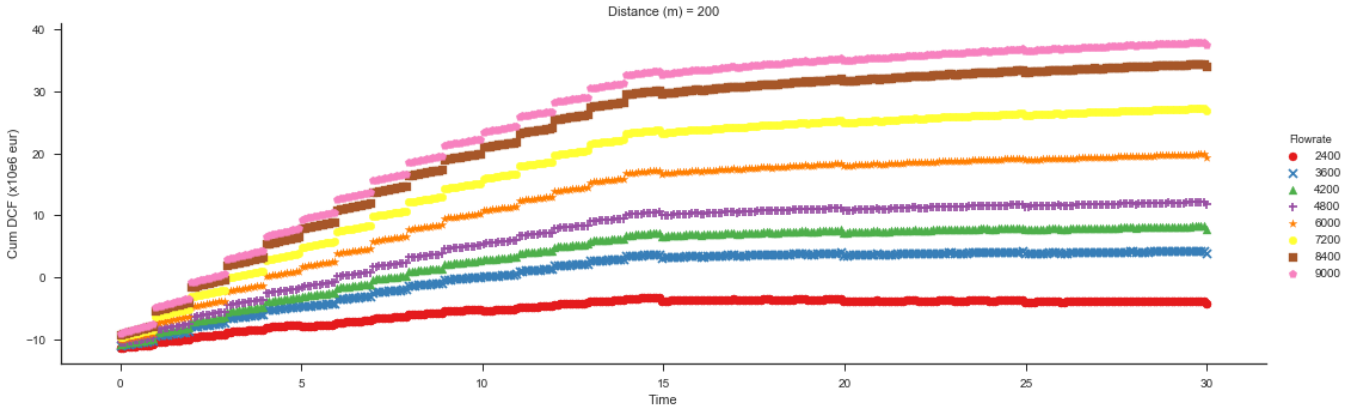

Figure B.0.1: The influence of flow rate between 2400 and 9000 m^3/day on the cumulative discounted cashflows of the projects

C

The Interdependency of Water Density, Viscosity and Temperature

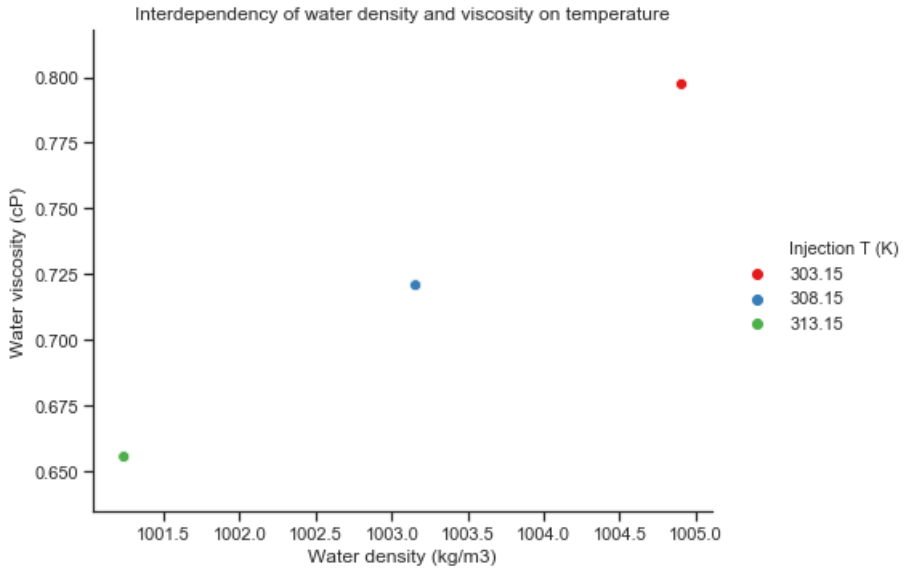

Figure C.0.1: The interdependency of water density, viscosity and temperature

D

The Influence of the Distance Between a Non-Sealing Fault and Wells on the NPV

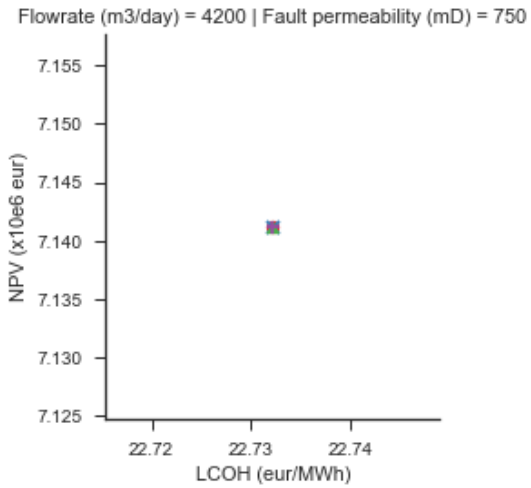

Figure D.0.1: The influence of 100, 200, 300 and 400 m distance between the wells and fault on the NPV and the LCOH in the presence of a non-sealing fault

E

Additional Development Results in the Presence of a Sealing Fault

E.1. NPV and Maximum Pore Pressures at Rates 2400 and 3000 m^3/day

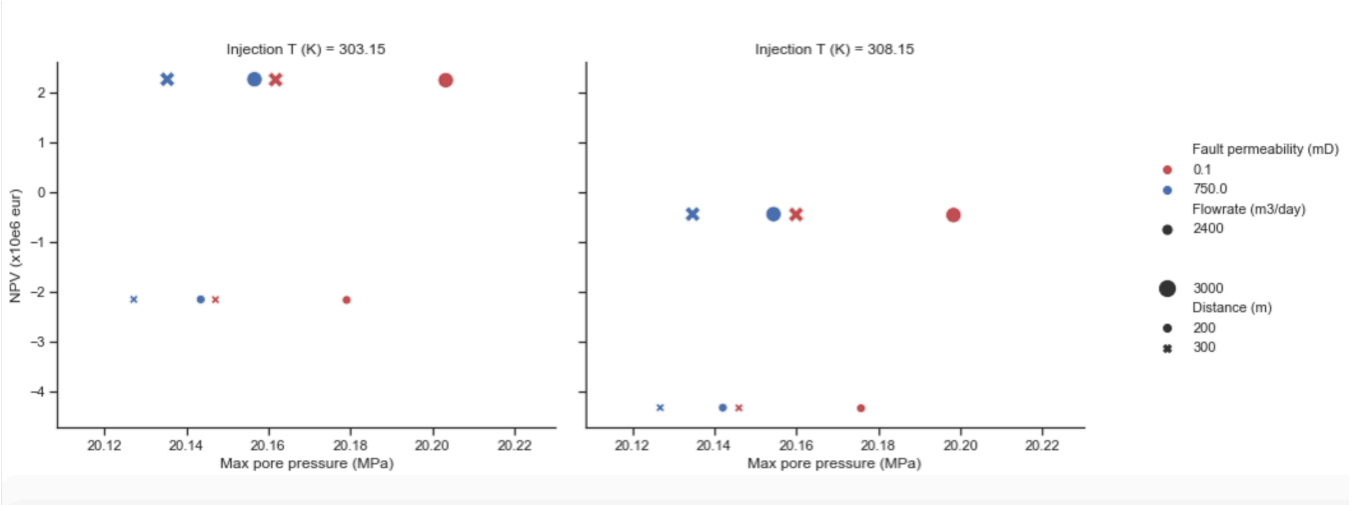

Figure E.1.1: NPV versus Maximum pore pressure for rates 2400 and 3000 m^3/day showing the influence of distance 200 m and 300 m between the wells and fault, fault permeability of 0.1 mD and 750 mD and injection temperature of 303.15 K and 308.15 K.

E.2. Fault Throw Influences on the NPV and the Pressure Build up

The following figures show the pressure build up in the two layers South from the fault and the NPV values as result of fault throws with lengths 0 m, 25m and 75 m, flow rates between 3600 and 6000 m^3/day increasing in steps of 600 m^3/day and in presence of a sealing fault (0.1 mD).

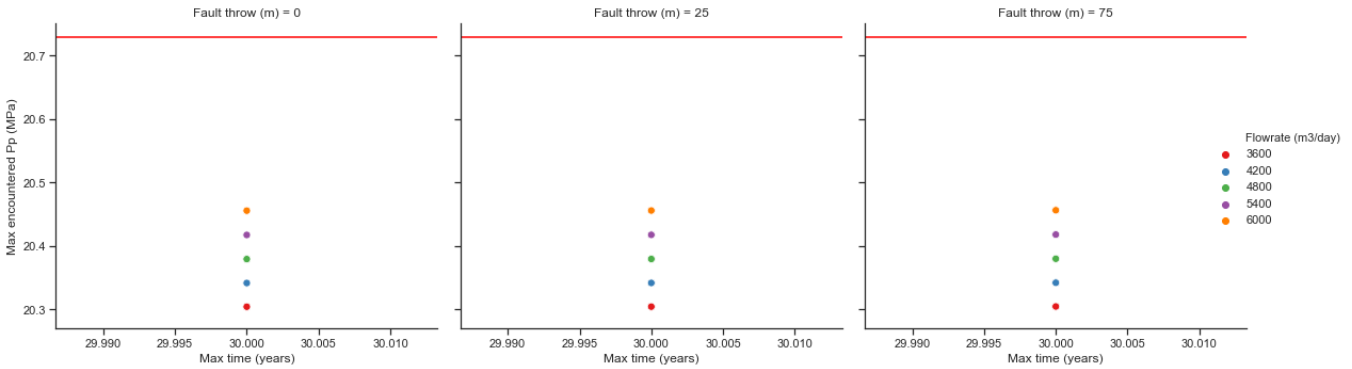

Figure E.2.1: The influence of fault throw in combination with flowrates on the maximum pressures encountered after 30 years of production in presence of a sealing fault

E.3. Additional Results on the NPV Outcomes

NPV vs Maximum Encountered Pore Pressures as a Result of the Fault Throw

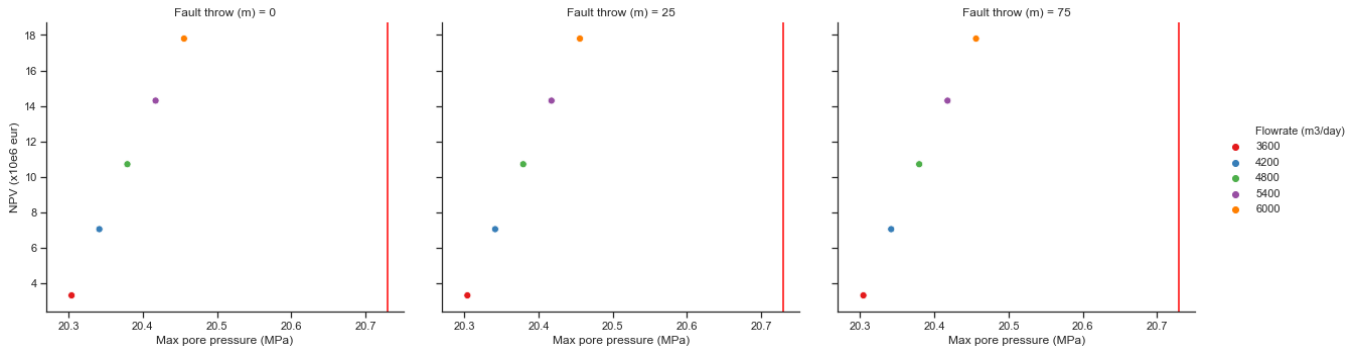

Figure E.3.1: NPV versus maximum pore pressures next to a sealing fault as result of fault throw

NPV Build Up

The combined influence of flowrate, distance between the wells and the fault and injection temperature on the NPV.

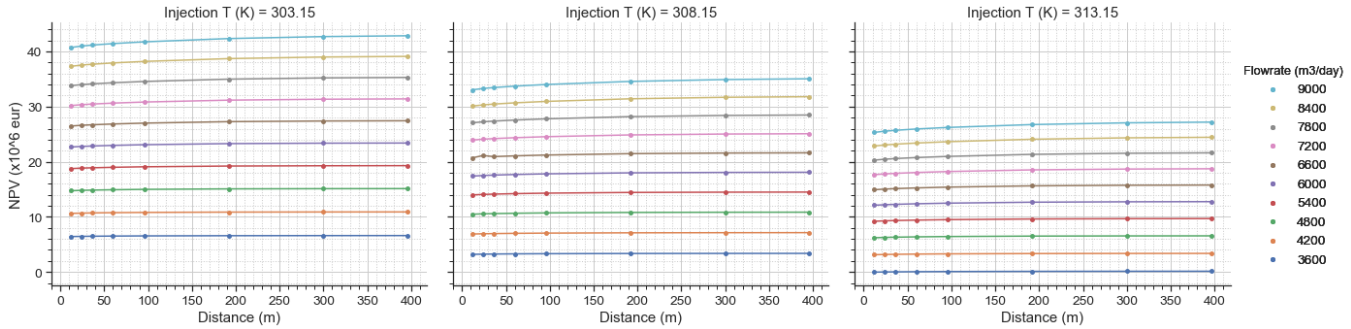

Figure E.3.2: The combined influence of injection temperature, distance between the fault and the wells and flowrates between 3600 and 9000 m^3/day on the NPV build up

E.4. Additional Results for the Friction Coefficient Influence

Maximum encountered pressure next to the fault as result of:

- Distance between the fault and the wells of 12 m, 24 m, 36 m, 60 m, 96 m, 192 m, 300 m and 396 m
- Flowrates between 3600 and 9000 m^3/day, increasing in steps of 600 m^3/day
- Injection temperatures of 303.15 K, 308.15 K and 313.15 K

Friction coefficient 0.4 and 0.47

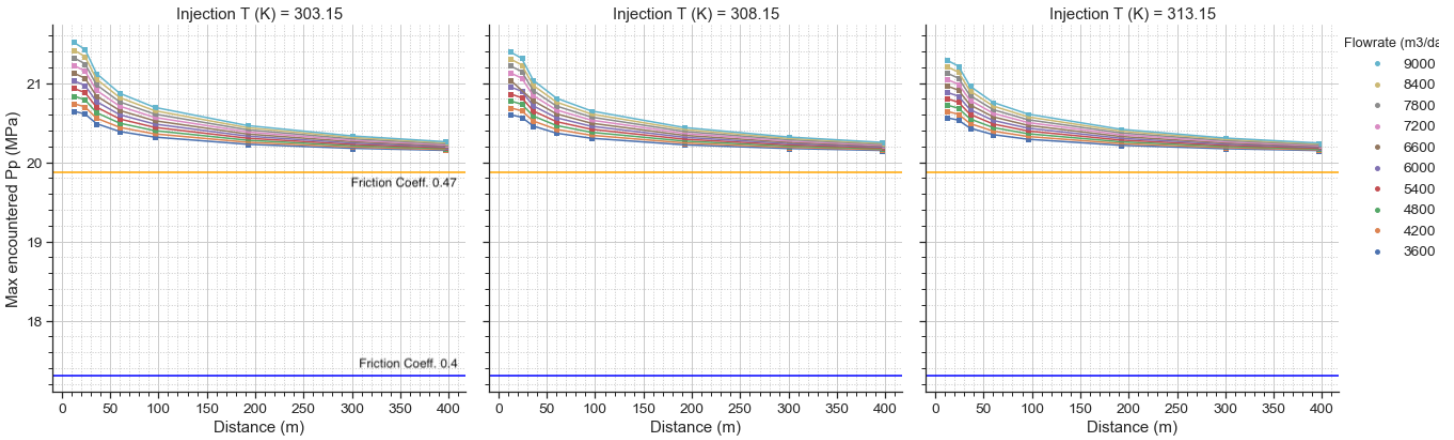

Figure E.4.1: Pressure build up in the second layer South from the fault causing failure as result of distance of 12 m, 24 m, 36 m, 60 m, 96 m, 192 m, 300 m and 396 m between the fault and the wells, flowrates between 3600 and 9000 m^3/day and injection temperatures of 303.15 K, 308.15 K and 313.15 K. Considered friction coefficients of the sandstone are 0.4 and 0.47

Friction coefficient 0.53, 0.54 and 0.6

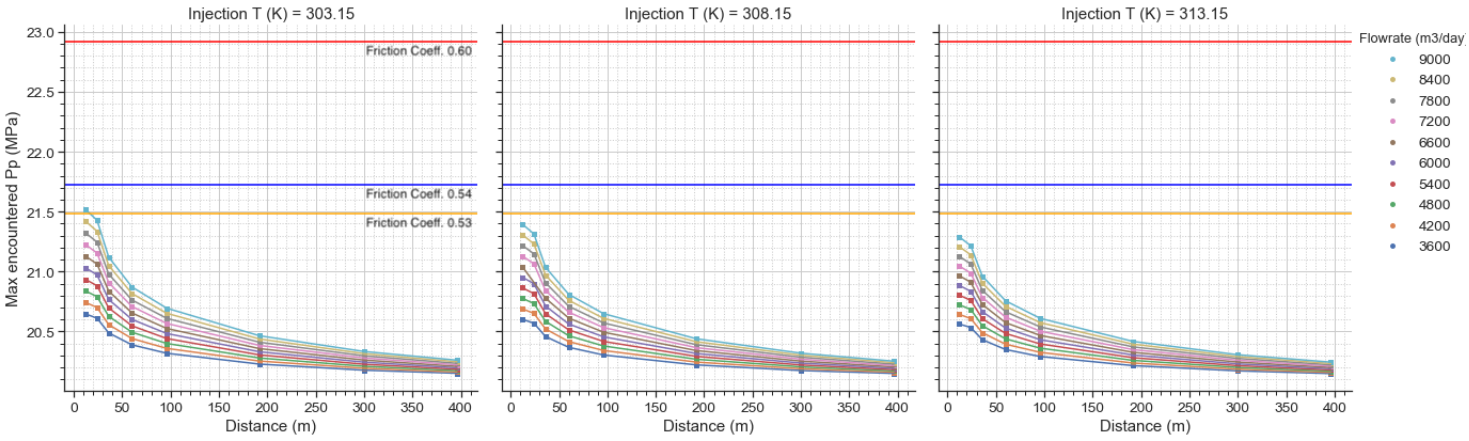

Figure E.4.2: Pressure build up in the second layer South from the fault causing failure as result of distance of 12 m, 24 m, 36 m, 60 m, 96 m, 192 m, 300 m and 396 m between the fault and the wells, flowrates between 3600 and 9000 m^3/day and injection temperatures of 303.15 K, 308.15 K and 313.15 K. Friction coefficients of the sandstone are 0.53, 0.54 and 0.6.

E.5. Reservoir Cross-Sections and Pressure Build Up Between the Fault and the Injector Well

How the pressure builds up next to the fault at different wells positions with respect to the fault is shown by the figures in this appendix. The figures show a slice of the reservoir, which taken over the entire length in the x-direction (E.5.1).

These build ups of the pressure next to the fault are as a result of:

- Distance between the fault and the wells of 12 m, 24 m, 36 m, and 192 m
- Flowrates 3600 and 5400 m^3/day

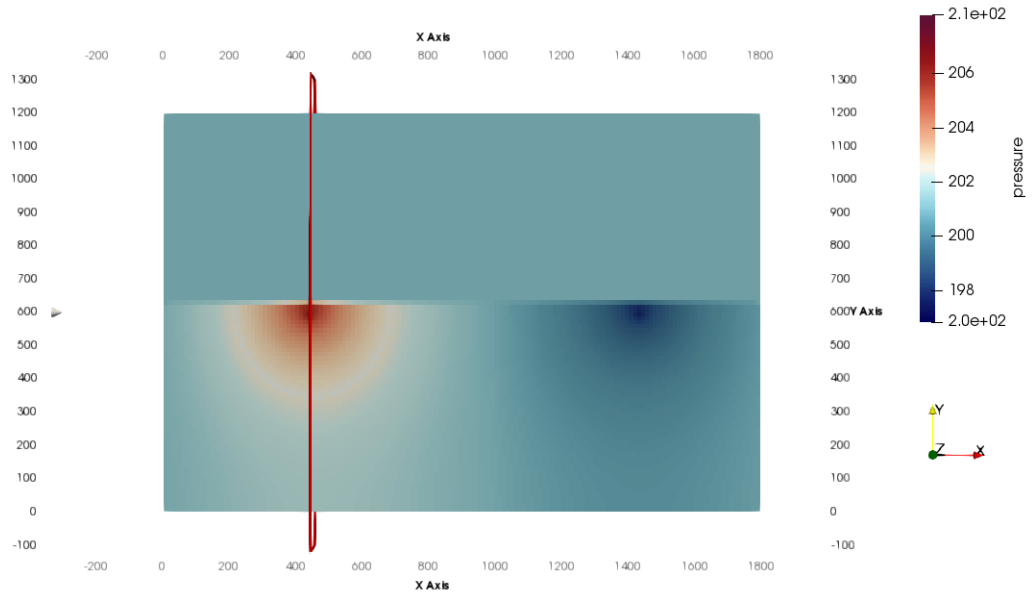

Figure E.5.1: Sub slice of the reservoir over the entire length in the x-direction used to show the pressure build up between the injector and the fault. The red and blue plume indicate the pressure change due to the injector and producer respectively.

Pressure build up as a result of flowrate 3600 m^3/day

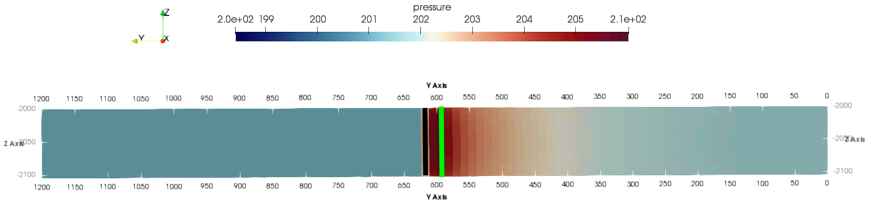

(a) X-view of the reservoir, wells placed 12 m from the fault

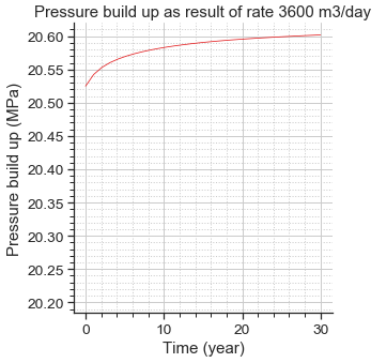

(b) Pressure build up next to the fault, wells placed 12 m from the fault

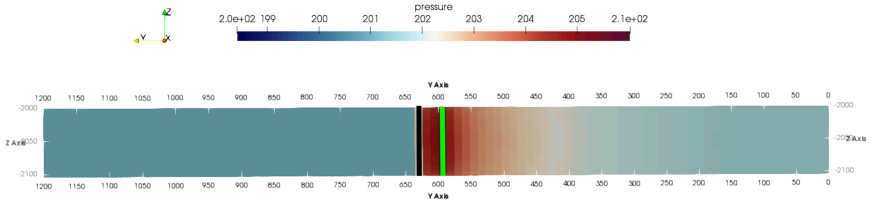

(c) X-view of the reservoir, wells placed 24 m from the fault

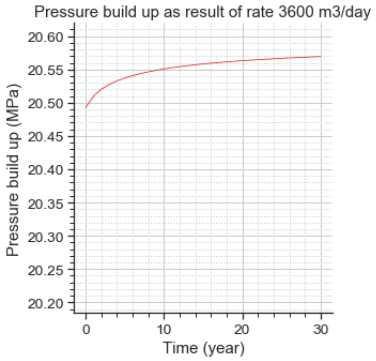

(d) Pressure build up next to the fault, wells placed 24 m from the fault

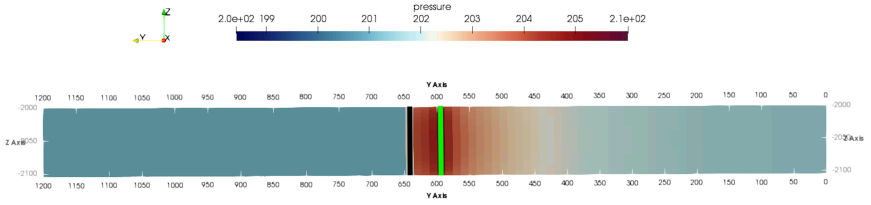

(e) X-view of the reservoir, wells placed 36 m from the fault

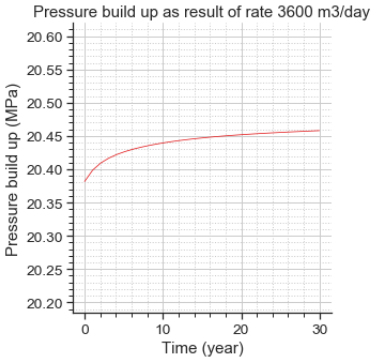

(f) Pressure build up next to the fault, wells placed 36 m from the fault

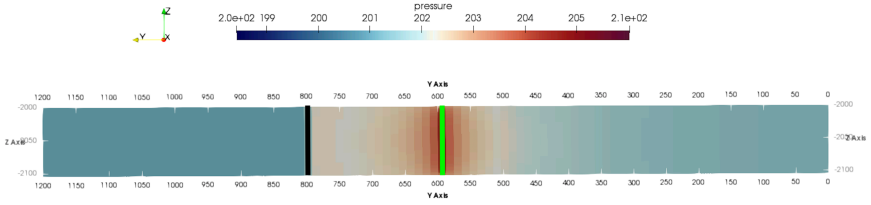

(g) X-view of the reservoir, wells placed 192 m from the fault

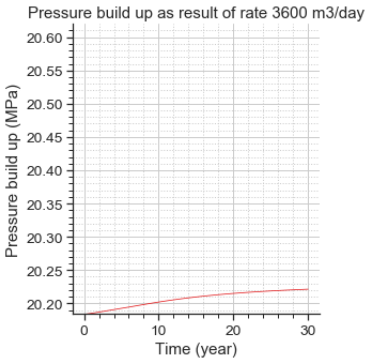

(h) Pressure build up next to the fault, wells placed 192 m from the fault

Figure E.5.2: X-angle view of the reservoir and pressure build up plots showing the pressure build up next to the fault as results of flowrate 3600 m^3/day and wells placed 12 m, 24 m, 36 m and 192 m from the fault. The injector well is indicated lime and the fault is indicated black.

Pressure build up as a result of flowrate 5400 m^3/day

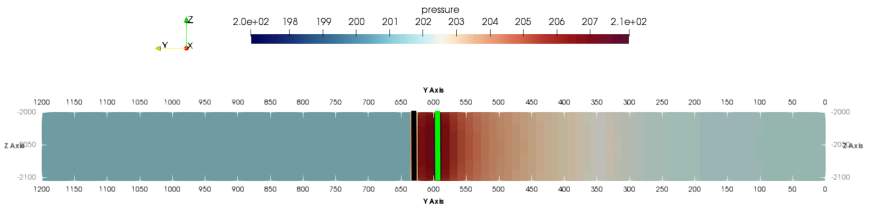

(a) X-view of the reservoir, wells placed 24 m from the fault

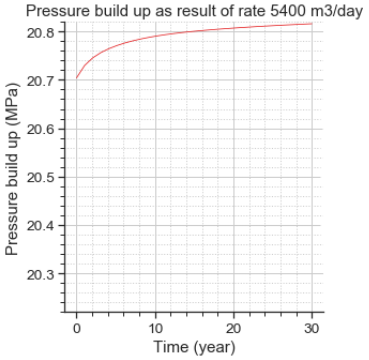

(b) Pressure build up next to the fault, wells placed 24 m from the fault

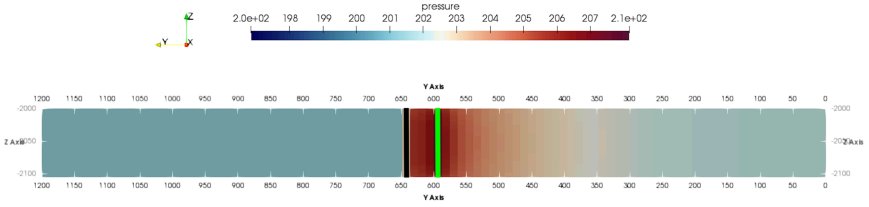

(c) X-view of the reservoir, wells placed 36 m from the fault

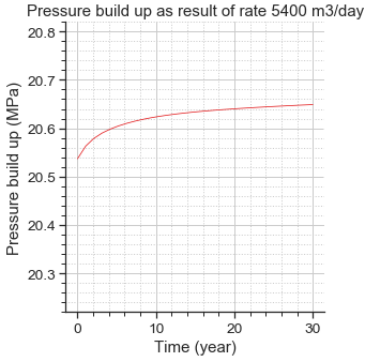

(d) Pressure build up next to the fault, wells placed 36 m from the fault

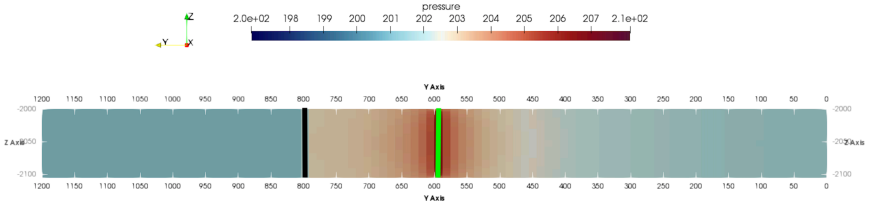

(e) X-view of the reservoir, wells placed 192 m from the fault

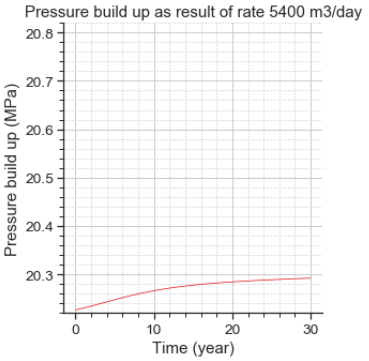

(f) Pressure build up next to the fault, wells placed 192 m from the fault

Figure E.5.3: X-angle view of the reservoir and pressure build up plots showing the pressure build up next to the fault as results of flowrate 5400 m^3/day and wells placed 24 m, 36 m and 192 m from the fault. The injector well is indicated lime and the fault is indicated black.

F.1. NPV Build Up During Production

Combined influence of flowrate, distance between the wells and the fault and injection temperature on the NPV.

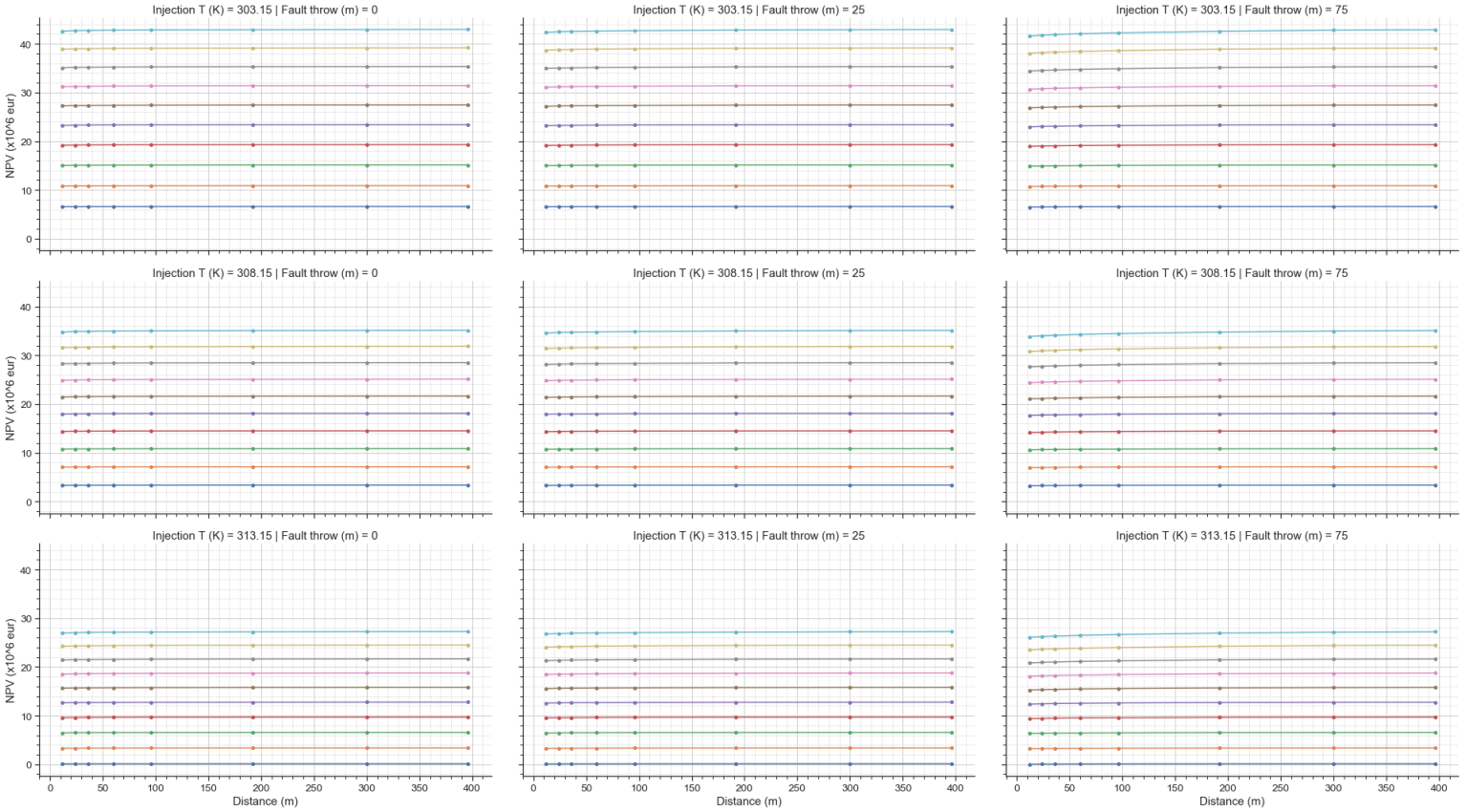

Figure F.1.1: The combined influence of injection temperature, distance between the fault and the wells and flowrates between 3600 and 9000 m^3/day on the NPV build up in presence of a medium sealing fault (0.75 mD)

F.2. Maximum Encountered Pressures Next to the Fault

Maximum encountered pressures next to a medium sealing fault after 30 years as result of injection temperatures, distance between 12 and 396 m and flowrates between 3600 and 9000 m^3/day.

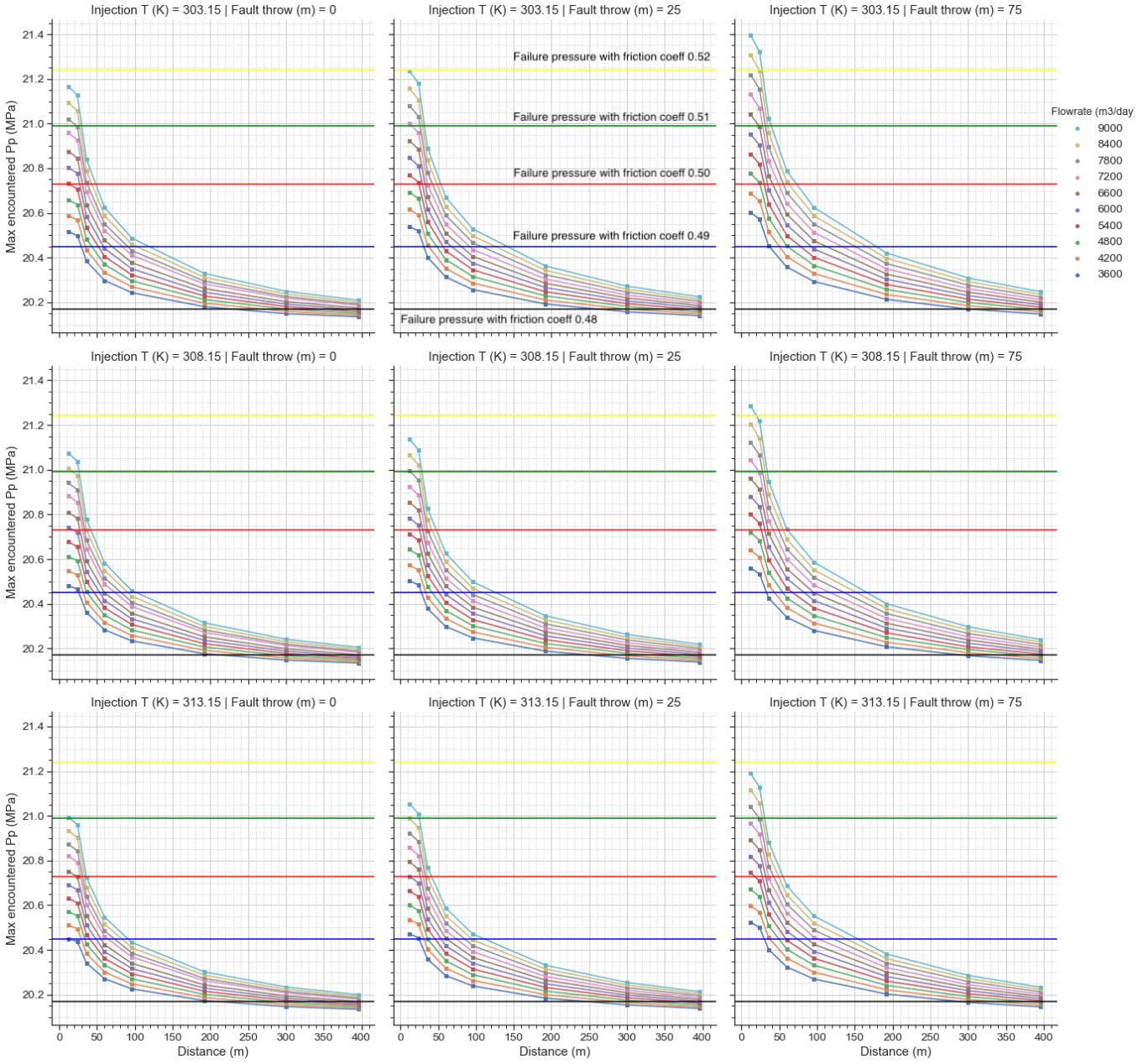

Figure F.2.1: Maximum encountered pressures next to a medium sealing fault after 30 years as result of distance of 12 m, 24 m, 36 m, 60 m, 96 m, 192 m, 300 m and 396 m between the fault and the wells, flowrates between 3600 and 9000 m^3/day and injection temperatures of 303.15 K, 308.15 K and 313.15 K. The horizontal lines indicate the failure pressures as result of coefficients 0.48 (Black), 0.49 (Blue), 0.5 (Red), 0.51 (Green) and 0.52 (Yellow).

NPV and Maximum Encountered Pressures next to the Fault

NPV and maximum encountered pressures next to a medium sealing fault after 30 years as result of injection temperatures, distance between 12 and 396 m and flowrates between 3600 and 9000 m^3/day and fault throw.

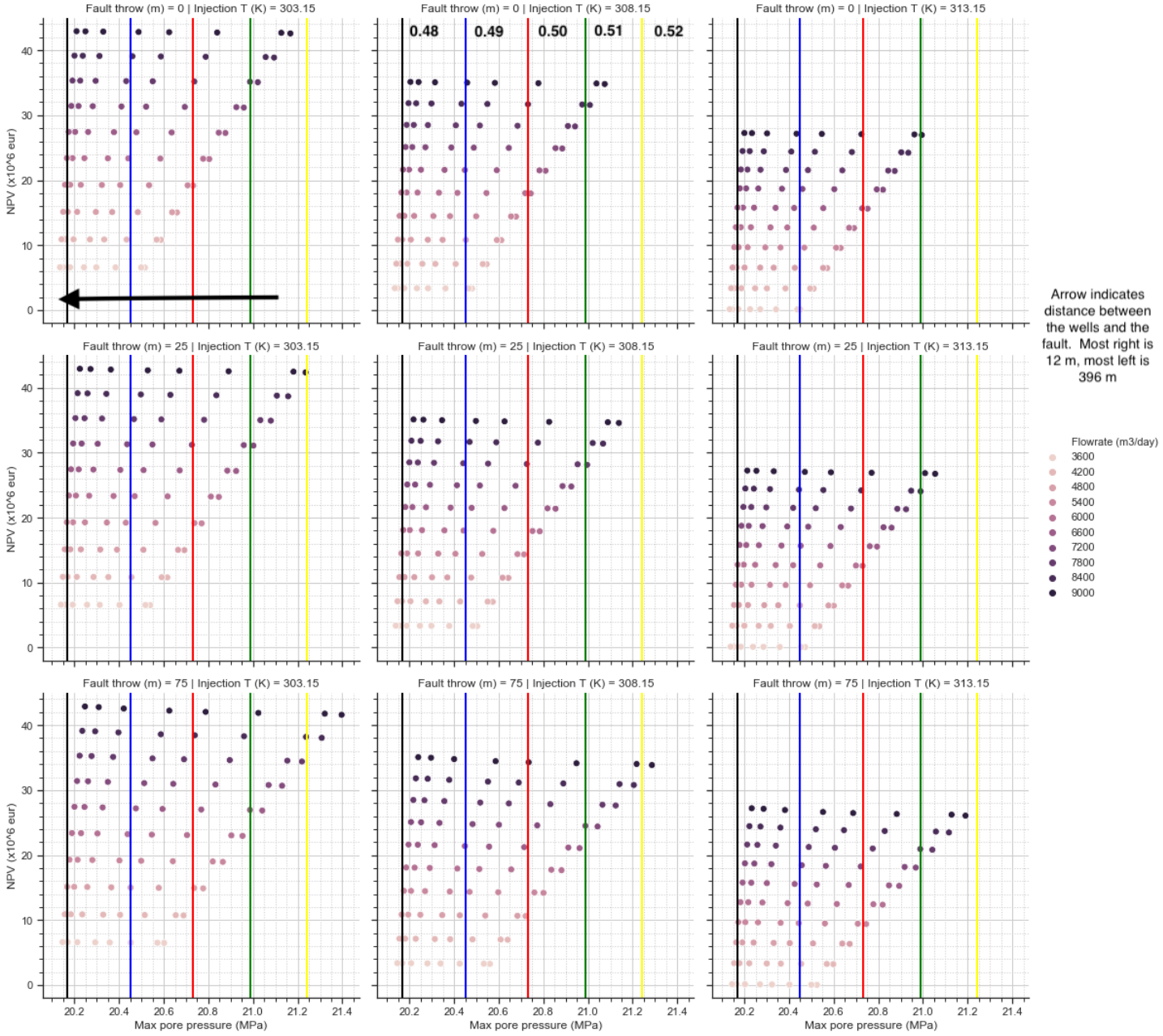

Figure F.2.2: NPV and Maximum encountered pore pressures after 30 years as result of rates between 3600 and 9000 m^3/day in presence of a medium sealing fault. The vertical lines indicate the failure pressures for friction coefficients: 0.48 (Black), 0.49 (Blue), 0.50 (Red), 0.51 (Green) and 0.52 (Yellow). The arrow indicates increasing distance between the wells and the fault from right to left. Most right indicates 12 m between the wells and the fault and most left is 396 m.

G

Additional Development Results in Presence of a Fully Transparent Fault

G.1. Maximum Encountered Pressures Next to the Fault

Maximum encountered pressures next to the Fault after 30 years as result of injection temperatures, distance between 12 and 396 m and flowrates between 3600 and 9000 m^3/day.

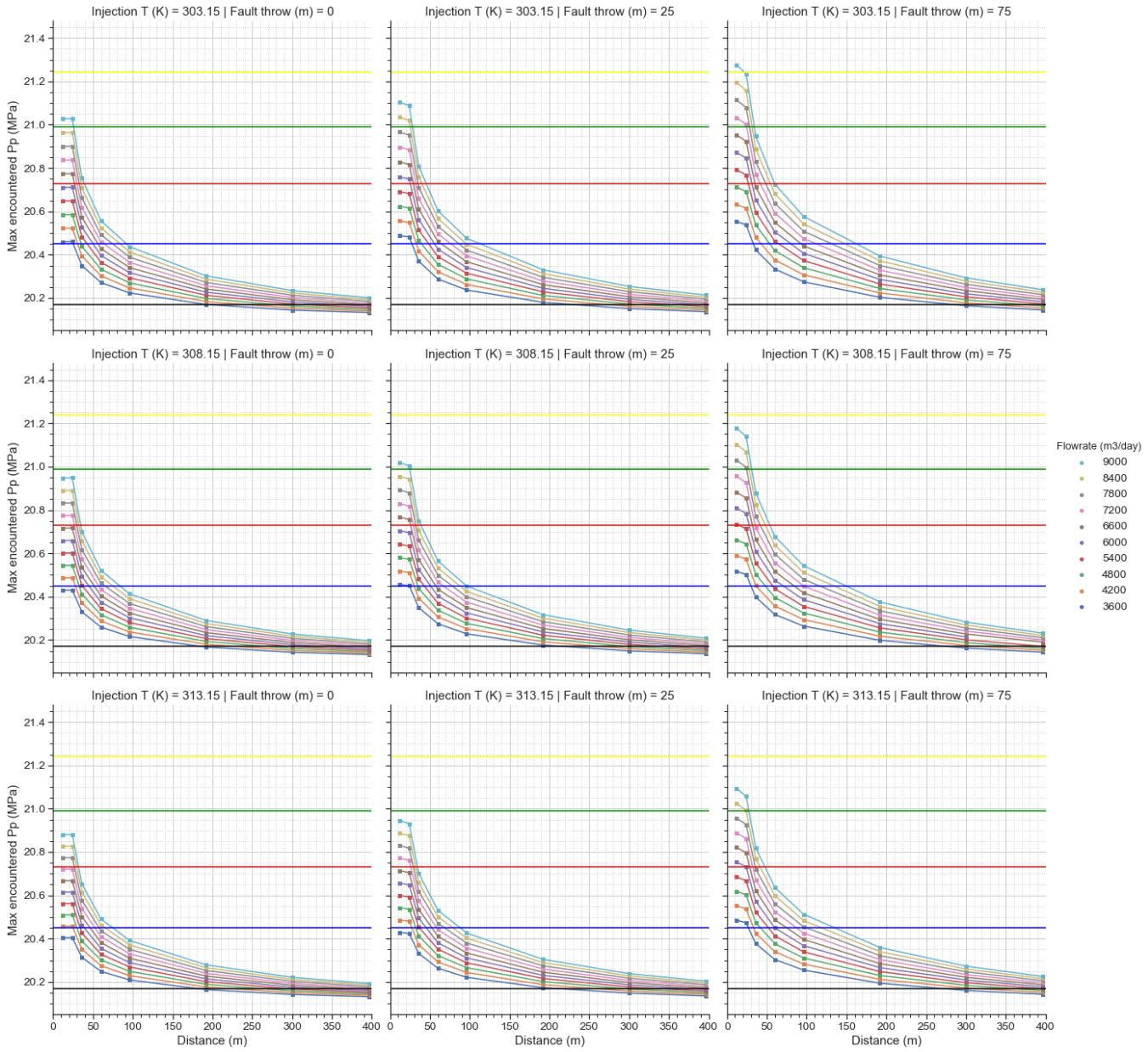

Figure G.1.1: Maximum encountered pressures next to a fully transparent fault after 30 years as result of distance of 12 m, 24 m, 36 m, 60 m, 96 m, 192 m, 300 m and 396 m between the fault and the wells, flowrates between 3600 and 9000 m^3/day and injection temperatures of 303.15 K, 308.15 K and 313.15 K. The horizontal lines indicate the failure pressures as result of coefficients 0.48 (Black), 0.49 (Blue), 0.5 (Red), 0.51 (Green) and 0.52 (Yellow).

G.2. Pressure Distribution in the Reservoir as Result of Increasing Fault Throw

Figures G.2.2, G.2.3 and G.2.4 show the pressure distribution along a transparent fault as result of increasing fault throw, flowrate 9000 m^3/day and 303.15 K injection temperature. The pressure distribution is shown for distance between the wells and the fault of 12 m and 24 m. The figures show a slice of the reservoir, which is taken over the entire length in the x-direction, as shown by figure G.2.1.

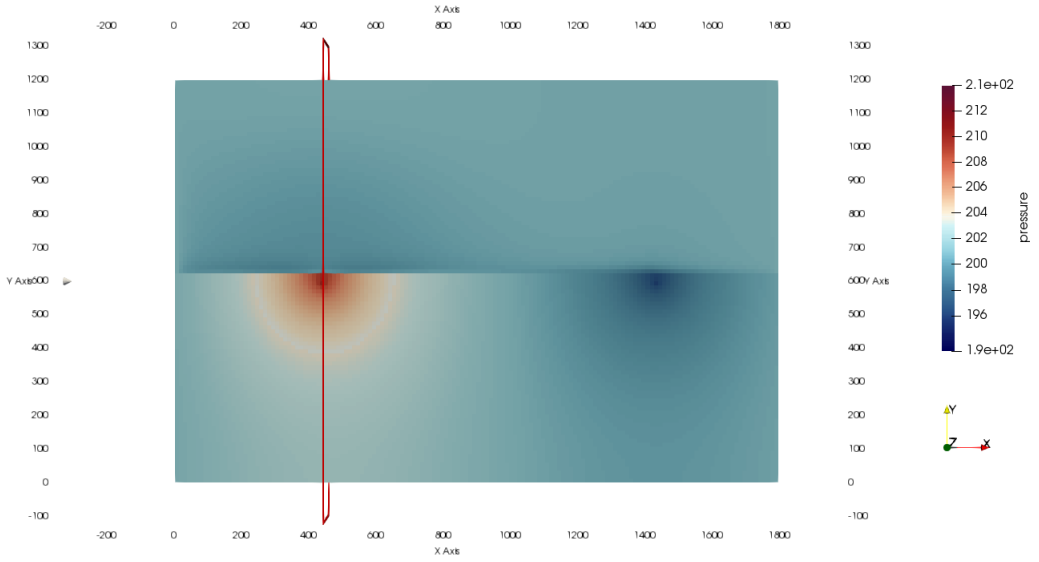

Figure G.2.1: Sub slice of the reservoir over the entire length in the x-direction used to show the pressure distribution between the injector and a transparent fault. The red and blue plume indicate the pressure change due to the injector and producer respectively.

Fault Throw of 0 m

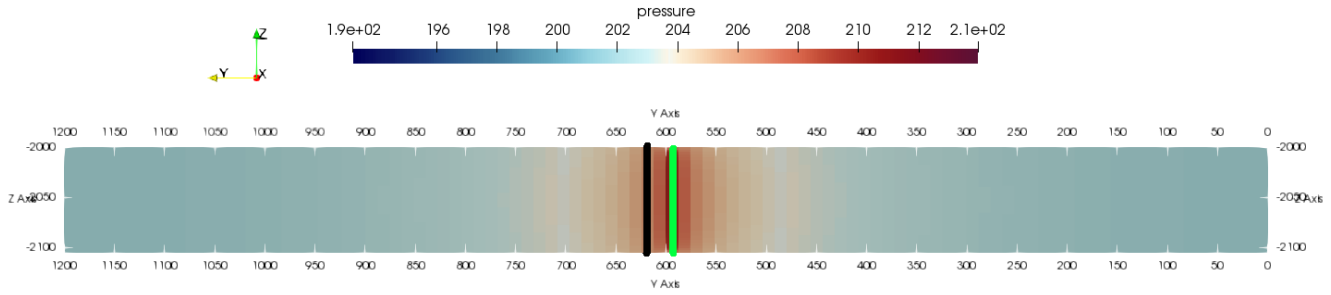

(a) Pressure distribution when the wells are placed 12 m from the fault

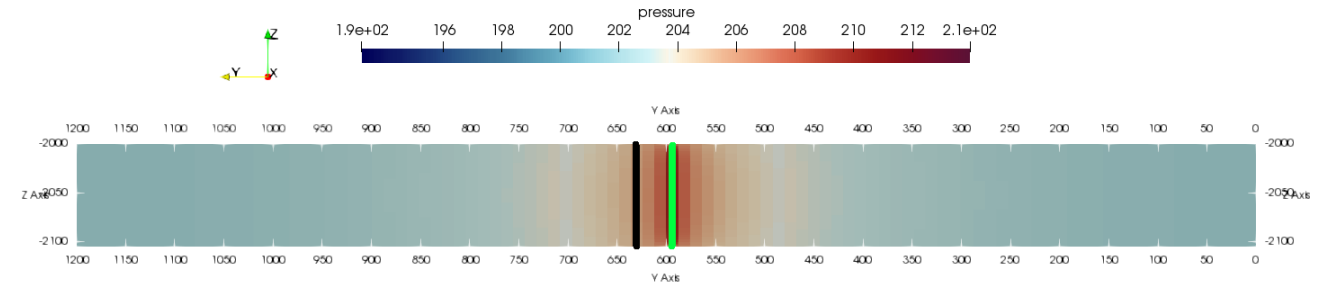

(b) Pressure distribution when the wells are placed 24 m from the fault

Figure G.2.2: X-angle view of the reservoir showing the pressure distribution between the injection well and a transparent fault as result of the presence of 0 m fault throw. This pressure distribution results from a flowrate of 9000 m^3/day and 303.15 K injection temperature and the wells are placed 12 m and 24 m from the fault.

Fault Throw of 25 m

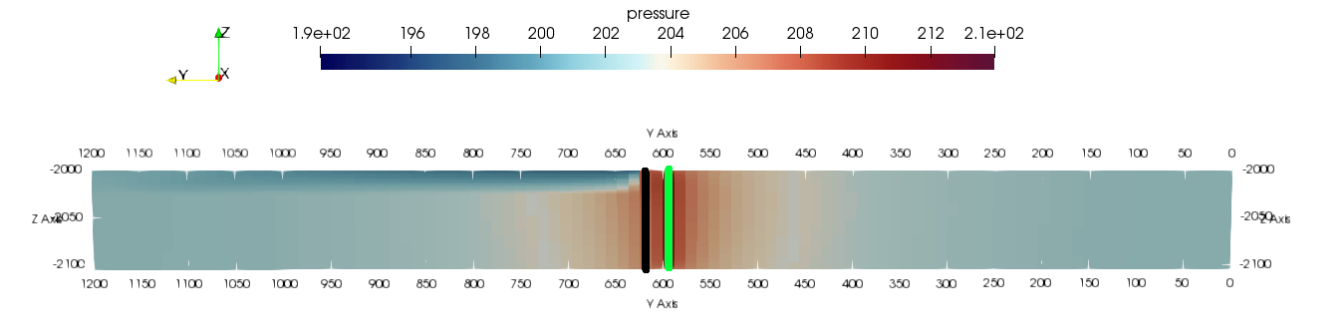

Figure G.2.3: X-angle view of the reservoir showing the pressure distribution between the injection well and a transparent fault as result of the presence of 25 m fault throw. This pressure distribution results from a flowrate of 9000 m^3/day and 303.15 K injection temperature and the wells are placed 12 m from the fault.

Fault Throw of 75 m

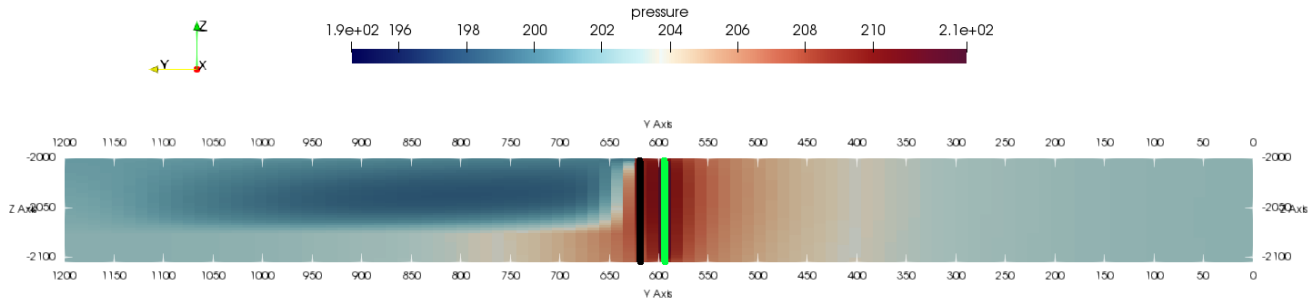

Figure G.2.4: X-angle view of the reservoir showing the pressure distribution between the injection well and a transparent fault as result of the presence of 75 m fault throw. This pressure distribution results from a flowrate of 9000 m^3/day and 303.15 K injection temperature and the wells are placed 12 m from the fault.

G.3. NPV and Maximum Encountered Pressures Next to the Fault

NPV and maximum encountered pressures next to a transparent fault after 30 years as result of varying injection temperatures, distance between the fault and wells ranging between 12 and 396 m, flowrates between 3600 and 9000 m^3/day and fault throws.

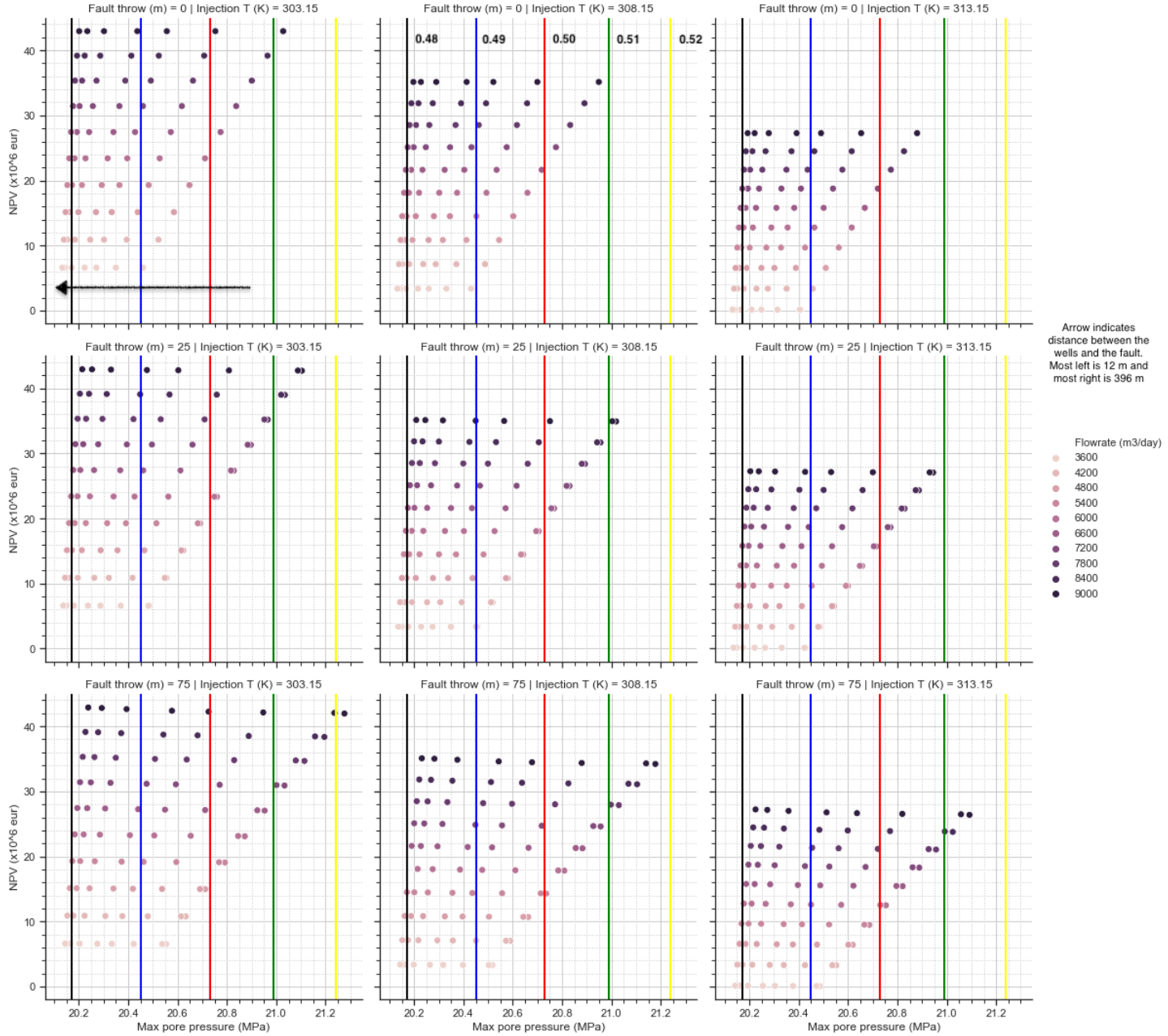

Figure G.3.1: NPV and Maximum encountered pore pressures after 30 years as result of rates between 3600 and 9000 m^3/day in presence of a fully transparent fault. The vertical lines indicate the failure pressures for friction coefficients: 0.48 (Black), 0.49 (Blue), 0.50 (Red), 0.51 (Green) and 0.52 (Yellow). The arrow indicates increasing distance between the wells and the fault from right to left. Most right indicates 12 m between the wells and the fault and most left is 396 m.

H.1. Produced Energy over 30 years

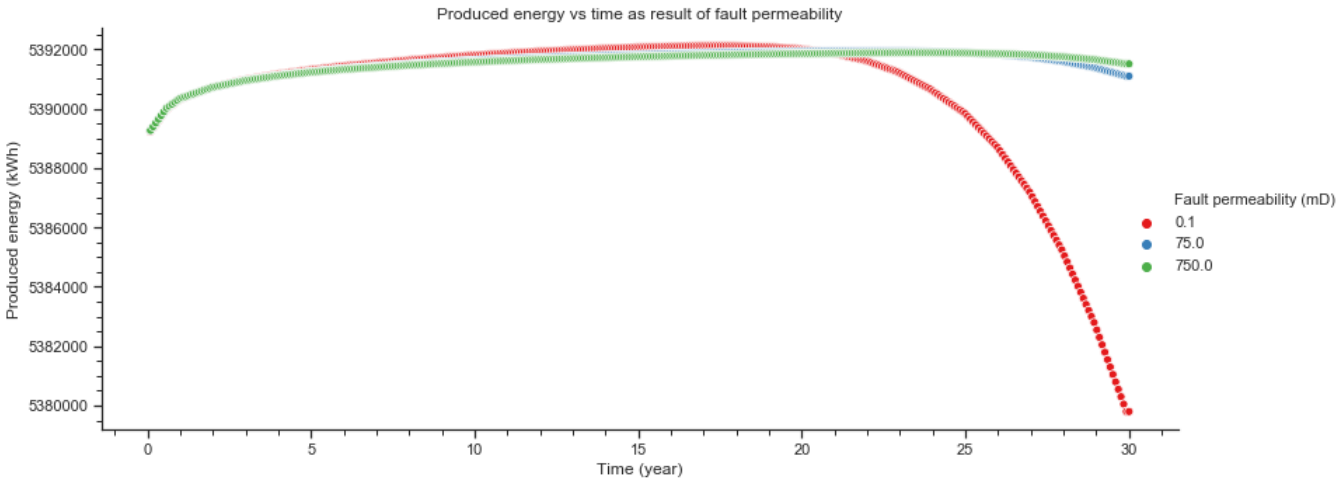

Figure H.1.1: Produced amount of Energy over 30 years in presence of a 0.1 mD, 75 mD and 750 mD fault at rate 4200 m^3/day

H.2. Production Temperature over 30 years

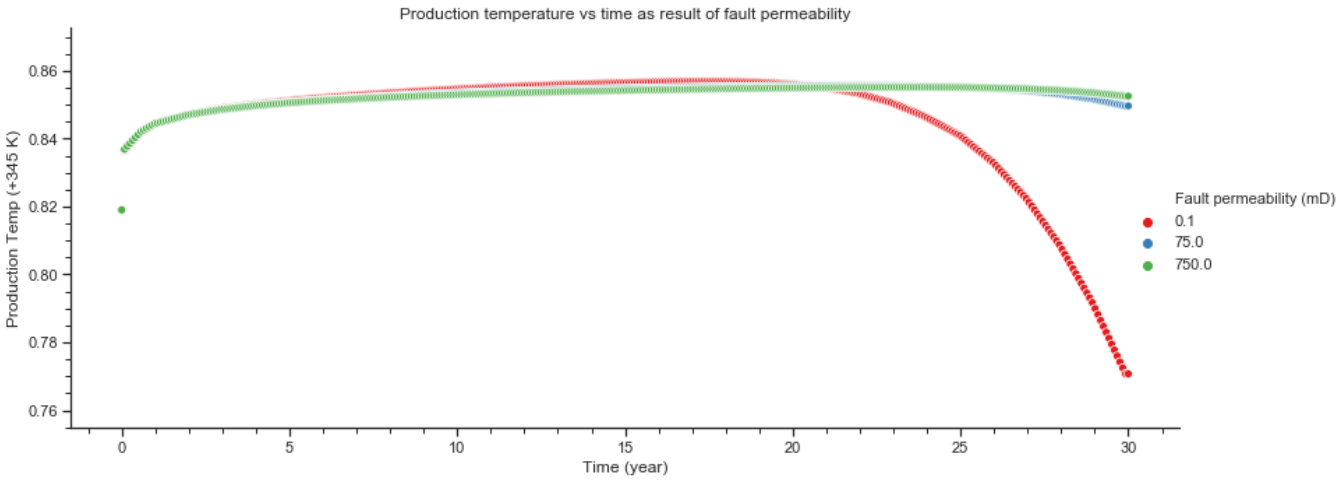

Figure H.2.1: Production temperature over 30 years in presence of a 0.1 mD, 75 mD and 750 mD fault at rate 4200 m^3/day

H.3. Cumulative Produced Energy after 30 years

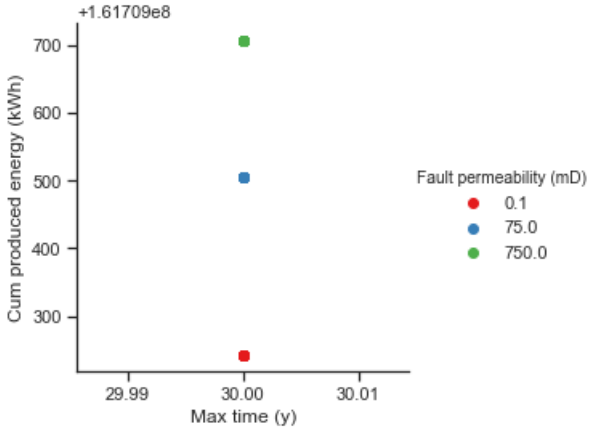

Figure H.3.1: Cumulative Produced Energy after 30 years in presence of a 0.1 mD, 75 mD and 750 mD fault at rate 4200 m^3/day

H.4. Pumping Costs over 30 years

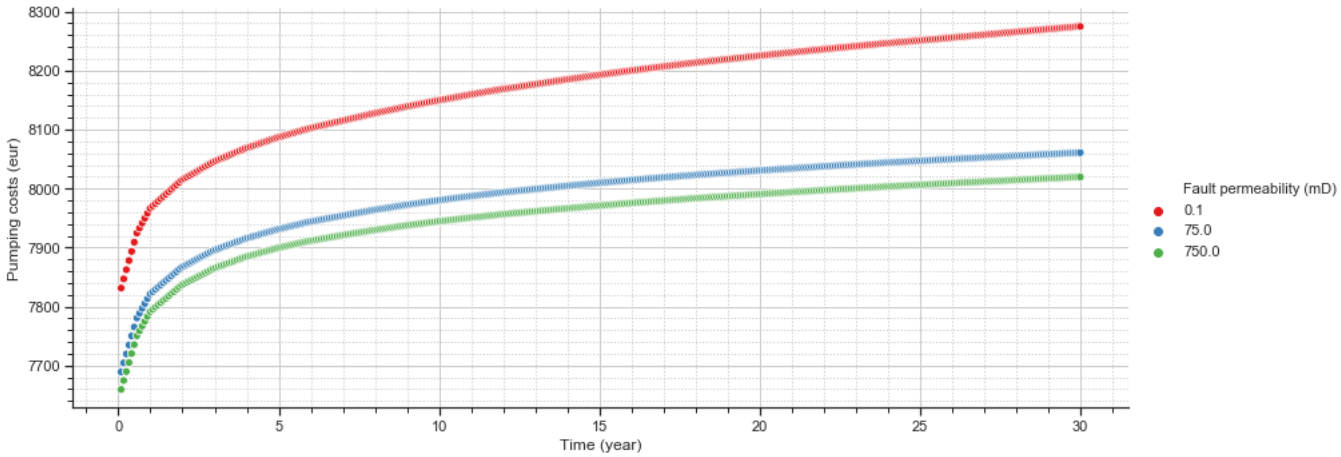

Figure H.4.1: Pumping Costs over 30 years in presence of a 0.1 mD, 75 mD and 750 mD fault at rate 4200 m^3/day

The results show the outcomes of the produced amount of energy and the temperature of the production water in the presence of a tranparent fault and fault throws of 0 m, 25 m, 50 m and 75 m.

I.1. Produced Temperature over 30 years

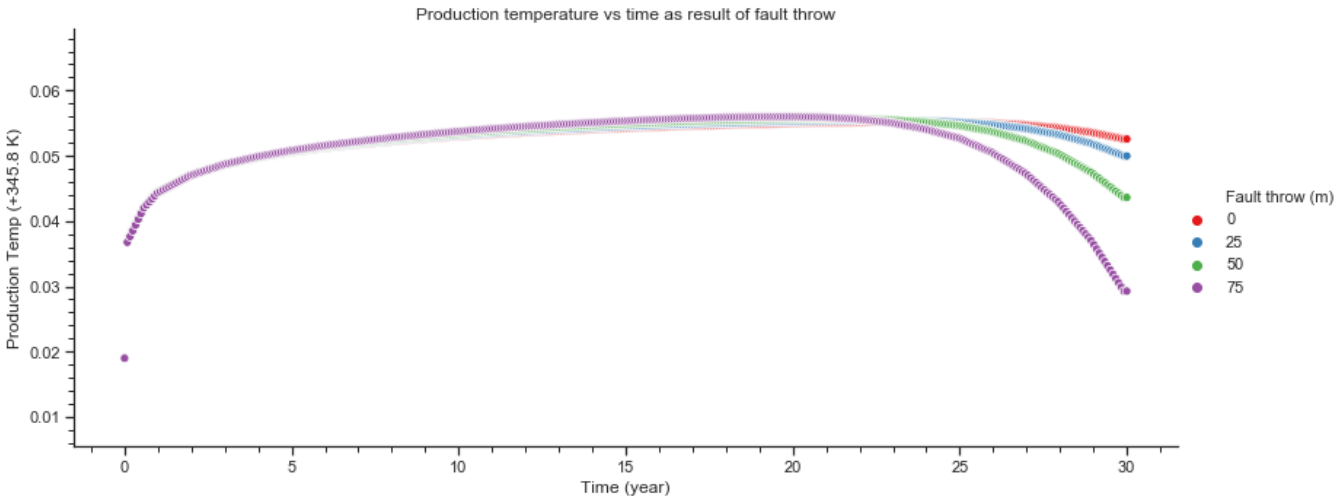

Figure I.1.1: Production temperature over 30 years in presence of a transparent fault and fault throws of 0 m, 25 m, 50 m and 75 m at rate 4200 m^3/day

I.2. Produced Energy over 30 years

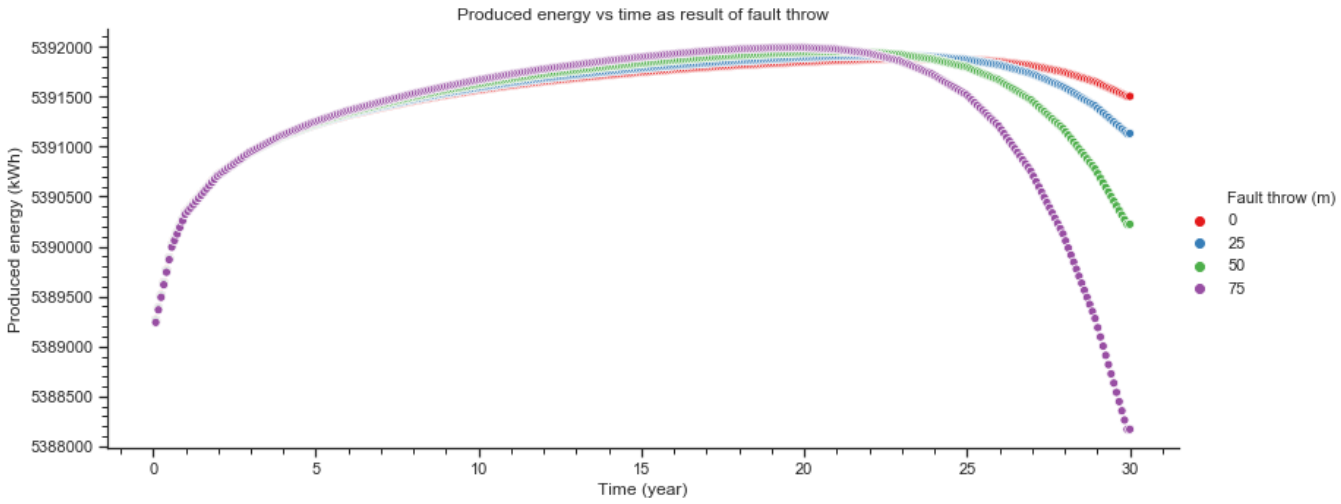

Figure I.2.1: Produced energy over 30 years in presence of a transparent fault and fault throws of 0 m, 25 m, 50 m and 75 m at rate 4200 m^3/day

J

Additional Comparison Results for the Presence of a Sealing, Medium Sealing and Fully Transparent Fault

J.1. Comparison of the NPV Outcomes

The comparison of the NPV outcomes for the Three Different Faults at a Constant Flowrate and Injection Temperature. For the figure the following parameter values are assumed:

- A constant flowrate of 9000 m^3/day
- Distance between the wells and the faults of 12 m, 60 m, 192 m and 396 m
- Constant injection temperature of 303.15 K
- Zero fault throw

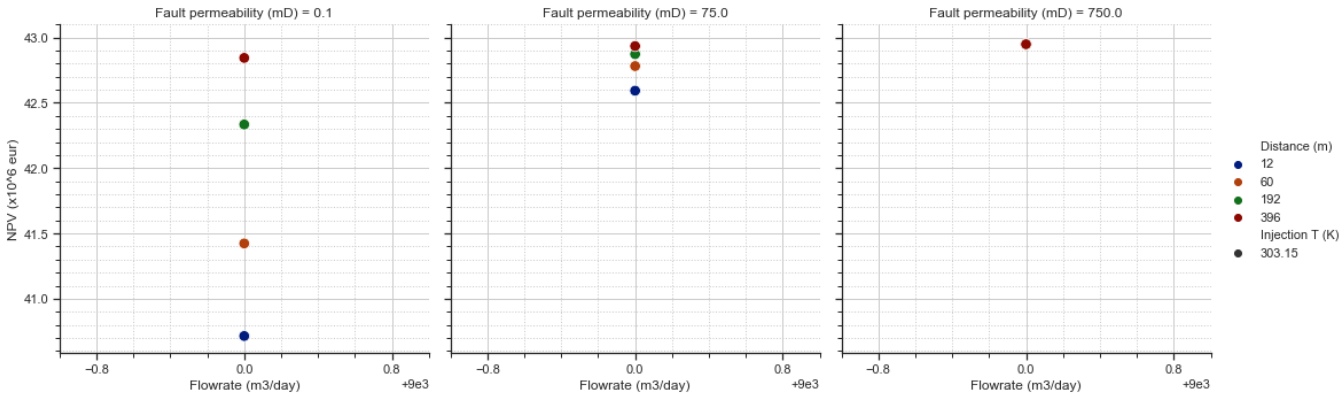

Figure J.1.1: Comparison of the NPV outcomes at a constant flowrate of 9000 m^3/day and constant injection temperature at 303.15 K. For increasing distance between the fault and the wells of 12 m, 60 m, 192 m and 396 m and zero fault throw.

NPV outcomes in Presence of 75 m throw

For the figure the following parameter values are assumed:

- Flowrate: 3600, 5400, 7200 and 9000 m^3/day
- Distance between the wells and the faults of 12 m, 60 m, 192 m and 396 m
- Injection temperature: 303.15 K, 308.15 K and 313.15 K
- 75 m fault throw

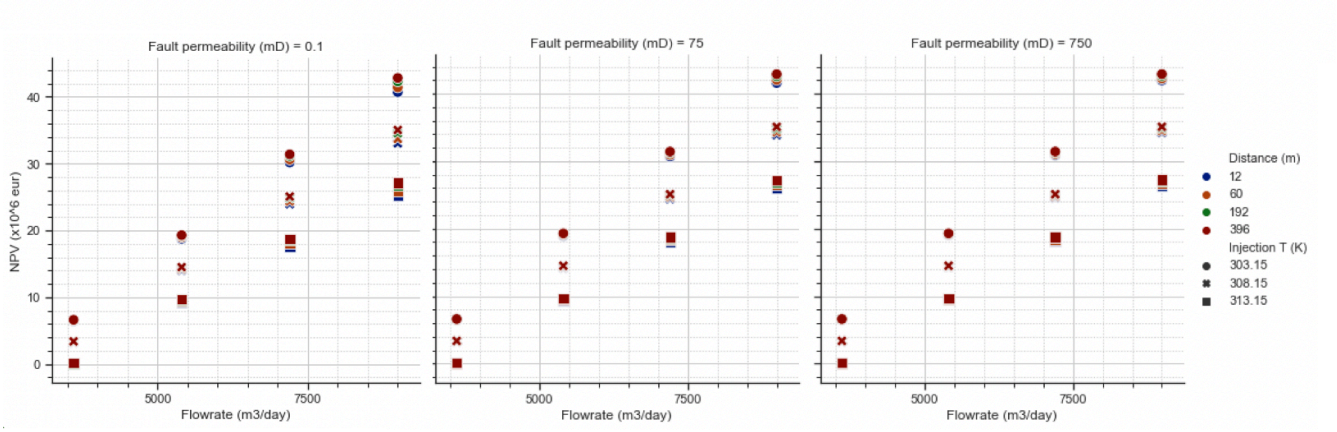

Figure J.1.2: Comparison of the combined influence of injection temperature, distance between the fault and the wells and flowrates between 3600 and 9000 m^3/day on the NPV in presence of a sealing, a medium sealing and a transparent fault when 75 m throw is present

J.2. Comparison of The Produced Amount of Energy

The following figures show the comparison of the produced energy for a sealing, a medium sealing and a transparent fault. The figure is based on:

- Injection temperature: 303.15 K
- Flowrates: 3600, 5400, 7200 and 9000 m^3/day
- Distance between the fault and the wells: 12 m, 60 m, 192 m and 396 m
- Fault throw: 0 and 75 m

Produced Energy in the Presence of Zero Fault Throw

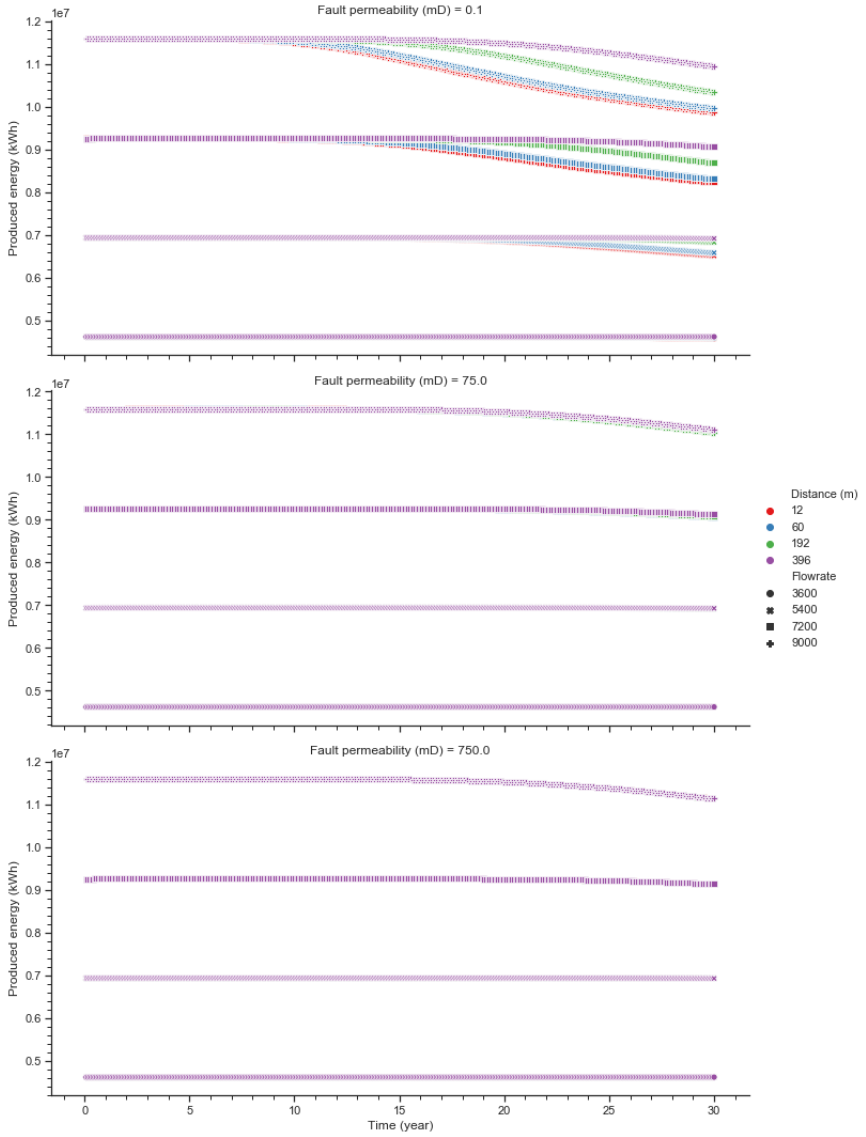

Figure J.2.1: The combined influence of an injection temperature of 303.15 K, distance between the fault and the wells and flowrates between 3600 and 9000 m^3/day on the produced energy in presence of a sealing fault, medium sealing and a transparent fault

Produced Energy in the Presence of 75 m Fault Throw

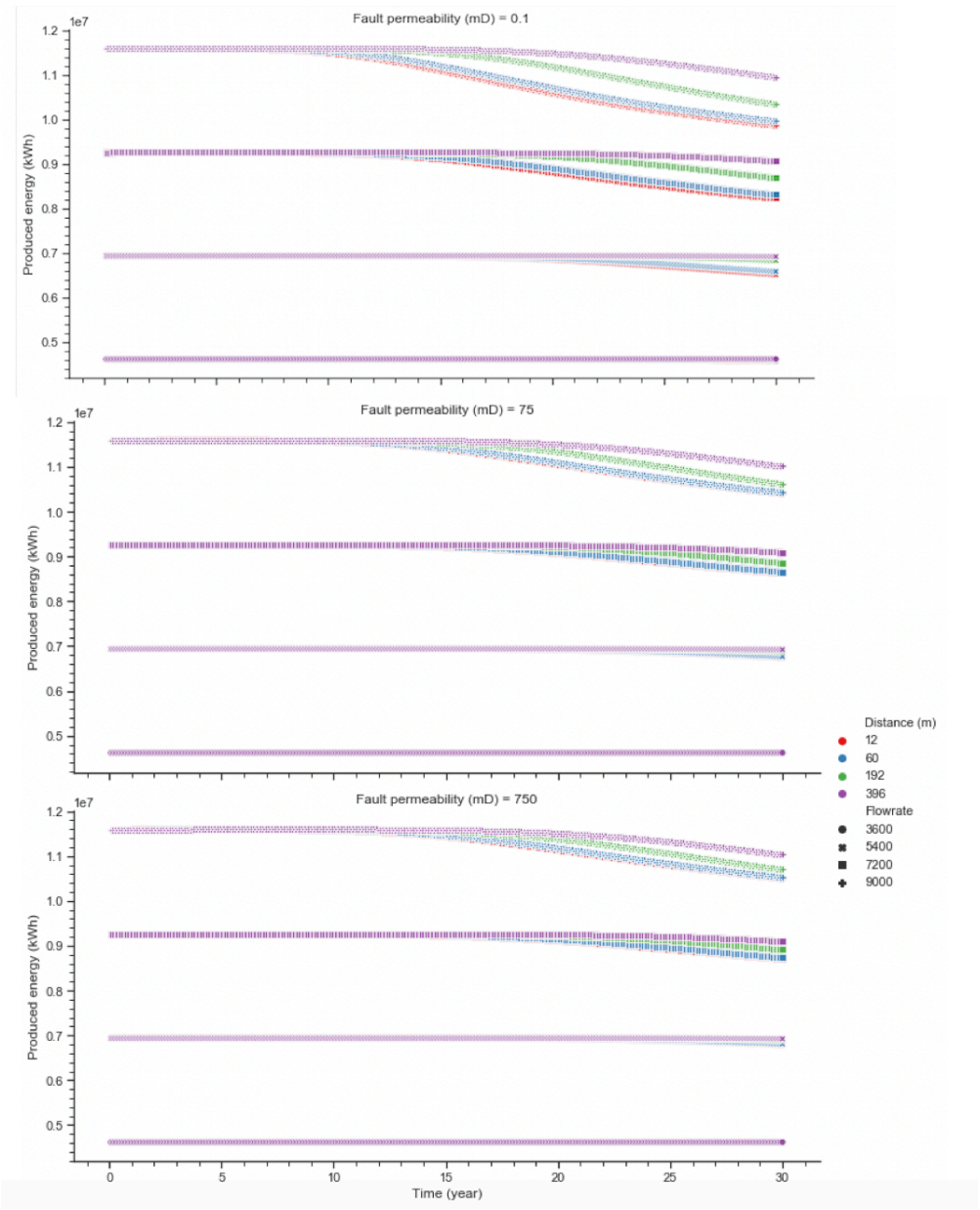

Figure J.2.2: The combined influence of an injection temperature of 303.15 K, distance between the fault and the wells and flowrates between 3600 and 9000 m^3/day on the produced energy in presence of a sealing fault, medium sealing and a transparent fault when 75 m throw is present.

J.3. Comparison of The Production Temperature

The following figures show the comparison of the produced energy for a sealing, a medium sealing and a transparent fault. The figure is based on:

- Injection temperature: 303.15 K
- Flowrates: 3600, 5400, 7200 and 9000 m^3/day
- Distance between the fault and the wells: 12 m, 60 m, 192 m and 396 m
- Fault throw: 0 m

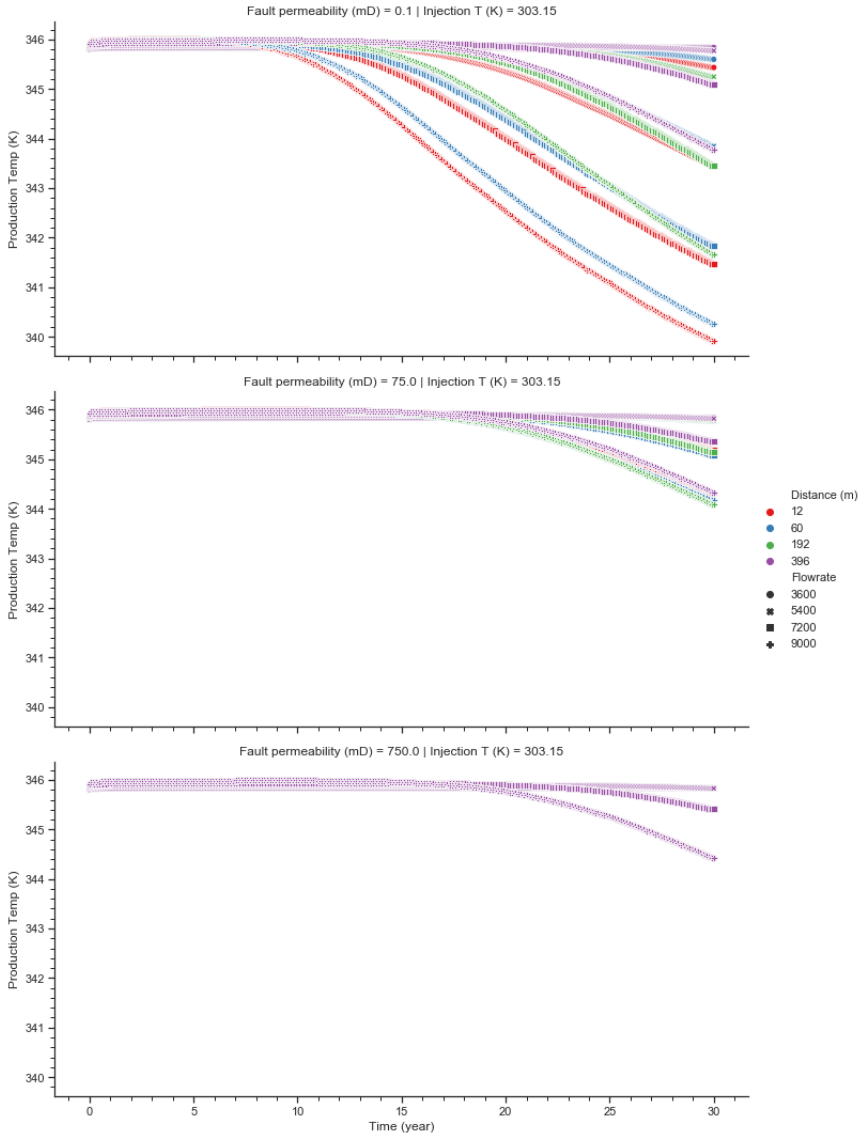

Figure J.3.1: The combined influence of an injection temperature of 303.15 K, distance between the fault and the wells and flowrates between 3600 and 9000 m^3/day on the temperature of the production water in the presence of a sealing fault, medium sealing and a transparent fault

J.4. Comparison of The Pumping Costs

The following figures show the comparison of the pumping costs for a sealing, a medium sealing and a transparent fault. The figure is based on:

- Injection temperature: 303.15 K
- Flowrates: 3600, 5400, 7200 and 9000 m^3/day
- Distance between the fault and the wells: 12 m, 60 m, 192 m and 396 m
- Fault throw: 0 and 75 m

The Pumping Costs in the Presence of Zero Fault Throw

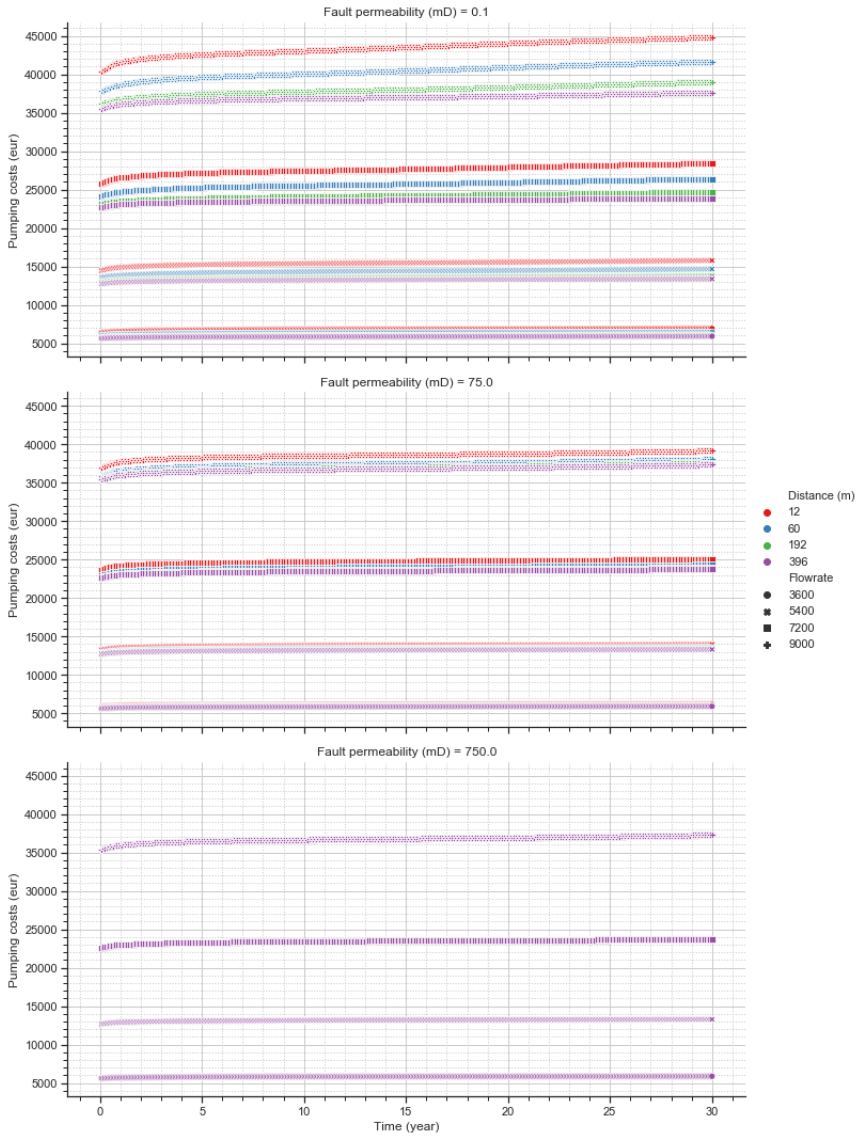

Figure J.4.1: The combined influence of an injection temperature of 303.15 K, distance between the fault and the wells and flowrates between 3600 and 9000 m^3/day on the pumping costs in presence of a sealing, a medium sealing and a transparent fault and zero throw.

The Pumping Costs in the Presence of 75 m Fault Throw

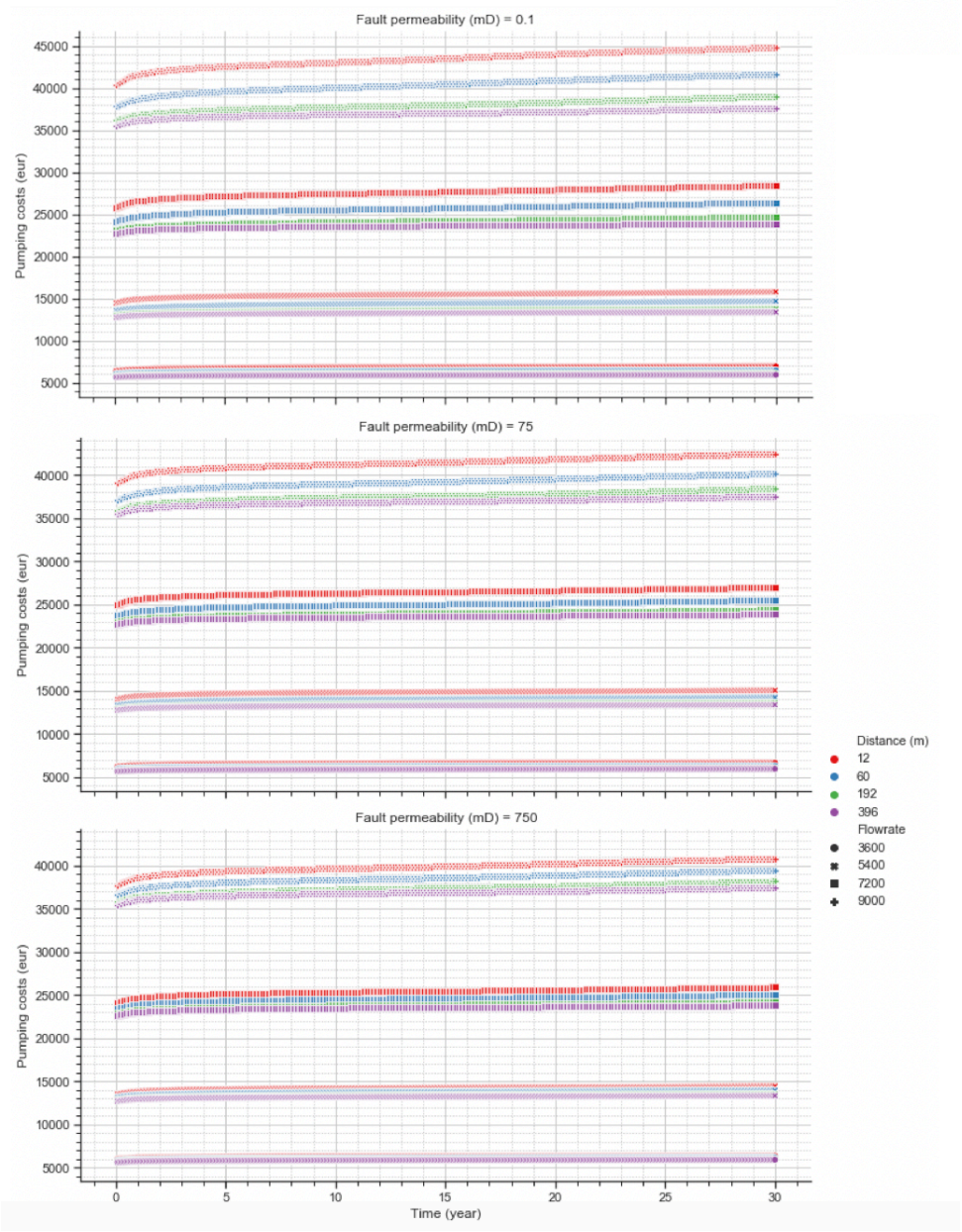

Figure J.4.2: The combined influence of an injection temperature of 303.15 K, distance between the fault and the wells and flowrates between 3600 and 9000 m^3/day on the pumping costs in presence of a sealing, a medium sealing and a transparent fault and 75 m throw.

J.5. NPV and Maximum Encountered Pore Pressures

The comparison of the combination in NPV and maximum encountered pore pressures next to the fault for the three fault types. For the figure the following parameter values are assumed:

- Flowrate: 3600, 5400, 7200 and 9000 m^3/day
- Distance between the wells and the faults of 12 m, 60 m, 192 m and 396 m
- Injection temperature: 303.15 K, 308.15 K and 313.15 K
- Fault throw: 0 m, 25 m and 75 m

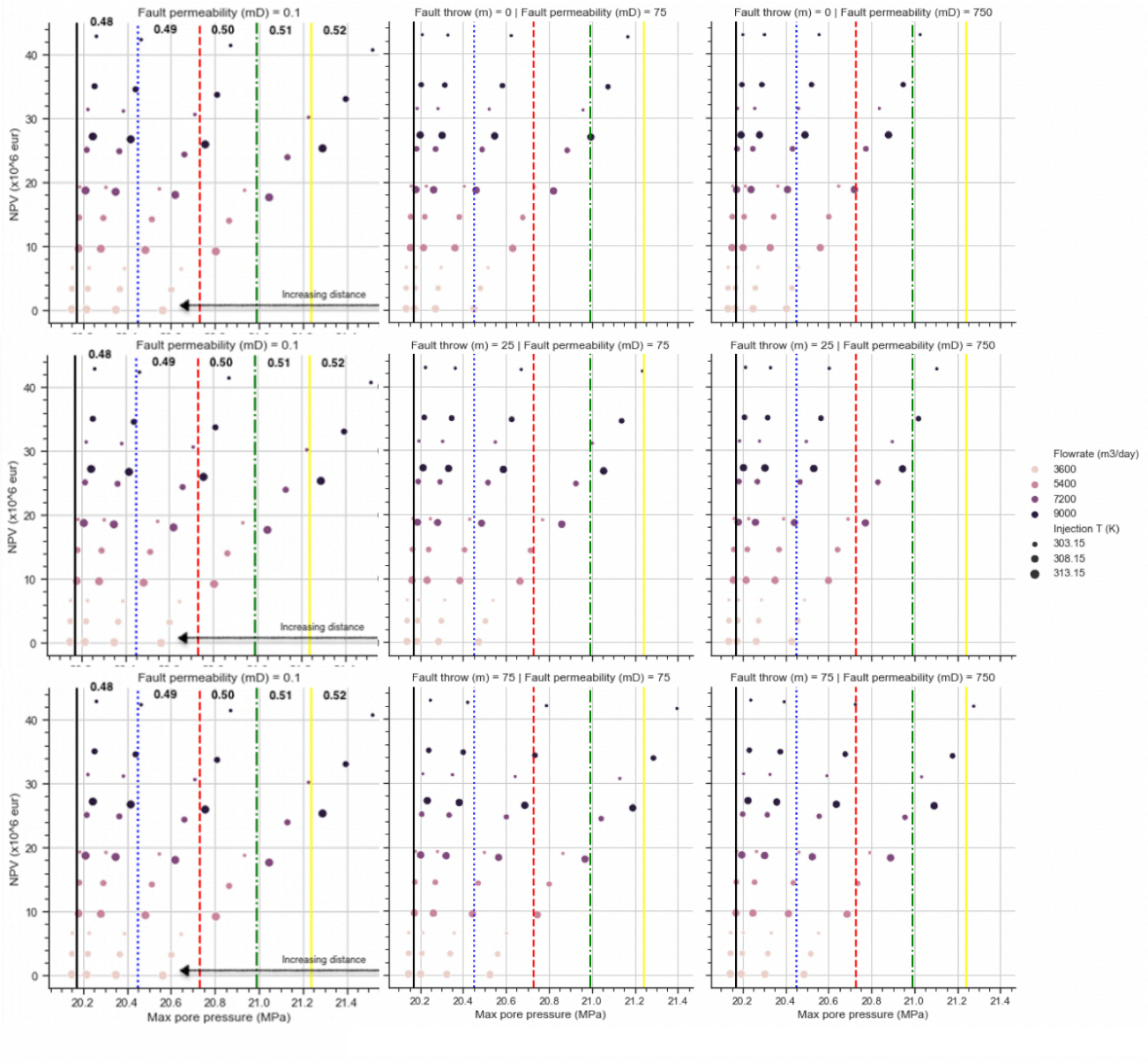

Figure J.5.1: Comparison of the combined NPV and maximum encountered pore pressures next to the fault in presence of a sealing, a medium sealing fault and a transparent fault. Showing the influence of the injection temperature, distance between the fault and the wells and flowrates between 3600 and 9000 m^3/day on the NPV in presence of a sealing, a medium sealing and a transparent fault.

J.6. Encountered BHP Values

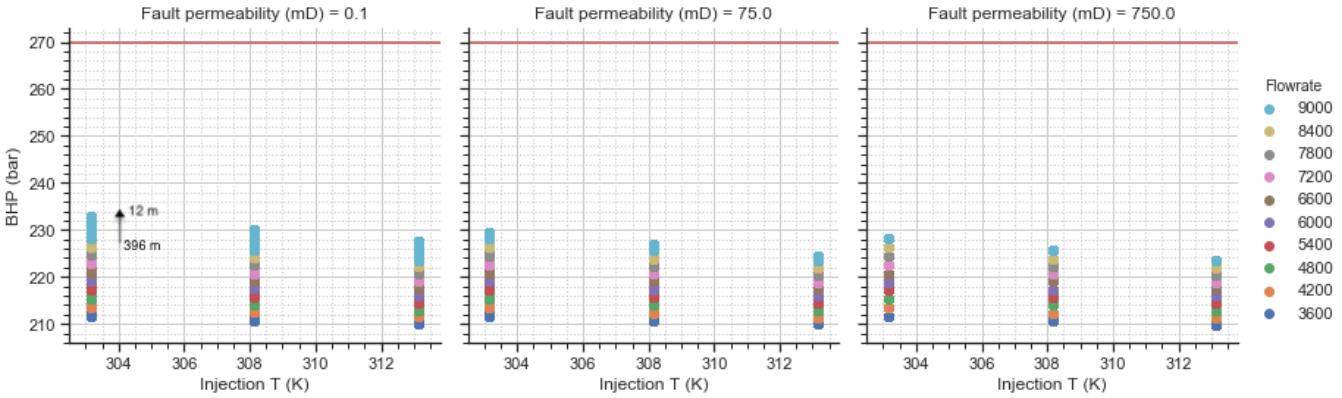

Figure J.6.1: Comparison of the maximum BHP values in a homogeneous reservoir in the presence of a sealing, medium sealing and transparent fault. The results show the combined influence of the injection temperatures, flowrates between 3600 and 9000 m^3/day and distance between the fault and the wells between 12 m and 396 m (indicated by the arrow). The maximum allowable BHP is 270 bar, determined according to the protocol set up by SodM and TNO-AGE (2013). This maximum allowable BHP is indicated by the red horizontal line.

All results are shown for the presence of a sealing and a transparent fault in a heterogeneous DSSM reservoir. The figures are based on the following parameters, except if mentioned differently:

- Injection temperatures: 303.15 K and 313.15 K
- Flowrates: 3600, 5400, 7200 and 9000 m^3/day
- Distance between the fault and the wells: 60 m, 90 m, 180 m and 390 m
- Fault throw: 0 m

K.1. Comparison of The Produced Amount of Energy

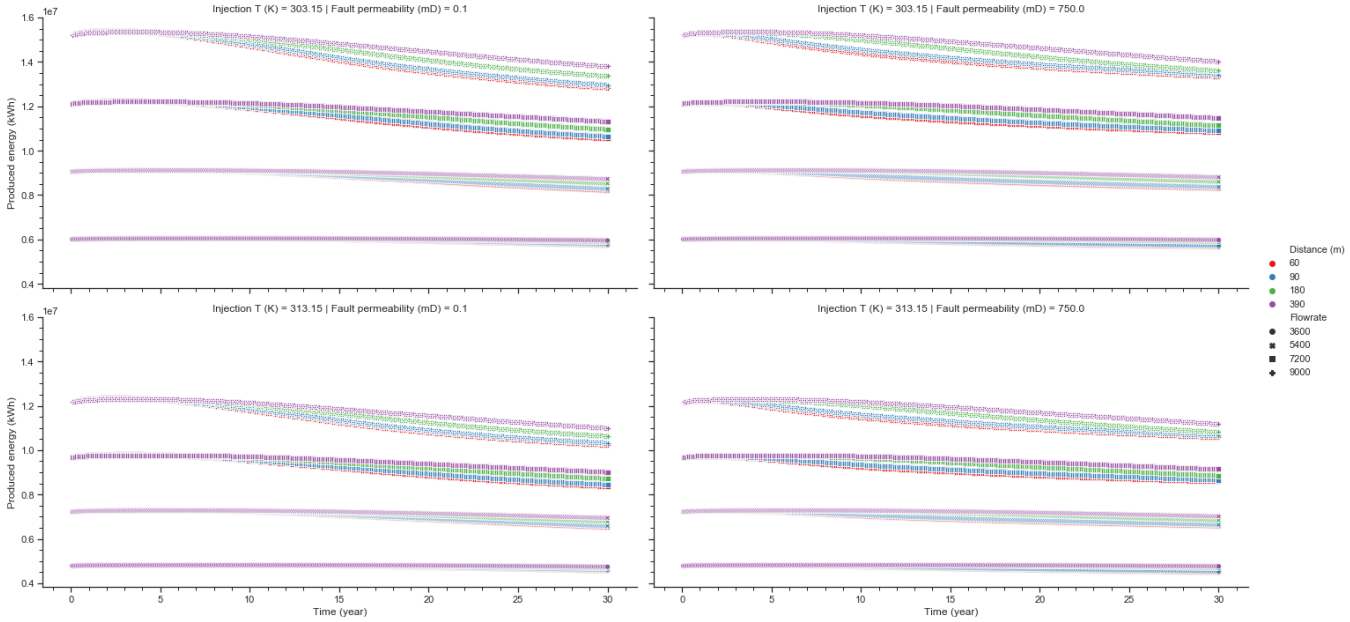

Figure K.1.1: Comparison of the produced energy in the presence of a sealing and a fully transparent fault in the heterogeneous DSSM reservoir. As a result of the influence of injection temperature, distance between the fault and the wells and flowrates between 3600 and 9000 m^3/day

K.2. Comparison of The Required Amount of Pumping Energy

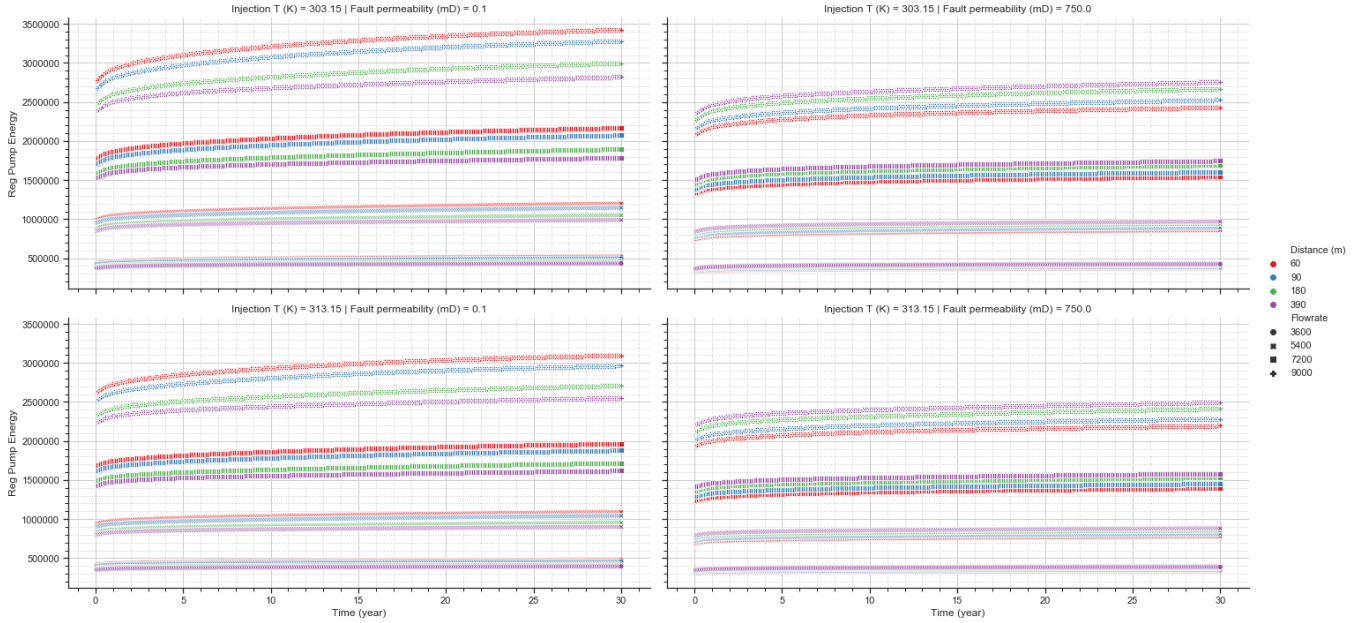

Figure K.2.1: Comparison of the required amount of pumping energy in the presence of a sealing and a fully transparent fault in the heterogeneous DSSM reservoir. As a result of the influence of injection temperature, distance between the fault and the wells and flowrates between 3600 and 9000 m^3/day

K.3. Permeability and Pressure Distribution in Presence of A Sealing and a Transparent Fault

The comparison of the heterogeneity and pressure distribution in the presence of a sealing and a fully transparent fault in a heterogeneous DSSM reservoir. The figure is based on:

- Injection temperature: 303.15 K
- Flowrate: 9000 m^3/day
- Distance between the fault and the wells: 60 m
- Fault throw: 0 m

Transparent Fault and Distance Between the Fault and the Wells of 60 m

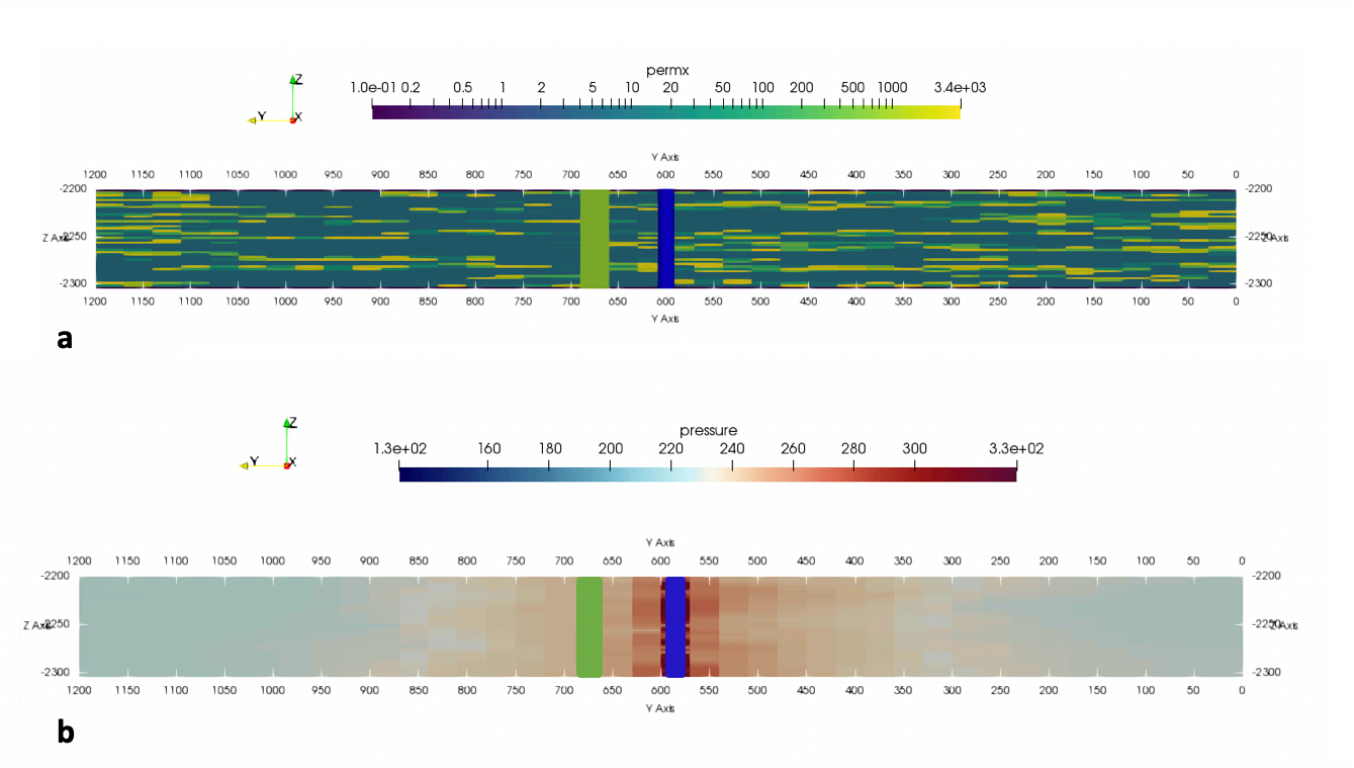

Figure K.3.1: X-view slice of the reservoir showing the permeability and pressure distribution in the DSSM reservoir when the wells are placed 60 m from a transparent fault. As a result of 303.15 K injection temperature and a flowrate of 9000 m^3/day. The permeability and pressure distribution are visualized in figures a and b respectively.

Transparent Fault and Distance Between the Fault and the Wells of 390 m

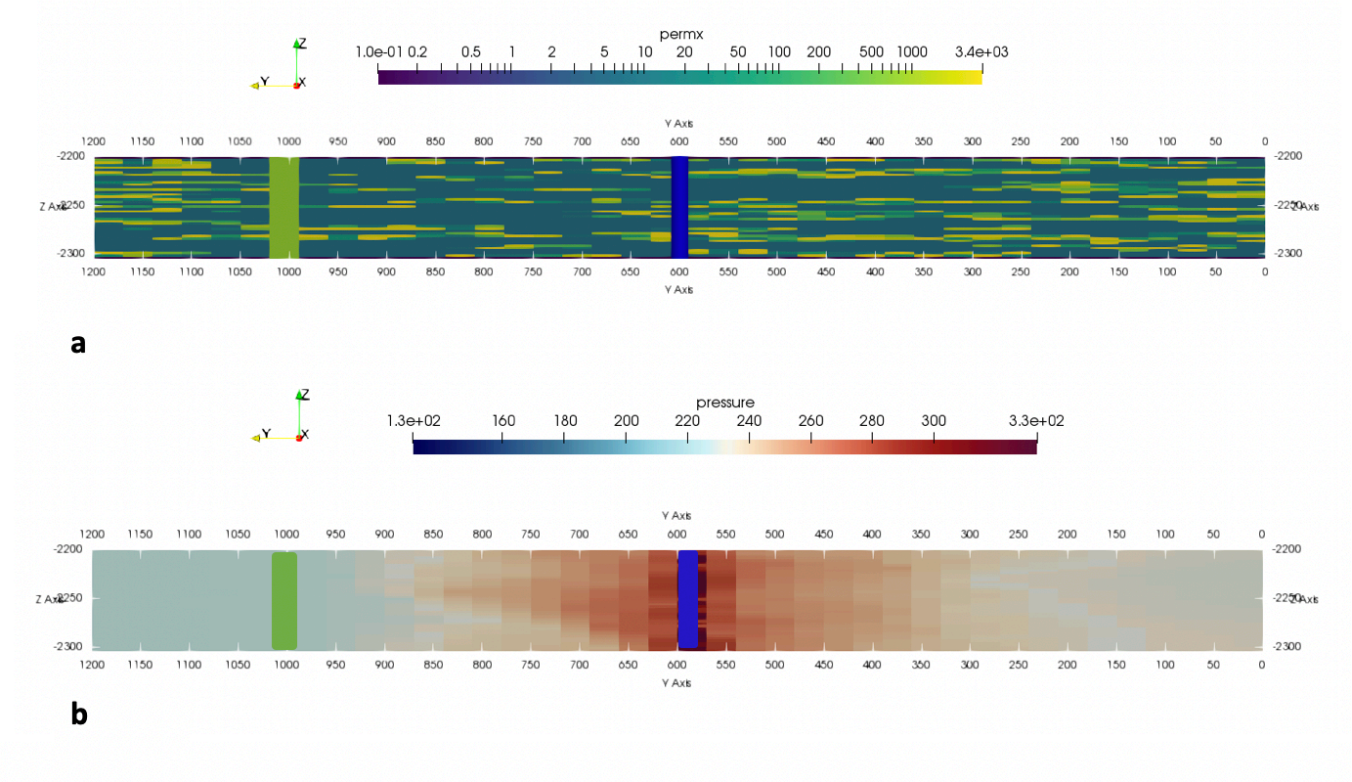

Figure K.3.2: X-view slice of the reservoir showing the permeability and pressure distribution in the DSSM reservoir when the wells are placed 390 m from a transparent fault. As a result of 303.15 K injection temperature and a flowrate of 9000 m^3/day. The permeability and pressure distribution are visualized in figures a and b respectively.

Sealing Fault and Distance Between the Fault and the Wells of 60 m

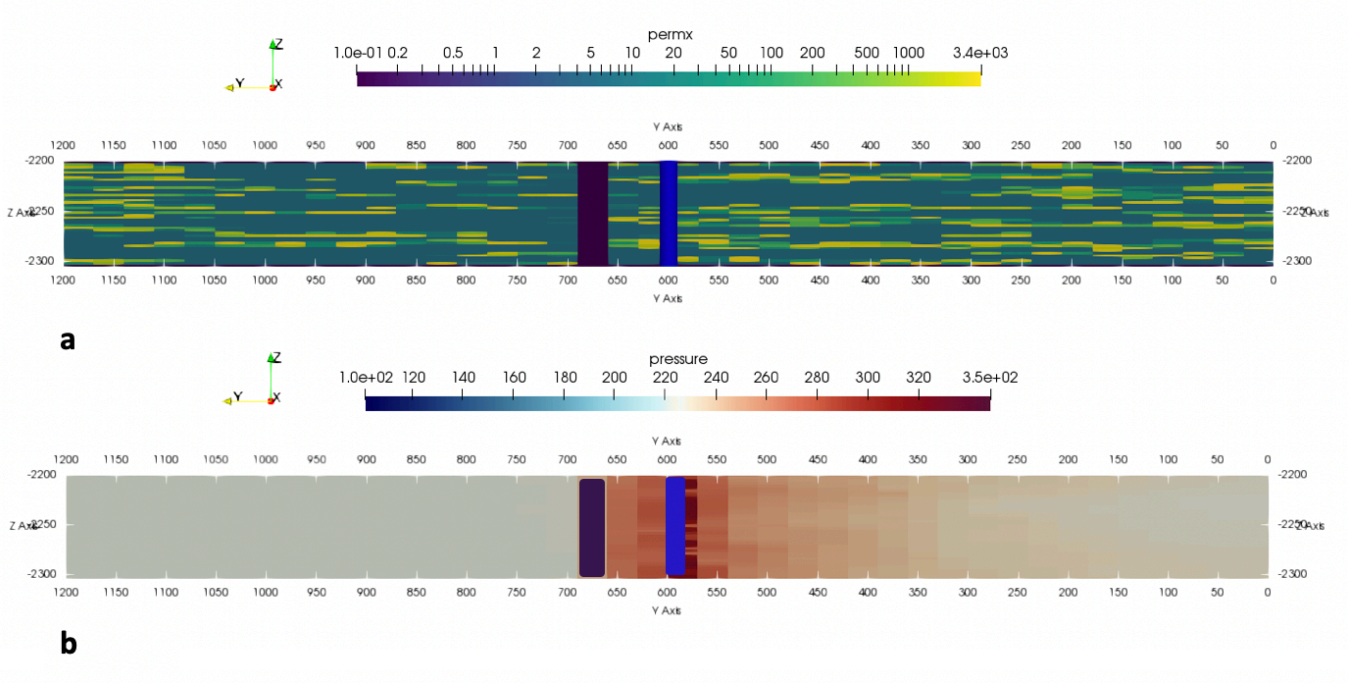

Figure K.3.3: X-view slice of the reservoir showing the permeability and pressure distribution in the DSSM reservoir when the wells are placed 60 m from a sealing fault. As a result of 303.15 K injection temperature and a flowrate of 9000 m^3/day. The permeability and pressure distribution are visualized in figures a and b respectively.

Sealing Fault and Distance Between the Fault and the Wells of 390 m

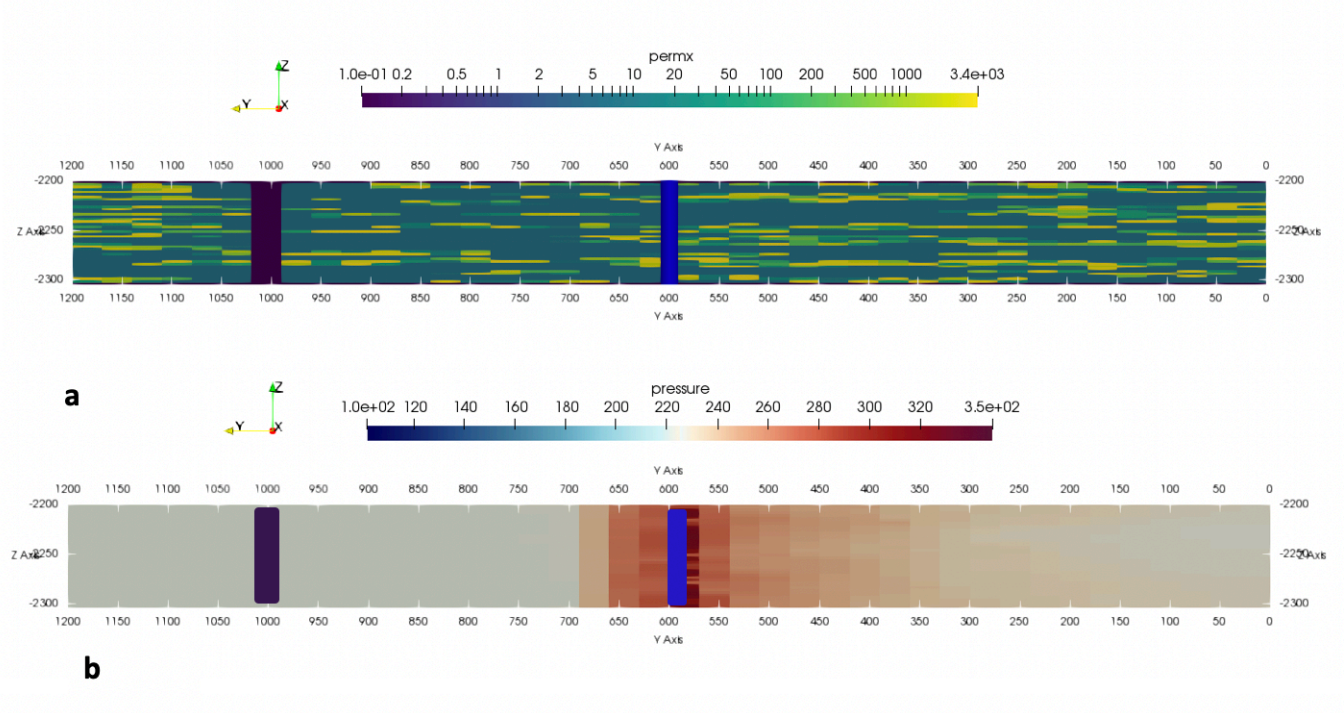

Figure K.3.4: X-view slice of the reservoir showing the permeability and pressure distribution in the DSSM reservoir when the wells are placed 390 m from a sealing fault. As a result of 303.15 K injection temperature and a flowrate of 9000 m^3/day. The permeability and pressure distribution are visualized in figures a and b respectively.

K.4. Encountered BHP values

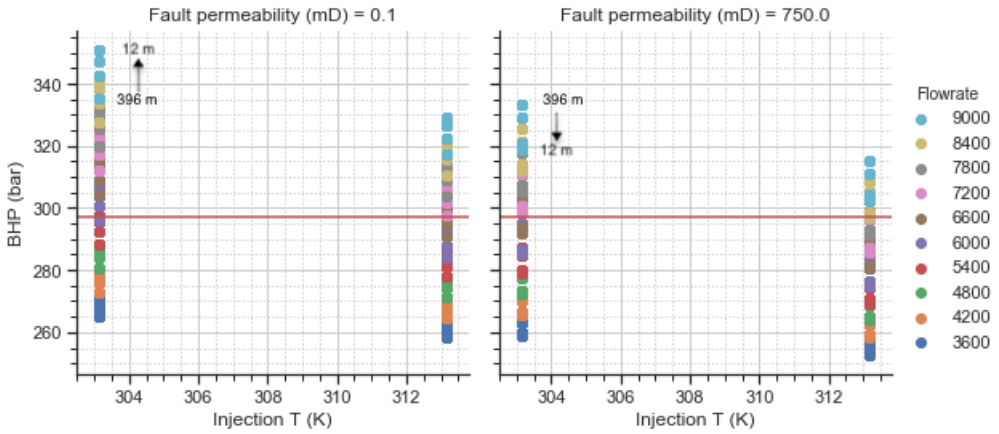

Figure K.4.1: Comparison of the maximum encountered BHP values in the heterogeneous Delft Sandstone reservoir in the presence of a sealing and a transparent fault. The results show the combined influence of 303.15 K and 313.15 K injection temperatures, flowrates between 3600 and 9000 m^3/day and distance between the fault and the wells of 60 m, 90 m, 180 m and 390 m (indicated by the arrow). The maximum allowable BHP is 297 bar, determined according to the protocol set up by SodM and TNO-AGE (2013). This maximum allowable BHP is indicated by the red horizontal line.

Closer View on the BHP Values

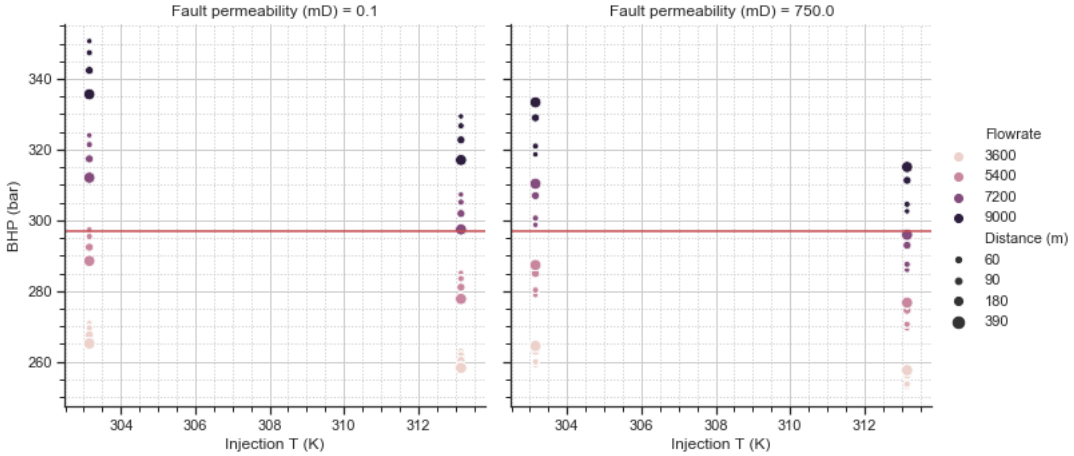

Figure K.4.2: Closer view on the comparison of the maximum encountered BHP values in the heterogeneous Delft Sandstone reservoir in the presence of a sealing and a transparent fault. The results show the combined influence of 303.15 K and 313.15 K injection temperatures, flowrates between 3600 and 9000 m^3/day and distance between the fault and the wells of 60 m, 90 m, 180 m and 390 m (indicated by the arrow). The maximum allowable BHP is 297 bar, determined according to the protocol set up by SodM and TNO-AGE (2013). This maximum allowable BHP is indicated by the red horizontal line.

K.5. Economic Sensitivity Results

Normal Gas Price of 0.016 eur/kWh

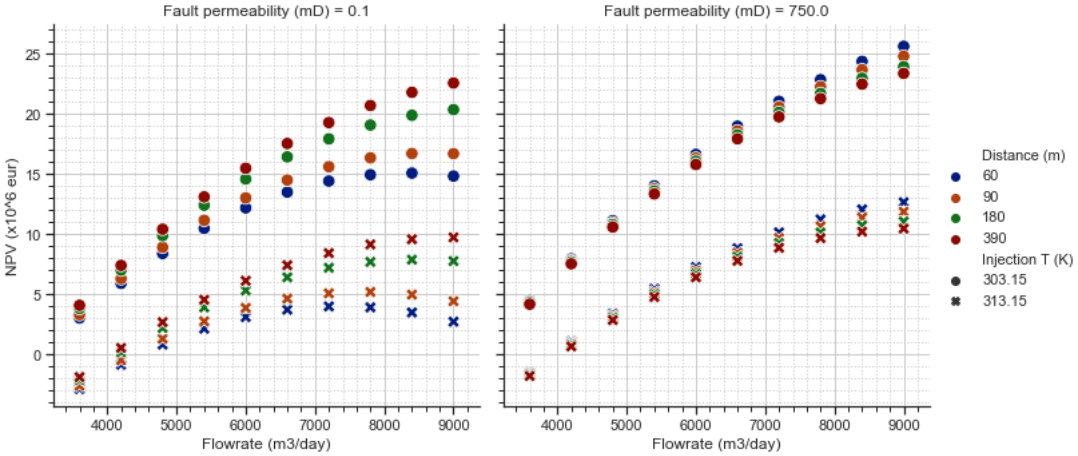

Figure K.5.1: NPV outcomes of the heterogeneous reservoir in the presence of a sealing fault and a transparent fault. The results show the combined influence of 303.15 K and 313.15 K injection temperatures, flowrates between 3600 and 9000 m^3/day and distance between the fault and the wells of 60 m, 90 m, 180 m and 390 m.

Exclusion of the SDE+ Subsidy and a Low Gas Price

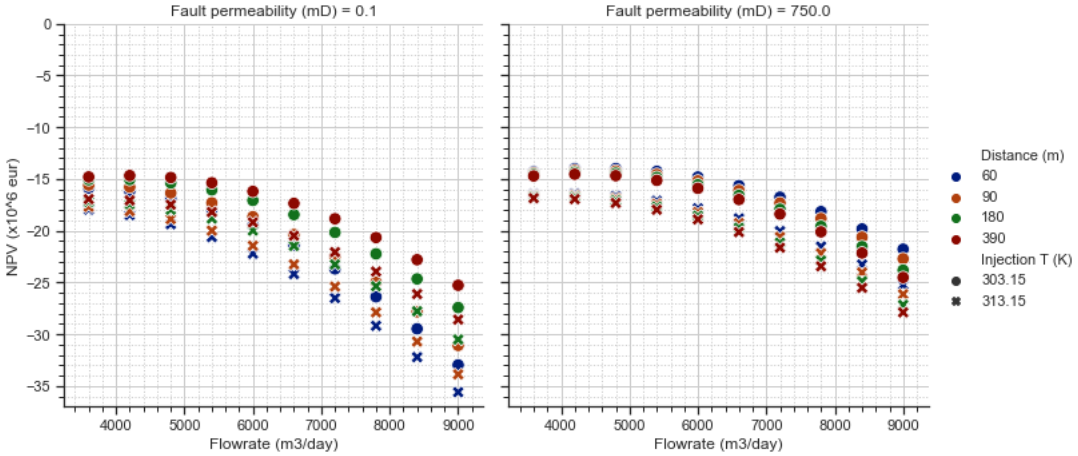

Figure K.5.2: NPV outcomes of the heterogeneous reservoir when a low gas price is combined with SDE+ subsidy exclusion in the presence of a sealing fault and a transparent fault. The results show the combined influence of 303.15 K and 313.15 K injection temperatures, flowrates between 3600 and 9000 m^3/day and distance between the fault and the wells of 60 m, 90 m, 180 m and 390 m.

Bibliography

Anderson, E. (1951). *The dynamics of faulting and dyke formation with applications to Britain*. 2d ed. Edinburgh, Oliver and Boyd.

Baisch, S., Koch, C., Stang, H., and et.al. (2016). Defining the framework for seismic hazard assessment in geothermal projects v0.1. Technical report, Q-con GmbH and IF Technology B.V.

Bakker, R. (2019). Fault stability DAP well. Unpublished report, Delft University of Technology.

Belastingdienst (2019). *Handboek milieubelastingen 2019'*. https://download.belastingdienst.nl/belastingdienst/docs/handboek_milieubelast_2019_ml0301z91fd.pdf [Accessed: 05-11-19].

Bonte, D., van Wees, J.-D., and Verweij, J. (2012). Subsurface temperature of the Onshore Netherlands: new temperature dataset and modelling. *Netherlands Journal of Geosciences*, 91-4:491–515.

Buijze, L., van Bijsterveldt, L., Cremer, H., Paap, B., and et.al. (2019a). Review of induced seismicity in geothermal systems worldwide and implications for geothermal systems in the netherlands. *Netherlands Journal of Geosciences*, 98(13).

Buijze, L., van Bijsterveldt, L., Cremer, H., Paap, B., and et.al. (2019b). Review of worldwide geothermal projects: mechanisms and occurrence of induced seismicity. Technical report, TNO.

Burg, J. (2018). Script to Structural Geology. Technical report, ETH Zurich Research Collection.

Candela, T., Wassing, B., Ter Heege, J., and Buijze, L. (2018). How earthquakes are induced. *Science*, 360:598–600.

CBS (2019). *Aardgas en elektriciteit, gemiddelde prijzen van energieverbruikers*. https://opendata.cbs.nl/statline/#/CBS/nl/dataset/81309NED/table?fromstatweb [Accessed: 02-11-19].

Daniilidis, A., Alpsoy, B., and Herber, R. (2017). Impact of technical and economic uncertainties on the economic performance of a deep geothermal heat system. *Renewable Energy*, 114(Part B):805–816.

Daniilidis, A., Doddema, L., and Herber, R. (2016). Risk assessment of the groningen geothermal potential: From seismic to reservoir uncertainty using a discrete parameter analysis. *Geothermics*, 64:271–288.

Daniilidis, A., Hamidreza, M., and Bruhn, D. (2020a). Interdependencies between physical, design and operational parameters for direct use geothermal heat in faulted hydrothermal reservoirs. *Geothermics*, 86(101806).

Daniilidis, A., Khait, M., Saeid, S., and et.al. (2020b). A high performance framework for the optimization of geothermal systems, comparing energy production and economic output. In *World Geothermal Congress 2020*.

de Boer, S., Bourdon, E., Butterman, G., and et.al. (2016). *Evaluatie Algemeen instrumentarium geothermie'*.

Den Hartog Jager, D. (1996). Fluviomarine sequences in the lower cretaceous of the west netherlands basin: correlation and seismic expression. *Geology of gas and oil under the Netherlands*, Springer:229–241.

DeVault, B. and Jeremiah, J. (2002). Tectonostratigraphy of the nieuwerkerk formation (delfland subgroup), west netherlands basin. *AAPG Bulletin*, 86:1679–1707.

Dinoloket (2020). *Delft Sandstone Member SLDND*. https://www.dinoloket.nl/delft-sandstone-member-sldnd [Accessed: 20-03-20].

DiPippo, R. (2016). *Geothermal Power Generation: Developments and Innovation*. Woodhead Publishing.

Doddema, L. (2012). The influence of reservoir heterogeneities on geothermal doublet performance. *Default journal*.

Donselaar, M., Groenenberg, R., and Gilding, D. T. (2015). Reservoir geology and geothermal potential of the delft sandstone member in the west netherlands basin. In *World Geothermal Congress 2015*.

Dutch Government (2020). *Mijnbouwwet*. https://wetten.overheid.nl/BWBR0014168/2020-03-18 [Accessed: 27-04-20].

EBN (2017). Energie in Nederland. https://www.energieinnederland.nl/2017 [Accessed: 13-01-20].

Fitts, C. (2013). *Groundwater Science*. 2nd ed. Elsevier Science Publishing Co Inc.

Gaucher, E., Schoenball, M., Heidbach, O., Zang, A., and et.al. (2015). Induced seismicity in geothermal reservoirs: A review of forecasting approaches. *Renewable and Sustainable Energy Reviews*, 52:1473–1490.

Gilding, D. (2010). Heterogeneity determination of the delft subsurface for heat flow modelling. Master's thesis, Applied Earth Sciences, Delft University of Technology.

Grasso, J. (1992). Mechanics of seismic instability induced by the recovery of hydrocarbons. *Pure and Applied Geophysic*, 193(3):507–534.

Hanson, P. (2019). Phases of a Geothermal Project Pt1. https://www.geoenergymarketing.com/energy-blog/phases-of-a-geothermal-project-pt-1/ [Accessed: 03-11-19].

Heidbach, O., Barth, A., Müller, B., and et.al (2016). Wsm quality ranking scheme, database description and analysis guidelines for stress indicator. Technical report, World Stress Map Technical Report 16-01, GFZ German Research Centre for Geoscience. http://www.world-stress-map.org/fileadmin/wsm/pdfs/WSM_TR_16-01.pdf [Accessed: 09-01-20].

Herber, R. (2020). *Personal Communication*. Member of the Dutch Mining Council and Professor Geo-Energy at the RijksUniversiteit Groningen.

Hillis, R. (2000). Pore pressure/stress coupling and its implications for seismicity. *Exploration Geophysics*, 31:1448–454.

Jaeger, J. and Cook, N. (1979). *Fundamentals of rock mechanics (third edition)*. Chapman and Hall, London U.K.

Khait, M. and Voskov, D. (2018a). Adaptive parameterization for solving of thermal/compositional nonlinear flow and transport with buoyancy. *SPE Journal*.

Khait, M. and Voskov, D. (2018b). Operator-based linearization for efficient modeling of geothermal processes. *Geothermics*, 74:7–18.

Kidambi, T. and Kumar, G. (2016). Mechanical earth modeling for a vertical well drilled in a naturally fractured tight carbonate gas reservoir in the persian gulf. *Journal of Petroleum Science and Engineering*, 141:38–51.

Lukawski, M., Anderson, B., Augustine, C., and et.al. (2014). Cost analysis of oil, gas, and geothermal well drilling. *Journal of Petroleum Science and Engineering*, 118:1–14.

Mechelse, E. (2017). The in-situ stress field in the Netherlands: Regional trends, local deviations and an analysis of the stress regimes in the northeast of the Netherlands. Master's thesis, Applied Earth Sciences, Delft University of Technology.

Mezger, W. (2014). The Shale Oil Potential of the Posidonia Formation in the Netherlands. Master's thesis, Applied Earth Sciences, Delft University of Technology.

Michon, L., van Balen, R., Merle, O., and et.al. (2003). The Cenozoic evolution of the Roer Valley Rift Systemintegrated at a European scale. *Tectonophysics*, 367:101–126.

Mijnlieff, H., van Kempen, B., van der Molen, R., and et.al (2017). Specificaties geologisch onderzoek voor geothermieprojecten – rapportagevereisten sde+ en rnes. Technical report, TNO. https://www.rvo.nl/sites/default/files/2017/12/Specificaties%20Geologisch%20onderzoek%20SDE%20en%20RNES%20april%202017.pdf, [Accessed: 05-01-20].

Ministerie van Economische Zaken en Klimaat (2019). Staatscourant van het Koninkrijk der Nederlanden, nr 9735. https://zoek.officielebekendmakingen.nl/stcrt-2019-9735 [Accessed: 05-11-19].

Moeck, I., Kwiatek, G., and Zimmermann, G. (2009). Slip tendency analysis, fault reactivation potential and induced seismicity in a deep geothermal reservoir. *Journal of Structural Geology*, 31(10):1174–1182.

Morris, A., Ferill, D., and Henderson, D. (1996). Slip-tendency analysis and fault reactivation. *Geology*, 24(3):275–278.

National Research Council (2013). *Induced Seismicity Potential in ENERGY TECHNOLOGIES*. Washington, DC: The National Academies Press.

Nelskamp, S. and Verweij, J. (2016). Using basin modeling for geothermal energy exploration in the netherlands - an example from the west netherlands basin and roer valley graben. Technical report, TNP. https://www.nlog.nl/sites/default/files/west%20netherlands%20basin_nelskamp%20and%20verweij_tno-060-ut-2012-00245.pdf [Accessed: 17-03-20].

Neuzil, C. (1994). How permeable are clays and shales? *Water Resources Research*, 30:145–150.

O'Sullivan, M., Pruess, K., and Lippmann, M. (2000). State of the art geothermal reservoir simulation. *Geothermics*, 30(4):395–429.

Osundare, O., Teodoriu, C., Faclone, G., and et.al. (2018). Estimation of plugging and abandonment costs based on different eu regulations with application to geothermal wells. In *43rd Workshop on Geothermal Reservoir Engineering*.

Pennington, W., Davis, S., Carlson, S., and et.al. (1986). The evolution of seismic barriers and asperities caused by the depressuring of fault planes in oil and gas of south texas. *Bulletin of the Seismological Society of America*, 76(4):939–948.

Platt, J., Xia, H., and Schmidt, W. (2018). Rheology and stress in subduction zones around the aseismic/seismic transition. *Progress in Earth and Planetary Science*, 5(24).

Platteeuw, I. (2018). Initiation of Fault Reactivation. Master's thesis, Applied Earth Sciences, Delft University of Technology.

Pluymaekers, M., Kramers, L., van Wees, J., and et.al. (2012). Reservoir characterisation of aquifers for direct heat production: Methodology and screening of the potential reservoirs for the netherlands. *Netherlands Journal of Geosciences*, 91-4:621–636.

Preuss, S., Herrendörfer, R., Gerya, T., and et.al (2019). Seismic and aseismic fault growth lead to different fault orientations. *Reviews of Geophysics*, 124(8):8867–8889.

Rijksdienst voor Ondernemend Nederland (2019a). Regeling nationale EZ subsidies - Risico's dekken voor Aardwarmte, Handleiding Garantiestelling tegen het risico van misboring. *Zevende en achtste openstelling*.

Rijksdienst voor Ondernemend Nederland (2019b). SDE+ najaar 2019. https://www.rvo.nl/sites/default/files/2019/10/Brochure%20SDE%20najaar%202019.pdf [Accessed: 04-11-19].

Rijksoverheid (2019). Wijzigingen vennootschapsbelasting, belastingplan 2020. https://www.rijksoverheid.nl/onderwerpen/belastingplan/belastingwijzigingen-voor-ondernemers/vennootschapsbelasting [Accessed: 06-11-19].

Romera, J. (2020). *iapws.iapws97 module*. https://iapws.readthedocs.io/en/latest/iapws.iapws97.html [Accessed: 27-04-20].

Saeid, S., Al-Khoury, R., Nick, H., and et.al. (2015). A prototype design model for deep low-enthalpy hydrothermal systems. *Renewable Energy*, 77:408–422.

Samuelson, J. and Spiers, C. (2012). Fault friction and slip stability not affected by co 2 storage : Evidence from short-term laboratory experiments on north sea reservoir sandstones and caprocks. *International Journal of Greenhouse Gas Control*, 11.

Schoof, F., van der Hout, M., van Zanten, J., and et.al. (2018). Masterplan Aardwarmte in Nederland. Technical report, Platform Geothermie, DAGO, Stichting Warmtenetwerk, EBN. https://www.ebn.nl/wp-content/uploads/2018/05/20180529-Masterplan-Aardwarmte-in-Nederland.pdf [Accessed: 02-11-19].

Schoots, K. and Hammingh, P. (2019). Klimaat- en Energieverkenning 2019. Technical report, Den Haag: Planbureau voor de Leefomgeving. https://www.pbl.nl/sites/default/files/downloads/pbl-2019-klimaat-en-energieverkenning-2019-3508.pdf [Accessed: 04-10-19].

Schwarts, S. and Rokosky, J. (2007). Slow slip events and seismic tremor at circum□pacific subduction zones. *Reviews of Geophysics*, 45(3).

Shetty, S. (2017). Numerical strategy for uncertainty quantification in low enthalpy geothermal projects. Master's thesis, Applied Earth Sciences, Delft University of Technology.

SodM (2016). Methodiek voor risicoanalyse omtrent geinduceerde bevingen door gaswinning. Technical report. Versie 1.2, Den Haag.

SodM (2017). Staat van de sector geothermie. Technical report. https://www.sodm.nl/documenten/rapporten/2017/07/13/staat-van-de-sector-geothermie [Accessed: 11-04-20].

SodM (2018). *Aardwarmteproject nabij Venlo uit voorzorg stil gelegd na aardbeving*. https://www.sodm.nl/actueel/nieuws/2018/09/06/aardwarmteproject-nabij-venlo-uit-voorzorg-stil-gelegd-na-aardbeving [Accessed: 03-03-20].

SodM and TNO-AGE (2013). Protocol bepaling maximale injectiedrukken bij aardwarmtewinning – versie 2. Technical report. https://www.sodm.nl/documenten/publicaties/2013/11/23/protocol-bepaling-maximale-injectiedrukken-bij-aardwarmtewinning, [Accessed: 13-04-20].

Stichting Platform Geothermie (2019). *Hoe duurzaam is aardwarmte? 'Factsheet Duurzaamheid'*. https://geothermie.nl/images/Factsheets/20190729_mp_hoe_duurzaam_is_geothermie.pdf [Accessed: 17-03-20].

Straver, F. (2019). *SodM komt met nieuwe eisen, want ook groene energie moet veilig zijn*. https://www.trouw.nl/duurzaamheid-natuur/sodm-komt-met-nieuwe-eisen-want-ook-groene-energie-moet-veilig-zijn~b201d0b0/ [Accessed: 27-04-20].

Taghipour, M., Ghafoori, M., and et. al. (2019). Estimation of the current stress field and fault reactivation analysis in the asmari reservoir, sw iran. *Petroleum Science*, 16:513–526.

Takahashi, M., Mizoguchi, M., Kitamura, K., and et.al. (2007). Effects of clay content on the frictional strength and fluid transport property of faults. *Journal of Geophysical Research: Solid Earth*, 112(8).

TNO (2019). *Economic model (Thermogis)*. https://www.thermogis.nl/en/economic-model [Accessed: 02-11-19].

TNO (2020). *Nlog (kaart boringen)*. https://www.nlog.nl/kaart-boringen [Accessed: 02-03-20].

Trading Economics (2020). *Natural Gas 1990-2020*. https://tradingeconomics.com/commodity/natural-gas [Accessed: 10-04-20].

Van Adrichem Boogaert, H. and Kouwe, W. (1993). Stratigraphic nomenclature of the Netherlands, revision and update by Rijks Geologische Dienst (RGD) and Netherlands oil and gas exploration and production association (NOGEPA). *Mededelingen Rijks Geologische Dienst*, 50.

van Adrichem, et. al. (2014). Handboek geothermie 2014. https://www.kasalsenergiebron.nl/content/user_upload/Handboek_Geothermie_DEEL_1_-_2014.pdf [Accessed: 05-11-19].

van Balen, R., van Bergen, F., de Leeuw, C., and et.al. (2000). Modelling the hydrocarbon generation and migration in the West Netherlands Basin, the Netherlands. *Netherlands Journal of Geosciences*, 79:29–44.

van den Bosch, R., Flipse, B., and Vorage, R. (2013). Stappenplan Winning Aardwarmte voor Glastuinbouw. Technical report, Kas als energiebron. https://www.kasalsenergiebron.nl/content/research/14899_Stappenplan_Aardwarmte_12-2013.pdf [Accessed: 06-10-19].

van der Welle, A. and Lensing, S. (2018). Conceptadvies SDE+ 2019. Overzicht basisbedragen en algemene parameters en uitgangspunten. Publicatienummer 3300, Planbureau voor de leefomgeving.

van Dongen, B. (2019a). The economic potential of deep, direct use geothermal systems in the Netherlands. Master's thesis, Applied Earth Sciences, Delft University of Technology.

van Dongen, B. (2019b). *Personal Communication*. Pipeline Engineer.

van Wijhe, D. (1987). Structural evolution of inverted basins in the Dutch offshore. *Tectonophysics*, 137:171–219.

van 't Spijker, H. and Ungemach, P. (2016). Definition of Electrosubmersible Pump (ESP) design and selection workflow. https://www.kasalsenergiebron.nl/content/user_upload/Definition_of_ESP_design-_final_version_20160629_-public_v2.pdf [Accessed: 02-11-19].

Vondrak, A., Donselaar, M. E., and et.al. (2018). Reservoir architecture model of the nieuwerkerk formation (early cretaceous, west netherlands basin): diachronous development of sand-prone fluvial deposits. *Geological Society, London, Special Publications*, 469:423–434.

Voskov, D. (2017). Operator-based linearization approach for modeling of multiphase multi-component flow in porous media. *Journal of Computational Physics*, 337:275–288.

Waltham, T. (2009). *Foundations of Engineering Geology*. 3rd ed. Taylor & Francis, New York.

Wang, Y., Khait, M., Voskov, D., and et.al. (2019). Benchmark test and sensitivity analysis for Geothermal Applications in the Netherlands. In *44th Workshop on Geothermal Reservoir Engineering*.

Wang, Y., Voskov, D., Khait, M., and et.al. (2020). An efficient numerical simulator for geothermal simulation: A benchmark study. *Applied Energy*, 264(114693).

Wiebes, E. (2018). *Beleidsbrief Geothermie* . https://www.rijksoverheid.nl/documenten/kamerstukken/2018/02/08/kamerbrief-over-geothermie [Accessed: 11-04-20].

Willems, C., Hamidreza, N., Weltje, G., and et.al. (2017). An evaluation of interferences in heat production from low enthalpy geothermal doublets systems. *Energy*, 135:500–512.

Zoback, M. D., Barton, C., and et. al. (2003). Determination of stress orientation and magnitude in deep wells. *International Journal of Rock Mechanics and Mining Sciences*, 40(7–8):1049–1076.